ISBN 978-82-326-6215-9 (printed ver.)
ISBN 978-82-326-6338-5 (electronic ver.)
ISSN 1503-8181 (printed ver.)
ISSN 2703-8084 (electronic ver.)

NTNU
Norwegian University of
Science and Technology

Doctoral theses at NTNU, 2023:39

Marcel Ulrich Ahrens

Development of an ammonia-water absorption-compression heat pump at high temperature operation

Doctoral thesis
Marcel Ulrich Ahrens

NTNU
Norwegian University of
Science and Technology
Thesis for the degree of
Philosophiae Doctor
Faculty of Engineering
Department of Energy and Process Engineering

Doctoral theses at NTNU, 2023:39
NTNU
NTNU
Norwegian University of
Science and Technology

Marcel Ulrich Ahrens

Development of an ammonia-water absorption-compression heat pump at high temperature operation

Thesis for the degree of Philosophiae Doctor

Trondheim, February 2023

Norwegian University of Science and Technology
Faculty of Engineering
Department of Energy and Process Engineering

NTNU
Norwegian University of
Science and Technology

NTNU
Norwegian University of Science and Technology

Thesis for the degree of Philosophiae Doctor

Faculty of Engineering
Department of Energy and Process Engineering

ISBN 978-82-326-6215-9 (printed ver.)
ISBN 978-82-326-6338-5 (electronic ver.)
ISSN 1503-8181 (printed ver.)
ISSN 2703-8084 (electronic ver.)

Doctoral theses at NTNU, 2023:39

PRINTED IN NORWAY
NO - 1598

NORDIC SWAN ECOLABEL
Printed matter
2041 0731

Printed by Skipnes Kommunikasjon AS

Preface

This doctoral thesis was submitted to the Norwegian University of Science and Technology (NTNU) in partial fulfilment of the requirements for the degree of Philosophiae Doctor (Ph.D.).

The PhD period lasted from October 2018 to November 2022 and included the equivalent of six months of course work and one year of departmental teaching and research duties. The research work was carried out in the Refrigeration group at the Department of Energy and Process Engineering, under the supervision of Professor Trygve Magne Eikevik (EPT) and the co-supervision of Professor Armin Hafner (EPT), Dr Ignat Tolstorebrov (EPT) and Professor Ruzhu Wang (Shanghai Jiao Tong University, China). An external research stay with a total duration of three months was undertaken at the Danish Technological Institute (DTI) in Aarhus, Denmark, in the period from May 2021 to September 2021.

This PhD position was created and financed by NTNU Energy. The research work was funded and supported by HighEFF – Centre for an Energy Efficient and Competitive Industry for the Future, an 8-years' Research Centre under the FME-scheme (Centre for Environment-friendly Energy Research, 257632) with financial support from the Research Council of Norway and user partners of HighEFF.

All financial support is gratefully acknowledged.

Marcel Ulrich Ahrens
November 2022
Trondheim, Norway

Acknowledgements

Once I heard, and I find it very appropriate, that the time as a PhD candidate can be described as the course of a roller coaster with alternating ups and downs. The fact that I have successfully completed this journey and can now present the following work is due to a variety of individuals whom I would like to thank in the following for their various forms of support!

Above all, this work would not have been possible without the support and guidance of my PhD supervisor, Professor Trygve Magne Eikevik, and my co-supervisors, Professor Armin Hafner, Dr Ignat Tolstorebrov and Professor Ruzhu Wang. Thank you very much for all the interesting and often inspiring discussions on how to deal with the small and big challenges related to the PhD work, among many other topics. I am grateful for this unique opportunity and the development I have experienced. This challenging project has helped me to grow as a researcher and to expand my skills.

To succeed in the scientific environment, it is essential to accomplish tasks as a team and to pursue the larger objectives together. I want to thank all my co-authors, peers and partners from academia and industry for their outstanding support and successful collaboration. I would also like to thank all the students I have had the privilege to supervise and who have supported my research in various ways with their work.

To all my colleagues in various positions at NTNU who have contributed to an engaging and welcoming atmosphere, I thank you for your support. Special thanks to all my PhD fellows and friends from Trondheim and around the world for making my time in the office and especially outside the university unforgettable with many shared activities and memories!

On a personal note, I would like to thank my partner Tiana for her endless support and understanding during these unique and often challenging years. Thank you for constantly reminding me of the crucial things in life and all the adventures we have experienced together.

Finally, none of this would have been possible without my family's unconditional love and support. Thank you for everything you have done for me and for always having my back.

Thank you!

Abstract

Decarbonization of the industrial sector is one of the most important measures to tackling global warming. Energy demand and associated greenhouse gas (GHG) emissions are continuously increasing in various industrial processes. The increasing demand in the industry for energy-efficient, cost-effective, and environmentally friendly energy systems results in a growing interest in using heat pumps. Integrating high temperature heat pumps (HTHPs) for waste heat recovery and supply temperatures of more than 100 °C is a sustainable solution for many industrial high temperature applications.

This study investigates the absorption-compression heat pump (ACHP) using the zeotropic ammonia-water mixture as working fluid. The ACHP system combines the technologies of an absorption and vapor compression heat pump with the ability of achieving high supply temperatures above 120 °C with large temperature lifts ($> 60\,K$) and non-isothermal heat transfer ($T_{glide} > 30\,K$). The working principle and characteristics of different ACHP cycles were discussed and an overview of the current state-of-the-art was elaborated with respect to experimental investigations available in the literature.

The existing solutions and challenges for the realization of ACHP systems with focus on the application at high temperature operation were identified: the compressor design with respect to discharge temperature and lubrication; the design and operation of the absorber and desorber; the establishment of efficient liquid-vapor mixing and distribution; and the selection and cavitation protection of the solution pump. It was concluded that the oil-free operation of the ACHP system can lead to improved efficiency and reduced costs by saving on the required oil infrastructure. This can further improve the competitiveness of ACHP systems for the usage in industrial high temperature applications compared to conventional energy supply systems.

The analysis of an existing dairy plant, which uses heat pumps for heating and cooling at multiple temperature levels, revealed that the process efficiency can be significantly improved with a waste heat recovery rate of more than 95%. This reduced the primary energy demand by 37.9% and emitted GHG emissions by 91.7%. The ACHP system supplied a temperature of 95 °C and a temperature lift of 33.5 K. An average COP of 5.8 was achieved with a Carnot efficiency of more than 50%. The results demonstrated that ACHP systems are reliable and efficient in commercial high temperature applications up to 100 °C. The potential application area can be further expanded by increasing the achievable heat sink supply temperature above 120 °C.

Based on the identified challenges and demands, the task description of the experimental ACHP prototype was specified, and a simulation model of the ACHP cycle with single-stage solution circuit was developed using Engineering Equation Solver. This model was used to investigate the system behaviour of the ACHP system and to determine the design parameters of the ACHP prototype. The energy and exergy analysis revealed that the use of liquid injection during the vapor compression process is a sufficient measure to decrease the discharge temperature and to provide lubrication. The determined design parameters were the basis for the design of applicable and feasible component section solutions.

The main component sections for the defined research areas were designed to meet the specifications, considering existing limitations for available components on the market and their potential for modifications. A numerical simulation model of an oil-free liquid-injected twin-screw compressor was developed and used to reduce the limiting compressor discharge temperature and achieve the desired oil-free system operation.

The investigation revealed that it is preferable to inject the lean solution with a low NH_3 mass fraction (40%), and an injection ratio of 10% of the compressor's suction mass flow rate is required. The distribution of the lean solution over multiple injection ports located at the beginning (360°) and in the middle of the compression phase (450° or 495°) can ensure a continuous liquid film. The liquid film is utilized for sealing, lubrication, and decreasing of the discharge temperature. The obtained findings are considered as a kind of best-case analysis and were used to determine modifications to an existing compressor and to design the required injection line.

The outcome of the conducted research work is the ACHP prototype with a maximum heat capacity of up to 200 kW and a maximum operating pressure and temperature of 40 bar and 190 °C, respectively. Together with the pressurized water heat source and sink circuits, the test facility allows the investigation of different component sections and application cases with heat sink outlet temperatures up to 140 °C. The ACHP prototype is an important tool for the validation of numerical models, testing new elements and optimization of the control strategy.

This thesis has successfully completed the aim of the development of an ammonia-water absorption-compression heat pump at high temperature operation. The results were disseminated in the context of three published journal articles, several peer-reviewed conference papers, and other presentations. This project was done in collaboration with industrial partners and generated spin-off projects.

Contents

Preface ..... **I**

Acknowledgements ..... **III**

Abstract ..... **V**

Contents ..... **VII**

List of Figures ..... **XI**

List of Tables ..... **XIII**

Nomenclature ..... **XV**

1 Introduction **1**

1.1 Motivation 1

1.2 Research objectives 4

1.3 Thesis outline 5

1.4 Scientific publications 6

1.4.1 Journal publications 6

1.4.2 Peer-reviewed conference publications 6

2 Background **9**

2.1 Introduction 9

2.2 The ammonia-water absorption-compression heat pump 10

2.2.1 Cycle configurations 14

2.3 State-of-the-art 16

2.3.1 Identified challenges 18

2.3.2 Summary of existing solutions 20

2.4 Potential use of ACHP in industrial applications 22

2.5 Summary 24

3 Design of the Experimental ACHP Prototype 25
3.1 Task description of the experimental ACHP prototype 25
3.2 Design of the ACHP system 27
3.2.1 System analysis 27
3.2.2 Determination of design parameters 32
3.2.3 Summary 34
3.3 Design of the compressor section 35
3.3.1 Numerical investigation of oil-free liquid-injected screw compressors 37
3.3.2 Summary 39
3.4 Design of the desorber and absorber with mixing sections 40
3.4.1 Liquid-vapor mixing section 41
3.4.2 Summary 42
3.5 Solution pump section 43
3.6 Summary 44
4 The Experimental ACHP Prototype 45
4.1 System description 46
4.2 Components 47
4.2.1 Liquid-vapor separator 47
4.2.2 Compressor with liquid injection line 48
4.2.3 Solution pump 49
4.2.4 Absorber and mixing section 49
4.2.5 High-pressure receiver 50
4.2.6 Internal heat exchanger 51
4.2.7 Expansion valve 51
4.2.8 Desorber 51
4.2.9 Auxiliary system 52

4.3 Measuring system 53
4.3.1 Instrumentation 53
4.3.2 DAQ and data handling 54
4.4 System charging and safety considerations 55
4.5 Control system 56
4.5.1 Test procedure 56
5 Summary of Research Work 57
5.1 Article I – Identification of existing challenges and future trends for the utilization of ammonia-water absorption-compression heat pumps at high temperature operation 58
5.2 Article II – Integrated HTHPs and thermal storage tanks for combined heating and cooling in the industry 59
5.3 Article III – Numerical investigation of an oil-free liquid-injected screw compressor with ammonia-water as refrigerant for high temperature heat pump applications 61
6 Conclusions 63
7 Suggestions for Future Work 67
Bibliography 69
A. Additional Information 77
A.1. Simulation model – EES code 77
A.2. Simulation results 80
A.3. Detailed P&IDs 81
A.4. Measurement & control system 82
B. Collection of Publications 83

List of Figures

Figure 1.1. Breakdown of the final energy and process heating demand in the EU industry. .. 1
Figure 1.2. Integration of heat pump driven energy systems into industrial processes. 2
Figure 2.1. Schematic of the basic absorption-compression heat pump cycle. 11
Figure 2.2. Example of a simplified ACHP cycle in ammonia-water log p-(1/T) diagram. ... 12
Figure 2.3. Schematic representations of different ACHP cylces. 14
Figure 2.4. Overview of identified challenges. 18
Figure 2.5. Overview of recent developments and existing solutions for ACHP systems..... 20
Figure 3.1. Schematic of the simulation model and the detailed compressor configuration. . 28
Figure 3.2. Effects of circulation ratio and desorber pressure on selected parameters. 33
Figure 3.3. Different potential compressor configurations. 35
Figure 3.4. Mass and energy flows associated with each control volume. 37
Figure 3.5. Simulation setup of the compressor model with defined boundary conditions. ... 38
Figure 3.6. Schematic of PHE operated as absorber in falling film and bubble mode. 41
Figure 3.7. 3D model of the experimental ACHP prototype with research focus areas. 44
Figure 4.1. Picture of the experimental ACHP prototype on-site in the NTNU laboratory.... 45
Figure 4.2. Flow diagram of the experimental ACHP prototype with measuring points..... 46
Figure 4.3. Schematic of the liquid-vapor separator with indicated flows..... 47
Figure 4.4. Schematic of the compressor section with liquid injection line. 48
Figure 4.5. Schematic of the absorber and mixing section. 49
Figure 4.6. Flow diagram of the auxiliary system with heat source and sink circuits. 52
Figure 5.1. Sequential order of the conducted research work. 57
Figure 5.2. Integrated energy supply system of the investigated dairy. 59
Figure 5.3. Temperature evolution for different injection angles.. 62
Figure A.1. Effects of circulation ratio and desorber pressure at 60 °C inlet temperature. 80
Figure A.2. Effects of circulation ratio and desorber pressure at 70 °C inlet temperature. 80
Figure A.3. Detailed P&ID of the experimental ACHP prototype with instrumentation. 81
Figure A.4. Detailed P&ID of the auxiliary system with heat source and sink circuits..... 81
Figure A.5. Detailed P&ID in LabVIEW with measurement and controlling points. 82

List of Tables

Table 2.1. Overview of experimental investigations on the different ACHP cycles..... 16
Table 3.1. Component input parameters..... 29
Table 3.2. Simulation input parameters used. 30
Table 3.3. Simulation results for Case 1 without liquid injection. 30
Table 3.4. Simulation results for Case 2 with a liquid injection ratio of 10%. 31
Table 3.5. Input parameter range for the thermodynamic model in EES. 33
Table 3.6. Determined design parameters. 34
Table 4.1. Plate characteristics of the different PHE units used..... 50
Table 4.2. Range and accuracy of measuring instruments connected to the test facility. 53

Nomenclature

Abbreviations

ACHP	Absorption-compression heat pump
CM	Compressor
CV	Control volume
DAQ	Data acquisition system
EES	Engineering Equation Solver
EU	European Union
FS	Full scale
GHG	Greenhouse gas
GWP	Global warming potential
HTHP	High temperature heat pump
IHX	Internal heat exchanger
NH_3	Ammonia
PHE	Plate heat exchanger
RES	Renewable energy source
RTD	Reference temperature detection
VCHP	Vapor compression heat pump

Roman Letters

COP	Coefficient of performance [-]
CR	Circulation ratio [-]
h	Specific enthalpy [$kJ \cdot kg^{-1}$]
L/D	Plate length to gap ratio [-]
$\dot{m}$	Mass flow rate [$kg \cdot s^{-1}$]
p	Pressure [bar]
$\dot{Q}$	Thermal load [kW]
s	Specific entropy [$kJ \cdot kg^{-1} \cdot K^{-1}$]
T	Temperature [°C]
x	Ammonia mass fraction [$kg \cdot kg^{-1}$]
W/D	Plate width to gap ratio [-]
$\dot{W}$	Power [kW]

Greek symbols

ε	Thermal efficiency [-]
ζ	Injection ratio [-]
η	Efficiency [-]
θ	Rotational angle of male rotor [rad]

Subscripts

comp	Compressor
dis	Discharge
HP	High-pressure
in	Inlet
inj	Injection
int	Intermediate
isen	Isentropic
j	Index
leak	Leakage
LP	Low-pressure
ls	Lean solution
min	Minimum
out	Outlet
pp	Pinch point
suc	Suction

1 Introduction

This chapter introduces the motivation and main research objectives of the doctoral work, the thesis structure and a list of scientific publications within the scope of this thesis.

1.1 Motivation

Decarbonization of the industrial sector is one of the most important keys to tackling global warming [1]. Energy demand and associated greenhouse gas (GHG) emissions in various industrial processes are continuously increasing [2]. With the increasing impacts of climate change, there is growing consensus on the importance of improving the energy efficiency of industrial processes and reducing direct GHG emissions, for instance from fossil fuel combustion, to create environmentally friendly, cost-effective, and sustainable energy systems.

In 2015, the total industrial energy demand in the European Union (EU) was 2950 TWh/a, of which thermal energy accounted for the majority, with 81% (2390 TWh/a) [3,4]. The demand for process heating represented 1952 TWh/a (66% of the total) and was required at different temperature levels, whereby 37% was in the lower temperature range below 200 °C. More than 77% of the energy supply came from fossil fuels, while only about 12% came exclusively from renewable energy sources (RES). Figure 1.1 shows the breakdown of the industrial energy demand in the EU by broad application with the process heating demand by different temperature levels and the energy sources used to fulfil this demand [5].

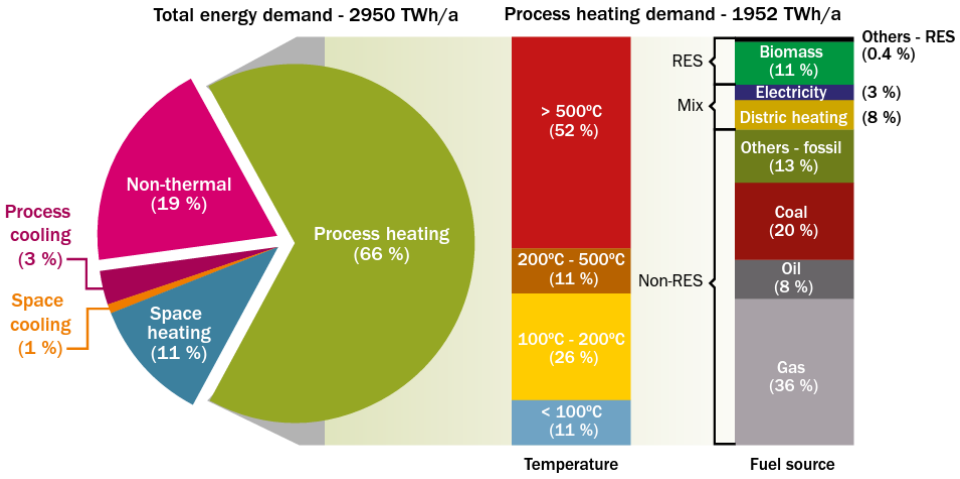

Figure 1.1. Breakdown of the total industrial energy demand in the EU by broad application (left) and process heating demand by temperature level (centre) and energy sources used (right) [5].

The available waste heat potential in the EU is estimated at approximately 300 TWh/year, of which one-third is below 200 °C, often referred to as low temperature waste heat [6]. At the same time, large amounts of potentially usable low-grade waste heat are often not exploited by now. Due to this, it is essential to develop more efficient and environmentally friendly ways to provide thermal energy as usable heat and cold for industrial applications.

Many industries requiring both cooling and heating have separate systems for these tasks. Having a combined system capable of providing both demands while utilizing available waste heat can significantly increase the overall energy efficiency. By integrating heat pumps, most of the energy can be recovered from available waste heat. This significantly reduces the required primary energy (electric power), reflected in the coefficient of performance (COP). At the same time, GHG emissions are reduced and can even be eliminated by using renewable energy sources. Figure 1.2 shows the integration of a heat pump driven energy system into an industrial process with a given heat pump COP of 4.0 and a waste heat recovery rate of 75%.

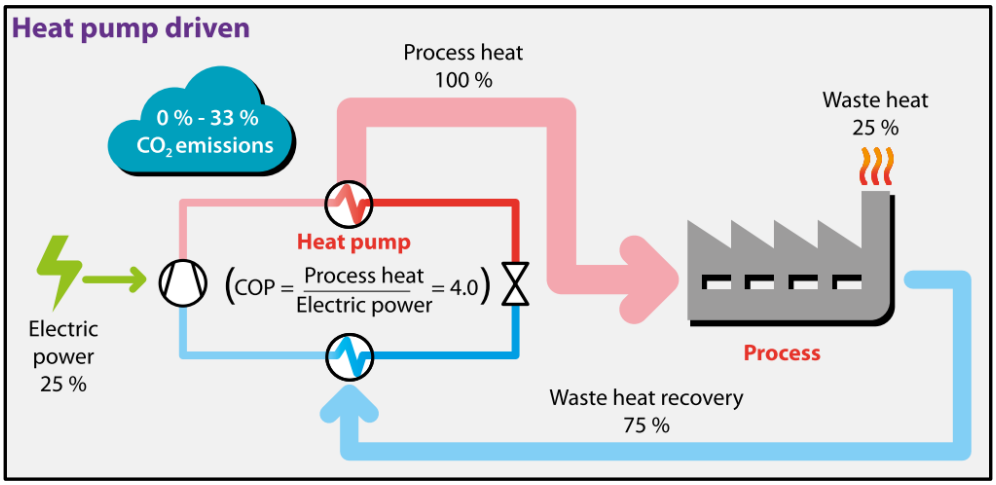

Figure 1.2. Integration of heat pump driven energy systems into industrial processes [5].

The integration of high temperature heat pumps (HTHPs) with a heat supply temperature above 100 °C is a promising approach for many industrial applications [7]. Suitable HTHP solutions have been increasingly investigated in recent years [8]. In the heat pump technology, a lot of achievements were made, especially at lower heat supply temperatures, but fewer at high temperatures above 90 °C. Ongoing research is focused on further increasing the delivery temperatures, as great utilization potential exists for high temperature applications up to 150 °C and more due to the prevailing industry conditions [9].

The *Heat Pumping Technology Annex 58* about HTHPs by the *International Energy Agency* is intended to provide an overview of the current state-of-the-art and demonstration cases for different technologies with heat supply temperatures above 120 °C [10]. It is stated that many development projects are underway with different technologies and varying technology readiness levels, capacities, expected costs and achievable temperature levels. Typical systems in current demonstration cases are vapor compression heat pump (VCHP) systems, often using artificial refrigerants or mechanical vapor recompression systems using water as refrigerant. The use of natural refrigerants with low global warming potential (GWP) and known impacts and burdens on the atmosphere, such as ammonia and water, is of particular interest regarding environmental sustainability when developing new HTHP solutions [11–13].

One of the suitable heat pump solutions for various industrial high temperature applications is the absorption-compression heat pump (ACHP) system with the zeotropic ammonia-water mixture as working fluid. The ACHP is often named a vapor compression cycle with solution circuit, compression/absorption cycle or hybrid absorption–compression heat pump. It combines the technologies of an absorption and vapor compression heat pump using a zeotropic mixture of ammonia and water as working fluid. As a result, heat is extracted and released at temperature glides ($T_{glide} > 30\ K$). The compression ratio can be reduced, when compared with conventional VCHPs utilizing single fluid refrigerants, via adjusting the concentration to the given boundary conditions. These characteristics, combined with the ability to achieve high sink temperatures above 100 °C at large temperature lifts ($> 60\ K$) and high COPs, make the ACHP system a valuable solution for the use and integration in high temperature heat supply application in the industry [14].

The utilization and improvement of HTHP technology and its integration into industrial processes is one of the main objectives of the Centre for an Energy Efficient and Competitive Industry for the Future (HighEFF) [15]. It is designed to achieve ambitious goals for the development and demonstration of technologies that can help to improve the energy efficiency and reduce emissions from the industry. A main emphasis is on the development and use of HTHP systems with natural refrigerants to exploit available waste heat and improve the efficiency of industrial processes. The HighEFFLab project supports this effort by developing and testing different systems and components through the establishment of new experimental test facilities [16]. Following the current trend and aiming to cover a broad spectrum in the development of potential HTHP systems using natural refrigerants, the experimental ACHP prototype is one of these installations.

1.2 Research objectives

The primary objective of this PhD thesis is to contribute to the evolution of high-temperature heat pump technology through the development of an experimental ACHP prototype using ammonia-water mixture as refrigerant. With the ability to experimentally investigate various high-temperature operating conditions, this work aims to enhance the understanding of the ACHP system and contribute to the extension of the potential application range. Emphasis is on the identification, implementation and testing of recent developments and further potential improvements of the entire ACHP system and specific components. To achieve the main objective, the following sub-objectives are proposed:

- Identification of existing demands and challenges for the utilization of ACHP systems at high temperature operation.
- Development of a numerical simulation tool to investigate and describe different concepts and operating conditions of the ACHP system.
- Determination of requirements and design parameters for the development of the experimental ACHP prototype based on results of previous literature work and conducted simulations.
- Design of the experimental ACHP prototype for defined requirements and operation parameters based on the identified state-of-the-art findings and developments.
- Commissioning and description of the constructed experimental ACHP prototype for the investigation of various operating conditions and main components.
- Identification and elaboration of the possible use of the ACHP prototype in relation to the overall system and specific components within the scope of future work.

This PhD project aims to build and establish new knowledge and competencies in the design and application of ACHP systems with ammonia-water mixture as working fluid. The motivation is to support the decarbonization of industrial high temperature processes with enlarged application range by providing higher supply temperatures and improved system efficiencies. The research work provides the basis to perform further investigations and establish cooperations with academic and industrial partners.

1.3 Thesis outline

This thesis is structured by seven chapters representing an overview and summary of the conducted research work for the development of the experimental ACHP prototype and covering the results and findings presented in three journal articles and several peer-reviewed conference papers. These chapters can be summarized as:

- **Chapter 1** introduces the demand and motivation for the doctoral research work, highlights the research objectives and approach, and provides the list of scientific publications.
- **Chapter 2** provides the background of the thesis on the absorption-compression heat pump with ammonia-water as refrigerant. The functionality and properties of the ACHP cycle are described and an overview of the stat-of-the-art with existing challenges and possible solutions is presented. Finally, the potential use of ACHP systems in industrial applications is discussed.
- **Chapter 3** addresses the development and design of the experimental ACHP prototype with the methodology used. The task description of the planned installation along with the design of ACHP system and main component sections are outlined.
- **Chapter 4** presents the developed experimental ACHP prototype based on the previous obtained findings and specifications. The functionality and detailed design are described along with the specific component solutions. Furthermore, the installed measuring system and operating procedure for the performance of experiments are presented.
- **Chapter 5** summarizes the published research work by elaborating a brief description and highlighting main results and findings for each publication.
- **Chapter 6** concludes the thesis by presenting the main findings and contributions of the conducted research work and its value to the ACHP technology at high temperature operation.
- **Chapter 7** suggests future research work enabled by the development of the experimental ACHP prototype that can further improve the technology and enhance the useability in industrial applications.

1.4 Scientific publications [*]

The research findings conducted during the PhD project were published in three peer-reviewed journal articles. All articles are subject to evaluation and are attached in the Appendix. The author contributions for each article are indicated based on the CRediT classification [17]. The PhD candidate was the corresponding first author of all these articles and was responsible for conceptualization, methodology, formal analysis, investigation, visualization, and writing of the original draft as well as the review and editing process.

1.4.1 Journal publications

Article I M.U. Ahrens, M. Loth, I. Tolstorebrov, A. Hafner, S. Kabelac, R.Z. Wang and T.M. Eikevik (2021). **Identification of Existing Challenges and Future Trends for the Utilization of Ammonia-Water Absorption-Compression Heat Pumps at High Temperature Operation**. In: *Applied Sciences* 11, 4635. DOI: 10.3390/app11104635

Article II M.U. Ahrens, S.S. Foslie, O.M. Moen, M. Bantle and T.M. Eikevik (2021). **Integrated high temperature heat pumps and thermal storage tanks for combined heating and cooling in the industry.** In: *Applied Thermal Engineering* 189, 2021, 116731. DOI: 10.1016/j.applthermaleng.2021.11673

Article III M.U. Ahrens, I. Tolstorebrov, E.K. Tønsberg, A. Hafner, R.Z. Wang and T.M. Eikevik (2022). **Numerical investigation of an oil-free liquid-injected twin screw compressor with ammonia-water as refrigerant for high temperature heat pump applications.** In: *Applied Thermal Engineering* 219, 2023, 119425. DOI: 10.1016/j.applthermaleng.2022.119425

1.4.2 Peer-reviewed conference publications

In addition to the journal articles, the author has contributed to the publication of several peer-reviewed conference papers in international and national conference proceedings within the scope of the thesis subject during the doctoral research period. A selection of the contributions published with the PhD candidate as first author is listed here and is attached in the Appendix.

[*] The latest versions of all publications are available at the following link, either directly as download or as link to the original publications: https://www.ntnu.edu/employees/marcel.u.ahrens

Paper I M.U. Ahrens, A. Hafner and T.M. Eikevik (2019). **Compressors for ammonia-water hybrid absorption-compression heat pumps.** In: *Proceedings of the 8th IIR International Conference on Ammonia and CO2 Refrigeration Technologies*, Ohrid, Republic of North Macedonia, 11-13 April.

Paper II M.U. Ahrens, A. Hafner and T.M. Eikevik (2019). **Development of Ammonia-Water Hybrid Absorption-Compression Heat Pumps.** In: *Proceedings of the 25th IIR International Congress of Refrigeration*, Montreal, Canada, 24-30 August.

Paper III M.U. Ahrens, I.S. Ertesvåg and T.M. Eikevik (2020). **Exergy analysis of a combined absorption-compression heat pump with ammonia-water mixture as working fluid.** In: *Proceedings of the 14th IIR Gustav Lorentzen Conference on Natural Refrigerants*, Kyoto (Online), Japan, 6-9 December.

Paper IV M.U. Ahrens, E.K. Tønsberg, I. Tolstorebrov, A. Hafner and T.M. Eikevik (2021). **Modelling approach for a liquid-injected ammonia-water screw compressor.** In: *Proceedings of the 10th International Conference on Compressors and Coolants,* Bratislava (Online), Slovakia, 13-15 January.

Paper V M.U. Ahrens, H. Selvnes, L. Henke, M. Bantle and A. Hafner (2021). **Investigation on heat recovery strategies from low temperature food processing plants: Energy analysis and system comparison.** In: *Proceedings of the 9th IIR International Conference on Ammonia and CO2 Refrigeration Technologies*, Ohrid (Online), Republic of North Macedonia, 16-18 September.

Paper VI M.U. Ahrens, E.K. Tønsberg, I. Tolstorebrov, A. Hafner and T.M. Eikevik (2022). **Modeling and simulation of oil-free liquid-injected screw compressors using ammonia-water mixture as working fluid.** In: *Proceedings of the 15th IIR Gustav Lorentzen Conference on Natural Refrigerants*, Trondheim, Norway, 13-15 June.

Paper VII M.U. Ahrens, A. Brækken, S.S. Foslie, O.M. Moen, K.A. Lovas, M. Bantle, A. Hafner and T.M. Eikevik (2022). **Performance analysis of high temperature heat pumps and thermal energy storages for a dairy.** In: *Proceedings of the 15th IIR Gustav Lorentzen Conference on Natural Refrigerants*, Trondheim, Norway, 13-15 June.

2 Background

This chapter provides the background of the doctoral thesis to enhance the understanding of the ammonia-water absorption-compression heat pump (ACHP) working principle and making the content of this thesis comprehensible to the reader. It provides a summarized overview on the current state-of-the-art by identifying existing challenges, possible solutions, and the use of HTHPs in industrial applications at high temperature operation.

2.1 Introduction

The ACHP system combines the technologies of an absorption and vapor compression heat pump (VCHP) using the zeotropic mixture of ammonia and water as working fluid. Heat is extracted and released at temperature glides and can be matched to the given heat source and sink conditions by adjusting the overall working fluid concentration and changing the circulation ratio through the solution circuit. The required compression ratio for a given temperature lift can be reduced compared with conventional VCHPs utilising single fluid refrigerants. These characteristics combined with the ability to achieve high sink temperatures above 100 °C at large temperature lifts and high coefficient of performance (COP), make the ACHP system a valuable solution to provide heat at high temperatures in various industrial applications [18].

The first patent in relation to ACHP cycles was published by Osenbrück in 1895 [19]. Detailed theoretical studies were first conducted by Altenkirch in 1950 and indicated a large potential for energy savings [20]. Due to the energy-saving potential and the increasing urgency to substitute the ozone-depleting chlorofluorocarbons (CFCs) in combination with the energy crisis in the 1970s, research activities increased rapidly since the 1980s and several experimental plants were built in this context. In 1997, Groll [21] summarized the research activities by reviewing more than 40 papers in a detailed overview. It was concluded that despite the investigation of various cycle configurations as well as the commissioning and operation of several large-scale pilot plants, considerable work remained to be done before the ACHP could be used commercially.

In the following years, research activities continued and were stimulated by the increasing energy demand in the industrial sector, with growing awareness of the problem of GHG emissions and the increasing motivation for HTHP solutions using natural refrigerants. The ACHP with single-stage solution circuit was successfully brought to commercial use with

standard refrigeration components, as reported by Baksaas and Grandum [22] and Risberg et al. [23]. Until today, several units have been installed for commercial use in various industrial applications, achieving heat sink temperatures of up to 100 °C and temperature lifts of up to 75 K, as described by the company *Hybrid Energy AS*.

The first commercial installations of the ACHP encouraged the growing interest in this system and led to extensive theoretical investigations in recent years to identify optimal operation conditions and potential applications. Van de Bor et al. [24] numerically investigated the optimal performance of compression-resorption heat pumps for 50 specific industrial cases in the chemical process industry indicated that energetically and economically competitive applications can be achieved. Jensen et al. [25] examined design parameters for the utilization of ACHP systems with heat supply temperatures above 100 °C. Qing et al. [26] continued with the thermodynamic analysis of feasible operating regions of ACHP cycles with two-stage compression. Furthermore, special focus was placed on possible system improvements to further expand the achievable process parameters, such as the heat supply temperature of more than 100 °C and an increased system efficiency, in order to compete with conventional solutions for use in high temperature applications [27–29]. This thesis supports these efforts by developing an experimental prototype of an ACHP system at high temperature operation to improve the understanding of the overall system, investigate a variety of potential component solutions and to develop and evaluate further improvements.

2.2 The ammonia-water absorption-compression heat pump

The most basic type of the ACHP system with ammonia-water mixture as working fluid is often referred to as Osenbrück cycle in recognition of its inventor Osenbrück (1895) [19]. This ACHP cycle with a single-stage solution circuit consists of seven main components, namely: three heat exchangers, a liquid-vapor separator, an expansion valve, a solution pump, and a compressor. Figure 2.1 shows a schematic representation of this basic ACHP cycle.

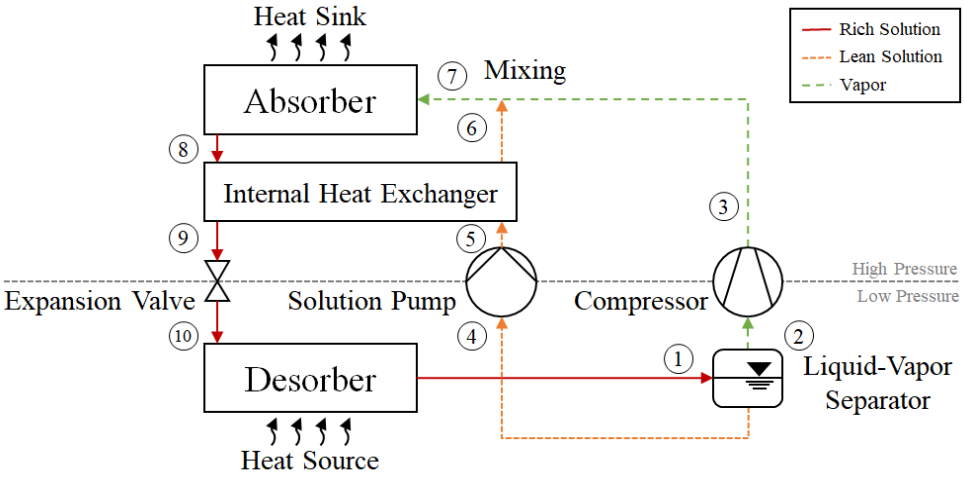

Figure 2.1. Schematic of the basic absorption-compression heat pump cycle.

In the ACHP cycle, evaporator and condenser are namely replaced by desorber and absorber transferring heat with the heat source and sink. Throughout the entire heat transfer process with the heat source in the desorber, the temperature increases and the solubility of the ammonia in water decreases, causing ammonia vapor to expel. As a result, a two-phase mixture leaving the desorber towards the liquid-vapor separator (1). The low-pressure vapor and ammonia-lean solution are separated in the liquid-vapor separator before being directed to the compressor (2) and solution pump (4). The compressor increases the pressure and temperature of the vapor (2 to 3), while the pump elevates the pressure of the lean solution correspondingly (4 to 5). To improve the cycle performance, an internal heat exchanger (IHX) is installed to interconnect the solution streams. Heat is exchanged between the lean and rich solution, resulting in a temperature increase of the lean solution (5 to 6) and a decrease of the rich solution (8 to 9). At the high-pressure side, the lean solution (6) is then mixed with the superheated NH_3 vapor from the compressor (3) at the inlet of the absorber (7). In the absorber, vapor is absorbed by the liquid and the generated heat is transferred to the heat sink fluid. During the absorption process, the NH_3 mass fraction in the solution phase gradually increases and a saturated solution emerges at the outlet of the absorber (8). The ammonia-rich solution then flows through the IHX (8 to 9) before being throttled down to the low-pressure level (9 to 10) returning to the desorber inlet (10) and thus completing the cycle.

Figure 2.2 shows a log p-(1/T) diagram of saturated liquid for ammonia-water mixture with the main components and flows of the described ACHP cycle. This representation illustrates the qualitative working principle and characteristics of the ACHP system with the zeotropic mixture of ammonia and water, not the actual compression paths or temperature levels.

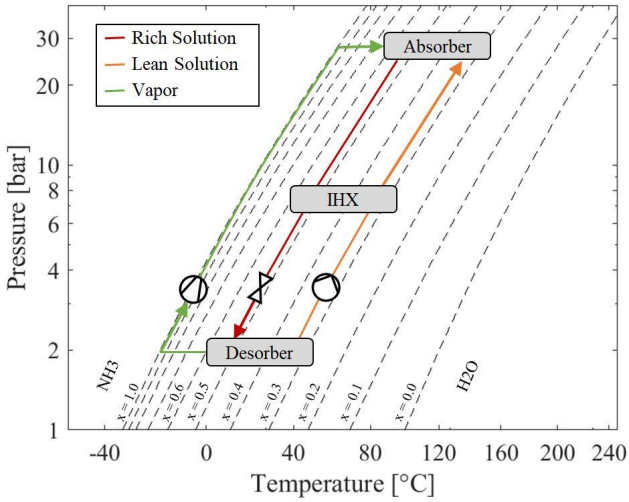

Figure 2.2. Example of a simplified ACHP cycle in ammonia-water log p-(1/T) diagram.

The ammonia-water mixture used in the ACHP system is a zeotropic mixture consisting of two solution components with different boiling points [30]. The large boiling point difference of the working fluid and the implementation of the additional solution circuit provides two additional degrees of freedom in the choice of the ammonia mass fraction and the circulation ratio for the ACHP cycle compared to conventional VCHP cycles [21]. This increases the flexibility and complexity when designing the ACHP system. Any given available source inlet temperature does not automatically define the required low-pressure level, but the set ammonia mass fraction of the lean solution is also decisive. Further, the circulation ratio (CR), specified as the ratio between the mass flow rates of the lean and rich solution

$$CR = \frac{\dot{m}_{lean}}{\dot{m}_{rich}} \tag{2.1}$$

influences the difference in ammonia mass fraction between the lean and rich solution. For a given ammonia mass fraction of the rich solution (equivalent to the system charge), the ammonia mass fraction of the lean solution can be controlled via the circulation ratio or, vice versa, the required system charge can be determined for a given operation point. Increasing the circulation ratio reduces the difference in ammonia mass fraction of the two solution streams.

Thus, the temperature glide with the secondary system and the capacity of the system are adjusted accordingly. Due to the non-isothermal heat transfer that takes place in the absorber and desorber of the ACHP cycle, instead of using the Carnot COP for operating between constant heat source and sink temperature levels:

$$COP_{Carnot} = \frac{T_{sink}}{T_{sink} - T_{source}} \tag{2.2}$$

the theoretical limit value for the coefficient of performance is often determined as described by Lorenz (1895) [31]:

$$COP_{Lorenz} = \frac{T_{log,mean,sink}}{T_{log,mean,sink} - T_{log,mean,source}} \tag{2.3}$$

Here, the constant temperature levels are substituted by the logarithmic mean temperatures of the secondary fluids for heat sink and source using Equation 2.3:

$$\mathrm{T_{log,mean}} = \frac{\mathrm{T_{secondary\ fluid,in}} - \mathrm{T_{secondary\ fluid,out}}}{\ln \frac{\mathrm{T_{secondary\ fluid,in}}}{\mathrm{T_{secondary\ fluid,out}}}} \tag{2.4}$$

The ability to vary the NH_3 mass fraction of the working fluid and the circulation ratio between the mass flow rates of the lean and rich solution ensures high flexibility and adaptability of the operating parameters to changing boundary conditions. In general, the following advantages for the ACHP system can be pointed:

- Capacity control by changing the overall NH_3 mass fraction of the working fluid mixture, resulting in a change in the low-pressure gas density. Hereby, at constant speed and volume flow of the compressor, the mass flow of the vapor and thus the capacity of the heat pump is changed.
- Exploitation of the occurring non-isothermal heat transfer in desorber and absorber can be matched to heat source and sink and thus reduce the irreversibility of the system and enable large temperature spans with comparatively high achievable COPs. The process follows the Lorenz rather than the Carnot process and becomes more effective as the temperature spread over the heat source and sink increases.
- Compared to VCHP cycles with pure ammonia as refrigerant, higher heat sink temperatures can be achieved with lower discharge vapor pressure and reduced pressure ratios when water is used as solvent.

2.2.1 Cycle configurations

Based on the most basic ACHP cycle introduced in Figure 2.1, authors such as Amrane et al. (1991) [32], Hultén and Berntsson (2002) [33] and Jensen (2015) [18] examined various possible process modifications. These included for instance the use of additional components, such as heat exchangers for desuperheating the vapor before the mixing, internal heat exchange, or cooling circuits. Subsequently, the system was further adapted and improved, although its complexity increased. More advanced cycle configurations have been developed in addition to these modifications of the ACHP cycle with single-stage solution cycle. Figure 2.3 shows three cycle configurations of the ACHP, which have been assigned individual designations due to the modifications made and specific characteristics.

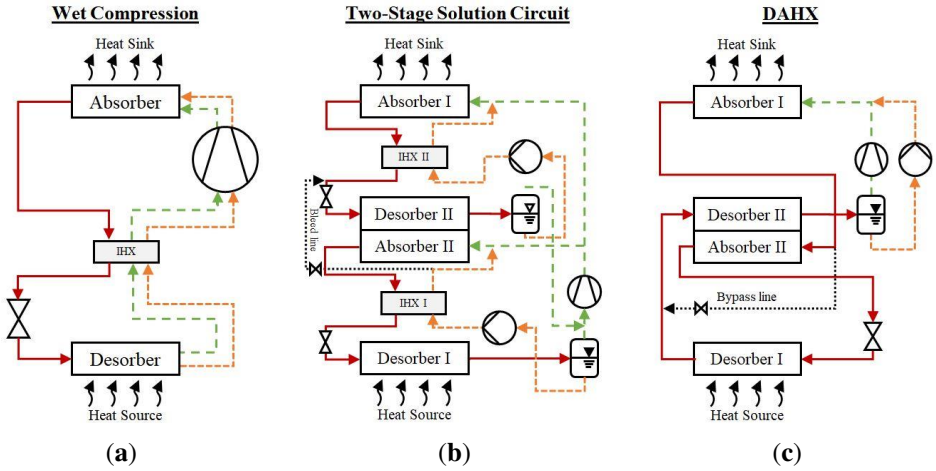

Figure 2.3. Schematic representations of (a) a wet compression cycle, (b) ACHP with two-stage solution circuit and (c) with single circuit and desorber/absorber heat exchange (DAHX) [Article I].

The wet compression cycle, also known as wet compression-resorption cycle, is shown in Figure 2.3a and was investigated by Bergmann and Hivessy (1990) [34], Itard and Machielsen (1994) [35] and Itard (1995) [36]. Contrary to dry compression with a separate solution circuit, the ammonia-water mixture leaving the desorber in a wet-vapor state is conveyed to the compressor without additional phase separation. Thus, a two-phase compression takes place, intended to reduce the compressor discharge temperature and the required compression work by decreasing the superheating of the vapor phase through continuous cooling by the present liquid. To achieve a good system performance, an extensive internal heat exchange and a suitable compressor with high isentropic efficiency are important. A disadvantage of the basic

wet compression approach is the loss of flexibility since the circulation ratio and mixture composition can no longer be varied during operation.

To keep the flexibility of the ACHP cycle combined with the advantages of increased internal heat exchange, the modification of the single-stage solution circuit towards the two-stage solution circuit, as shown in Figure 2.3b, was investigated by Radermacher (1988) [37], Rane and Radermacher (1991) [38] and (1993) [39]. Here, two solution circuits are staggered, connected with an intermediate absorber-desorber pair for internal heat exchange. Occurring concentration differences between the solution circuits are compensated by a bleed line. The lean solution from the low temperature circuit is fed into the rich solution of the high temperature circuit. This modification and the reduced temperature differences for each stage enable the system to achieve high temperature lifts of up to 100 K at comparatively modest pressure ratios, which can be achieved with a single compressor stage. Compared to a single fluid VCHP, a reduction in the required pressure ratio of 40% to 65% and a resulting improvement in COP can be achieved for a given temperature lift [40]. However, because both stages are supplied with vapor by the compressor, the capacity will be reduced by 45%. This leads to a necessary increase in mass flow, which however can have a positive effect on the selection and performance of a suitable compressor.

The vapor compression cycle with solution circuit and desorber/absorber heat exchange (DAHX) cycle, as shown in Figure 2.3c, was investigated by Groll and Radermacher (1994) [41]. In this approach, the gliding temperature intervals of desorber and absorber are further increased, allowing them to overlap. A portion of the heat transferred internally from absorber II to desorber II. As a result, the DAHX cycle only requires one solution pump and compressor while having similar characteristics to a two-stage solution circuit. Due to the internal heat exchange, the required pressure ratio for a temperature lift of 75 K can be reduced by up to 75% compared to a single fluid VCHP, with a possible COP increase of more than 40%. However, using only one solution circuit results in a loss of flexibility regarding the temperature glides, whereby the temperature intervals are dependent on the pressure ratio and can no longer be selected independently.

Based on the presented characteristics of the different cycles, it can be concluded that each cycle features specific advantages for different requirements and applications. The ACHP with single-stage solution circuit is considered most suitable for most industrial applications with the advantage of adjustable temperature glides and capacity. Wet compression can help to solve

occurring challenges such as high compressor discharge temperatures. The two-stage solution circuit is considered a promising approach for applications with the highest required temperature lift and small temperature glide, while the DAHX cycle achieves considerable temperature glides with lower temperature lift [42].

2.3 State-of-the-art

In the following, the state-of-the-art for the ACHP system using ammonia-water mixture as working fluid is examined based on the experimental work carried out. The experiments conducted until 1994 were comprehensively discussed by Groll (1997) [21], with an update of experiments until 2001 by Nordtvedt (2005) [43]. Based on these results, an updated overview of conducted experimental investigations was prepared and is presented in detail in Article I in the Appendix. Table 2.1 provides a summarized overview of selected parameters of the experimental investigations on the different ammonia-water ACHP cycles.

Table 2.1. Summarized overview of experimental investigations on the different ACHP cycles.

Cycle type	**Capacity [kW]**	T_{source} **[°C]**	T_{sink} **[°C]**	**COP [-]**	**Compressor design**	**Absorber/ Desorber design**
ACHP with single-stage solution circuit	7 to 4500	95 to 15	25 to 115	2.1 to 11.3	Piston, (twin) screw	Shell/tube, corrugated PHE
Wet Compression	1.4 to 1000	70 to 3	15 to 92	1.4 to 4.4	Screw, scroll, liquid ring	Shell/tube, tube/tube
ACHP with two-stage solution circuit	4.2	4 to -5	96 to 104	1.0c	Piston	Shell/tube vertical
ACHP with single circuit and DAHX	5.0	0 to -6	58 to 74	0.9c	Piston	Shell/tube vertical

The ACHP cycle with single-stage solution circuit is the most frequently experimentally investigated cycle, accounting for 16 publications identified from 1983 until 2021. The installed capacities range from laboratory plants starting from 7 kW up to industrial pilot plants with capacities ranging from 160 kW up to 4500 kW. Almost identical inlet temperatures were often selected for heat source and heat sink temperatures, whereby a larger temperature glide was usually achieved on the heat sink side. The highest achieved heat sink outlet temperature was at constant 115 °C during a steam generation process with many other attempts frequently ranging below 100 °C due to the limitation of the open water auxiliary circuits used. The achieved COPs range from 2.1 to 11.3, whereby a direct comparison is difficult due to the

different temperature levels and stages of optimization (insulation, compressor size, selected pinch point in heat exchanger).

Regarding the compressor design, oil-lubricated reciprocating compressors with single or two-stage compression were employed in most of the investigations. Two times twin screw compressors with oil lubrication and oil cooling were used. Only four cases of oil-free operation involving three reciprocating compressors (two single-stage and one two-stage compression) and one screw compressor were tested. The oil-lubricated two-stage reciprocating compressors often achieved the highest temperature lifts, which is in proportion to the required pressure ratio. Here, intercooling with an additional heat exchanger between the compression stages was frequently used to reduce the occurring discharge temperature. In the absorber and desorber design, an evolution from shell-and-tube to corrugated plate heat exchangers (PHE) was observed, and the alignment changed from horizontal to vertical. In this context, several innovative approaches have been employed. The connection of several PHEs in series to extend the effective heat transfer length in combination with different operation modes, described as falling film and bubble mode, and mixing techniques were evaluated.

The wet compression cycle was investigated in five experimental studies. The first of these are industrial pilot plants with capacities of 500 kW and 1000 kW, which follow in time with the first installation of the single-stage ACHP pilot plants. Then a wet compression laboratory facility was investigated with one of the smallest capacities of all ACHP cycles at 1.4 kW. The tested temperature levels vary in all investigations with the shared feature of a larger temperature gradient over the heat sink. Single-stage compressors lubricated with solution were used for all investigations, although a wide variation of different compressor types was tested. Except for the liquid ring compressor employed by Itard (1998) [44], all types were considered suitable for use in wet compression cycles. However, for efficient and reliable use, the authors highlight the importance of modifications, such as the selection of suitable bearings and the design of the liquid injection system [34,45–47]. For the design of absorber and desorber, an evolution from horizontal to vertical arrangement was observed. Additionally, Torstensson and Nowacki (1991) [47] tested a coaxial arrangement of a tube-to-tube heat exchanger. Itard (1998) [44] employed plate-fin heat exchangers with the aim of increasing the heat transfer area as a precursor to the commonly used corrugated PHE.

The ACHP with two-stage solution circuit and the ACHP with single-stage circuit with DAHX have both been studied only once by a group of researchers led by Radermacher [38,41]. The

researchers modified an existing single-stage laboratory facility designed by Rane et al. (1989) [48] to investigate the different cycle configurations as previously described. The ACHP with two-stage solution circuit investigated by Rane and Radermacher (1991) [38] had a capacity of 4.2 kW and achieved a total temperature lift of 100.5 K with almost identical temperature glides ranging from 4 °C to -5 °C for the source and from 96 °C to 104 °C for the sink. This enables simultaneous use for cooling and heating and results in a determined cooling COP of 1.

Groll and Radermacher (1993) [41] achieved during the investigation of the ACHP with single-stage circuit with DAHX a capacity of 5 kW with a total temperature lift of 68.7 K with temperature glides ranging from 0 °C to -6 °C for the source and from 58 °C to 74 °C for the sink. Despite the lower temperature lift and required pressure ratio, the achieved cooling COP at 0.9 is smaller than the cooling COP obtained for the ACHP with two-stage solution circuit. For both investigations, oil-free two-stage reciprocating compressors with water cooling were used and vertically arranged shell-and-tube heat exchangers were installed as absorber and desorber. Groll and Radermacher (1993) [41] identified a potential COP increase of over 40% by optimizing the compressor for use in the ACHP with single-stage circuit with DAHX.

2.3.1 Identified challenges

Based on the experimental work presented and discussed, different challenges for the realization and improvement of ACHP systems were identified. Figure 2.4 presents an overview of the identified challenges and allocates them to the different system component sections.

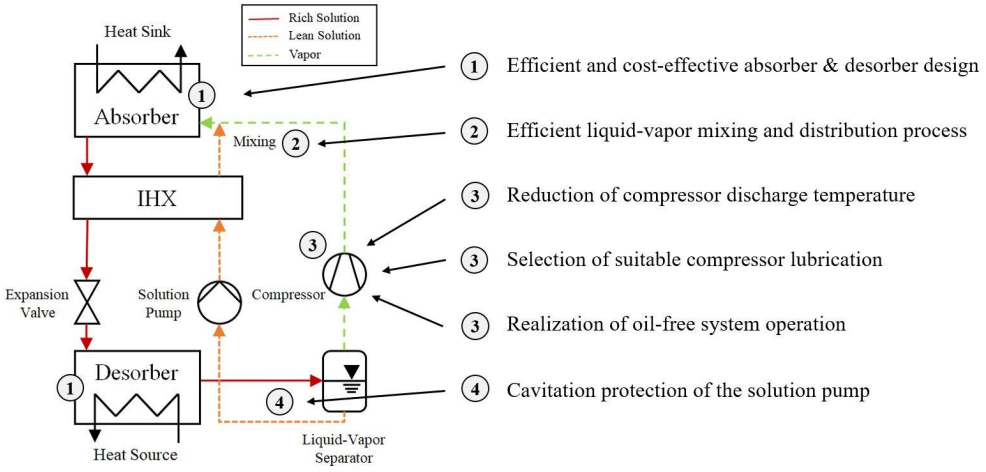

Figure 2.4. Overview of identified challenges allocated to the different system components.

The individual challenges allocated to the different system components are explained in more detail below:

1. **Absorber (and desorber) design:** An efficient design of the absorber and desorber is an important factor in improving the performance of the system. Therefore, an advanced understanding of the occurring heat transfer phenomena is essential, especially for the absorber at high temperature and high-pressure operation.

2. **Liquid-vapor mixing and distribution process:** When using plate-plate heat exchanger, an appropriate selection of the operation mode together with the establishment of an effective liquid-vapor mixing and distribution are essential to achieve high overall heat transfer coefficients and overall system performances.

3. **Compressor discharge temperature:** Occurring discharge temperatures during the compression of ammonia vapor constrain the achievement of higher sink outlet temperatures, as they can cause problems, such as decomposition of used lubricating oils and material problems in the compressor.

3. **Compressor lubrication:** When oil is used to lubricate the compressor, additional components are needed for separation and cooling, raising the complexity and costs. In addition, the oil tends to penetrate the whole circuit, which requires a recirculation system and can have a negative impact on the heat pump performance.

3. **Oil-free operation of the system:** Compressors that can be operated oil-free or with lubrication done by the refrigerant are often associated with higher equipment costs due to necessary modifications or are unavailable for commercial use.

4. **Solution pump:** Due to the saturated liquid leaving the liquid-vapor separator, cavitation caused by changing low-pressure conditions related to rapid changes in compressor operation and system operating conditions is a major challenge for the selection and reliable operation of the solution pump in ACHP systems.

2.3.2 Summary of existing solutions

Figure 2.5 summarizes the existing solutions for the realization of ACHP systems in a mind map. The classification is based on the performed experimental work and accompanying theoretical studies. The fields highlighted in green indicate the currently most frequently used solutions for commercial applications of each system part.

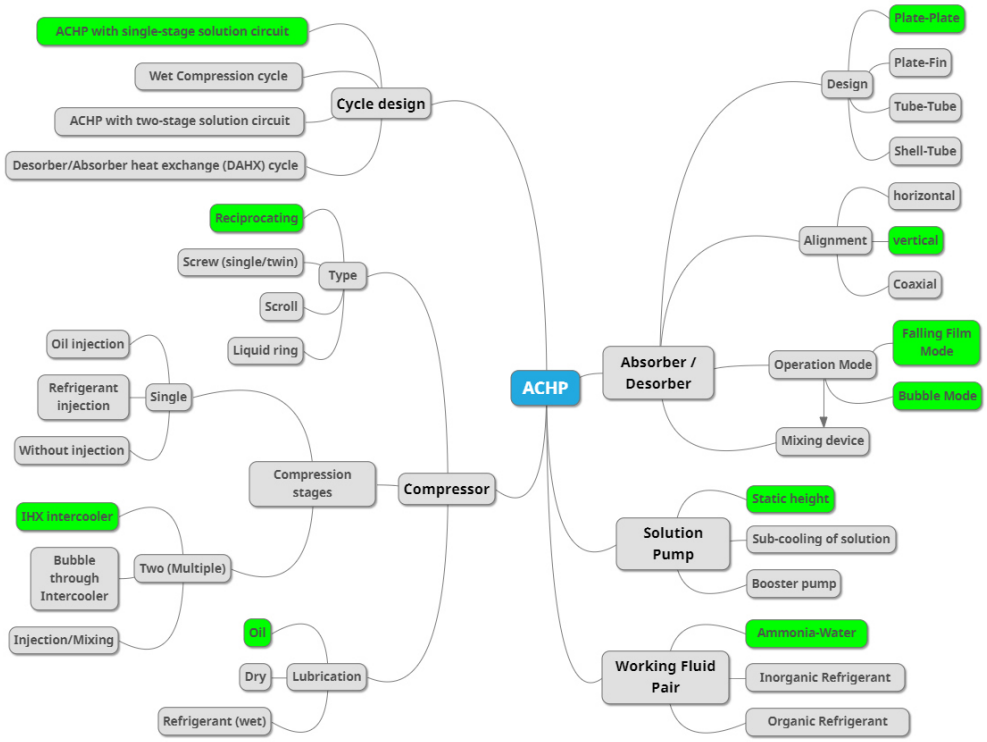

Figure 2.5. Overview of recent developments and existing solutions for realization of ACHP systems (fields highlighted in green indicate the currently most frequently used solutions for commercial applications of each system part) [Article I].

Four different cycle configurations were discussed and tested for the design of the ACHP system, whereby the ACHP with single-stage solution circuit was most frequently investigated and is used commercially today. The compressor as a major component and constraint for achieving higher heat sink outlet temperatures, features a wide range of solutions. To enable high temperature lifts and sink outlet temperatures it is necessary to provide a high discharge pressure and pressure ratio. During compression of the ammonia vapor the discharge temperature is comparatively high due to the relatively low density and specific heat capacity of ammonia in the superheated vapor phase [49]. With the aim of reducing occurring

compressor discharge temperatures and costs, several types with different compression stages and lubrication solutions were used and studied. Positive displacement compressors, such as reciprocating and screw compressors, have been identified as promising compressor solutions due to the higher achievable pressure ratios and lower swept volumes when compared with dynamic compression systems. For commercial applications, oil-lubricated reciprocating compressors with two-stage compression and intercooling are currently employed.

For the absorber and desorber design, different designs with varying alignments were investigated. In commercial applications, vertically aligned PHEs are used in different operating modes with the associated devices for liquid-vapor mixing and distribution. The plates can be pressed with different shapes to increase turbulence, fluid distribution and surface area [50]. Due to these features, the design can be much more compact. However, the specific design and operation, especially at high pressures, remain the subject of ongoing research to further increase efficiency while reducing the required size and cost.

Different approaches for the solution pump have been investigated to reduce the risk of cavitation in the mainly used centrifugal pumps. Besides the general reduction of pressure losses upstream of the pump inlet by the appropriate design of the piping, it is important to place the pump as low as possible in the system to generate a pressure increase due to the static height of the upstream liquid column in the liquid-vapor separator. Other approaches include external sub-cooling of the lean solution or the use of an additional booster pump. Despite numerous theoretical studies on alternative working fluid pairs, experimental experience in ACHP systems is mainly limited to the use of ammonia-water.

While one system configuration is currently most frequently used for commercial applications, the use and combination of other solutions is explicitly not excluded to overcome existing challenges and further improve the ACHP system performance. Depending on the circumstances, a follow-up and combination of different component solutions can be a promising approach to improve the achievable operating parameter and efficiency to increase the suitable application range and competitiveness compared to VCHPs and other conventional solutions for industrial high temperature applications.

2.4 Potential use of ACHP in industrial applications

The purpose of this sub-chapter is to examine the potential use of ACHP systems in industrial applications. The presented content is based on the insights gained from the analysis of the integrated energy system of a green-field dairy during winter (Article II) and summer (Paper VII) operation. A further potential application is presented in the theoretical investigation of different strategies for the recovery of available low-grade waste heat from a CO_2/NH_3- cascade refrigeration system by using high-temperature heat pumps (Paper V). The integrated energy systems are designed with interconnected heat pump systems to supply all cooling and heating demands of the various consumers at different temperature levels. The system design must consider varying operation conditions caused by changing production periods and seasonal variations. Auxiliary systems, such as dry chiller or electric heater, can be installed as back-up to compensate for occurring fluctuations in demand.

In the context of the intended and essential decarbonization and efficiency improvement of industrial processes, there is great demand for the integration and use of HTHPs. Food processing plants in particular offer great potential for initial improvement measures due to the simultaneous cooling and heating requirements in achievable temperature ranges for heat pump solutions that are currently ready for the market [51]. Most of this energy is generated using fossil fuels, and the decarbonization of these processes is key for a green transition of the industry [52]. In conventional plants the heating demand is traditionally covered by fossil fuel boilers, while the cooling demand is covered by a separate refrigeration system. By integrating industrial heat pump systems that can provide both process cooling and heating, the overall efficiency of the system can be significantly increased while reducing the energy demand. As a result, the need for fossil fuels can be reduced and/or eliminated altogether. Combined with a steady reduction in the share of fossil fuels in power generation, this can lead to a significant reduction in GHG emissions and reduce grid dependency and cost.

Conducted investigations focusing on the integration of HTHPs reveal the great potential for the achievable application range and given characteristics of ACHP systems, as summarized by Jiang et al. (2022) [53]. The existing temperature glide in the desorber and absorber combined with the large achievable temperature lift and range enables simultaneous supply for both cooling and heating demands. The use in combination with multiple heat pump systems can be reasonable if there exists heating demand at different temperature levels. In this case, different heat pump systems can be connected directly or by using thermal storage tanks to serve all

energy consumers. The demand of the different consumers will often vary depending on the process and ambient conditions. The use of thermal storage tanks can help to buffer possible demand peaks and fluctuations while increasing the operational stability of the heat pump systems.

The analysis of the integrated energy system of the investigated dairy in summer and winter operation demonstrated that a reliable operation with nearly constant efficiencies is achievable. A waste heat recovery rate of up to 95% was achieved with little external heat input. The ACHP system is used as HTHP stage, delivering a supply temperature of 95 °C at a temperature lift of 33.5 K. An average COP of 5.8 is achieved with a Carnot efficiency of more than 50%. The demand fluctuations occurring during the operation period require efficient capacity control to obtain good results despite part load operation of the heat pump systems.

The results obtained show that ACHP systems operate reliable and efficient in commercial application cases up to 100 °C. By increasing the achievable supply temperatures, the potential application range can be further increased. Furthermore, there is a great demand for supplying higher supply temperatures, which are required in many industrial processes with existing energy systems based on steam or with the general demand of higher process temperatures.

The investigation of different waste heat recovery strategies (Paper V) indicated great potential for savings in overall energy consumption and GHG emissions through the increased integration of HTHPs and heat recovery rates. The results for the investigated cases indicate that the integration of heat pumps can lead to potential GHG emissions reductions of up to 35% even in locations with comparatively low CO_2 equivalent of the energy sources used, such as electricity in Norway. The possible oil-free operation of the ACHP system can lead to improved efficiency and reduced costs by saving on oil components. This can further improve the competitiveness for the use of ACHP system in industrial applications compared to conventional systems.

2.5 Summary

Growing interest in ACHP systems has been recognized over the last years and was supported by the successful implementation of the first commercial units. A variety of theoretical and experimental studies were addressed to the improvement of achievable operating parameters and system efficiency to increase the competitiveness of the ACHP system in comparison to VCHPs and conventional solutions for industrial high temperature applications. Large variety of cycle configurations of the ACHP system with specific characteristics were developed and investigated. The ACHP with a single-stage solution circuit is the most studied configuration and the only one in commercial use today.

To extend the application range of the ACHP system, the existing challenges and solutions were identified and presented based on the conducted research. The compressor is a major constraint to achieve higher heat sink outlet temperatures of more than 120 °C, with existing challenges in terms of discharge temperature, lubrication, and oil-free operation of the system. Different types and configurations of heat exchangers have been used. For the design and operation of absorber and desorber, a clear trend towards vertically arranged PHEs has emerged. However, the optimal design to achieve effective liquid-vapor distribution and high overall heat transfer coefficients remains challenging. The ability to determine and predict the parameters required for the design and control of absorber and desorber more accurately is an important goal for the wider deployment of ACHP systems in industrial applications at high temperature operation. Different strategies to avoid cavitation in the solution pump were successfully implemented and tested, thus widely solving this problem discussed in earlier literature.

In summary, further numerical investigations and especially experimental work are required to develop and test novel concepts to improve the usability and performance of ACHP systems for high temperature applications with heat supply temperatures past 120 °C.

3 Design of the Experimental ACHP Prototype

This chapter presents an outline of the theoretical and numerical approaches (methodology) used in the development and design of the experimental ACHP prototype. The ACHP cycle with a single-solution circuit is the commercially deployed and most frequently investigated ACHP system so far and is used in the further study. The task description of the planned installation is defined based on the previously presented objectives and identified challenges. The design of the ACHP system with the main component sections, namely compressor, desorber and absorber with mixing and solution pump, are addressed, and the results are summarized for the implementation in the experimental ACHP prototype. The component sections refer thereby to the defined research focus areas in relation to the identified challenges.

3.1 Task description of the experimental ACHP prototype

There is a growing interest in the use of HTHPs, such as the ACHP system, in industrial applications at high temperature operation. Experimental investigations and industrial applications are currently mainly limited to reach heat sink outlet temperatures of up to 100 °C with a potential maximum of 120 °C, as demonstrated in Chapter 2.

The maximum operational range of ammonia-water ACHP with a single-stage solution cycle using standard refrigeration components up to 28 bar can reach up to 111 °C with single-stage dry compression and up to 126 °C with two-stage dry compression, based on theoretical studies by Jensen (2015) [18]. The upper limit of the achievable temperature results from a constrained compressor discharge temperature of 170 °C and a minimum NH_3 mass fraction of 0.95 at the compressor inlet. Higher heat sink temperatures can be achieved by using components designed for higher operating pressure and temperature. With the compressor as main constraint, different configurations, and measures to reduce the compressor discharge temperature, such as intercooling, liquid injection, or wet compression can be applied.

The aim of the development of the experimental ACHP prototype is to increase the achievable heat sink outlet temperature past 120 °C up to 140 °C and to optimize the system performance by exploiting the developments and improvements of recent years. Furthermore, the optimization of process parameters and specific components should be possible through extensive testing. To achieve these goals, the following specifications and requirements are defined for the experimental ACHP prototype (based on findings presented in Paper II):

1. The system components must be designed and selected to operate at high temperatures and high pressures to achieve the desired increase in heat sink outlet temperature.
2. To investigate the different research focus areas of the ACHP system, the respective connections of the main components must be designed interchangeably and with sufficient installation space.
3. It must be possible to vary the operating parameters of the ACHP system and to set the temperatures of heat source and heat sink inlets individually to test and analyse various potential operating conditions.
4. The auxiliary system providing heat source and sink, and the measuring instruments used must provide a sufficient operating range to ensure the desired flexibility of the ACHP system.
5. When selecting and dimensioning components, the resulting size and capacity must be considered for the given infrastructure of the NTNU laboratory.
6. The use of the ammonia-water mixture as the working fluid and the desired high-temperature operation imposes additional requirements on the ACHP system, such as material compatibility and oil-free operation:
    - When designing the system and selecting the components, all wetted parts must be made of ammonia-compatible material. Ammonia and aqueous ammonia are fully compatible with materials such as iron, steel, stainless steel, and aluminium but cause corrosion problems in contact with copper, zinc and copper-based alloys [49].
    - The oil-free operation of components such as the compressor is desirable to keep the system and in particular the heat exchanger free of lubricant oil. Especially high temperatures and possible water content in the NH_3 vapor flow increase the complexity and cost of the oil separation process. Incomplete separation results in lubricating oil being carried in other system parts, such as the heat exchanger, which can negatively affect the heat transfer properties and require additional components for oil recirculation [54].

3.2 Design of the ACHP system

For the development and design of the experimental ACHP prototype, the ACHP cycle with single-stage solution circuit is investigated. Reaching higher sink outlet temperatures is highly constrained by the ammonia vapor compression process. Thus, the possibility of intercooling to reduce the occurring temperature during the compression process is required. The modification of the ACHP system by employing additional IHXs as well as liquid injection options are potential possibilities, as stated earlier and comprehensively investigated by Jensen (2015) [18]. The best results in terms of achievable heat sink outlet temperature and system COP were obtained with two-stage compression and intercooling with an additional IHX downstream the original IHX. However, compared to other options with additional IHX or bubble through intercooler, the liquid injection achieved good improvements. Furthermore, the number of required components is reduced, and installation costs may be decreased. Altogether, the modification of the ACHP system with the use of liquid injection is a promising approach to achieve the desired oil-free operation while improving the achievable system parameters. The investigations further demonstrated that the resulting design parameters are highly influenced by the selection of the ammonia mass fraction of the rich solution and the circulation ratio. It is therefore crucial to identify a suitable combination range for the specification of the design parameters [14]. In the following, the impact of the liquid injection on the ACHP system is analysed, and the design parameters of the experimental ACHP prototype are determined.

3.2.1 System analysis

To investigate the effect of liquid injection on the overall system performance, an energy and exergy analysis was conducted. For this purpose, a simulation model of the basic ACHP cycle with single-stage solution circuit was developed and implemented in Engineering Equation Solver (EES) [55]. Each component is modelled based on steady-state mass and energy balances. The model ensures that the second law of thermodynamics is fulfilled in all components and includes several assumptions to simplify the simulation. Pressure and temperature losses in the components and piping are neglected. Further, the liquid-vapour mixing is adiabatic, and equilibrium exists between the two phases in absorber, desorber and separator. The thermodynamic properties of the ammonia-water mixture are determined using the built-in function *"CALL NH3H2O (123,T,P,x:T,P,x,h,s,u,v,q)"* based on the Ibrahim and Klein (1993) [56] equation of state. The function requires three independent properties (for instance, temperature, pressure and NH_3 mass fraction) to determine the thermodynamic

properties of the ammonia-water mixture in subcooled, saturated, and superheated conditions. The correlation is applicable for temperatures ranging from 230 K to 600 K at equilibrium pressures between 0.2 bar to 110 bar. Figure 3.1 shows (a) the schematic of the simulation model and (b) the detailed compressor configuration with state points for the liquid injection.

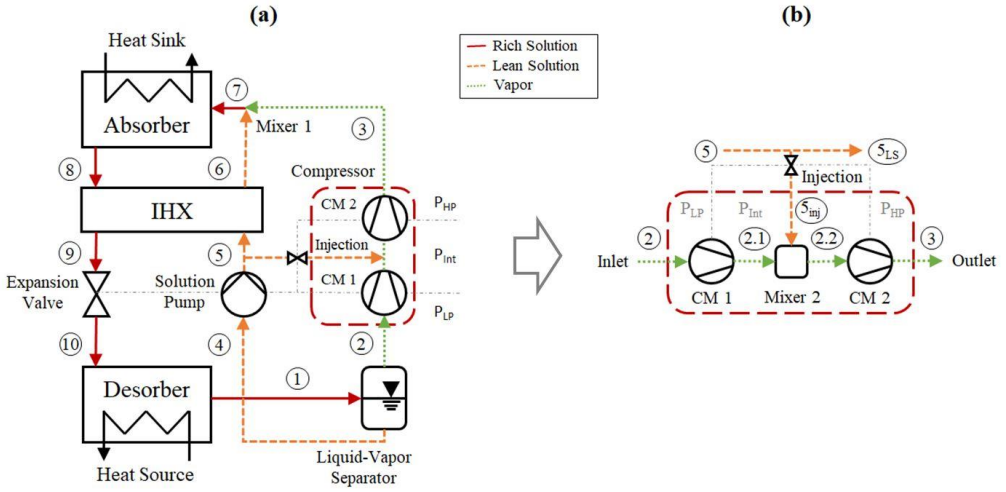

Figure 3.1. Schematic of (a) the simulation model and (b) the detailed compressor configuration.

The compressor configuration was extended by splitting the compression process from the low-pressure level (p_{LP}) to the high-pressure (p_{HP}) level into two stages (CM 1 and CM 2), with the possibility of liquid injection as mixing (Mixer 2) between the two stages at intermediate pressure (p_{Int}). Three additional state points were introduced for the simulation and further analysis of the split compression procedure with liquid injection: 2.1 – Outlet conditions of the first compressor stage (CM 1), 5_{inj} – Injection of lean solution and 2.2 – Inlet conditions of the second compressor stage (CM 2). The intermediate pressure level is determined with $p_{Int} = \sqrt{p_{LP} \cdot p_{HP}}$. For the execution of the simulations, the injection ratio (ζ) is introduced as the ratio of the injection mass flow rate to the vapor mass flow rate from the liquid-vapor separator. This results in $\dot{m}_{5,inj} = \dot{m}_{2.1} \cdot \zeta$ for the injection mass flow rate, $\dot{m}_{2.2} = \dot{m}_{2.1} + \dot{m}_{5,inj}$ for the mass flow rate leaving CM 2 and $\dot{m}_{5,ls} = \dot{m}_5 - \dot{m}_{5,inj}$ for the lean solution mass flow rate. To determine the state points of the compression process, the following procedure was used:

1. State point 2.1 – after real compression in CM 1 with

$$h_{2.1} = \frac{\left(h_{2.1,isen} - h_2\right) + h_2 \cdot \eta_{isen,CM1}}{\eta_{isen,CM1}} \qquad \text{Eq. (3.1)}$$

2. State point 2.2 – after mixing in Mixer 2 with

$$h_{2.2} = \frac{\left(h_{2.1} \cdot \dot{m}_{2.1} + h_{5,inj} \cdot \dot{m}_{inj}\right)}{\dot{m}_{2.2}} \quad \text{Eq. (3.2)}$$

$$x_{2.2} = \frac{\left(x_{2.1} \cdot \dot{m}_{2.1} + x_{5,inj} \cdot \dot{m}_{inj}\right)}{\dot{m}_{2.2}} \quad \text{Eq. (3.3)}$$

3. State point 3 – after real compression in CM 2 with

$$h_3 = \frac{\left(h_{3,isen-} h_{2.2}\right) + h_{2.2} \cdot \eta_{isen,CM2}}{\eta_{isen,CM2}} \quad \text{Eq. (3.4)}$$

More detailed information can be found in the EES model in Appendix A.1.

To analysis the effect of liquid injection on the system performance, different cases with changing injection ratios and varying input parameters such as the pressure levels, circulation ratio and inlet temperatures were investigated. For this, constant input parameters were defined for the different components of the model as presented in Table 3.1.

Table 3.1. Component input parameters.

Component	Input	Value	Unit
Compressor	η_{isen}	0.79	-
Compressor	η_{motor}	0.9	-
Pump	η_{isen}	1.0	-
Pump	η_{motor}	0.9	-
Desorber	ε	0.9	-
Desorber	$\Delta T_{pp,min}$	5	K
IHX	ε	0.9	-
Absorber	$\Delta T_{pp,min}$	5	K

Two cases, one without injection (Case 1) and one with an injection ratio of 10% of the compressor inlet mass flow (Case 2) are compared, with the aim of achieving a heat sink outlet temperature of up to 120 °C. Table 3.2 presents the input parameters used for the simulation of the two cases.

Table 3.2. Simulation input parameters used.

Parameter		Case1		Case 2	
		Value	Unit	Value	Unit
Injection ratio	ζ	0.0	-	0.1	-
Circulation ratio	CR	0.5	-	0.5	-
Heat capacity	$\dot{Q}_{sink}$	200	kW	200	kW
Low-pressure level	p_{LP}	7	bar	7	bar
High-pressure level	p_{HP}	35	bar	35	bar
Heat source inlet temperature	$T_{source,in}$	60	°C	60	°C
Heat sink inlet temperature	$T_{sink,in}$	60	°C	60	°C

The simulation results for the different stream points are shown in Table 3.3 and

Table 3.**4** for the case without and with 10% injection ratio, respectively.

Table 3.3. Simulation results for Case 1 without liquid injection.

Stream j	$\dot{m}_j$ $\left[\mathrm{kg/s}\right]$	x_j $\left[\mathrm{kg/kg}\right]$	T_j [°C]	p_j [bar]	h_j $\left[\mathrm{kJ/kg}\right]$	s_j $\left[\mathrm{kJ/kgK}\right]$
1	0.281	0.734	54.9	7.0	702	2.75
2	0.140	0.992	54.9	7.0	1397	4.84
2.1$_{isen}$	0.140	0.992	120.1	15.7	1530	4.84
2.1	0.140	0.992	133.3	15.7	1565	4.93
2.2	0.140	0.992	133.3	15.7	1565	4.93
3$_{isen}$	0.140	0.992	209.1	35.0	1729	4.93
3	0.140	0.992	224.4	35.0	1771	5.01
4	0.140	0.475	54.9	7.0	7	0.65
5	0.140	0.475	55.3	35.0	11	0.65
5$_{inj}$	0.000	0.475	55.6	15.7	11	0.66
5$_{ls}$	0.140	0.475	55.3	35.0	11	0.65
6	0.140	0.475	85.3	35.0	148	1.05
7	0.281	0.734	126.0	35.0	960	3.09
8	0.281	0.734	88.6	35.0	248	1.21
9	0.281	0.734	75.0	35.0	179	1.01
10	0.281	0.734	28.9	7.0	179	1.08
Sink$_{in}$	0.779	0.000	60.0	10.0	252	0.83
Sink$_{out}$	0.779	0.000	120.9	10.0	509	1.54
Source$_{in}$	1.213	0.000	60.0	1.6	252	0.84
Source$_{out}$	1.213	0.000	33.9	1.6	142	0.49

Table 3.4. Simulation results for Case 2 with a liquid injection ratio of 10%.

Stream j	$\dot{m}_j$ $\left[\mathrm{kg/s}\right]$	x_j $\left[\mathrm{kg/kg}\right]$	T_j [°C]	p_j [bar]	h_j $\left[\mathrm{kJ/kg}\right]$	s_j $\left[\mathrm{kJ/kgK}\right]$
1	0.289	0.734	54.9	7.0	702	2.75
2	0.144	0.992	54.9	7.0	1397	4.84
2.1$_{isen}$	0.144	0.992	120.1	15.7	1530	4.84
2.1	0.144	0.992	133.3	15.7	1565	4.93
2.2	0.159	0.945	95.1	15.7	1424	4.56
3$_{isen}$	0.159	0.945	133.9	35.0	1554	4.56
3	0.159	0.945	144.5	35.0	1588	4.64
4	0.144	0.475	54.9	7.0	7	0.65
5	0.144	0.475	55.3	35.0	11	0.65
5$_{inj}$	0.014	0.475	55.6	15.7	11	0.66
5$_{ls}$	0.130	0.475	55.3	35.0	11	0.65
6	0.130	0.475	85.3	35.0	148	1.05
7	0.289	0.734	124.4	35.0	940	3.04
8	0.289	0.734	88.6	35.0	248	1.21
9	0.289	0.734	76.4	35.0	186	1.03
10	0.289	0.734	29.1	7.0	186	1.10
Sink$_{in}$	0.800	0.000	60.0	10.0	252	0.83
Sink$_{out}$	0.800	0.000	119.4	10.0	502	1.52
Source$_{in}$	1.239	0.000	60.0	1.6	252	0.84
Source$_{out}$	1.239	0.000	34.1	1.6	143	0.50

The results in Table 3.1 were used as a reference to roughly estimate the effects of liquid injection on the system. By injecting 10% of lean solution during the divided compression process, all values from the injection point forward to the absorber inlet were changed. The NH_3 mass fraction and inlet temperature to the second compressor stage (CM 2) were reduced. As a result, the discharge temperature of the second compressor stage was significantly reduced from 224.4 °C to a manageable temperature for existing compressors of 144.5 °C. The total required compression work was reduced from 58.4 kW to 55.9 kW, despite the increased mass flow rates. The pump work remains in the range between 0.54 kW and 0.55 kW. With the constant heat load of 200 kW, this resulted in a system COP increase from 3.4 to 3.5 with the use of liquid injection.

Based on the determined simulation results, an exergy analysis was conducted for all components within the ACHP system. The methodology and detailed results are presented in Paper III in the Appendix. The second compressor stage, absorber and first compressor stage are identified as main sources of irreversibility with the highest exergy destruction rates for both cases investigated. The overall exergy destruction rate was reduced from 32.2 kW to

30.3 kW for the case with liquid injection. The greatest improvement was achieved in the liquid-vapor mixing section upstream of the absorber by reducing the compressor discharge temperature and the associated approximation of the vapor and lean solution temperatures. Additional exergy destruction through the injection was compensated by the improvements in the liquid-vapor mixing, thus improving overall system exergy efficiency from 52.2% to 53.8%.

The results revealed that besides reducing the compressor discharge temperature, liquid injection can improve the overall system efficiency. Considering the intended objectives for the ACHP system, such as increasing the achievable sink outlet temperature and oil-free system operation, the implementation of a compressor configuration with the injection of the lean solution during the compression process provides a promising approach. However, further investigations are required for the design and realization of this solution in the experimental ACHP prototype.

3.2.2 Determination of design parameters

The ACHP system model with injection of lean solution was used for the determination of design parameters. The aim was to define an appropriate combination range for the design of the experimental ACHP prototype to meet the defined task description. Simulations with varying input parameters were conducted, and the effects on the defined target parameters of achieving a high heat sink outlet temperature and system COP were evaluated. The occurring compressor discharge temperature and the maximum reachable high-pressure level were limiting factors in achieving higher values. The resulting volume and mass flow rates further restrict the availability of components for the technical installation.

For this investigation, the thermodynamic model in EES (see Appendix A.1) was used with the previously defined component input parameters (see Table 3.1). The isentropic efficiency of the compressor was reduced to 0.6 to compensate for uncertainties due to liquid injection in the design of the compressor section. This adjustment follows the experimental results stated by Zaytsev et al. (2006) [57] for the achieved isentropic efficiencies of a twin-screw compressor in wet compression. Based on the previous results, the compression ratio was set to a fixed value of 5 with a constant injection ratio of 10% for all simulations. The circulation ratio, the low-pressure level and the inlet temperatures of the heat source and the heat sink were varied as input parameters within a reasonable range to perform the simulations and provide a parametric study. Table 3.5 shows the range of the input parameter used for the simulations.

Table 3.5. Input parameter range for the thermodynamic model in EES.

Parameter	Symbol	Value	Unit
Circulation ratio	CR	0.4 to 0.8	-
Desorber pressure level	p_{LP}	3 to 8	bar
Heat source inlet temperature	$T_{source,in}$	50 to 70	°C
Heat sink inlet temperature	$T_{sink,in}$	50 to 70	°C

Figure 3.2 shows an exemplary selection of simulation results for varying circulation ratios with a focus on the achieved heat sink outlet temperature and COP for different desorber pressure levels at constant source inlet temperature of 50 °C. More results are provided in Appendix A.2.

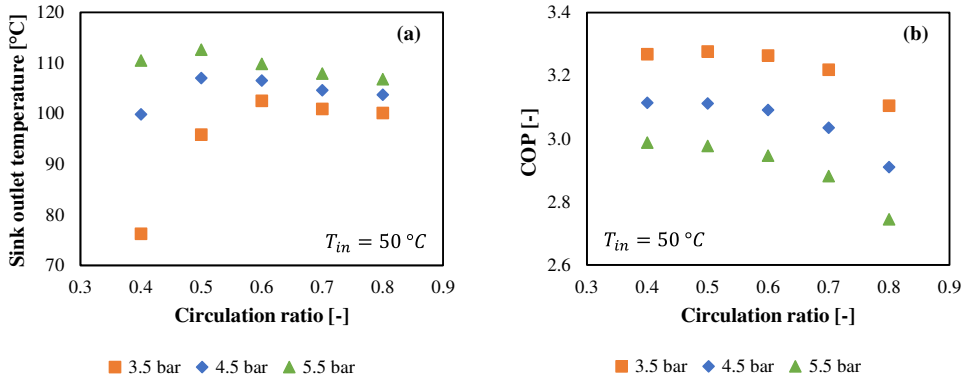

Figure 3.2. Effects of circulation ratio and desorber pressure on (a) heat sink outlet temperature and (b) COP at constant source inlet temperature of 50 °C.

The results revealed the influence of the circulation ratio and the NH_3 mass fractions on the achievable system parameters, as previously described in Section 2.2. The ammonia mass fraction of the lean solution depends on the prevailing equilibrium condition in the separator and decreases at lower source inlet temperatures. The required NH_3 mass fraction of the rich solution correlates proportionally to this, while a higher circulation ratio reduces the difference in ammonia mass fraction between both solution streams.

With increasing desorber pressure and corresponding absorber pressure, higher heat sink outlet temperatures were achieved. The same trend was observed for increased inlet temperatures. However, the discharge temperature limitation becomes more critical by reaching temperatures of almost 200 °C. With increasing circulation ratios, a strong increase in the sink outlet

temperature can be seen at the beginning, with a maximum in the range of 0.5 to 0.6 and an almost constant trend thereafter.

With increasing inlet temperatures, the COP remained almost constant but was reduced for higher desorber pressure. At the same time, an increasing circulation rate decreases the COP due to the reduced capacity at constant compressor power consumption. A circulation ratio of between 0.5 to 0.6 yielded the highest COP values. These results are in line with previous investigations and findings presented in the literature by Nordtvedt (2005) [43] and Jensen et al. (2015) [14]. Based on the results of this study, the design parameters for the design of the experimental ACHP prototype are defined as listed in Table 3.6.

Table 3.6. Determined design parameters.

Design parameter	Value	Unit
Pressure range	Up to 40	bar
Temperature range	Up to 190	°C
Heat sink capacity	Up to 200	kW
Circulation ratio	0.5 to 0.6	-
NH_3 mass fraction (rich solution)	0.6 to 0.75	kg/kg

3.2.3 Summary

The experimental ACHP prototype is designed as ACHP cycle with single-stage solution circuit with the possibility of liquid injection for the compressor configuration. Liquid injection can be realized with lean solution downstream of the solution pump or rich solution upstream of the expansion valve. The design parameters are specified to cover a wide range of operating conditions to ensure the desired flexibility in the performance of different investigations.

- A thermodynamic model of the ACHP cycle with a single-stage solution cycle was developed and used in EES.
- The conducted system analysis revealed that the use of liquid injection is a valid approach for the design of the ACHP system.
- Design parameters were determined to meet the defined requirements of the experimental ACHP prototype.
- The results serve as a basis for the design of applicable and feasible solutions for the component sections.

3.3 Design of the compressor section

To enable high temperature lifts and heat sink outlet temperatures, it is necessary to provide a high discharge pressure and pressure ratio. During the compression of the ammonia vapor the discharge temperature is comparatively high due to the relatively low density and specific heat capacity of ammonia in the superheated vapor phase [49]. High discharge temperatures reduce the COP of the system and cause various problems, such as chemical decomposition of the working fluid, carbonization of the lubricant and collapse of seals [18]. Additionally, liquid portions can be included even for dry compression depending on the temperature and pressure level due to the characteristics of the ammonia-water mixture. Therefore, the compressor must be resistant to small amounts of liquid in the vapor stream during the compression. This is, furthermore, a fundamental requirement for wet compression. According to an extensive analysis by Zaytsev (2003) [45] and in agreement with the findings presented in Article I, positive displacement compressors, such as reciprocating and screw compressors, have been identified as promising compressor solutions due to the higher achievable pressure ratios and the lower swept volumes when compared with dynamic compression systems. With the aim of reducing the superheat occurring during compression and maintaining the discharge temperature in an acceptable range for the compressor, different potential compressor solutions are available for the implementation, as shown in Figure 3.3.

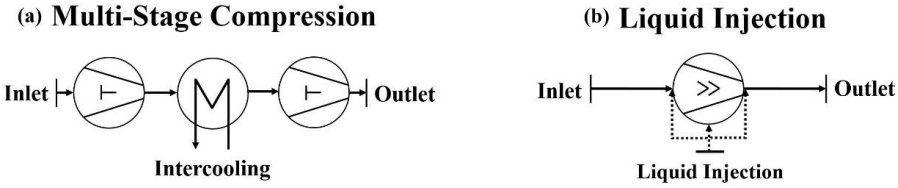

Figure 3.3. Potential compressor configurations: (a) multi-stage compression with intercooling through an additional IHX and (b) single-stage compression with liquid injection [Article I].

The first possible solution, as shown in Figure 4a, is to divide the compression into two or more stages with an additional IHX for cooling the vapor after each stage. Therefore, multi-stage compression with intercooling can increase the achievable pressure ratio. The functionality of this solution with two-stage reciprocating compressors and intercooler connected to the lean solution circuit has been experimentally proven by various authors [22,43,58,59]. Moreover, there are other approaches to the implementation of intercooling. Jensen (2015) [18] investigated the effect of the positioning of the intercooler (upstream or downstream of the

contained solution IHX between rich and lean solution) as well as other alternatives, such as the use of a bubble through intercooler or mixing option with liquid injection. It was concluded that the solution with an additional IHX downstream of the contained solution IHX can most effectively reduce the discharge temperature and costs for a multi-stage compression system.

Another promising solution, as shown in Figure 4b, is the use of a liquid-resistant single-stage compressor with the implementation of liquid injection (oil or oil-free using the working fluid) during the compression process. The injection can take place at various locations during the compression cycle and provides different functions, such as sealing, lubrication, and lowering the vapor temperature during compression [54]. The point of injection and amount of the injected liquid is a matter of optimization [57]. If all the liquid is carried along with the vapor, it is defined as wet compression [33]. Bergmann and Hivessy (1990) [34] stated that liquid injection makes the compressor operation smoother and more silent compared to dry compression. However, especially for the operation as wet compression the isentropic efficiencies obtained are often comparatively low due to the complexity of the compression process, causing various challenges in the design and optimization of the compressor and the injection system [60,61].

To solve the identified challenge of the compressor discharge temperature and enable the desired oil-free system operation, a single-stage compression with liquid injection is considered a feasible compressor configuration for the implementation in the experimental ACHP prototype. For the realization of the injection line, both the lean solution downstream of the solution pump or the rich solution upstream of the expansion valve can be utilized. The preliminary thermodynamic analysis suggests that both desorption of gaseous ammonia from the liquid phase and full evaporation are achievable during the compression process with liquid injection, irrespective of the subcooled state of the injected lean or rich solution. An investigation within the scope of Paper I has shown that there is a growing interest and supply of compressors for ammonia with pressures up to 60 bar and more. However, yet no commercially available compressor can entirely meet the specified requirements. Therefore, a numerical investigation of an oil-free liquid-injected twin-screw compressor using ammonia-water mixture was conducted to enhance the understanding of the thermodynamical behaviour during the compression process and to plan the design of the compressor section. A summary of the study conducted in Article III and the obtained key findings is presented below.

3.3.1 Numerical investigation of oil-free liquid-injected screw compressors (Article III)

A quasi-one-dimensional numerical model of an oil-free liquid-injected twin-screw compressor was developed using the object-orientated Modelica language. It was implemented and simulated in the Dymola 2020 simulation environment [62] and the commercial TIL-Suite 3.5 [63] and TILMedia 3.5 [64] libraries provided by *TLK-Thermo GmbH*. The model consists of multiple control volumes representing the respective rotor cavities and considers the effects of liquid injection, leakage flows and heat losses. Figure 3.4 illustrates the mass and energy flows associated with each control volume (CV) implemented in the compressor model.

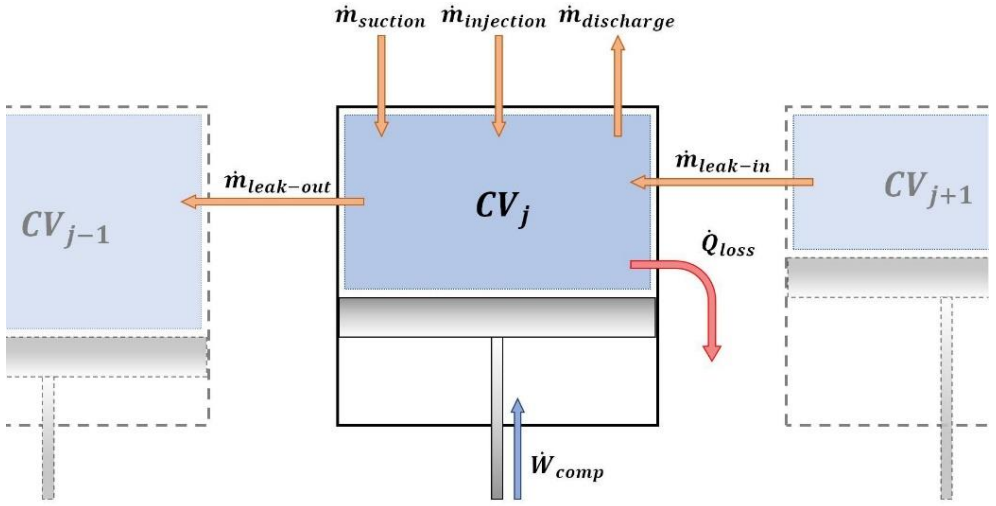

Figure 3.4. Mass and energy flows associated with each control volume [Paper IV].

Within the scope of the study, the effects of varying NH_3 mass fractions of the injected solution, injection amounts, injection positions and compressor speeds on different parameters of the compression process were investigated. To perform the simulations, boundary conditions for pressure, temperature and NH_3 mass fraction were defined based on the specified design parameters, and constant input values were set for the parameter of the investigated compressor. The defined boundary conditions are based on the expected operation conditions for the screw compressor in the experimental ACHP prototype. Figure 3.5 illustrates the simulation setup with the defined boundary conditions for the suction, injection, and discharge ports.

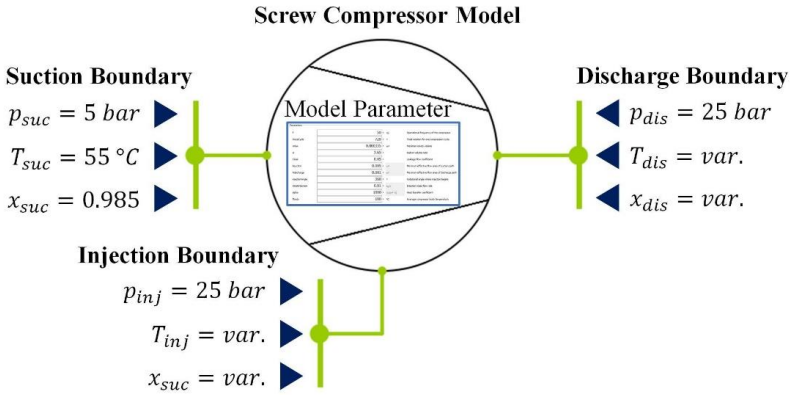

Figure 3.5. Simulation setup of the compressor model with defined boundary conditions [Article III].

The results revealed a strong influence of occurring internal leakages, varying NH_3 mass fractions of the injected solution and changing injection amounts and positions on the evolution of temperature, pressure, and compression power. A reduction in the ammonia content at constant injection mass flow rate reduced the values for discharge temperature, over-pressure and required compression power due to the higher specific heat capacity of the increased water content. Further, the presence and residence time of liquid in the rotor cavity (wet compression) to provide sufficient lubrication and sealing of the compressor were a function of the NH_3 mass fraction of the injected solution. The lowest and therefore best results of the investigated parameters were obtained with pure water, and it is therefore preferable to inject the lean solution in the ACHP system under the given conditions.

Increasing the injection amount led to a further reduction of the investigated parameter values and an extension of the occurring wet compression phase. If the injection amount becomes too large, negative effects such as under-compression and backflow from the discharge port with resulting pressure pulsation will occur. By positioning the injection port at the beginning of the compression phase at 360° and injecting an amount of about 10% of the compressor's suction mass flow rate, continuous wet compression was achieved. The split and distribution of the injection to several injection ports located at the beginning and in the middle of the compression phase (450° or 495°) supported the provision of a constant liquid film and reduced occurring under-compression and backflow. A reduction of the compressor speed from 62.5 Hz to 25 Hz with varying injection ratios in the range of 0%, 5% and 10% led to increased leakage flows, resulting in a drop of the volumetric efficiency from 0.97 to 0.88. As a result, an increased injection ratio is required to maintain constant values of the investigated parameters. Thus, it is necessary to adjust and optimize the injection amount to the respective operating conditions.

Due to existing limitations in the model caused by the simplified representation of leakage paths and other losses along with further unknown uncertainties, the results are considered as a kind of best-case analysis. Nevertheless, the performed study fulfils the purpose of providing information about the expected behaviour and preferable integration and design of the compressor section of the ACHP systems. The results for the lowest required injection amounts and the distribution of injection positions enable the development and design of the compressor and injection line for the experimental ACHP prototype.

3.3.2 Summary

The compressor section for the experimental ACHP prototype will be designed as an oil-free single-stage twin-screw compressor with the possibility of liquid injection. Since commercially available compressors were found to be unable to fulfil all the defined requirements, further modifications and experimental investigations are required. Based on the conducted research, the following conclusions for the design of the compressor section are drawn:

- Liquid injection with about 10% of the compressor's suction mass flow rate is required to lower the compressor discharge temperature and increase the efficiency of the compression process by sealing and lubricating the compressor.
- Lean solution with a comparatively low NH_3 mass fraction of about 0.4 should be injected, as the higher water content creates a greater cooling effect for identical injection amounts and reduces the required compression power more significantly.
- Splitting and distributing the injection over multiple ports located at the beginning (360°) and in the middle of the compression phase (450 or 495°) can improve the provision of a continuous liquid film, whereby a portion of the liquid must, in any case, be injected at the beginning of the compression phase.
- Injection amount and ratio must be adjusted and optimized depending on the operating conditions to enable an efficient performance with identical parameters by reducing occurring leakage flows.
- Lubrication and cooling of the bearings and compressor screws using the injected solution to achieve oil-free operation must be addressed and requires further investigations and possibly the use of improved components.

3.4 Design of the desorber and absorber with mixing sections

The desorber and absorber are critical components of ACHP systems to achieve higher system efficiencies and to obtain higher sink outlet temperatures [59,65]. For the use in ACHP systems with the zeotropic ammonia-water mixture as refrigerant, various requirements are defined for the properties of the heat exchanger used. In addition to the general requirements, such as the reduction of size and pressure losses, the suitability for the desired operating parameters must be considered [66]. To reduce installation costs, compact heat exchangers with a high area density (m^2/m^3) of the heat transfer surface combined with a high overall heat transfer coefficient ($kW/(m^2K)$) are desired [67,68]. Furthermore, the establishment of effective liquid-vapor mixing and the complete and continuous wetting of the heat transfer surfaces are important [69].

The plates can be pressed with different shapes to increase turbulence, fluid distribution and surface area [50]. Due to these features, the design can be much more compact. In addition, PHE can provide high overall heat transfer coefficients, good wettability and liquid-vapor mixing [65]. Various approaches have been and are being investigated to improve the design and operation of desorbers and absorbers [70]. In general, it was concluded that longer plates combined with good distribution of the mixture and operation in counter-flow with the coolant have positive effects on the performance. Jung et al. (2014) [65] stated that increasing the ratio of plate length to gap (L/D) is more important than the ratio of width to gap (W/D) for more effective operation.

Several possibilities are available for the implementation of the desorber and absorber. Due to the similarity of the operating conditions and requirements, the desorber is often designed and operated like a flooded evaporator. Thus, the solution enters at the bottom and flows upwards with the increasingly forming vapor phase during the ammonia desorption process. Táboas et al. (2010) [71] stated for a bubble desorber, that pressure has only a slight influence and mass flux a major influence. Experimental data from Nordtvedt (2005) [72] for PHE desorber were between 0.4 to 1.5 $kW/(m^2K)$.

The absorber can be operated in falling film mode, where lean solution slides from top to bottom as a thin film on the surface of the vertical plate and vapor filling the free space is absorbed into the liquid film, releasing heat to the coolant. Another approach is to operate the absorber in bubble mode, where the lean solution and vapor are mixed at the bottom before entering the absorber and flow upwards in counter-flow with the coolant [73]. Furthermore, it is possible to

operate several PHEs in line using different operating modes to increase the effective heat exchanger plate length and utilise the advantages of both the respective operation modes [59,74]. Figure 3.6 shows a schematic representation of a plate heat exchanger operated as absorber in falling film and bubble mode.

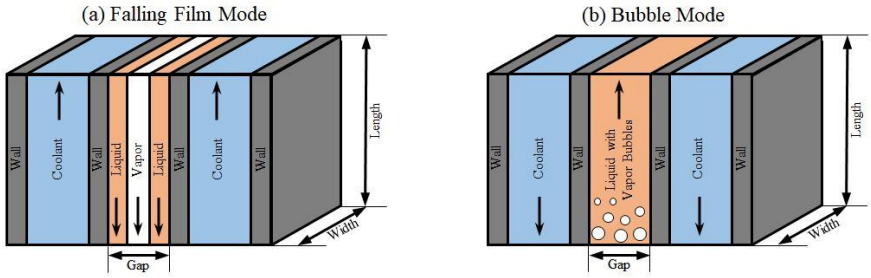

Figure 3.6. Schematic of PHE operated as absorber in (a) falling film and (b) bubble mode [Article I].

Bubble mode operation in the absorber of PHE in a ACHP cycle was investigated by An et al. (2013) [73]. Based on experiments with different sized PHE, they concluded that higher pressure is a more significant factor for increasing the heat exchanger performance than the size. The maximum overall heat transfer coefficients achieved for different PHE sizes were between 0.96 to 1.61 kW/m²K. In contrast, Lee et al. (2002) [75] reported values between 0.3 to 0.55 kW/(m²K) at lower temperatures in a PHE test facility. More experimental data from Nordtvedt (2005) [72] for bubble and falling film absorber were between 0.6 to 1.4 kW/(m²K). Due to many parameters affecting the absorption and desorption process, which are not all documented in these sources, a direct comparison or deducing trends becomes impossible. However, it can be concluded that the overall heat transfer coefficients can vary considerably depending on the given operation conditions and other factors such as the liquid-vapor distribution. Therefore, it is important to further examine the options and requirements for the design of the liquid-vapor mixing section upstream the absorber.

3.4.1 Liquid-vapor mixing section

The implementation of the liquid-vapor mixing, and the distribution process depends on the selected operating mode of the absorber. The overall objective is to provide a uniform distribution of the two phases with a minimum pressure drop for an effective absorption process to achieve high heat exchanger efficiencies and heat sink outlet temperatures. Baksaas and Grandum (1999) [22] investigated the design of the mixing section for an absorber in falling film mode. For this purpose, the lean solution was injected via a vertically aligned nozzle into

the ammonia vapor stream at some distance upstream of the absorber inlet. The aim was to achieve a homogeneous mixture and an adiabatic adjustment of the streams prior to the heat transfer in the absorber. However, the objective was not met as the results demonstrated that the liquid is collected at the bottom of the tube and irregularly floods the first channels when entering the absorber. By modifying the mixing section in the form of a parallel injection of the lean solution into the ammonia vapor stream directly at the absorber inlet, a more homogeneous distribution and improved heat exchanger efficiency were obtained [76].

When operating in bubble mode, the liquid-vapor mixture enters the absorber at the bottom. This eliminates the described problem of uneven liquid distribution in the first channels due to gravity. For the mixing section, the ammonia vapor can thus be injected into the lean solution stream using nozzles. The injection point for the mixing can be placed prior to the absorber inlet to achieve an alignment of the two phases. This can help to provide a homogenous liquid-vapor distribution for an effective absorption process at the inlet of the absorber, resulting in a reduction of the required effective heat exchanger plate length. The configuration of the mixing section, together with the use of equipment such as nozzles and the correct positioning prior to the absorber needs to be addressed and requires further research.

3.4.2 Summary

The desorber and absorber sections of the experimental ACHP prototype are designed as two in series connected PHE units. Since commercially available PHE units are restricted in the available plate length at high-pressure and temperature operation. The following conclusions for the design of the desorber and absorber, and the liquid-vapor mixing sections are drawn:

- The use of corrugated PHE is feasible for the design of the desorber and absorber.
- Sufficient liquid-vapor distribution is essential to achieve high heat exchanger efficiencies and improve the design since theoretical studies often use homogenous approaches.
- Longer heat exchanger plates are beneficial for achieving high heat transfer coefficients and sufficient liquid-vapor distribution (influence of the L/D ratio is greater than the W/D ratio).
- When operating at high pressure and temperature levels, PHE's effective heat transfer area can be further increased by connecting multiple heat exchanger units in series.
- The possibility and sufficient space to relocate the absorber inlet flow from bottom to top, together with different liquid-vapor mixing setups will be provided for experimental testing.

3.5 Solution pump section

Different commercially available pumps are used, mainly centrifugal pumps for industrial-scale installations and diaphragm pumps for smaller laboratory-scale facilities. Occurring cavitation is a major challenge for the selection and operation of the solution pump in ACHP systems. The saturated lean solution entering from the liquid-vapor separator is very sensitive to changing low-pressure conditions caused by rapid changes in the operational speed of the solution pump or the compressor.

To reduce the risk of cavitation, different approaches are available. In general, it is important to reduce occurring pressure losses in the pump intake line and smoothly change the pump and compressor's operational speed. The use of an upstream booster pump or a special design of the separator to provide enough static height of the liquid column for a pressure increase upstream of the solution pump was investigated by various researchers [43,65,76].

Furthermore, Risberg et al. (2004) [23] and Markmann et al. (2019) [76] introduced an option to keep the low-pressure level in the separator stable and reduce the risk of cavitation due to rapid pressure changes by controlling the liquid level in the high-pressure receiver by regulating the expansion valve.

The application of external subcooling of the lean solution, as used by Rane et al. (1989) [48], is another potential solution for additional cavitation protection in the experimental ACHP prototype with varying operating conditions. A straight tube-in-tube heat exchanger solution with sufficient diameter can minimise occurring pressure losses while providing the desired subcooling.

3.6 Summary

For the development and design of the experimental ACHP prototype, the ACHP cycle with single-stage solution circuit was investigated. The task description was defined to achieve the specified research objectives, including the identified challenges and demands for the use of ACHP system at high temperature operation. A simulation model was developed and used to design the ACHP system and specify the design parameter for the development of the experimental ACHP prototype. The main component sections were designed to meet the defined specifications while existing limitations for available components on the market and potential modifications were addressed. Figure 3.7 shows the 3D model of the experimental ACHP prototype with the highlighted component sections for the defined research focus areas.

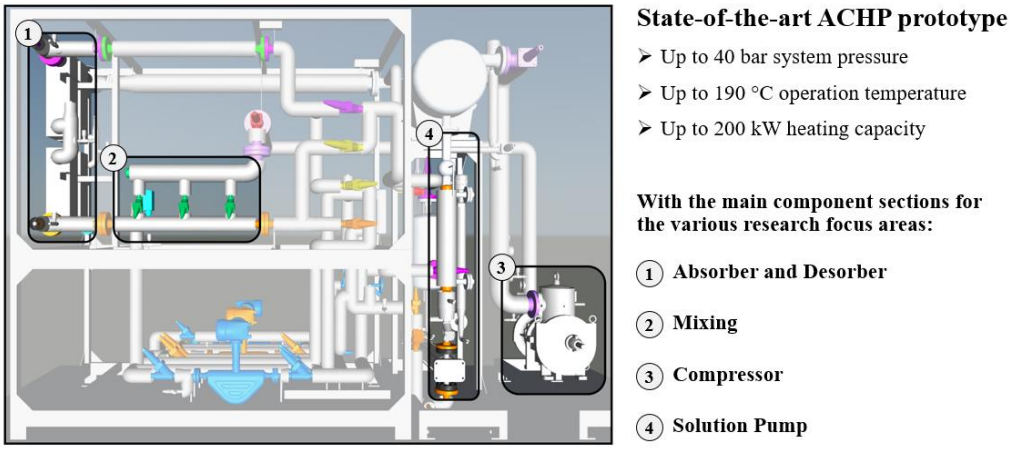

Figure 3.7. 3D model of the experimental ACHP protype with the defined research focus areas.

4 The Experimental ACHP Prototype

This chapter presents the experimental ACHP prototype named *"Osenbrück 4.0 Heat Pump"* as part of the HighEFFLab [16]. It is the result of the conducted doctoral research work and located in the NTNU laboratory in Trondheim. The overall objective was to further advance the ACHP technology for the use in high temperature applications through the development of an experimental research installation. The experimental ACHP prototype provides the possibility to experimentally elaborate novel solutions for existing challenges of the different component sections, verify numerical models, and validate achievable operation conditions for potential use cases in various industrial applications. The system is designed for a maximum operating pressure of 40 bar and an operational temperature range from -10 °C to 190 °C with a maximum heat capacity of up to 200 kW. All heat-carrying components are insulated with 30 mm thick rock wool to minimize thermal losses to the ambient. The installation site is constructed as a machinery room to guarantee the required safety standards when handling ammonia. Figure 4.1 shows the experimental ACHP prototype on-site in the NTNU laboratory.

Figure 4.1. Picture of the experimental ACHP prototype on-site in the NTNU laboratory.

In the following, the overall system design is introduced, focusing on the general functions and including component sections. The main components are described in detail with the functionality and design. The measuring system is presented, and the system charging with safety considerations is discussed. Finally, the control system and test procedure are presented.

4.1 System description

The complete test facility consists of the experimental ACHP prototype with heat source and sink circuits, referred to as the auxiliary system. Figure 4.2 shows the flow diagram of the experimental ACHP prototype with measuring points and highlighted component sections.

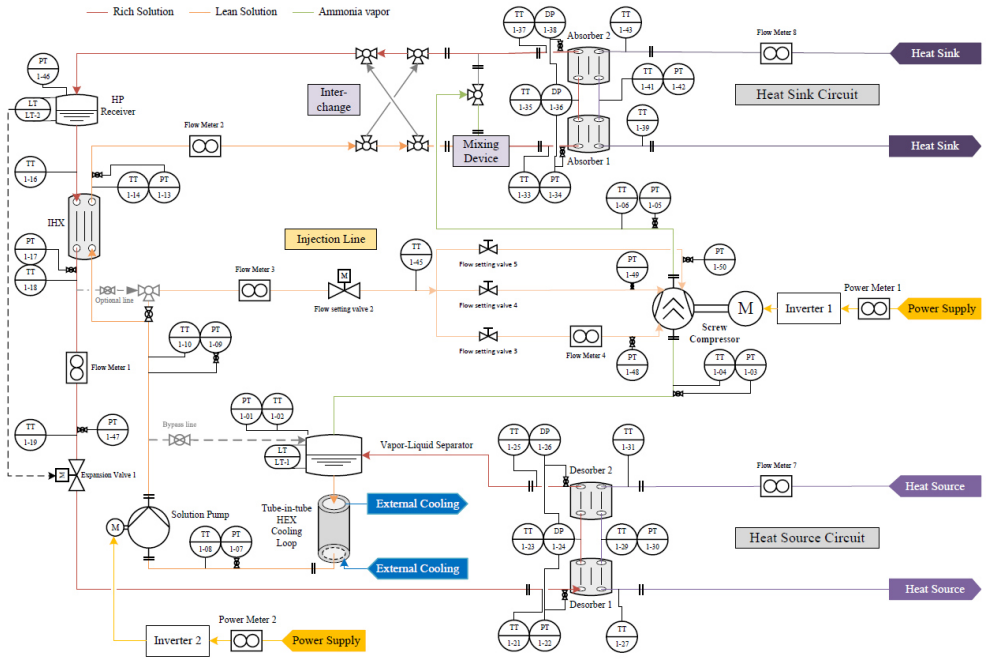

Figure 4.2. Flow diagram of the experimental ACHP prototype with measuring points.

The flow diagram and general arrangement of the main components of the experimental ACHP prototype are based on the basic ACHP cycle schematic presented and described in Figure 2.1. For the implementation of the research focus areas described in Chapter 3, the ACHP system was further extended, as indicated by the highlighted component sections. Starting from the liquid-vapor separator, a tube-in-tube heat exchanger is installed to sub-cool the lean solution with external cooling water. An injection line with the possibility to inject the lean or rich solution through different injection ports into the screw compressor used is implemented. For the investigation of the absorber with different operating modes, a flow interchange of the solution streams with sufficient space for the associated mixing section is provided. A variety of measuring instruments are installed at all main components to determine all required operating and performance parameters (pressure, temperature, mass flow rate, density) for the analysis and evaluation of experimental investigations. The detailed piping and instrumentation diagram (P&ID) of the experimental ACHP prototype is given in Appendix A.3.

4.2 Components

The functionality and design of the main components shown in Figure 4.2 are described below.

4.2.1 Liquid-vapor separator

The liquid-vapor separator receives the rich solution leaving the desorber in two-phase flow, and distributes the vapor phase to the compressor at the top and the lean liquid phase to the solution pump at the bottom. The separator volume is the main storage of the solution and serves as a buffer for reliable system operation during changing operating conditions. When designing the separator, it must be ensured that the volume is in proportion to the expected volume flows during system operation to ensure stable system performance with changing operating parameters. Since the mixture exists at vapor-liquid equilibrium (VLE), small drops in the prevailing pressure caused by increasing compressor speed will result in the desorption of ammonia from the liquid phase. This leads to vapor formation, which can cause the liquid flow to the solution pump to interrupt and/or cavitation to occur.

It is designed as a horizontal vessel connected with a long pipe at the bottom, serving as inlet of the solution pump. The volume for the liquid-vapor separator is 204 litres with a minimum liquid column of 1.6 m above the solution pump. To further ensure the safe operation of the solution pump in the intended test operations, the intake pipe is designed as tube-in-tube heat exchanger. Thus, external cooling can be applied to sub-cool the lean solution at the inlet of the solution pump. Figure 4.3 shows a schematic of the liquid-vapor separator with indicated flows.

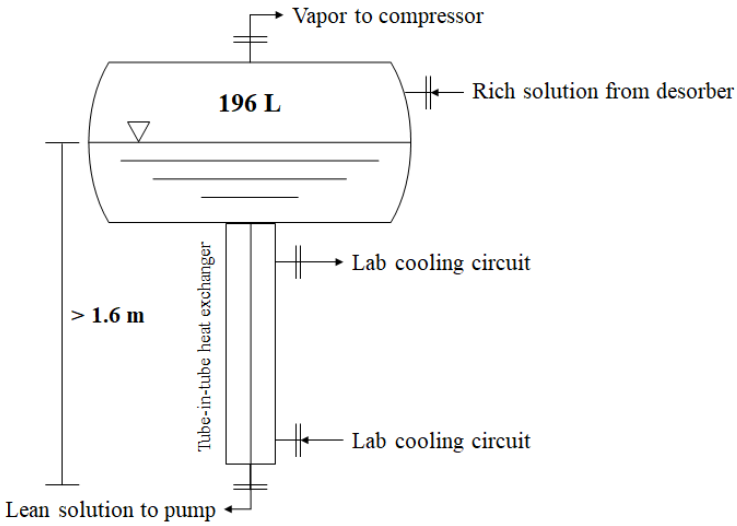

Figure 4.3. Schematic of the liquid-vapor separator with indicated flows.

The design maximizes the liquid column with minimal volume to increase the upstream pressure to the solution pump through static height and prevent the formation of vapor and cavitation at the inlet. The given cross-section of the horizontal vessel ensures a large surface area for the liquid phase to enable improved evaporation. Both measures can help to reduce the required volume and refrigerant charge.

4.2.2 Compressor with liquid injection line

The compressor is critical for achieving higher sink outlet temperatures and system efficiencies. An oil-free twin-screw compressor with the possibility of liquid injection was selected based on the performed numerical study in Section 3.3.1. Since there was no ready-to-use compressor option available on the market, the required modifications for the oil-free operation and liquid injection were made to an existing compressor, following the results of the numerical study. The aim is to reduce the occurring compressor discharge temperature by using liquid injection of the rich or lean solution of the ACHP system. The injected liquid provides lubrication and sealing to ensure oil-free system operation.

The compressor has an inbuilt volume ratio of 3.65 and is manufactured with three independent injection ports. The main injection port supplies all bearings with liquid and injects the liquid into the compression chamber at the beginning of the compression process. Two more injection ports are placed at the end of the compression phase, injecting in the male and female rotor cavities. The total injection flow rate and distribution and operation of the different injection ports can be regulated via flow setting valves during operation. Pressure, temperature, and mass flow rates are measured. Figure 4.4 shows the schematic of the compressor section with liquid injection line and connected injection ports.

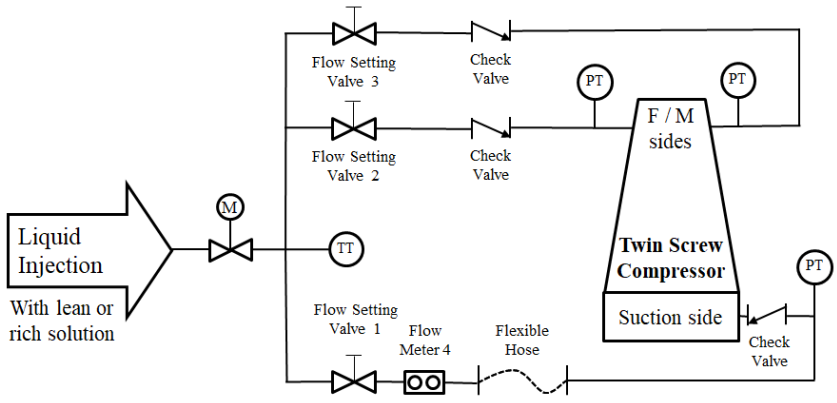

Figure 4.4. Schematic of the compressor section with liquid injection line.

4.2.3 Solution pump

The solution pump delivers the liquid phase from the bottom of the liquid-vapor separator to the high-pressure side of the test facility. For this, a relatively small and, depending on the operating point, changing volume flow must be handled at the maximum possible pressure ratio to compensate for pressure losses occurring in the IHX and mixing section upstream of the absorber. This ability and corrosion resistance to the ammonia-water mixture are important factors when selecting a suitable solution pump.

The selected solution pump is a multistage, in-line centrifugal pump of type *CRN 3-31 S-FGJ-T-E-HQQE* special model with a controlled motor supplied by *Grundfos*. The solution pump is equipped with 31 impeller stages and can deliver volume flows from 0 to 4.5 m³/h with a maximum achievable pump head of up to 200 m. The maximum operating pressure is 50 bar with a maximum solution temperature of 120 °C. For variable regulation of the volume flow, the solution pump is equipped and operated by a frequency converter of type *FC202 – 3 kW* from *Danfoss A/S*.

4.2.4 Absorber and mixing section

The absorber and mixing section consists of three parts: flow interchange, mixing section, and two in-series connected absorber PHE units. It is designed to investigate different heat exchanger units and operation modes and the corresponding liquid-vapor distribution. Figure 4.5 shows the schematic installation of the complete absorber and mixing section

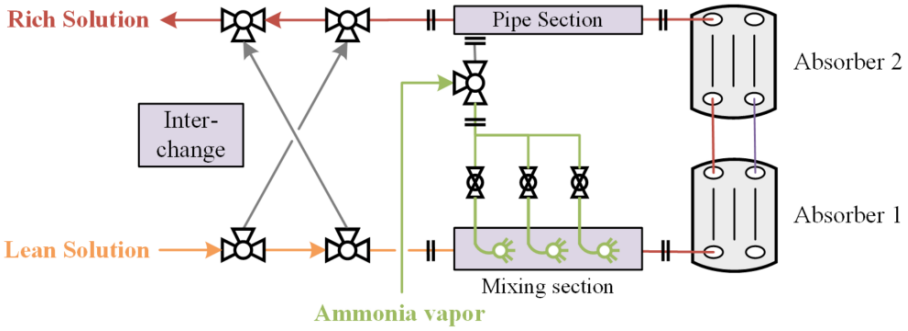

Figure 4.5. Schematic of the absorber and mixing section.

The flow interchange allows for switching the direction of the rich and lean solution streams to operate the absorber in falling film and bubble mode. To provide the desired bubble mode operation, the mixing section is placed upstream of the absorber section and connected to the inlet at the bottom of the lower absorber unit. The mixing section consists of three individual

mixing ports (nozzles) to spray and distribute the vapor in the lean solution stream. The mixing ports are equally distributed with a spacing of 0.215 m, with a distance from 0.94 m to 1.37 m from the mixing points' centre to the absorber inlet.

To ensure efficient liquid-vapor distribution over the entire heat transfer area and thus achieve high effective heat transfer rates, an increased ratio of plate length to the gap distance (L/D) is advantageous for the design of the absorber section. The absorber section is equipped with two vertically aligned and in-series connected nickel-brazed PHE units of type *AlfaNova XP52-40H*, supplied by *Alfa Laval AS*. The PHE units are made of stainless steel with a maximum pressure of 58 bar and an operating temperature of up to 225 °C. Therefore, the available overall length is technically limited, and it is required to split the section into two units to increase the overall plate length. Each PHE unit is designed with 40 corrugated plates with a high corrugation angle and a total heat transfer area of 2.22 m², resulting in 19 channels with a total volume of 1.81 litres for the refrigerant side and 20 channels with a total volume of 1.90 litres for the secondary fluid. Table 4.1 summarizes the plate characteristics of the different PHE units used.

Table 4.1. Plate characteristics of the different PHE units used.

Parameter	Absorber	Desorber	IHX
Number of plates [-]	40	40	20
Total heat transfer area [m²]	2.22	2.22	0.61
Overall length [m]	0.53	0.53	0.31
Overall width [m]	0.11	0.11	0.11
Gap distance [mm]	2.48	2.48	2.42
Aspect ratio L/D [-]	213.7	213.7	128.1
Aspect ratio W/D [-]	44.4	44.4	45.5

4.2.5 High-pressure receiver

The high-pressure receiver is a vertically oriented cylindrical vessel with a volume of 18 litres. It is placed downstream of the absorber and upstream of the IHX. The solution enters through the inlet port at the top and leaves the receiver through the outlet port with extraction from the bottom. The purpose of the high-pressure receiver is to ensure that the strong solution enters the IHX in liquid phase to maintain a high heat transfer rate. Further, rich solution is stored in

the high-pressure receiver to alter the system parameters. The variation of the liquid level can be used to control and adjust the operating conditions of the ACHP system.

4.2.6 Internal heat exchanger

The internal heat exchanger is operated in counter-flow and increases the efficiency of the ACHP system by further cooling the rich solution and simultaneously heating the lean solution prior to the mixing process. The rich solution's temperature reduction increases the heat source's possible heat intake. Heating the lean solution reduces the temperature difference with the superheated ammonia vapor and accelerates the equalization and absorption processes.

The IHX used is a nickel-brazed PHE of type *AlfaNova XP27-20H*, supplied by *Alfa Laval AS*. It is made of stainless steel with a maximum pressure of 54 bar and an operating temperature of up to 225 °C. The PHE unit is designed with 20 corrugated plates with a high corrugation angle and a total heat transfer area of 0.61 m², resulting in 9 channels with a total volume of 0.45 litres for the rich solution side and 10 channels with a total volume of 0.5 litres for the lean solution side. Table 4.1 summarizes the plate characteristics of the PHE unit used for the IHX.

4.2.7 Expansion valve

The expansion valve downstream of the IHX ensures an almost isenthalpic reduction of the pressure with the associated decrease in temperature of the rich solution before entering the desorber. The opening degree of the expansion valve is used for controlling the high-pressure level, and thus a linear operating characteristic is preferable. The *ICM 20A* model is used as expansion valve together with the associated *ICAD 600A* actuator, both supplied by *Danfoss A/S*. The digital actuator enables precise adjustment of the opening degree and thus control of the high-pressure level.

4.2.8 Desorber

The desorber is connected in counterflow with the heat source on the secondary side and transfers the heat into the ACHP system. Due to the previously expansion, the rich solution exists in the two-phase region and enters the desorber with small vapor mass fraction. The heat intake results in further desorption of the ammonia from the liquid phase. To minimize occurring flow barriers due to the increasing vapor phase, the PHE units are arranged vertically, and the solution enters at the bottom and is directed to the top. An increased gap distance can additionally be beneficial for this purpose.

The desorber section is equipped with two vertically aligned and in series connected nickel-brazed PHE units of type *AlfaNova X52-40L*, supplied by *Alfa Laval AS*. The PHE units are made of stainless steel with a maximum pressure of 58 bar and an operating temperature of up to 225 °C. Each PHE unit is designed with 40 corrugated plates with a low corrugation angle and a total heat transfer area of 2.22 m², resulting in 19 channels with a total volume of 1.81 litres for the refrigerant side and 20 channels with a total volume of 1.90 litres for the secondary fluid. Table 4.1 summarizes the plate characteristics of the desorber PHE units used.

4.2.9 Auxiliary system

The auxiliary system is a pressurised water system and serves as heat source and sink circuits for the experimental ACHP prototype and is connected via the respective absorber and desorber heat exchanger sections, as indicated in Figure 4.2. It is designed to provide independently adjustable inlet temperatures and volume flow rates for the heat source and sink circuits. Most of the energy is transferred and reused internally. Surplus heat can be released to the laboratory's cooling system via an additional heat exchanger and a temperature-controlled flow regulating valve. Figure 4.6 shows the flow diagram of the auxiliary system with connections.

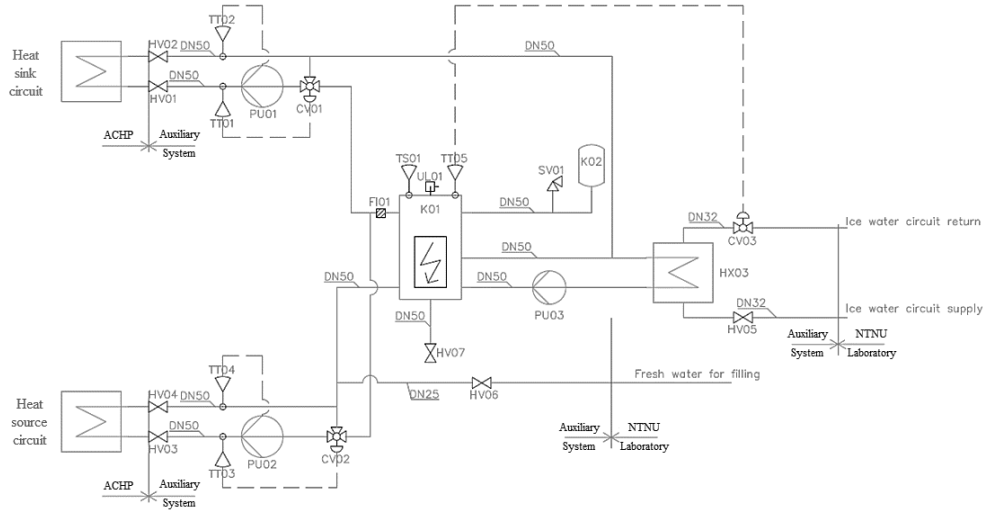

Figure 4.6. Flow diagram of the auxiliary system with heat source and sink circuits and connections.

The auxiliary system consists of a single buffer tank (K01) with a volume of 200 litres and electrical heater, and an expansion tank (K02) with a volume of 50 litres. It is designed to operate in a temperature range from 0 °C up to 140 °C with a maximum system pressure of 10 bar (PN10) and can handle a heat capacity of up to 200 kW at the heat sink side. The heat

source and sink circuits are equipped with regulated three-way valves (CV01 and CV02) and variable speed circulation pumps (PU01 and PU02) with a specific flow rate of 1.2 l/s and a maximum delivery head of 30 m.

4.3 Measuring system

For the measurement of all relevant process parameters, a variety of measuring instruments are installed in the entire ACHP system and the auxiliary system, as indicated in Figure 4.2.

4.3.1 Instrumentation

Table 4.2 lists the measuring instruments used with measuring parameters, range, and accuracy.

Table 4.2. Range and accuracy of the measuring instruments connected to the test facility.

Instrument	Parameter	Range	Accuracy
PT100 RTD - 1/3 DIN	Temperature	0-200 °C	± (0.15+0.002·T) [°C]
Absolute pressure transmitter	Pressure	0-40 bar	± 0.1% FS
		0-40 bar	± 0.25% FS
		0-16 bar	± 0.1% FS
		0-16 bar	± 0.25% FS
		0-10 bar	± 0.25% FS
Differential pressure transmitter	Pressure	0-3 bar	± 0.05% FS
Coriolis flow meter – NH_3-H_20 streams	Mass flow	4.5-95 kg/min	± 0.1% FS
	Density	100-3000 kg/m³	± 1 kg/m³
Coriolis flow meter – Liquid injection	Mass flow	0.2-4 kg/min	± 0.2% FS
	Density	500-1400 kg/m³	± 0.01 kg/litre
Coriolis flow meter – Aux. system	Mass flow	5-100 kg/min	± 0.2% FS
	Density	500-1400 kg/m³	± 0.01 kg/litre
Frequency converter VLT FC202	Power	0-110 kW	± 1.0% FS
	Power	0-3 kW	± 1.0% FS

All temperature measuring points are equipped with PT100 resistance temperature detectors (RTD) with a defined measuring range between 0 °C and 200 °C and 1/3 DIN accuracy. The sensors are mounted in stainless steel thermowells with a small diameter and are aligned against the flow direction of the measuring medium. The sensors are connected to the data acquisition system (DAQ) with shielded 4-wire cables. The measurement chain for selected measuring points was calibrated on site against an *AMETEK RTC-157 reference temperature calibrator* in the range from -10 °C to 110 °C, achieving an accuracy of 0.1 °C and stability of 0.01 °C.

The pressure measuring points are equipped with absolute pressure transmitters with an accuracy of 0.25% of full scale (FS) and two different measuring ranges for the low-pressure side (up to 16 bar) and the high-pressure side (up to 40 bar). The entire measurement chain of a low-pressure transmitter was calibrated on-site against a *FLUKE 719 Pro electric pressure calibrator* in the range from 0.5 bar to 7 bar, achieving an accuracy of 0.005 bar. A transmitter with a higher accuracy of 0.1% FS is installed at the inlet of the desorber and absorber on the refrigerant side. This increases the accuracy of the entire measuring chain across all heat exchanger sections with the two interconnected differential pressure transmitters with a variable measuring range of up to 3 bar and an accuracy of 0.05% FS.

Coriolis flow meters determine the mass flows and densities of all liquid streams in the ACHP and auxiliary system. The models and measuring ranges differ with respect to the calculated mass flows of the respective measuring streams. The accuracies are based on the manufacturer's specifications for the models selected.

The consumed power is determined with an accuracy of 1.0% FS using the frequency converters for the compressor (110 kW) and the solution pump (3 kW).

4.3.2 DAQ and data handling

The DAQ acquires and processes the analogue measurement signals of all installed measuring instruments and is based on *National Instrument* components with *LabVIEW* software. It consists of a *NI cRIO-9045* controller in conjunction with various modules for the specific measuring instruments. The system stores 5 readings per second for each measuring point. After reaching steady-state conditions, the readings will be logged and stored over a period of at least five minutes. The logged values are then averaged and serve as the basis for further calculations of the performance parameters of the system. A detailed overview of the P&ID view implemented in *LabVIEW,* including all measuring and control points, is given in Figure A.5 in the Appendix.

4.4 System charging and safety considerations

During the initial commissioning, the experimental ACHP prototype is charged with an ammonia mass fraction of 0.45. For a total system charge of 55 kg, an ammonia mass of 25 kg and a water mass of 30 kg are specified. Prior to the filling process, the system is vacuumed to remove the remaining nitrogen from the leakage and pressure testing of the system. In the first step, distilled or demineralized water is added to the liquid-vapor separator. The system is vacuumed again to remove the oxygen contained in the water. After that, ammonia is slowly added to the liquid-vapor separator, dissolving the ammonia in the water. As a result, the system pressure increases until reaching its stagnation pressure.

The use of ammonia requires the consideration and implementation of safety measures, which are specified in the *NS-EN 378 1-4:2006* standards. Ammonia is toxic and dangerous to health in increased quantities. At the same time, it is flammable above specific saturation volumes and requires special attention. This includes a warning system for different concentration levels in the air and a ventilation system connected to the ambient or a scrubber to reduce the ammonia content. For safe operation during experiments, the experimental ACHP prototype is placed in a location designed as a machinery room. The room is equipped with NH_3 sensors, ATEX-protected electrical installations, and an emergency ventilation system. The room access is protected, and only trained personnel is allowed to enter and work on the ammonia-containing equipment. Personal protection measures are located inside the room and at a close distance around. The control and monitoring of the test facility during experiments are performed from the remote-control station located outside the room.

4.5 Control system

The remote-control system operates the compressor, the solution pump, the expansion valve, the injection line valve, and the heat source and sink circulation pumps (computer/DAQ). Manual valves installed in the three individual liquid injection lines are used to achieve additional flow rate adjustments for the compressor injection. The heat source and sink inlet temperatures are set and controlled by three-way valves connected to the buffer tank, and the respective circuit return flows. PID controllers regulate the opening degrees to control the inlet temperatures. The temperature of the buffer tank is set and controlled by the electric heater with PID controller. Surplus heat is released to the laboratory cooling circuit via the additional heat exchanger and the temperature-regulated flow setting valve. Before starting an experiment, the system must be prepared by opening and closing the required manual shut-off valves to set the desired stream flow directions.

4.5.1 Test procedure

(1) After powering all system parts, the circulation pumps in the heat source and sink circuits are turned on.

(2) The buffer tank, heat source and sink inlet temperatures are set and the system heats up.

(3) The expansion valve is set to fully open.

(4) The solution pump is started to pump the solution and heat the system.

(5) The compressor is started and ramped up to 30% speed. The main injection valve is opened to provide liquid injection towards the bearings for lubrication and cooling.

(6) When the desorber pressure is stable, the expansion valve is gradually closed until the required absorber pressure for complete absorption is achieved.

(7) The solution pump and compressor speed are then adjusted to the desired capacity and operating point. The liquid injection flow rates towards the different compressor injection ports are adjusted accordingly via the use of the installed flow setting valves.

(8) The mass flow rates of the heat source and sink circuits are set to the specified values.

(9) The heat pump is operated until steady-state conditions are obtained.

(10) All measuring points are logged in the DAQ for the duration of the experiment.

5 Summary of Research Work

This chapter provides a summary of the research work conducted in accordance with the research objectives of this thesis. The published articles contribute to the achievement of the defined sub-objectives of the doctoral work. Article I review the state-of-the-art with existing challenges and future trends for the utilization of ACHP systems. Article II presents operational data to provide an overview of the current use and potential future demand of ACHP systems in industrial high-temperature heat pump applications. Article III addresses the numerical investigation of an oil-free liquid-injected screw compressor to overcome existing limitations due to high compressor discharge temperatures and to develop novel oil-free solutions for the design of the compressor section. The development process of the experimental ACHP prototype was further supported by several peer-reviewed conference papers published on various related topics. The experimental ACHP prototype, as described in Chapter 4, is the cumulative result of all these studies. The sequential order of the conducted research work in combination with the respective scientific publications is illustrated in Figure 5.1.

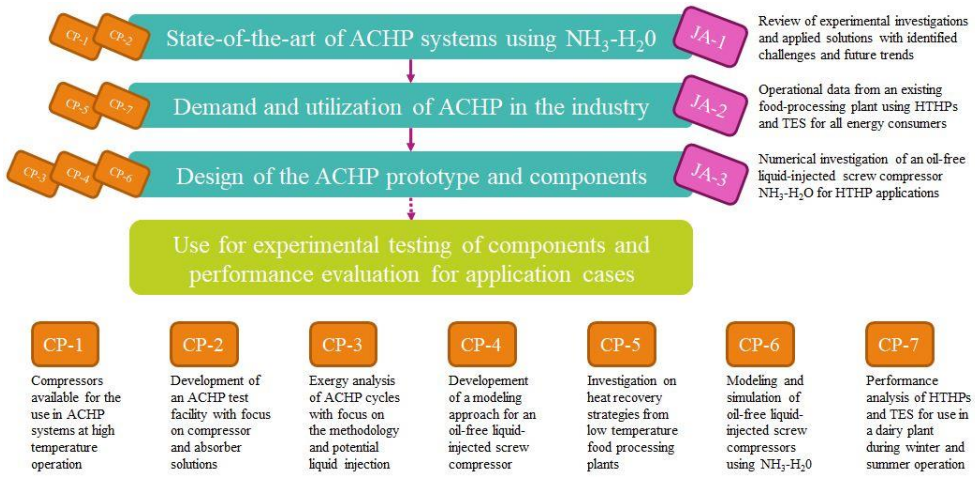

Figure 5.1. Sequential order of the conducted research work.

The following summary of the published research work is intended to briefly describe the main research topics and highlight the key contributions of each journal article. More information and discussions on the results and findings of the conducted research work can be found in the attached publications in Appendix B.

5.1 Article I – Identification of existing challenges and future trends for the utilization of ammonia-water absorption-compression heat pumps at high temperature operation

This article investigates existing challenges and future trends for the utilization of ACHP systems with ammonia-water mixture as refrigerant at high temperature operation. The working principle and advantages of the basic ACHP cycle and experimentally investigated cycle configurations were presented. An overview of the current state-of-the-technology was elaborated based on experimental investigations described in the literature.

In this context, 23 references were evaluated with capacities ranging from 1.4 kW to 4500 kW, heat sink outlet temperatures between 45 °C to 115 °C and achieved COPs from 1.4 to 11.3. Existing challenges for the realization of ACHP systems with focus on the application at high temperature operation were identified. These challenges include the compressor concerning the discharge temperature and lubrication, the absorber and desorber design and operation, the establishment of efficient liquid-vapor mixing and distribution, and the selection and cavitation protection of the solution pump.

To address these challenges, recent developments and promising solutions for the different component sections were highlighted and summarized in a mind map. Furthermore, possible trends for future studies were identified and discussed. The purpose of this study was to serve as a starting point for further research by linking theoretical approaches, possible solutions and experimental results as a source for further developments in the utilization of ammonia-water ACHP systems at high temperature operation.

This article includes and extends the content and results from the published conference Paper I and Paper II. The results and findings obtained from this research serve as the background for the doctoral thesis and form the basis for the development and design of the experimental ACHP prototype and the presented component solutions.

5.2 Article II – Integrated HTHPs and thermal storage tanks for combined heating and cooling in the industry

This article investigates the integrated energy system of a newly built dairy in Bergen, Norway. The aim was to determine the energy consumption and system performance to demonstrate the feasibility of such energy systems and improve the acceptability for further applications among potential users. The dairy features a novel and innovative energy system consisting of heat pumps using exclusively natural refrigerants to supply all cooling and heating demands.

A combination of three ammonia chillers (2400 kW_{th}, -1.5 °C/40 °C) for the cooling demands, two ammonia heat pumps (1577 kW_{th}, 20 °C/67 °C) for heat recovery and supply of building heat, and one ACHP (Hybrid heat pump) (940 kW_{th}, 60 °C/95 °C) to provide the highest supply temperature are implemented. Thermal energy storage tanks are provided for each temperature level to supply the respective energy consumers, as shown in Figure 5.2.

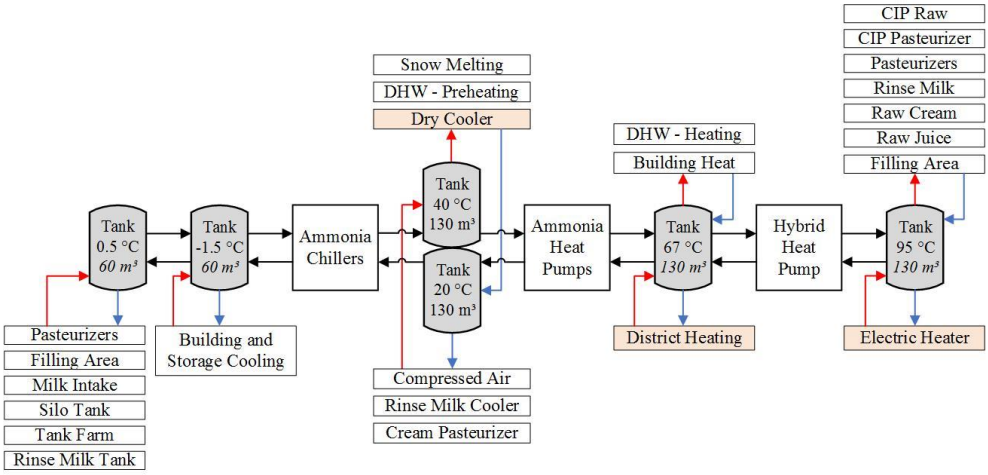

Figure 5.2. Integrated energy supply system of the investigated dairy.

The thermal energy storage tanks link the heat pump systems and help to balance fluctuations in demand and enhance operational stability. The additionally installed auxiliary systems, namely the dry cooler, district heating and electric heater, can be used if required. The energy consumption and system performance analysis are based on available process data for a comparable energy-intensive winter week in February, with an increased demand for building heating.

The results demonstrated that the integrated energy system is capable to efficiently meet the demands with minimal need for the auxiliary systems. Demand peaks were compensated, and an overall system COP of 4.1 was achieved, with Carnot efficiencies ranging from 53% to 65% for the installed heat pump systems. The process achieved a waste heat recovery rate of over 95%, which accounts for 32.7% of the total energy used. As a result, energy consumption was reduced by 37.9% and GHG emissions by up to 91.7% compared to conventional dairy systems.

Paper VII extends the analysis with an additional summer week in June to provide a wider perspective in the annual operation with varying conditions. Here, the demand for building heat is significantly reduced under otherwise similar process conditions. Excess heat is released via the dry coolers due to the reduced heat demand. The dry coolers are used to release the surplus heat in this case. The installed heat pump systems and the overall process achieve almost identical performance values. This demonstrates that the integrated energy system can be used efficiently for changing environmental conditions.

The results and findings from this research work describe the potential usage of ACHP systems in industrial applications at high temperature operation.

5.3 Article III – Numerical investigation of an oil-free liquid-injected screw compressor with ammonia-water as refrigerant for high temperature heat pump applications

This study investigates a numerical model of an oil-free twin screw compressor with ammonia-water mixture as refrigerant and liquid injection. The compressor was identified as main constraint to increase the heat sink supply temperature of absorption-compression heat pump systems past 120 °C. The implementation of liquid injection can reduce the occurring superheat of the vapor during compression, while an existing liquid film can provide lubrication and sealing, enabling oil-free operation of the compressor and thus the entire ACHP system. A quasi-one-dimensional numerical model was developed using the Modelica language. The developed screw compressor model consists of moving control volumes containing the working fluid in liquid vapor equilibrium and performing the compression process without mechanical losses. It considers the effects of leakages, heat losses, and the variation in NH_3 mass fractions.

Within the scope of this study, the effects of varying NH_3 mass fractions of the injected solution, injection amounts, injection positions and compressor speeds on different parameters of the compression process were investigated. To perform the simulations, boundary conditions for pressure, temperature and NH_3 mass fraction were defined based on the specified design parameters, and constant input values were set for the parameter of the investigated compressor.

The results of this study revealed a strong influence of occurring internal leakages, varying NH_3 mass fractions of the injected solution, and changing injection flows and positions on the evolution of temperature, pressure, and compression power. The injection with reduced NH_3 mass fraction was beneficial for the reduction of the investigated values for discharge temperature, discharge pressure and compression power. The lowest values were obtained for the injection with pure water. An increased discharge temperature is generally beneficial for high temperature heat pump applications. However, it is limited by the material properties of the compressor. Thus, it was concluded that the injection of the lean solution should be preferred for the application in the ACHP system.

Increased injection flow rates led to a further reduction in the investigated compression parameters. With the injection of 0.01 kg/s (about 5% of the compressor's suction mass flow rate) of lean solution, the temperature was sufficiently reduced, and the pressure evolution was adapted to the externally applied pressure ratio. Thereby, under-compression and backflow from the discharge end were minimized. This is important for the efficient and sustainable

operation of the compressor. Figure 5.3 shows an example of the temperature evolution in relation to the injection angle.

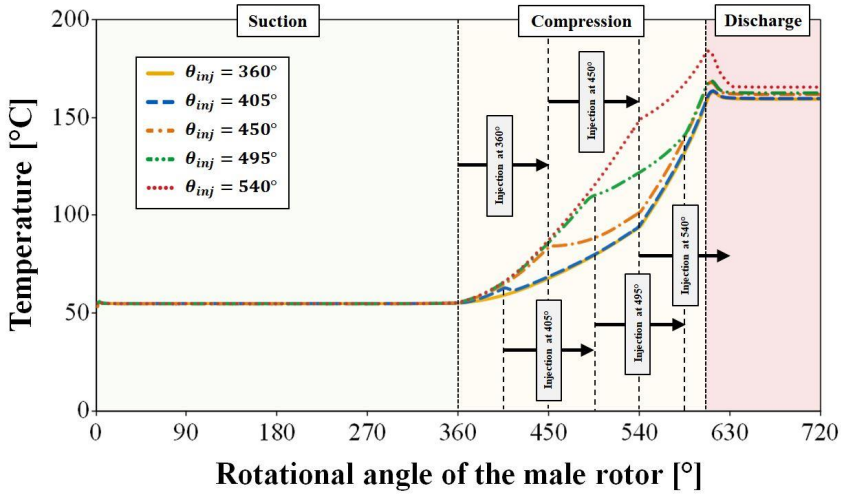

Figure 5.3. Example of the temperature evolution for different injection angles (θ_{inj}) with a constant NH_3 mass fraction of 0.4, a leakage coefficient of 0.05 m^{-1} and an injection mass flow of 0.01 kg/s.

When injecting through a single injection port, full wet compression was only observed when injecting at 360° (at the beginning of the compression phase) but was not achieved continuously throughout the entire compression phase with the given injection rate of 5%. Thus, the injection rate must be increased to about 10% of the compressor's suction mass flow rate (0.02 kg/s) to ensure a continuous liquid film that provides sufficient lubrication and sealing. Thereby, the placement of one injection port at 360° is important for ensuring a continuous liquid film.

The distributing of liquid injection via two injection ports, one at 360° and an additional port in the mid-compression phase (450° or 495°, respectively), was investigated. Here, the smaller portion of approx. 25% was at the beginning of the compression phase (360°), and the remaining portion (approx. 75%) was injected via the port in the mid-compression phase. With this measure, the continuous provision of full wet compression can be supported and occurring under-compression and backflow can be reduced. Changes in the compressor speed will affect the compressor's volumetric efficiency, and the injection rate and ratio must be adjusted.

This article includes and extends the content and results from the published conference Paper IV and Paper VI. The results and findings obtained from this research were used to determine possible modifications to an existing screw compressor and serve as basis for the development and design of the compressor section with injection line for the experimental ACHP prototype.

6 Conclusions

This thesis has successfully completed the aim of the development of an ammonia-water absorption-compression heat pump at high temperature operation. To accomplish this aim, investigations were conducted on various research topics in accordance with the defined research objectives. The results were disseminated in the context of three published journal articles, several peer-reviewed conference papers, and other presentations. The cumulative result is the experimental ACHP prototype with a maximum heat capacity of up to 200 kW and a maximum operating pressure and temperature of up to 40 bar and 190 °C, respectively. Together with the pressurized water heat source and sink circuits, the developed test facility allows for variable investigations of different component solutions and varying application cases with heat sink outlet temperatures up to 140 °C.

The current state-of-the-art was presented and the existing challenges were identified.

The working principle and characteristics of different ACHP cycles were discussed. An overview of the current state-of-the-art was elaborated based on experimental investigations available in the literature. In this context, 23 references were evaluated with heat capacities ranging from 1.4 kW to 4500 kW, heat sink outlet temperatures between 45 °C to 115 °C and achieved COPs from 1.4 to 11.3. The existing solutions and challenges for the realization of ACHP systems with a focus on the application at high temperature operation were identified: the compressor design with respect to discharge temperature and lubrication; the design and operation of the absorber and desorber; the establishment of efficient liquid-vapor mixing and distribution, and the selection and cavitation protection of the solution pump.

The possible use and further demand for ACHP in industrial applications were addressed.

The integrated energy system of an existing dairy plant was investigated, which uses heat pumps to supply all energy consumers at multiple temperature levels. The ACHP system supplied a temperature of 95 °C and a temperature lift of 33.5 K. An average COP of 5.8 was achieved with a Carnot efficiency of more than 50%. The results demonstrated that ACHP systems are reliable and efficient in commercial high temperature applications up to 100 °C. Further theoretical studies on the potential use of the ACHP system for heat recovery in industrial food processes revealed that GHG emission reductions of up to 35% are achievable even in locations with comparatively low CO_2 equivalent of the energy sources used, such as electricity in Norway.

Furthermore, there is a great demand for higher supply temperatures required in many processes with existing steam systems or general demand for higher process temperatures. The potential application area can be further expanded by increasing the achievable heat sink supply temperatures above 120 °C. The oil-free operation of the ACHP system can lead to improved efficiency and reduced costs by saving on the required oil infrastructure. This can further improve the competitiveness of ACHP systems for usage in industrial high temperature applications compared to conventional energy supply systems.

A numerical system model was developed and used in EES to investigate the ACHP cycle.

Based on the identified challenges and demands, the task description of the experimental ACHP prototype was specified, and a simulation model of the ACHP cycle with single-stage solution circuit was developed in EES. This model was used to investigate the system behaviour of the ACHP system and to determine the design parameters of the experimental ACHP prototype. The energy and exergy analysis revealed that the use of liquid injection during the vapor compression process is a valid approach for the design of the ACHP system. The determined design parameters were the basis for the design of applicable and feasible component solutions.

Component solutions for the design of the experimental ACHP prototype were developed.

The main component sections for the defined research focus areas were designed to meet the specifications, considering existing limitations for available components on the market and their potential for modifications. A numerical simulation model of an oil-free liquid-injected twin-screw compressor was developed and used to reduce the limiting compressor discharge temperature and achieve the desired oil-free system operation.

The investigation revealed that it is preferable to inject the lean solution with a low NH_3 mass fraction of about 0.4, and an injection ratio of 10% of the compressor's suction mass flow rate is required. The distribution of the lean solution over multiple injection ports located at the beginning (360°) and in the middle of the compression phase (450° or 495°) can ensure a continuous liquid film for sealing, lubrication and decreasing of the discharge temperature. Thereby, a portion of the liquid must be injected at the beginning of the compression phase, and the total amount must be adjusted for varying operating conditions. The obtained findings were used to determine modifications to an existing compressor and to design the required injection line. Due to the existing limitations and simplified assumptions in the model, the simulation results are considered as a kind of best-case analysis, and the experimental testing and validation for the further improvement are planned and required.

The use of PHE was identified as an appropriate solution for the design of the desorber and absorber sections of the experimental ACHP prototype. The optimal operating mode and design improvements will be the subject of further investigations. For this purpose, the possibility and sufficient space were provided to change the flow direction to the absorber inlet from the bottom to the top, along with different liquid-vapor mixing arrangements for the experimental testing.

The selected solution pump is a multi-stage, in-line circulation pump placed at a low point below the liquid-vapor separator and connected with minimal possible pressure losses in the pipe. To further ensure the safe operation of the solution pump in the intended test operations, the intake pipe is designed as a tube-in-tube heat exchanger. Thus, external cooling can be applied to sub-cool the lean solution at the inlet of the solution pump.

Design and functions of the experimental ACHP prototype were presented and described.

The experimental ACHP prototype was developed with the overall objective to further advance the ACHP technology for the use in a wide range of industrial high temperature applications. For this, the defined research focus areas were equipped with the presented solutions for the main component sections. The heat source and sink circuits were designed to experimentally investigate the ACHP system and specific component sections for varying operating conditions. A variety of measuring instruments were installed at all main components to determine all required operating and performance parameters for the analysis and evaluation of the experimental investigations. For the commissioning of the system, the charging process and safety considerations for handling NH_3 were presented. The control system and test procedure were developed and described to ensure the safe operation of the experimental ACHP prototype during the performance of experimental investigations.

The results of the conducted research work serve as a basis for a variety of possible further investigations, which involve the testing and evaluation of the implemented component solutions and the development of novel approaches.

7 Suggestions for Future Work

The ammonia-water absorption-compression heat pump prototype and related infrastructure were designed and established to offer flexibility in possible operating conditions. This enables the conduction of experiments with a broad range of boundary conditions to investigate and evaluate various operating conditions for different industrial application cases. The presented component sections for the defined research focus areas were designed to address the identified challenges for achieving higher heat sink supply temperatures and system efficiencies. Additional system and component modifications for follow-up studies can be applied at any time.

The experimental ACHP prototype serves as a starting point for further investigations. It will be involved in different research projects in cooperation with both academic and industrial partners in the coming years. Comprehensive experimental investigations for evaluating and improving the implemented component solutions offer great potential for further studies. Suggestions for future work are presented and discussed in the following:

- Many industrial processes feature characteristic demand fluctuations over different periods, ranging from a minute base to seasonal changes. The resulting load variations influence the performance of the installed heat pump system. The testing and improvement of control strategies for part-load operation and the development of dynamic models of the ACHP system can help to further improve the design, operation, and part-load performance.

- The ACHP prototype represents the right tool for the development and experimental testing of novel concepts with respect to the defined research focus areas and the system control. Furthermore, the ACHP prototype can be used to validate and improve numerical simulation models and results. This will increase the precision of such models and can strengthen the confidence of end users in values determined for application cases.

- The development and investigation of concepts for steam generation using the ACHP system can enable and enhance the replacement of today's widely used conventional energy systems relying on fossil fuel. This will be investigated and demonstrated as part of the EU project ENOUGH[2].

[2] https://enough-emissions.eu/demonstrator/150c-steam-production-heat-pump/ (accessed: 20.11.2022)

Bibliography

[1] International Energy Agency, Net Zero by 2050 - A Roadmap for the Global Energy Sector, 2021. https://www.iea.org/reports/net-zero-by-2050 (accessed: 20.09.2022).

[2] International Energy Agency, Energy Efficiency 2O18: Analysis and outlooks to 2040, 2018. https://www.iea.org/reports/energy-efficiency-2018 (accessed: 20.09.2022).

[3] T. Fleiter, R. Elsland, M. Rehfeldt, J. Steinbach, U. Reiter, G. Catenazzi, M. Jakob, C. Rutten, R. Harmsen, F. Dittmann, P. Riviere, P. Stabat, Heat Roadmap Europe 2050. Deliverable 3.1: Profile of heating and cooling demand in 2015, 2017.

[4] Eurostat, Energy Balances, (2019). https://ec.europa.eu/eurostat/web/energy/data/energy-balances (accessed: 10.10.2022).

[5] R. de Boer, A. Marina, B. Zühlsdorf, C. Arpagaus, M. Bantle, V. Wilk, B. Elmegaard, J. Corberán, J. Benson, Strengthening Industrial Heat Pump Innovation: Decarbonizing Industrial Heat, 2020. https://www.sintef.no/globalassets/sintef-energi/industrial-heat-pump-whitepaper/2020-07-10-whitepaper-ihp-a4.pdf (accessed: 10.10.2022).

[6] M. Papapetrou, G. Kosmadakis, A. Cipollina, U. La Commare, G. Micale, Industrial waste heat: Estimation of the technically available resource in the EU per industrial sector, temperature level and country, Appl. Therm. Eng. 138 (2018) 207–216. https://doi.org/10.1016/j.applthermaleng.2018.04.043.

[7] K.M. Adamson, T.G. Walmsley, J.K. Carson, Q. Chen, F. Schlosser, L. Kong, D.J. Cleland, High-temperature and transcritical heat pump cycles and advancements: A review, Renew. Sustain. Energy Rev. 167 (2022) 112798. https://doi.org/10.1016/J.RSER.2022.112798.

[8] F. Schlosser, M. Jesper, J. Vogelsang, T.G. Walmsley, C. Arpagaus, J. Hesselbach, Large-scale heat pumps: Applications, performance, economic feasibility and industrial integration, Renew. Sustain. Energy Rev. 133 (2020). https://doi.org/10.1016/j.rser.2020.110219.

[9] C. Arpagaus, F. Bless, M. Uhlmann, J. Schiffmann, S.S. Bertsch, High temperature heat pumps: Market overview, state of the art, research status, refrigerants, and application potentials, Energy. 152 (2018) 985–1010. https://doi.org/10.1016/j.energy.2018.03.166.

[10] HPT, Annex 58 - High-Temperature Heat Pumps, (2022). https://heatpumpingtechnologies.org/annex58/ (accessed: 10.10.2022).

[11] B. Zühlsdorf, J.K. Jensen, S. Cignitti, C. Madsen, B. Elmegaard, Analysis of temperature glide matching of heat pumps with zeotropic working fluid mixtures for different temperature glides, Energy. 153 (2018) 650–660. https://doi.org/10.1016/j.energy.2018.04.048.

[12] G.F. Frate, L. Ferrari, U. Desideri, Analysis of suitability ranges of high temperature heat pump working fluids, Appl. Therm. Eng. 150 (2019) 628–640. https://doi.org/10.1016/j.applthermaleng.2019.01.034.

[13] D. Wu, B. Hu, R.Z. Wang, H. Fan, R. Wang, The performance comparison of high temperature heat pump among R718 and other refrigerants, Renew. Energy. 154 (2020) 715–722. https://doi.org/10.1016/j.renene.2020.03.034.

[14] J.K. Jensen, W.B. Markussen, L. Reinholdt, B. Elmegaard, On the development of high temperature ammonia-water hybrid absorption-compression heat pumps, Int. J. Refrig. 58 (2015) 79–89. https://doi.org/10.1016/j.ijrefrig.2015.06.006.

[15] SINTEF Energy, HighEFF - Centre for an Energy Efficient and Competitive Industry for the Future, (2022). https://www.sintef.no/projectweb/higheff/about/ (accessed: 10.10.2022).

[16] SINTEF Energy, HighEFFLab, (2022). https://www.sintef.no/projectweb/highefflab/ (accessed: 10.10.2022).

[17] A. Brand, L. Allen, M. Altman, M. Hlava, J. Scott, Beyond authorship: attribution, contribution, collaboration, and credit, Learn. Publ. 28 (2015) 151–155. https://doi.org/10.1087/20150211.

[18] J.K. Jensen, Industrial heat pumps for high temperature process applications, Doctoral Thesis, Technical University of Denmark, Kongens Lyngby, Denmark, 2015.

[19] A. Osenbrück, Verfahren zur Kälteerzeugung bei Absorptionsmaschinen, DPR 84084, 1895.

[20] E. Altenkirch, Kompressionskältemaschine mit Lösungskreislauf, Kältetechnik. 2 (1950) 251–259, 279–284, 310–315.

[21] E.A. Groll, Current status of absorption/compression cycle technology, in: ASHRAE Trans. Tec. Symp. Pap., 1997: pp. 361–374.

[22] H.S. Baksaas, S. Grandum, Initial tests of high temperature absorption/compression heat pump, in: Int. Sorption Heat Pump Conf., 1999: pp. 477–482.

[23] T. Risberg, B. Horntvedt, D. Madland, S.R. Nordtvedt, Process dynamics in an industrial prototype compression / absorption heat pump, in: 6th IIR Gustav Lorentzen Conf., International Institute of Refrigeration, Glasgow, 2004.

[24] D.M. Van De Bor, C.A. Infante Ferreira, A.A. Kiss, Optimal performance of compression-resorption heat pump systems, Appl. Therm. Eng. 65 (2014) 219–225. https://doi.org/10.1016/j.applthermaleng.2013.12.067.

[25] J.K. Jensen, L. Reinholdt, W.B. Markussen, B. Elmegaard, Investigation of ammonia / water hybrid absorption / compression heat pumps for heat supply temperatures above 100 ° C, in: Int. Sorption Heat Pump Conf., Center for Environmental Energy Engineering, 2014: pp. 1–10.

[26] C. Qing, P. Gao, C.L. Zhang, Thermodynamic analysis on feasible operating region of two-stage hybrid absorption-compression heat pump cycles, Int. J. Refrig. 121 (2021) 43–50. https://doi.org/10.1016/j.ijrefrig.2020.09.017.

[27] C.W. Jung, J.Y. Song, Y.T. Kang, Study on ammonia/water hybrid absorption/compression heat pump cycle to produce high temperature process water, Energy. 145 (2018) 458–467. https://doi.org/10.1016/j.energy.2017.12.141.

[28] L.G. Farshi, S. Khalili, A.H. Mosaffa, Thermodynamic analysis of a cascaded compression – Absorption heat pump and comparison with three classes of conventional heat pumps for the waste heat recovery, Appl. Therm. Eng. 128 (2018) 282–296. https://doi.org/10.1016/j.applthermaleng.2017.09.032.

[29] P. Gao, C. Qing, M.M. Chang, L.L. Shao, C.L. Zhang, Hybrid absorption-compression heat pump with two-stage rectification and subcooler, Appl. Therm. Eng. 181 (2020) 116027. https://doi.org/10.1016/j.applthermaleng.2020.116027.

[30] N.S. Ganesh, T. Srinivas, Evaluation of thermodynamic properties of ammonia- water mixture up to 100 bar for power application systems, J. Mech. Eng. Res. 3 (2011) 25–39.

[31] H. Lorenz, Die Ermittlung der Grenzwerte der thermodynamischen Energieumwandlung, Zeitschrift Für Die Gesammte Kälteindustrie, 2. (1895) 1-3,6-12.

[32] K. Amrane, M. V. Rane, R. Radermacher, Performance curves for single-stage vapor compression cycles with solution circuit, J. Eng. Gas Turbines Power. 113 (1991) 221–227. https://doi.org/10.1115/1.2906548.

[33] M. Hultén, T. Berntsson, The compression/absorption heat pump cycle - Conceptual design improvements and comparisons with the compression cycle, in: Int. J. Refrig., Elsevier, 2002: pp. 487–497. https://doi.org/10.1016/S0140-7007(02)00014-2.

[34] G. Bergmann, G. Hivessy, Experimental Hybrid Heat Pump of 1000kW heating capacity, in: 4th Int. Conf. Appl. Effic. Heat Pump Syst., Munich, 1990: pp. 27–40. https://doi.org/10.1007/978-3-662-30179-1_3.

[35] L.C.M. Itard, C.H.M. Machielsen, Considerations when modelling compression/resorption heat pumps, Int. J. Refrig. 17 (1994) 453–460. https://doi.org/10.1016/0140-7007(94)90005-1.

[36] L.C.M. Itard, Wet compression versus dry compression in heat pumps working with pure refrigerants or non-azeotropic mixtures, Int. J. Refrig. 18 (1995) 495–504. https://doi.org/10.1016/0140-7007(95)93788-L.

[37] R. Radermacher, An Example of the Manipulation of Effective Vapor Pressure Curves, J. Eng. Gas Turbines Power. 110 (1988) 647–651. http://asmedigitalcollection.asme.org/gasturbinespower/article-pdf/110/4/647/5596472/647_1.pdf (accessed: 23.03.2021).

[38] M. V. Rane, R. Radermacher, Experimental investigation on a two stage vapor compression heat pump with solution circuits: Performance enhancement with a bleed line, in: Absorpt. Heat Pump Conf., 1991: pp. 96–102.

[39] M. V. Rane, R. Radermacher, Feasibility study of a two-stage vapour compression heat pump with ammonia-water solution circuits: experimental results, Int. J. Refrig. 16 (1993) 258–264. https://doi.org/10.1016/0140-7007(93)90078-M.

[40] M. V. Rane, K. Amrane, R. Radermacher, Performance enhancement of a two-stage vapour compression heat pump with solution circuits by eliminating the rectifier, Int. J. Refrig. 16 (1993) 247–257. https://doi.org/10.1016/0140-7007(93)90077-L.

[41] E.A. Groll, R. Radermacher, Vapor Compression heat pump with solution circuit and desorber/absorber heat exchange, in: Int. Absorpt. Heat Pump Confernece, 1994: pp. 463–469.

[42] Q. Zhou, R. Radermacher, Development of a vapor compression cycle with a solution circuit and desorber/absorber heat exchange, Int. J. Refrig. 20 (1997) 85–95. https://doi.org/10.1016/S0140-7007(96)00072-2.

[43] S.R. Nordtvedt, Experimental and theoretical study of a compression / absorption heat pump with ammonia / water as working fluid, Doctoral Thesis, Norweigan University of Science and Technology, Trondheim, Norway, 2005.

[44] L.C.M. Itard, Wet compression-resorption heat pump cycles: thermodynamic analysis and design, Doctoral Thesis, Delft University of Technology, Delft, Netherlands, 1998.

[45] D. Zaytsev, Development of wet compressor for application in compression-resorption heat pumps, Doctoral Thesis, Technische Universiteit Delft, Delft, Netherlands, 2003.

[46] W.F. Malewski, Integrated absorption and compression heat pump cycle using mixed working fluid ammonia and water, in: 2nd Int. Work. Res. Act. Adv. Heat Pumps, Graz, 1988: pp. 35–44.

[47] H. Torstensson, J.-E. Nowacki, A sorption/compression heat pump using exhaust air as heat source, in: Absorpt. Heat Pump Conf., Tokyo, Japan, 1991: pp. 103–108.

[48] M. V. Rane, R. Radermacher, K.E. Herold, Experimental investigation of a single stage vapor compression heat pump with solution circuit, in: Adv. Ind. Heat Pumps Technol., San Francisco, California, 1989.

[49] J. Stene, Design and Application of Ammonia Heat Pump Systems for Heating and Cooling of Non-Residential Buildings, in: 8th IIR Gustav Lorentzen Conf. Nat. Work. Fluids, Copenhagen, 2008.

[50] A.K. Pratihar, S.C. Kaushik, R.S. Agarwal, Performance evaluation of a small capacity compression-absorption refrigeration system, Appl. Therm. Eng. 42 (2012) 41–48. https://doi.org/10.1016/j.applthermaleng.2012.03.011.

[51] C. Arpagaus, F. Bless, M. Uhlmann, J. Schiffmann, S.S. Bertsch, High temperature heat pumps: Market overview, state of the art, research status, refrigerants, and application potentials, Energy. 152 (2018) 985–1010. https://doi.org/10.1016/j.energy.2018.03.166.

[52] J.-M. Clairand, M. Briceño-León, G. Escrivá-Escrivá, A.M. Pantaleo, Review of Energy Efficiency Technologies in the Food Industry: Trends, Barriers, and Opportunities, IEEE Access. 8 (2020) 48015–48029. https://doi.org/10.1109/ACCESS.2020.2979077.

[53] J. Jiang, B. Hu, R.Z. Wang, N. Deng, F. Cao, C.-C. Wang, A review and perspective on industry high-temperature heat pumps, Renew. Sustain. Energy Rev. 161 (2022) 112106. https://doi.org/10.1016/J.RSER.2022.112106.

[54] D. Zaytsev, C.A. Infante Ferreira, Screw Compressor for Ammonia-Water Heat Pump Lubricated By the Process Mixture, in: Int. Compress. Eng. Conf. Sch., 2002.

[55] S.A. Klein, Engineering Equation Solver Academic Professional V10.650-3D, 2020. (n.d.). https://fchartsoftware.com/ees/mastering-ees.php (accessed: 23.09.2022).

[56] S.A. Ibrahim, O.M. Klein, Thermodynamic Properties of Ammonia-Water Mixtures, in: ASHRAE Trans. 99, 1993: pp. 1495–1502.

[57] C.A. Infante Ferreira, C. Zamfirescu, D. Zaytsev, Twin screw oil-free wet compressor for compression-absorption cycle, Int. J. Refrig. (2006). https://doi.org/10.1016/j.ijrefrig.2005.10.006.

[58] V. Bercescu, Aspects du fonctionnement d'une installation experimentale de pompe de chaleur avec compression mecanique et circulation additionelle de la solution, in: 16th Int. Congr. Refrig., Paris, 1983.

[59] J. Kim, S.R. Park, Y.J. Baik, K.C. Chang, H.S. Ra, M. Kim, Y. Kim, Experimental study of operating characteristics of compression/absorption high-temperature hybrid heat pump using waste heat, Renew. Energy. 54 (2013) 13–19. https://doi.org/10.1016/j.renene.2012.09.032.

[60] Y. Tian, H. Yuan, C. Wang, H. Wu, Z. Xing, Numerical investigation on mass and heat transfer in an ammonia oil-free twin-screw compressor with liquid injection, Int. J. Therm. Sci. (2017). https://doi.org/10.1016/j.ijthermalsci.2017.06.007.

[61] V. Gudjonsdottir, C.A. Infante Ferreira, A. Goethals, Wet compression model for entropy production minimization, Appl. Therm. Eng. 149 (2019) 439–447. https://doi.org/10.1016/j.applthermaleng.2018.12.065.

[62] Dassault Systems, DYMOLA Systems Engineering: Multi-Engineering Modeling and Simulation based on Modelica and FMI, (2022). https://www.3ds.com/products-

services/catia/products/dymola/ (accessed: 02.09.2022).

[63] TLK-Thermo GmbH, TIL Suite – Simulates thermal systems, (2022). https://www.tlk-thermo.com/index.php/en/software/til-suite (accessed: 02.09.2022).

[64] TLK-Thermo GmbH, TILMedia Suite – Software package for calculating the properties of thermophysical substances, (2022). https://www.tlk-thermo.com/index.php/en/software/tilmedia-suite (accessed at 2022-09-02).

[65] C.W. Jung, S.S. An, Y.T. Kang, Thermal performance estimation of ammonia-water plate bubble absorbers for compression/absorption hybrid heat pump application, Energy. 75 (2014) 371–378. https://doi.org/10.1016/j.energy.2014.07.086.

[66] B. Mongey, N.J. Hewitt, J.T. McMullan, P.C. Henderson, G.A. Molyneaux, Performance trends and heat transfer considerations in an ammonia-water resorption cycle, Int. J. Energy Res. 25 (2001) 41–51. https://doi.org/10.1002/1099-114X(200101)25:1<41::AID-ER697>3.0.CO;2-5.

[67] D.A. Reay, Compact heat exchangers, enhancement and heat pumps, in: Int. J. Refrig., 2002: pp. 460–470. https://doi.org/10.1016/S0140-7007(00)00005-0.

[68] A.K. Pratihar, S.C. Kaushik, R.S. Agarwal, Simulation of an ammonia - Water compression - Absorption refrigeration system for water chilling application, Int. J. Refrig. 33 (2010) 1386–1394. https://doi.org/10.1016/j.ijrefrig.2010.05.011.

[69] Y.T. Kang, A. Akisawa, T. Kashiwagi, Analytical investigation of two different absorption modes: falling film and bubble types, Int. J. Refrig. 23 (2000) 430–443.

[70] B. Markmann, Wärmeübergang bei der Absorption ammoniakreichen Dampfes durch wässrige Lösung im Plattenwärmeübertrager, Doktorbeit, Leibniz Universität Hannover, Hannover, Deutschland, 2020.

[71] F. Táboas, M. Vallès, M. Bourouis, A. Coronas, Flow boiling heat transfer of ammonia/water mixture in a plate heat exchanger, Int. J. Refrig. 33 (2010) 695–705. https://doi.org/10.1016/J.IJREFRIG.2009.12.005.

[72] S.R. Nordtvedt, Performance analysis of a plate type heat exchanger used as absorber in a combined compression/absorption heat pump, in: Int. Sorption Heat Pump Conf., Shanghai, China, 2002: pp. 235–239.

[73] S.S. An, C.W. Jung, M. Kim, S.R. Park, C. Kang, Y.T. Kang, Experimental and simulation study on the plate absorber for hybrid heat pump system, J. Mech. Sci. Technol. 27 (2013) 3903–3909. https://doi.org/10.1007/s12206-013-0935-8.

[74] S.R. Nordtvedt, B.R. Horntvedt, J. Eikefjord, J. Johansen, Hybrid Heat Pump for Waste Heat Recovery in Norwegian Food Industry, in: 10th Int. Heat Pump Conf., 2011.

[75] K.B. Lee, B.H. Chun, J.C. Lee, C.H. Lee, S.H. Kim, Experimental analysis of bubble mode in a plate-type absorber, Chem. Eng. Sci. 57 (2002) 1923–1929. https://doi.org/10.1016/S0009-2509(02)00089-1.

[76] B. Markmann, T. Tokan, M. Loth, J. Stegmann, K.H. Hartmann, H. Kruse, S. Kabelac, Experimental results of an absorption-compression heat pump using the working fluid ammonia/water for heat recovery in industrial processes, Int. J. Refrig. (2019). https://doi.org/10.1016/j.ijrefrig.2018.10.010.

A. Additional Information

A.1. Simulation model – EES code

```
{Procedures}
Procedure ihx(T;K;O;Z;X;M;N;E:R1;R2) {Procedure for IHEX}
i:= 1
Call nh3h2o(123;T;O;X:T[i];P[i];X[i];h[i];s[i];u[i];v[i];q[i]) {T[5], P_HP, ZZ}
i:= i +1
Call nh3h2o(123;K;O;X:T[i];P[i];X[i];h[i];s[i];u[i];v[i];q[i]) {T[12], P_HP, ZZ}
qh:= (h[1] - h[2]) * M {qh- ideal heat exchange from 5-6. M-Vapor flow rate}
i:= i + 1
Call nh3h2o(123;T;O;Z:T[i];P[i];X[i];h[i];s[i];u[i];v[i];q[i]) {T[5], P_HP, x_liquid}
i:= i + 1
Call nh3h2o(123;K;O;Z:T[i];P[i];X[i];h[i];s[i];u[i];v[i];q[i]) {T[10], P_HP, x_liquid}
qc:= (h[3] - h[4]) * N {qc- ideal heat exchange from 12-13.}
qihx:= 0
if(T<K) Then Goto 10
qmax:= min(qh;qc) {ideal heat exchange in IHEX}
qihx = qmax * E {actual heat exchange in IHEX}
10: R1:= h[1] - (qihx / M) {Return value for h[6]}
R2:= h[4] + (qihx / N) {Return value for h[13]}
End

Procedure absorber(Z[50..100];A[50..100];O;M;N;T_WA1;Y:C1;C2)
K[50]:= T_WA1 {Heat sink inlet temperature}
N:=N - 0,001 {Heat sink mass flow rate}{Adjust the accuracy}
10: i:=50 {Number of segments}
N:=N + 0,001 {Heat sink mass flow rate}{Adjust the accuracy}
r:= enthalpy('Water';P=O;T=K[50]) {Enthalpy of heat sink at the inlet absorber, O = P_A}
e[i] := r
D[i]:= Z[i]-K[50] {Temperature difference between mixed solution and heat sink }
Repeat
i:=i+1
q:=(A[i]-A[i-1])*M {Heat exchange between two points in the absorber}
e[i] := e[i-1]+(q/N) {indexed eNthalpy of the solution}
N:= (((A[i]-A[50])*M)/(e[i]-r)) {approxiMate heat sink mass flow rate}
L:= temperature('Water';P=O;h=e[i]) {Indexed temperature of the mixed solution}
D[i] := Z[i]-L {Indexed temerpature difference between mixed soLution and heat sink}
W[i]:= L
if(D[i]<Y) Then Goto 10 {If the temperature difference is beLow minimum temperature differences go to 10}
Until (i=100)
C1:= N {Return value of heat sink mass flow}
C2:= W[100] {Return value of heat sink temperature}
End

Function dsh(T;K;F;P;Z;M) {Function to determine thermal efficiency of the desuperheater.}
i:= 1
Call nh3h2o(123;T;P;Z:T[i];P[i];x[i];h[i];s[i];u[i];v[i];q[i]) {T[2], P_HP, x_vapour2}
i:= i +1
Call nh3h2o(123;K;P;Z:T[i];P[i];x[i];h[i];s[i];u[i];v[i];q[i]) {T[3], P_HP, x_vapour2}
i:= i + 1
Call nh3h2o(123;F;P;Z:T[i];P[i];x[i];h[i];s[i];u[i];v[i];q[i]) {T_wa2, P_HP, x_vapour2}
q:= (h[1] - h[2]) * M {actual heat exchange in dsh}
qmax:= (h[1] - h[3]) * M {ideal heat exchange in dsh}
epsilon:= q / qmax {dsh efficency}
dsh:= epsilon
End


{INPUT PARAMETERS}
eta_isentropic = 0,6
eta_motorc = 0,9 {Compressor motor efficency}
eta_motorp = 0,9 {Pump motor efficency}
epsilon_ihx = 0,9 {Thermal efficency of IHX}
epsilon_des=0,9 {Thermal efficency of desorber}
T_mindesorber= 5[K] {Minimum temperature differences in absorber}
T_minabsorber=5[K] {Minimum temperature differences in desorber}
PR = 5 [-]
P_D=3 {Pressure in sources}
```

```
P_A = 10 [bar] {Sink Pressure}
x_WA2=0 {Ammonia concertation in sink}
{Q_sink = 100 {Heat transfer rate to the sink}}


{BOUNDARY CONDITIONS}
w=0,1 {How much precent going to the compressor for cooling}
{CR = 0,5  {Circulation ratio}}
{P_HP = 20,5 [bar] {Absorber pressure}}
{P_LP = 3,0 [bar] {Desorber pressure}}
{m_dotvp1 = 0,132 [kg/s] {Compressor mass flow rate}}
T_Sourcein = 343,15 [K] {Inlet sources temperature}
T_WA1=343,15 [K] {Inlet sink temprature}


{Function}
P_MP = k*((P_LP*P_HP)^0,5) {Injection pressure}
Qihx = (h[5]-h[6])*m_dott {Heat transfer rate in the internal heat exchanger}
ZZ= ((x_vapour1*m_v)+(x_liquid*m_l))/(m_t) {Amonia concentraison in point 4-8}
h_4=((h[3]*m_dotvp2)+(h[13]*m_dota))/(m_dott) {Enthalpy in point 4 mixing}
m_dotl = CR*m_dott {Liquid mass flow rate in point 9-10}
m_dott = Q_absorber/DELTAh_absorber {Mass flow rate in point 4-8}
x[9]= x_liquid {Ammonia mass fraction in liquid point 9-13}
m_dotvp1= m_dott-m_dotl {mass flow rate at the inlet of the compressor}
x[1] = x_vapour1 {Ammonia mass fraction in vapour at the inlet of the compressor}
T_GlideDesorber = T_Sourcein-T_Sourceout {Temperature glide in desorber}
T_Glideabsorber = T_WA3-T_WA1 {Temperature glide in absorber}

x_vapour2 = ((x_liquid*m_cc)+(x_vapour1*m_vp1))/(m_vp2) {Ammonia mass fraction in vapour at the outlet of the
compressor. Point 2 and 3}
h_2i = (((h_2s-h[1])+(eta_isentropic*h[1]))/eta_isentropic) {Enthalpy at the injection stages in compressor before mixing }
m_dotvp2=m_dotvp1+m_dotcc {mass flow rate at the outlet of the compressor. Point 2 and 3}
m_dota= m_dotl-m_dotcc {Liquid mass flow rate in point 12-13}

h_2_inj = ((h_2i*m_vp1)+(m_cc*h[11]))/m_vp2 {Enthalpy at the injection stages after mixing in the compressor}

m_dotcc= m_dotvp1*w {Mass flow rate injection. Point 11}
PR= P_HP/P_LP {Pressure ratio}
h_2 = (((h_2i_inj-h_2_inj)+(eta_isentropic*h_2_inj))/eta_isentropic) {Enthalpy out of the compressor}


{Desorber}
T_WD2 = T_Sourcein-T_mindesorber {Temprature out of the desorber. Point WD2}
T_Sourceout = T[7]+T_mindesorber {Temperature out of the sources}
Call nh3h2o(123;T_Sourcein;P_D;0:T_Sourcein[17];P_Sourcein[17];x_Sourcein[17];h_Sourcein[17];s_Sourcein[17];
u_Sourcein[17];v_Sourcein[17];q_Sourcein[17]) {Inlet sources properties}
Call nh3h2o(123;T_Sourceout;P_D;0:T_Sourceout[18];P_Sourceout[18];x_Sourceout[18];h_Sourceout[18];
s_Sourceout[18];u_Sourceout[18];v_Sourceout[18];q_Sourceout[18]) {Outlet sources properties}
Q_des= (h[8]-h[7])*m_dott {Heat transfer rate from the sources}
m_dotwd= (Q_des*epsilon_des)/(h_Sourcein[17]-h_Sourceout[18]) {Mass flow rate in the sources}

{ABSORBER (Array [50]-[100])}
Call absorber(T[50..100];h[50..100];P_A;m_dott;m_dotWAApprox;T_WA1;T_minabsorber:m_dotWA;T_WA2)
DELTAh_absorber = h[4] - h[5] {Enthalpy difference through the absorber }
step_aa = DELTAh_absorber / 50 {Enthalpy difference through the absorber  in 50 steps}
A[50] = h[5] {Enthalpy of solution at point 5}
Duplicate i = 51;100
A[i] = A[i-1] + step_aa {Enthalpy of mixed solution trough the absorber}
End
Duplicate i =50;100
Call nh3h2o(234;P_HP;zz;A[i]:T[i];P[i];x[i];h[i];s[i];u[i];v[i];q[i]) {Properties in the absorber}
End

{DESUPERHEATER}
DELTAh_desuperheater = h[2] - h[3] {Enthalpy difference through the dsh}
Q_desuperheater = DELTAh_desuperheater*m_dotvp2*epsilon_dsh {Heat transfer rate to the sink from desuperheater}
Call nh3h2o(123;T_WA2;P_A;x_WA2:T_WA2[1];P_A[1];x_WA2[1];h_WA2;s_WA2;u_WA2;v_WA2;q_WA2) {Water
properties in the sink before desuperheater point WA2 }
```

```
h_WA3 = h_WA2+(Q_desuperheater/m_dotWA) {Enthalpy after desuperheater in the sink. Point WA3}
T_WA3 = temperature('Water';P=P_A;h=h_WA3) {Heat sink temperature after the desuperheater. Point WA3}
Call nh3h2o(123;T[2];P_HP;x_vapour2:T[14];P[14];x[14];h[14];s[14];u[14];v[14];q[14]) {Ammonia/water properties at the innlet of desuperheater. Point 2}
epsilondsh = dsh(T[14];T[3];T_WA2;P_HP;x_vapour2;m_dotvp2) {Efficency of desuperheater}


h_WA1 = enthalpy('Water';T=T_WA1;P=P_A) {Heat sink inlet enthalpy}
h_ApproxWA2 = enthalpy('Water';T=T[100] - T_mindesorber;P=P_A) {Guess value of heat sink outlet temperature}
m_dotWAApprox = Q_absorber/(h_ApproxWA2-h_WA1) {Guess value of heat sink mass flow rate}


{Loop}
{---- 1 ----}
Call nh3h2o(128;T_WD2;P_LP;1:T[1];P[1];x[1];h[1];s[1];u[1];v[1];q[1]) {After separator vapour}
{---- 2 ----}
Call nh3h2o(235;P_MP;x_vapour1;s[1]:T_2s;P_2s;x_2s;h_2s;s_2s;u_2s;v_2s;q_2s) {Injection stages before correction of isentropic efficiency and mixing}
Call nh3h2o(234;P_MP;x_vapour2;h_2_inj:T_2s_inj;P_2s_inj;x_2s_inj;h_2s_inj;s_2s_inj;u_2s_inj;v_2s_inj;q_2s_inj) {Injection stages after mixing}
Call nh3h2o(235;P_HP;x_vapour2;s_2s_inj:T_2i_inj;P_2i_inj;x_2i_inj;h_2i_inj;s_2i_inj;u_2i_inj;v_2i_inj;q_2i_inj) {After compression before correction of isentropic efficiency}
Call nh3h2o(234;P_HP;x_vapour2;h_2:T[2];P[2];x[2];h[2];s[2];u[2];v[2];q[2]) {After compressor}
{---- 3 ----}
Call nh3h2o(123;T[2];P_HP;x_vapour2:T[3];P[3];x[3];h[3];s[3];u[3];v[3];q[3]) {After desuperheter}
{---- 4 ----}
Call nh3h2o(234;P_HP;ZZ;h_4:T[4];P[4];x[4];h[4];s[4];u[4];v[4];q[4]) {After mixing}
{---- 5 ----}
Call nh3h2o(238;P_HP;ZZ;0:T[5];P[5];x[5];h[5];s[5];u[5];v[5];q[5]) {After absorber}
{---- 6 ----}
Call ihx(T[5];T[12];P_HP;x_liquid;ZZ;m_dott;m_dota;epsilon_ihx:h_6;h_13)
Call nh3h2o(234;P_HP;ZZ;h_6:T[6];P[6];x[6];h[6];s[6];u[6];v[6];q[6]) {After IHEX}
{---- 7 ----}
Call nh3h2o(234;P_LP;ZZ;h_6:T[7];P[7];x[7];h[7];s[7];u[7];v[7];q[7]) {After expansion valve}
{---- 8 ----}
Call nh3h2o(123;T_WD2;P_LP;ZZ:T[8];P[8];x[8];h[8];s[8];u[8];v[8];q[8]) {After desorber}
{---- 9 ----}
Call nh3h2o(128;T_WD2;P_LP;0:T[9];P[9];x[9];h[9];s[9];u[9];v[9];q[9]) {After separator liquid}
{---- 10 ----}
Call nh3h2o(235;P_HP;x_liquid;s[9]:T[10];P[10];x[10];h[10];s[10];u[10];v[10];q[10]) {After pump}
{---- 11 ----}
Call nh3h2o(234;P_MP;x_liquid;h[10]:T[11];P[11];x[11];h[11];s[11];u[11];v[11];q[11]) {Liquid injection}
{---- 12 ----}
Call nh3h2o(123;T[10];P_HP;x_liquid:T[12];P[12];x[12];h[12];s[12];u[12];v[12];q[12]) {After pump}
{---- 13 ----}
Call nh3h2o(234;P_HP;x_liquid;h_13:T[13];P[13];x[13];h[13];s[13];u[13];v[13];q[13]) {After IHEX}


{Calculation of COP}
W_comp1 = (m_dotvp1*(h_2s-h[1]))/(eta_motorc* eta_isentropic) {Compressor work up to the injection stages}
W_comp2 = (m_dotvp2*(h_2i_inj-h_2s_inj))/(eta_motorc* eta_isentropic) {Compressor work after injection stages}

W_comp = W_comp1+W_comp2 {Compressor work}
W_pump = ((h[10] - h[9]) * m_dotl)/eta_motorp {Pump work}
COP_heating = Q_sink / (W_comp + W_pump) {COP heating}
Q_sink = Q_desuperheater + Q_absorber {Heat transfer rate to the sink}

T_LM_sink = (T_WA1-T_WA3)/(ln(T_WA1/T_WA3)) {Logarithmic mean temperature of sink}
T_LM_sources = (T_Sourcein-T_Sourceout)/(ln(T_Sourcein/T_Sourceout)) {Logarithmic mean temperature of sources}
COP_LORENZ = T_LM_sink/(T_LM_sink-T_LM_sources) {Lorenz COP}

Tsink_out = T_WA3 - 271,15[°C]
```

A.2. Simulation results

Figure A.1 and Figure A.2 show further simulation results of the achieved heat sink outlet temperature and COP for varying circulation ratios at different desorber pressure levels and constant source inlet temperatures of 60 °C and 70 °C, respectively.

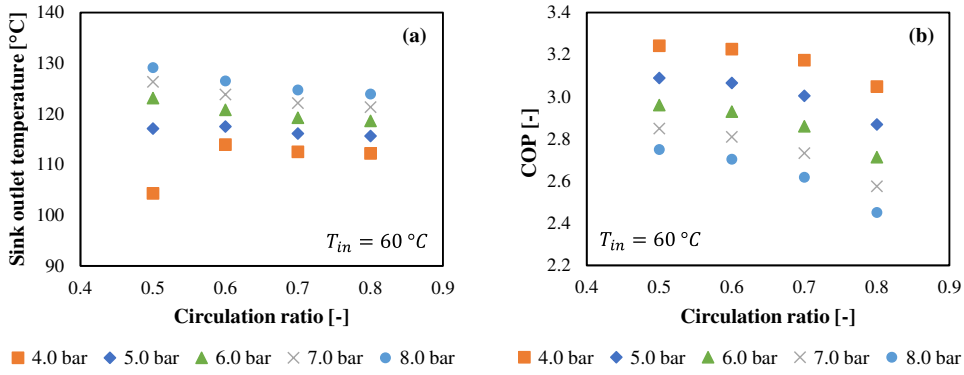

Figure A.1. Effects of circulation ratio and desorber pressure on (a) heat sink outlet temperature and (b) COP at constant source inlet temperature of 60 °C.

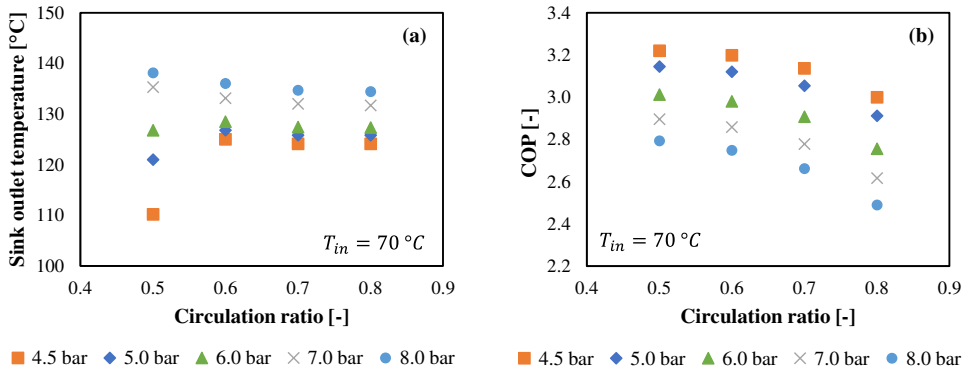

Figure A.2. Effects of circulation ratio and desorber pressure on (a) heat sink outlet temperature and (b) COP at constant source inlet temperature of 70 °C.

A.3. Detailed P&IDs

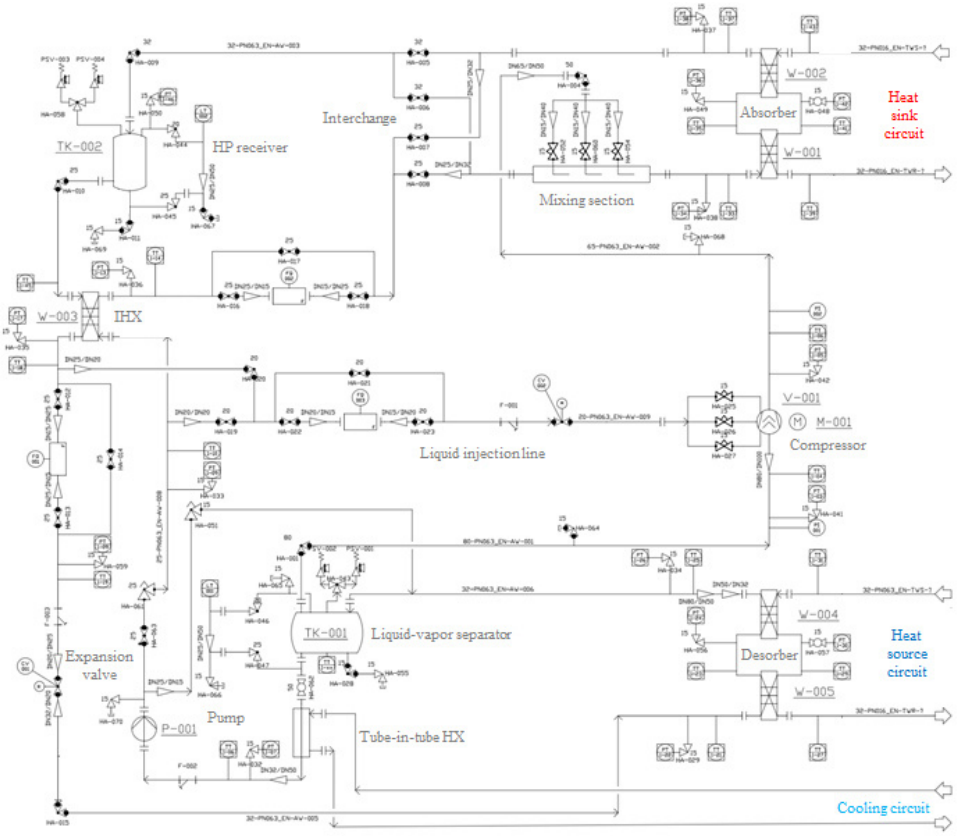

Figure A.3. Detailed P&ID of the experimental ACHP prototype with instrumentation.

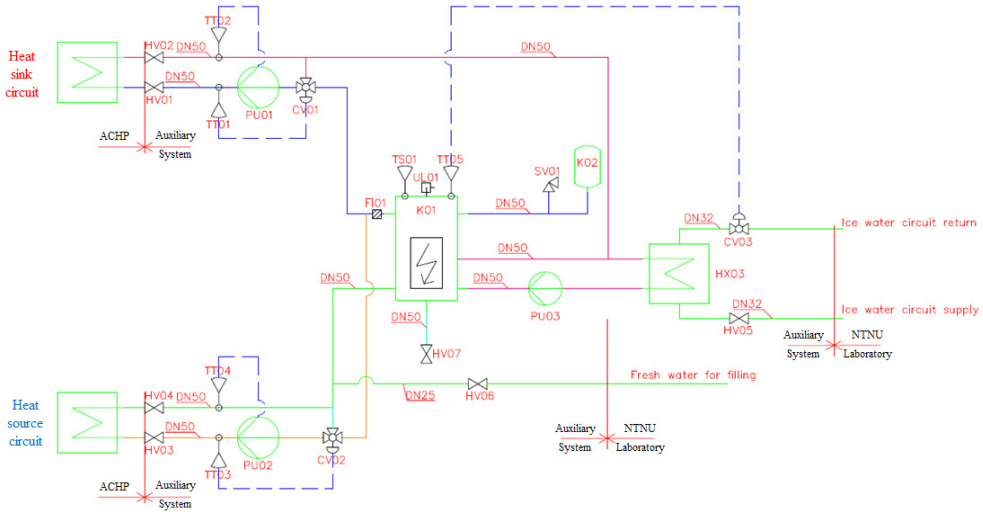

Figure A.4. Detailed P&ID of the auxiliary system with heat source and sink circuits.

A.4. Measurement & control system

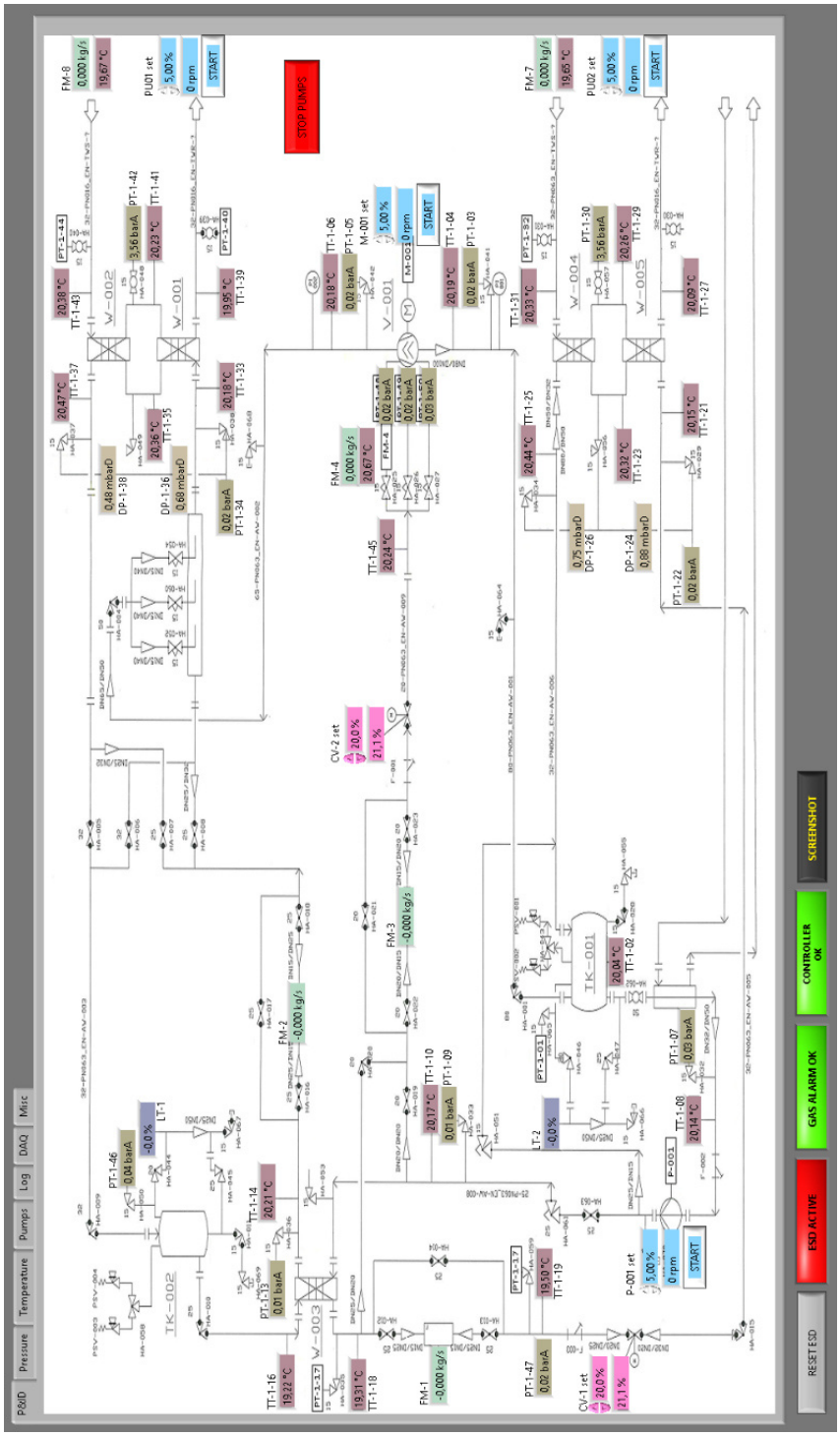

Figure A.5. Detailed P&ID in LabVIEW with measurement and controlling points.

B. Collection of Publications

Collection of published scientific contributions.

Article I

M.U. Ahrens, M. Loth, I. Tolstorebrov, A. Hafner, S. Kabelac, R.Z. Wang and T.M. Eikevik (2021). **Identification of Existing Challenges and Future Trends for the Utilization of Ammonia-Water Absorption-Compression Heat Pumps at High Temperature Operatio**n. In: *Applied Sciences* 11, 4635. DOI: 10.3390/app11104635

Author contributions: Conceptualization: M.U. Ahrens, M. Loth, I. Tolstorebrov, A. Hafner, S. Kabelac, R. Wang and T.M. Eikevik; Methodology: M.U. Ahrens, M. Loth and I. Tolstorebrov; Investigation: M.U. Ahrens, M. Loth and I. Tolstorebrov; Resources: M. Loth, A. Hafner, S. Kabelac, R. Wang and T.M. Eikevik; Writing - Original Draft: M.U. Ahrens; Writing - Review and Editing: M.U. Ahrens, M. Loth, I. Tolstorebrov, A. Hafner, S. Kabelac, R. Wang and T.M. Eikevik; Visualization: M.U. Ahrens; Supervision: I. Tolstorebrov, A. Hafner, S. Kabelac, R. Wang and T.M. Eikevik; Project Administration: M.U. Ahrens; Funding Acquisition: A. Hafner, S. Kabelac, R. Wang and T.M. Eikevik.

applied sciences

MDPI

Review

Identification of Existing Challenges and Future Trends for the Utilization of Ammonia-Water Absorption–Compression Heat Pumps at High Temperature Operation

Marcel Ulrich Ahrens [1,*], Maximilian Loth [2], Ignat Tolstorebrov [1], Armin Hafner [1], Stephan Kabelac [2], Ruzhu Wang [3] and Trygve Magne Eikevik [1]

[1] Department of Energy and Process Engineering, Norwegian University of Science and Technology, 7491 Trondheim, Norway; ignat.tolstorebrov@ntnu.no (I.T.); armin.hafner@ntnu.no (A.H.); Trygve.m.eikevik@ntnu.no (T.M.E.)

[2] Institute of Thermodynamics, Leibniz University Hannover, Am Welfengarten 1, 30167 Hannover, Germany; loth@ift.uni-hannover.de (M.L.); kabelac@ift.uni-hannover.de (S.K.)

[3] Institute of Refrigeration and Cryogenics, Shanghai Jiao Tong University, Shanghai 200240, China; rzwang@sjtu.edu.cn

* Correspondence: marcel.u.ahrens@ntnu.no; Tel.: +49-1729237476

Abstract: Decarbonization of the industrial sector is one of the most important keys to reducing global warming. Energy demands and associated emissions in the industrial sector are continuously increasing. The utilization of high temperature heat pumps (HTHPs) operating with natural fluids presents an environmentally friendly solution with great potential to increase energy efficiency and reduce emissions in industrial processes. Ammonia-water absorption–compression heat pumps (ACHPs) combine the technologies of an absorption and vapor compression heat pump using a zeotropic mixture of ammonia and water as working fluid. The given characteristics, such as the ability to achieve high sink temperatures with comparably large temperature lifts and high coefficient of performance (COP) make the ACHP interesting for utilization in various industrial high temperature applications. This work reviews the state of technology and identifies existing challenges based on conducted experimental investigations. In this context, 23 references with capacities ranging from 1.4 kW to 4500 kW are evaluated, achieving sink outlet temperatures from 45 °C to 115 °C and COPs from 1.4 to 11.3. Existing challenges are identified for the compressor concerning discharge temperature and lubrication, for the absorber and desorber design for operation and liquid–vapor mixing and distribution and the choice of solution pump. Recent developments and promising solutions are then highlighted and presented in a comprehensive overview. Finally, future trends for further studies are discussed. The purpose of this study is to serve as a starting point for further research by connecting theoretical approaches, possible solutions and experimental results as a resource for further developments of ammonia-water ACHP systems at high temperature operation.

Keywords: industrial heat pump; high temperature heat pump; absorption–compression heat pump; natural refrigerant; ammonia-water; solution circuit

Citation: Ahrens, M.U.; Loth, M.; Tolstorebrov, I.; Hafner, A.; Kabelac, S.; Wang, R.; Eikevik, T.M. Identification of Existing Challenges and Future Trends for the Utilization of Ammonia-Water Absorption–Compression Heat Pumps at High Temperature Operation. *Appl. Sci.* **2021**, *11*, 4635. https://doi.org/10.3390/app11104635

Academic Editor: Alberto Benato

Received: 14 April 2021
Accepted: 15 May 2021
Published: 19 May 2021

1. Introduction

Decarbonization of the industrial sector is one of the most important keys to reducing global warming. Energy demands and associated greenhouse gas (GHG) emissions in various industrial processes are continuously increasing [1]. Simultaneously, large amounts of potentially usable waste heat are available [2–4]. With climate change being one of the most significant topics of modern society, it is now globally recognized that there is a need to increase the energy efficiency of industrial processes and reduce direct GHG emissions, e.g., from burning of fossil fuels, in order to achieve environmentally friendly, cheap and sustainable energy systems [5–7]. Many industries requiring both cooling and heating

currently have separate systems for these tasks. Having a combined system capable of providing for both demands would be much more energy efficient. Due to this situation, the integration of high temperature heat pumps (HTHPs) with natural refrigerants is a promising approach for many industrial applications [8,9].

Following the trend towards more efficient and environmentally friendly ways of providing thermal energy from available waste heat as usable heat for industrial applications, suitable HTHP solutions have been increasingly investigated in recent years [10,11]. Many advances have been accomplished within the heat pump technology, in particular at lower heat delivery temperatures but a few at high temperatures above 90 °C [12,13]. However, ongoing research is seeking to further increase the delivery temperatures, as great demand and utilization potential exists for high temperature applications up to 150 °C due to the prevailing industry conditions [14]. Here, the use of natural refrigerants with low global warming potential (GWP) and known impacts and burdens on the atmosphere, such as ammonia and water, is of particular interest regarding environmental sustainability [15–17]. Therefore, the ammonia-water absorption–compression heat pump (ACHP) is considered a promising approach for heat pump applications in high temperature operations and is presented in more detail below.

The ACHP is often named a vapor compression cycle with solution circuit, compression/absorption cycle or hybrid absorption–compression heat pump. It combines the technologies of an absorption and vapor compression heat pump using a zeotropic mixture of ammonia and water as working fluid. As a result, heat is extracted and released at non-constant temperature glides. The required compression ratio can be reduced, when compared with conventional vapor compression heat pumps (VCHPs) utilizing single fluid refrigerants, by adjusting the concentration to the given boundary conditions. These characteristics, combined with the ability to achieve high sink temperatures above 100 °C at large temperature lifts and high coefficients of performance (COP), make the ACHP system a valuable solution for high temperature heat supply in the industry [18].

In 1895, the first patent concerning ACHP cycles was published by Osenbrück [19]. Detailed theoretical studies were first conducted by Altenkirch in 1950 and indicated a significant potential for energy savings [20]. Due to the energy saving potential and the increasing urgency to substitute the ozone-depleting chlorofluorocarbons (CFCs) combined with the energy crisis in the 1970s, research activities have increased rapidly since the 1980s, and several experimental plants have been built in this context. In 1997, Groll [21] summarized the research activities by reviewing more than 40 papers in a detailed overview. It was concluded that, despite the investigation of various cycle configurations and the commissioning and operation of several large-scale pilot plants, considerable work remained to be done before the ACHP could be used commercially.

In the following years, research activities continued and were stimulated by the increasing energy demand in the industrial sector with growing awareness of GHG emissions and the increased motivation for HTHP solutions using natural refrigerants. During the installation of further test and pilot plants, the ACHP with a single-stage solution circuit was successfully brought to commercial implementation using standard refrigeration components [22,23]. Until today, several units have been installed for commercial use in various industrial applications, achieving heat sink temperatures of up to 120 °C and temperature lifts of up to 75 K [24,25].

The first commercial installations of the ACHP encouraged the growing interest in the system. They have led to extensive theoretical investigations in recent years to identify optimal operating conditions and potential applications [26–29]. Furthermore, particular focus was placed on possible improvements to further expand the achievable process parameters, such as the sink outlet temperature and system efficiency, to compete with conventional solutions for use in high temperature applications [30–32].

The present work aims to support the current trends in the scientific field, focusing on developing and improving capable HTHP solutions for the use in industrial high temperature applications. For this reason, this study identifies the existing challenges and future trends for the utilization of the ACHP at high temperature operation against the background of recent research activities and findings. First, the ACHP cycle and various modifications are presented. This is followed by a comprehensive review of experimental work related to the described cycle modifications and the identification of existing challenges. Then, current developments and possible solutions are described and presented in a detailed overview. Finally, the future trends of research and innovation activities are defined based on the performed investigations.

2. The Ammonia-Water Absorption–Compression Heat Pump

The most basic type of the ACHP cycle using ammonia-water as a working fluid is the Osenbrück cycle, named after its inventor [19]. ACHP cycle with a single-stage solution circuit consists of seven main components: Three heat exchangers, a liquid–vapor separator, an expansion valve, a solution pump and a compressor. Figure 1 shows a simplified representation of this cycle.

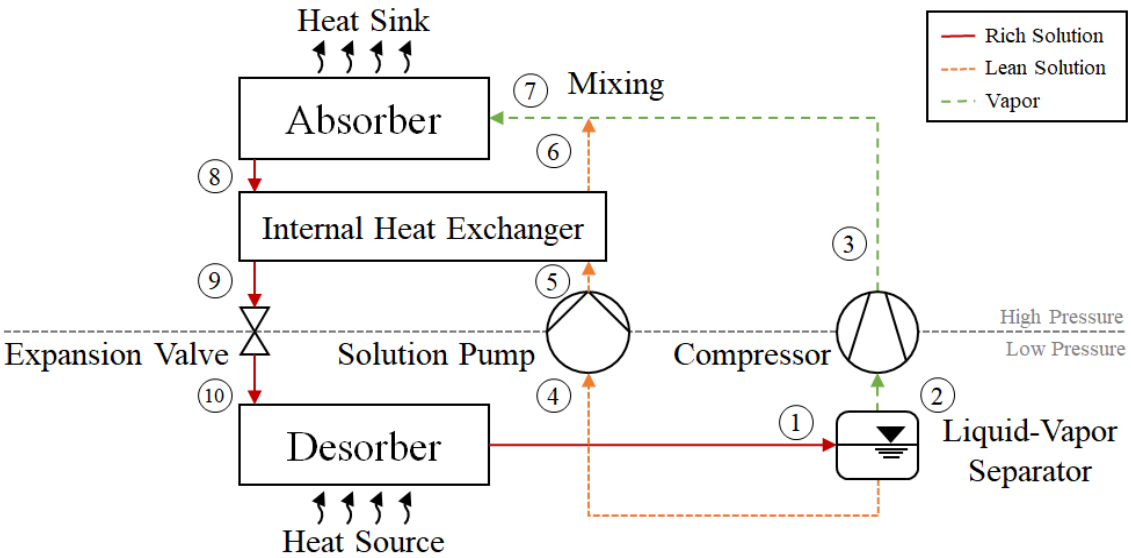

Figure 1. Schematic representation of a basic hybrid absorption–compression heat pump cycle.

In the ACHP cycle, the evaporator and condenser are replaced by desorber and absorber. Throughout the entire heat transfer process with the heat source in the desorber, the ammonia-water mixture is in the two-phase region and the ammonia concentration in the liquid phase decreases. Due to incomplete evaporation, a two-phase mixture leaves the desorber (1). A liquid–vapor separator is applied to separate the phases and ensure that only vapor enters the compressor (2) to be compressed to the high-pressure side of the cycle (3). The liquid phase, characterized as lean solution, is sent to the solution pump (4) where the pressure level increases (5). Then, the lean solution passes through an internal heat exchanger (IHX) to increase liquid temperature and improve overall cycle performance (5,6). After the IHX and compressor, the liquid and vapor streams are mixed, resulting in a liquid–vapor mixture (7). In the absorber, vapor is absorbed into the liquid phase rejecting heat to the heat sink. The ammonia concentration in the liquid phase gradually increases so that the saturated liquid leaving the absorber at the outlet is called rich solution (7,8). Heat is transferred from the rich

to the lean solution stream in the IHX (8,9) before the solution is throttled to the low-pressure level (9,10) returning to the desorber and completing the cycle.

Ammonia-water mixture as working fluid with a large boiling point difference and the implementation of the solution circuit provides two additional degrees of freedom compared to conventional VCHP cycles [21]. The ability to vary the working fluid composition and the circulation ratio between solution pump and compressor streams ensures high flexibility and adaptability of the operating parameters by changing boundary conditions. In general, the following advantages for the ACHP system can be pointed:

- Capacity control by changing the overall composition of the working fluid mixture, resulting in a change in the low-pressure gas density. Hereby, at constant speed and volume flow of the compressor, the mass flow of the vapor and thus the capacity of the heat pump is changed.
- Exploitation of the occurring temperature glides in desorber and absorber can be matched to heat source and sink and thus reduce the irreversibility of the system and enable large temperature spans with comparatively high COPs. The process follows the Lorenz rather than the Carnot process and becomes more effective as the temperature spread increases.
- Compared to pure ammonia, higher heat sink temperatures can be achieved with lower discharge vapor pressure and reduced pressure ratios when water is used as solvent.

Cycle Configurations of the Absorption–Compression Heat Pump

Based on the ACHP cycle introduced in Figure 1, several authors such as Amrane et al. (1991) [33], Hultén and Berntsson (2002) [34] and Jensen (2015) [18] examined various process modifications. These included extra components, such as additional heat exchangers for the internal heat exchange or cooling circuits. As a result, the system could be further adapted and improved, but the complexity has also increased. In addition to these modifications of the ACHP cycle with single-stage solution circuit, other advanced cycle configurations have been developed. Figure 2 shows three cycle configurations of the ACHP, which have been assigned individual designations due to the modifications made and specific characteristics.

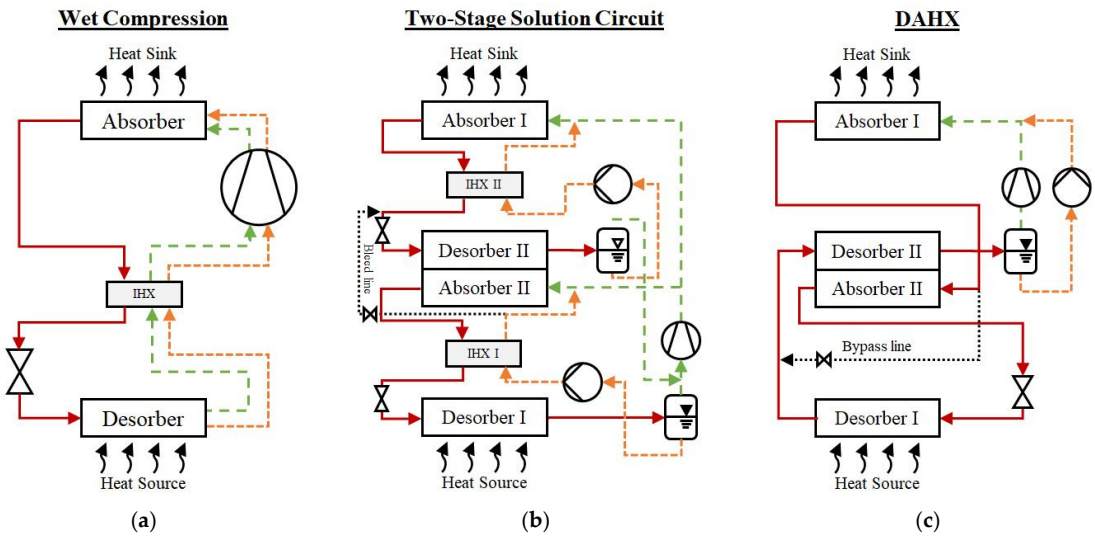

Figure 2. Schematic representations of (**a**) a wet compression cycle, (**b**) ACHP with two-stage solution circuit and (**c**) ACHP with single circuit and desorber/absorber heat exchange (DAHX).

The wet compression cycle, also known as wet compression-resorption cycle, is shown in Figure 2a and was investigated by Bergmann and Hivessy (1990) [35], Itard and Machielsen (1994) [36] and Itard (1995) [37]. Contrary to dry compression with a separate solution circuit, the ammonia-water mixture leaving the desorber in a wet-vapor state is conveyed to the compressor without additional phase separation. Thus, a two-phase compression takes place, intended to reduce the compressor discharge temperature and the required compression work by decreasing the superheating of the vapor phase through continuous cooling by the present liquid. To achieve a good system performance, an extensive internal heat exchange and a suitable compressor with high isentropic efficiency are important. A disadvantage of the basic wet compression approach is the loss of flexibility since the circulation ratio and mixture composition can no longer be varied during operation.

In order to keep the flexibility of the ACHP cycle combined with the advantages of increased internal heat exchange, the modification of the single-stage solution circuit towards the two-stage solution circuit, as shown in Figure 2b, was investigated by Radermacher (1988) [38], Rane and Radermacher (1991) [39] and (1993) [40]. Here, two solution circuits are staggered, connected with an intermediate absorber–desorber pair for internal heat exchange. Occurring concentration differences between the solution circuits are compensated by a bleed line. The lean solution from the low temperature circuit is fed into the rich solution of the high temperature circuit. This modification and the reduced temperature differences for each stage enable the system to achieve high temperature lifts of up to 100 K at comparatively modest pressure ratios, which can be achieved with a single compressor stage. Compared to a single fluid VCHP, a reduction in the required pressure ratio of 40% to 65% and a resulting improvement in COP can be achieved for a given temperature lift [41]. However, because both stages are supplied with vapor by the compressor, the capacity will be reduced by 45%. This leads to a necessary increase in mass flow, which however can have a positive effect on the selection and performance of a suitable compressor.

The vapor compression cycle with solution circuit and desorber/absorber heat exchange (DAHX) cycle, as shown in Figure 2c, was investigated by Groll and Radermacher (1994) [42]. In this approach, the gliding temperature intervals of desorber and absorber are further increased, allowing them to overlap. A portion of the heat transferred internally from absorber II to desorber II. As a result, the DAHX cycle only requires one solution pump and compressor while having similar characteristics to a two-stage solution circuit. Due to the internal heat exchange, the required pressure ratio for a temperature lift of 75 K can be reduced by up to 75% compared to a single fluid VCHP, with a possible COP increase of more than 40%. However, using only one solution circuit results in a loss of flexibility regarding the temperature glides, whereby the temperature intervals are dependent on the pressure ratio and can no longer be selected independently.

Figure 3 shows a simplified comparison of the described ACHP cycles for the operation in a defined temperature interval in a ln p–1/T diagram for ammonia-water mixture.

Here, all cycles start for identical composition and given source temperature at the same desorber pressure. The single-stage ACHP cycles require the largest pressure ratio to reach the desired sink temperature. The ACHP with two-stage solution circuit features two separate heat transfer arrows due to the extra absorber–desorber pair and reaches the absorber temperature at a lower pressure ratio. The DAHX cycle with the linked heat exchange requires the lowest pressure ratio.

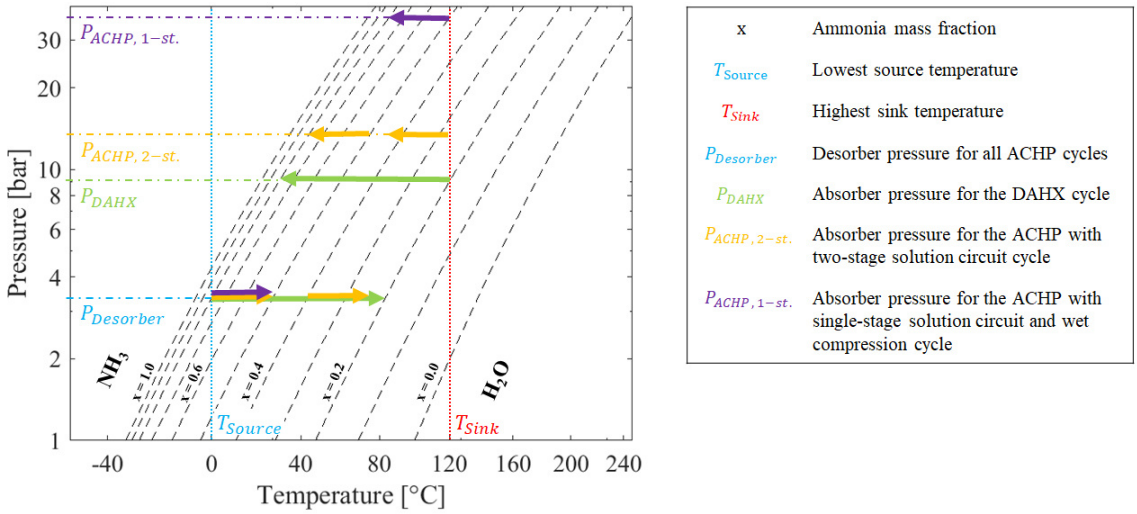

Figure 3. Simplified comparison of the described ACHP cycles in a ln p–1/T diagram (adapted from Groll (1997) [18]).

Based on the presentation of the cycle modifications, it can be concluded that each cycle provides specific advantages and associated application areas. The ACHP with single-stage solution circuit is considered most suitable for conventional applications with the advantage of adjustable temperature glides and capacity. Wet compression can help to solve occurring problems such as high compressor discharge temperatures. The two-stage solution circuit is considered a promising approach for applications with the highest temperature lift and small temperature glide, while the DAHX cycle achieves considerable temperature glides with lower temperature lift [43].

3. State of Technology

In the following, the state of technology for the ACHP system using ammonia-water mixture as working fluid will be examined based on the experimental work carried out. The experiments conducted until 1994 were comprehensively discussed by Groll (1997) [21] with an update of experiments until 2001 by Nordtvedt (2005) [44]. Based on these results, Table 1 presents an updated overview of conducted experimental investigations.

Table 1. Overview of experimental investigations on ammonia-water absorption–compression heat pump cycles.

Author (Location)	Year	Cap. [kW]	T_{source} [°C]	T_{sink} [°C]	$\Delta T_{m,lift}$ [K]	COP [-]	Compressor Design	Absorber Design	Desorber Design	Ref.
ACHP with single-stage solution circuit										
Bercescu et al. (Romania)	1983	15	24	59	n/a	4.9	oil, recip, t-st	n/a	n/a	[45]
Pop et al. (Romania)	1983	4500	36 to 30	45 to 55	16.9	2.6	dry, recip, s-st	Shell/tube horizontal	Shell/tube horizontal	[46,47]
Mučić, Scheuermann (Germany)	1984	160	60 to 45	25 to 78	−5.6	11.3	oil, recip, s-st	Shell/tube horizontal	Shell/tube horizontal	[48]
Stokar, Trepp (Switzerland)	1987	15	40 to 15	40 to 70	28.1	4.3	dry, recip, s-st	Shell/tube vertical	Shell/tube vertical	[49]
Mučić (Germany)	1989	1000	95 to 95 (const.)	115 to 115 (const.)	20.0	9.1	dry, screw, s-st	Shell/tube vertical	Shell/tube vertical	[50]
Rane et al. (USA)	1989	7	15 (avg.)	45 (avg.)	n/a	3.7	dry, recip, t-st	Shell/tube vertical	Shell/tube vertical	[51]
Baksaas, Grandum (Norway)	1999	60	48	48 to 100	n/a	2.1	oil, recip, t-st	Corrugated PHE	Corrugated PHE	[22]
Mongey et al. (North Ireland)	2001	13.5	42 to 27	42 to 57	15.2	3.7	oil, recip, s-st	Corrugated PHE	Corrugated PHE	[52]
FKW (Germany)	2003	27	43 to 35	60 to 72	27.0	4.3	oil, twin screw, s-st	Corrugated PHE	Corrugated PHE	[53]
Risberg et al. (Norway)	2004	300	50 to 15	50 to 85	36.9	n/a	oil, recip, t-st	Corrugated PHE	Corrugated PHE	[23]
Nordtvedt (Norway)	2005	47	50 to 17	50 to 93	38.7	2.4	oil, recip, t-st	Corrugated PHE	Corrugated PHE	[44]
Nordtvedt et al. (Norway)	2011	650	48 to 38	48 to 87	22.8	4.5	oil, recip, t-st	Corrugated PHE	Corrugated PHE	[24]
Kim et al. (Republic of Korea)	2013	10	50 to 30	50 to 90	28.9	3.0	oil, recip, t-st	Corrugated PHE	Corrugated PHE	[54]
Jung et al. (Republic of Korea)	2014	7.3	50 to 30	50 to 81	25.1	2.7	oil, recip, s-st	Corrugated PHE	Corrugated PHE	[55]
Markmann et al. (Germany)	2019	40	59 to 49	50 to 60	1.0	2.5	oil, twin screw, s-st	Corrugated PHE	Corrugated PHE	[56]
Ahrens et al. (Norway)	2021	940	67 to 60	73 to 95	20.1	5.9	oil, recip, t-st	Corrugated PHE	Corrugated PHE	[25]

Table 1. *Cont.*

Author (Location)	Year	Cap. [kW]	T_{source} [°C]	T_{sink} [°C]	$\Delta T_{m,lift}$ [K]	COP [-]	Compressor Design	Absorber Design	Desorber Design	Ref.
Wet compression cycle										
Malewski (Germany)	1988	500	35	60 to 80	n/a	4.4	wet, screw, s-st	Shell/tube horizontal	Shell/tube horizontal	[57]
Bergmann, Hivessy (Hungary)	1990	1000	25 to 5	15 to 85	27.9	4.4	wet, screw, s-st	Shell/tube horizontal	Shell/tube horizontal	[35]
Torstensson, Nowacki (Sweden)	1991	1.4	16 to 3	35 to 60	38.6	3.0_C	wet, scroll, s-st	Tube/tube coaxial	Tube/tube coaxial	[58]
Itard (Netherlands)	1998	13	44 to 38	40 to 53	5.3	3.1	wet, liquid ring, s-st	Plate-fin vertical	Plate-fin vertical	[59]
Zaytsev (Netherlands)	2003	18.9	70 to 65	76 to 92	16.3	1.4	wet, twin screw, s-st	Shell/tube vertical	Shell/tube vertical	[60]
ACHP with two-stage solution circuit										
Rane, Radermacher (USA)	1991	4.2	4 to −5	96 to 104	100.5	1.0_C	dry, recip, t-st	Shell/tube vertical	Shell/tube vertical	[39]
ACHP with single circuit and desorber/absorber heat exchange (DAHX)										
Groll, Radermacher (USA)	1994	5	0 to −6	58 to 74	68.7	0.9_C	dry, recip, t-st	Shell/tube vertical	Shell/tube vertical	[42]

Explanations: Cap.: Heating capacity; **$\Delta T_{m,lift}$:** Total temperature lift determined as the difference of the logarithmic mean temperatures; **COP:** $_C$: Cooling COP; **Compressor design:** oil: Oil-lubricated; dry: Oil-free; wet: Lubrication done by solution; recip: Reciprocating compressor; s-st: Single-stage compression; t-st: Two-stage compression; **Absorber/Desorber design:** PHE: Plate heat exchanger; **Ref.:** Reference.

As initially described, the first commercially used ACHP systems were commissioned in recent years. Here, the ACHP cycle with single-stage solution circuit using a two-stage compression with intercooling and desuperheater before the mixing at the absorber inlet was implemented. The ACHP cycle with single-stage solution circuit is the most frequently experimental investigated cycle, accounting for 16 publications identified from 1983 until 2021. The installed capacities range from laboratory plants starting from 7 kW up to industrial pilot plants with capacities ranging from 160 kW up to 4500 kW. An identical inlet temperature was often selected for source and sink temperatures of laboratory systems, whereby a larger temperature glide was usually achieved on the sink side. The highest achieved sink temperature was at constant 115 °C during a steam generation process, with many other attempts frequently ranged below 100 °C due to the limitation of the open auxiliary circuits used. Due to large temperature glides occurring in the heat sink and source of ACHP cycles, the total temperature lift $\Delta T_{m,lift}$ is employed to evaluate the experimentally achieved temperature lifts, as suggested by Lorenz (1895) [61]. The $\Delta T_{m,lift}$ was determined as the difference of the logarithmic mean temperatures of the secondary fluids for heat sink and source using Equations (1) and (2):

$$\Delta T_{m,lift} = \Delta T_{m,log,Sink} - \Delta T_{m,log,Source} \quad (1)$$

$$\Delta T_{m,log} = \frac{T_{secondary\ fluid,in} - T_{secondary\ fluid,out}}{\ln \frac{T_{secondary\ fluid,in}}{T_{secondary\ fluid,out}}} \quad (2)$$

For the total temperature lift of the ACHP cycle with single-stage solution circuit, values ranging from −5.6 K to 38.7 K were achieved. As mentioned earlier, through the temperature glides occurring in the heat source and sink in combination with a large total temperature lift, a simultaneous use for cooling and heating demands is possible, as shown by Nordtvedt (2005) [44]. COPs of 2.1 to 11.3 were achieved, whereby a direct comparison is difficult due to the different temperature levels and stages of optimization (insulation, compressor size, pinch in heat exchanger). Regarding the compressor design, oil-lubricated reciprocating compressors with single or two-stage compression were used in most investigations. Two times twin screw compressors with oil lubrication and oil cooling were used. Only four cases of oil-free operation involving three reciprocating compressors (two single-stage and one two-stage compression) and one screw compressor were tested. The oil-lubricated two-stage reciprocating compressors often achieved the highest temperature lifts, proportional to the required pressure ratio. Here, intercooling with an additional heat exchanger between the compression stages was frequently used to reduce the occurring discharge temperature. In the absorber and desorber design, an evolution from shell-and-tube to corrugated plate heat exchangers (PHE) can be seen, and the alignment changed from horizontal to vertical. In this context, several innovative approaches have been employed. Mučić and Scheuermann (1984) [48] investigated a subdivision of the heat exchanger surface with linking solution pumps. The connection of several PHEs to extend the effective heat transfer length in combination with different operation modes, described as falling film and bubble mode, as well as mixing techniques were evaluated during the investigations by several authors [20,21,41,50].

The wet compression cycle has been investigated in five experimental studies. The first of these are industrial pilot plants with capacities of 500 kW and 1000 kW, which follow in time with the first installation of the single-stage ACHP pilot plants. Then a wet compression laboratory facility was investigated with one of the smallest capacities of all ACHP cycles at 1.4 kW. The tested temperature levels vary in all investigations with the shared feature of a larger temperature gradient over the heat sink. Single-stage compressors lubricated with the solution were used for all investigations, although a wide variety of different compressor types was tested. Except for the liquid ring compressor employed by Itard (1998) [59], all types were considered suitable for use in wet compression cycles. However, for efficient and reliable use, the authors highlight the importance of modifications, such as selecting suitable bearings and the design of the liquid injection

system [35,57,58,60]. For the design of absorber and desorber, an evolution from horizontal to vertical arrangement was again observed. Additionally, Torstensson and Nowacki (1991) [58] tested a coaxial arrangement of a tube-to-tube heat exchanger. Itard (1998) [59] employed plate-fin heat exchangers with the aim to increase the heat transfer area as a precursor to the commonly used corrugated PHE.

The ACHP with a two-stage solution circuit and the ACHP with a single-stage circuit with DAHX have been studied only once by a group of researchers led by Radermacher [39,42]. The researchers modified an existing single-stage laboratory facility designed by Rane et al. (1989) [51] to investigate the different cycle configurations as previously described. The ACHP with two-stage solution circuit investigated by Rane and Radermacher (1991) [39] had a capacity of 4.2 kW and achieved a total temperature lift of 100.5 K with almost identical temperature glides ranging from 4 °C to −5 °C for the source and from 96 °C to 104 °C for the sink. This enables simultaneous use for cooling and heating and results in a determined cooling COP of 1. Groll and Radermacher (1994) [42] achieved during the investigation of the ACHP with single-stage circuit with DAHX a capacity of 5 kW with a total temperature lift of 68.7 K with temperature glides ranging from 0 °C to −6 °C for the source and from 58 °C to 74 °C for the sink. Despite the lower temperature lift and required pressure ratio, the achieved cooling COP at 0.9 is smaller than the cooling COP obtained for the ACHP with two-stage solution circuit. For both investigations, oil-free two-stage reciprocating compressors with water cooling were used and vertically arranged shell-and-tube heat exchangers were installed as absorber and desorber. Groll and Radermacher (1994) [42] identified a potential COP increase of over 40% by optimizing the compressor for use in the ACHP with single-stage circuit with DAHX.

Identified Existing Challenges

Based on the experimental work presented and discussed in Table 1, the following challenges for the realization of ACHP systems can be identified:

- **Compressor discharge temperature:** Occurring discharge temperatures constrain the achievement of higher sink temperatures, as they can cause problems, such as the decomposition of used lubricating oils and material problems in the compressor.
- **Compressor lubrication:** When oil is used to lubricate the compressor, additional components are needed for separation and cooling, raising the complexity and costs. In addition, the oil tends to penetrate the whole circuit, which requires a recirculation system and can have a negative impact on the heat pump performance.
- **Oil-free operation of the system:** Compressors that can be operated oil-free or for which lubrication is done by the solution are often associated with higher equipment costs due to necessary modifications or are unavailable for commercial use.
- **Absorber and desorber design:** An efficient design of the absorber and desorber is an important factor in improving the performance of the system. Therefore, an advanced understanding of the occurring heat transfer phenomena is essential, especially for the absorber at high temperature and high-pressure operation.
- **Liquid–vapor mixing and distribution process:** When using PHE, an appropriate selection of the operation mode together with effective liquid–vapor mixing and distribution are important to achieve high overall heat transfer coefficients and system performances.
- **Solution pump:** Cavitation caused by changing low pressure conditions related to rapid changes in compressor operation and operating conditions is a major challenge for the solution pump in ACHP cycles due to the saturated liquid leaving the liquid–vapor separator.

4. Identification of Recent Developments and Possible Solutions

The current working domain of ammonia-water ACHP with single-stage solution circuit using components up to 28 bar and dry compression are between 0 °C (freezing of solvent) and 127 °C (calculation by Jensen et al. (2015) [10]). The upper limit originates in a

constrained compressor discharge temperature of 170 °C. The same calculations indicate that by using several high-pressure components, an extension of the upper limit to 193 °C is possible. Additionally, sink temperatures of more than 127 °C can be achieved with 28-bar components through measures such as oil cooling, liquid injection or wet compression. In the following, recent developments and possible solutions for the implementation of ACHP systems are identified based on the performed experimental work and accompanying theoretical studies. The grouping is based on the identified challenges and the order on the relevance to improve system performance and achievable parameters.

4.1. Compressor Solutions

To enable high temperature lifts and sink discharge temperatures, it is necessary to provide a high discharge pressure and pressure ratio. During compression of the ammonia vapor the discharge temperature is comparatively high due to the relatively low density and specific heat capacity of ammonia in the superheated vapor phase [62]. High discharge temperatures reduce the COP of the system and cause various problems, such as chemical decomposition of the working fluid, carbonization of the lubricant and collapse of seals [18]. Additionally, liquid portions can be included even for dry compression depending on the temperature and pressure level due to the characteristics of the ammonia-water mixture. Therefore, the compressor must be resistant to small amounts of liquid in the vapor stream during the compression. This is, furthermore, a fundamental requirement for wet compression. According to an extensive analysis by Zaytsev (2003) [60] and in agreement with the findings presented in Table 1, positive displacement compressors, such as reciprocating and screw compressors, have been identified as promising compressor solutions due to the higher achievable pressure ratios and the lower swept volumes when compared with dynamic compression systems. To reduce the superheat occurring during compression and maintain the discharge temperature in an acceptable range for the compressor, different potential compressor solutions are available for the implementation besides simple single-stage compression, as shown in Figure 4.

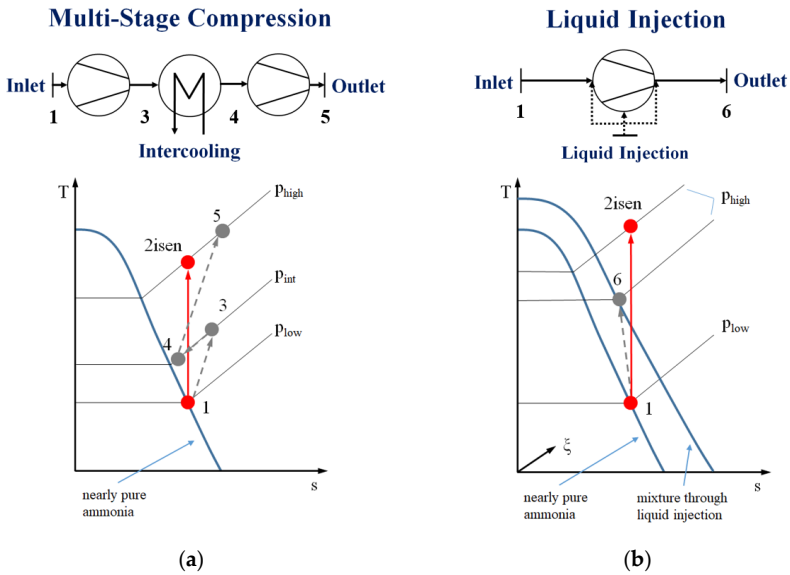

(**a**) (**b**)

Figure 4. Different potential compressor solutions (simplified) illustrated with T-s diagrams of nearly pure ammonia including isentropic compression (solid red line) compared to: (**a**) Divided multi-stage compression with intercooling through an additional IHX and (**b**) single-stage compression with liquid injection (dashed grey lines).

The simplified compression processes are illustrated in T-s diagrams for nearly pure ammonia to demonstrate the proposed possibilities. The isentropic compression (from point 1 to 2_{isen}) demonstrates the ideal compression process from the low-pressure to the high-pressure level. However, the achieved discharge temperature during real compression is significantly higher due to the occurring losses and irreversibility. Here, the identified maximum temperature for the compressor of 170 °C can be quickly exceeded. In the case of liquid injection, the composition of the working fluid changes during the compression process, adding another level to the representation.

As shown in Figure 4a, the first possible solution is to divide the compression into two or more stages with an additional IHX for cooling the vapor after each stage (from point 1 to 5). Therefore, multi-stage compression with intercooling can increase the achievable pressure ratio. The functionality of this solution with two-stage reciprocating compressors and intercooler connected to the lean solution circuit has been experimentally proven by various authors [22,44,45,54]. Moreover, there are other approaches for the implementation of intercooling. Jensen (2015) [18] investigated the effect of the positioning of the intercooler (upstream or downstream of the contained solution IHX between rich and lean solution) as well as other alternatives, such as the use of a bubble through intercooler or mixing option with liquid injection. He concluded that the solution with an additional IHX downstream the contained solution IHX can most effectively reduce the discharge temperature and costs for a multi-stage compression system.

Another promising solution, as shown in Figure 4b, is the use of a liquid-resistant single-stage compressor with the implementation of liquid injection (oil or oil-free using the working fluid) during the compression process (from point 1 to 6). The injection can take place at various compression grades (point of injection) and allows to provide different functions such as sealing, lubrication and lowering the vapor temperature during compression [63]. The point of injection and amount of the injected liquid is a matter of optimization [64]. If all the liquid is carried along with the vapor, it is defined as wet compression [34]. Bergmann and Hivessy (1990) [35] stated that the liquid injection makes the compressor operation smoother and more silent than dry compression. However, especially for operation as wet compression, the isentropic efficiencies obtained are often comparatively low due to the complexity of the compression process, causing various challenges in the design and optimization of the compressor and the injection system [65,66].

4.2. Absorber and Desorber Solutions

Absorber and desorber are critical components of ACHP cycles to achieve higher system efficiencies and obtain higher sink temperatures [54,55]. Many studies have been conducted to understand the characteristics of the occurring processes and thermodynamic properties [67,68]. For use in an ACHP system, various requirements are defined for the heat exchanger properties used. In addition to the general requirements, such as the reduction of size and pressure losses, the suitability for the desired operating parameters must be considered [52]. To reduce installation costs, compact heat exchangers with a high area density (m^2/m^3) of the heat transfer surface combined with a high overall heat transfer coefficient ($kW/(m^2K)$) are desired [69,70]. Furthermore, the establishment of effective liquid–vapor mixing and the complete and continual wetting of the heat transfer surfaces are important [71].

Based on the investigations carried out and the data presented in Table 1, the trend from horizontal to vertical shell-and-tube heat exchangers towards vertical PHE for use in ACHP systems can be recognized. The plates can be pressed with different shapes to increase turbulence, fluid distribution and surface area [72]. Due to these features, the design can be much more compact. In addition, PHE can provide high overall heat transfer coefficients, good wettability and liquid–vapor mixing [55]. Various approaches have been and are being investigated to improve the design and operation of absorber and desorber [73]. It was concluded that longer plates combined with good distribution of the mixture and operation in counter-flow with the coolant have positive effects on the

performance. Jung et al. (2014) [55] stated that increasing the ratio of plate length to gap (L/D) is more important than the ratio of width to gap (W/D) for more effective operation.

Several possibilities are available for the implementation. Due to the similarity of the operating conditions and requirements, the desorber is often designed and operated like a flooded evaporator. The absorber can be operated in falling film mode, where lean solution slides from top to bottom as a thin film on the surface of the vertical plate and vapor filling the free space is absorbed into the liquid film, releasing heat to the coolant. Another approach is to operate the absorber in bubble mode, where the lean solution and vapor are mixed at the bottom before entering the absorber and flow upwards in counter-flow with the coolant [74]. Furthermore, it is possible to operate several PHEs inline using different operating modes [24,54]. Figure 5 shows a schematic representation of a plate heat exchanger operated in counter-flow as absorber in falling film and bubble mode.

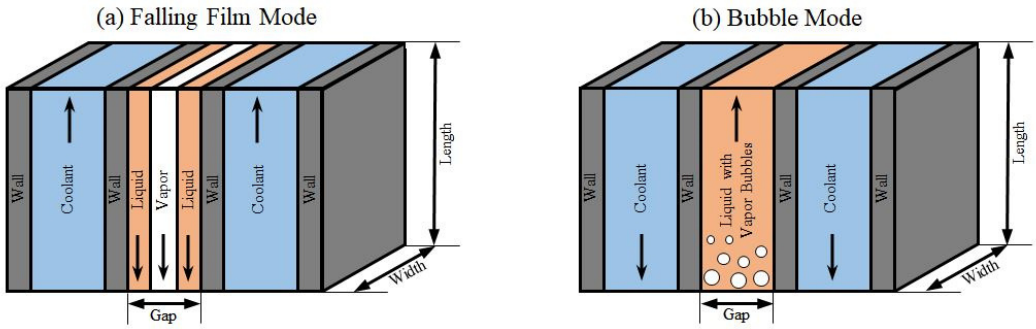

Figure 5. Schematic representation of a plate heat exchanger operated as absorber in (**a**) falling film and (**b**) bubble mode (adapted from Ahrens et al. (2019) [75]).

Bubble mode operation in the absorber of PHE in an ACHP cycle was investigated by An et al. (2013) [74]. They concluded that higher pressure is a more significant factor for increasing the heat exchanger performance than size based on experiments with different sized PHE. The maximum overall heat transfer coefficients achieved for different PHE sizes were between 0.96 and 1.61 kW/m^{2}K. In contrast, Lee et al. (2002) [76] reported values between 0.3 and 0.55 kW/(m^{2}K) at lower temperatures in a PHE test facility. More experimental data from Nordtvedt (2005) [77] for bubble and falling film absorber were between 0.6 and 1.4 kW/(m^{2}K) and for bubble desorber between 0.4 and 1.5 kW/(m^{2}K). Táboas et al. (2010) [78] stated for a bubble desorber, that pressure has only a slight influence and mass flux a major influence. Measured overall heat transfer coefficients varied between 2.5 and 4.1 kW/(m^{2}K). Due to many parameters affecting the absorption and desorption process, which are not all documented in these sources, a direct comparison or deducing trends becomes impossible. However, it can be concluded that the overall heat transfer coefficients can vary considerably depending on the given operating conditions and other factors such as the liquid–vapor distribution. Determining and predicting the required parameters more accurately for the design and controlling of ACHP cycles is an important goal to further disseminate ACHP technology for use in industrial applications.

4.3. Solution Pump Solutions

Cavitation is a major challenge for the solution pump in ACHP cycles. The saturated liquid coming from the liquid–vapor separator is very sensitive to changing low-pressure conditions caused by the compressor. The evaluation of the sources given in Table 1 shows that mainly centrifugal pumps for industrial pilot plants and diaphragm pumps for small laboratory facilities are used as solution pumps. To reduce the risk of cavitation, different approaches have been investigated. Besides the generally important reduction of pressure losses upstream of the pump inlet, the external subcooling of the lean solution, as used

by Rane et al. (1989) [51], is one possible solution. Additionally, experiments with an upstream booster pump or a special design of the separator to provide enough static height of the liquid level for the pressure increase upstream of the solution pump have been investigated by various researchers [44,55,56]. Furthermore, Risberg et al. (2004) [23] and Markmann et al. (2019) [56] introduced an option to control the liquid level in the high-pressure receiver by regulating the expansion valve to keep the low pressure stable and reduce the risk of cavitation due to rapid pressure changes.

4.4. Alternative Working Fluid Pairs

In general, all working fluid pairs suggested for absorption heat pumps may also be used in ACHP cycles [79]. The unique feature of a working fluid pair is a greater temperature glide during complete evaporation and condensation compared to the glide of heat source and sink, causing the partial phase change that makes a solution circuit necessary. For a comprehensive review and possible identification of interesting alternatives, Table 2 lists an overview of literature sources investigating alternative working fluid pairs besides ammonia-water for use in ACHPs. There are mainly theoretical studies with few experimental investigations on a laboratory scale (below 30 kW heating capacity).

Following the Montreal Protocol and Kyoto Protocol addressing the ozone depletion potential (ODP), the main issues in recent years have been the EU Regulation No. 517/2014 (2014) [80], also known as F-Gas Regulation, and the European Directive 2006/40/EC (2006) [81], establishing very strict limits on the GWP values of applicable refrigerants. Due to this legislation, many sources dealing with substances having an ODP > 0 or a GWP > 1000 are not listed and will not be discussed further. The Globally Harmonized System of Classification and Labelling of Chemicals (GHS) classification was carried out using the "GESTIS-Stoffdatenbank" [82]. Maximum workplace concentration (MAK) values are taken from the "DFG MAK- und BAT-Werte-Liste 2020" [83]. The applicable temperature range is defined so that saturation pressure is between 1 and 25 bar. If 200 °C is still possible at the sink with a vapor pressure below 25 bar, 200 °C is assumed to be the upper limit.

Table 2. Overview of alternative working fluid pairs proposed in the literature for use in ACHP cycles.

Author (Location)	Year	Exp.	Refrigerant	GHS	Absorbent	GHS	T_{min}/T_{max}	Ref.
Inorganic Refrigerant								
Åhlby, Hodgett (Sweden)	1990		NH_3 (1)		H_2O (2) /LiBr (3)	-/	0/200	[84]
Chatzidakis, Rogdakis (Germany)	1992		NH_3 (1)		H_2O (2) /LiBr (3)	-/	0/200	[85]
Tarique, Siddiqui (India)	1999		NH_3 (1)		NaSCN (4)		−35/160	[86]
Hannl (Austria)	2015	X	NH_3 (1)		$LiNO_3$ (5)		−40/200	[87]
Herold et al. (USA)	1991		H_2O (2)	-	LiBr (3)		0/200	[88]
Ansari et al. (India)	2018		H_2O (2)	-	LiBr (3)		0/200	[89]
Gudjonsdottir et al. (Netherlands)	2017		NH_3 (1) /CO_2 (6)		H_2O (2)	-	0/200	[90]
Groll, Kruse (Germany)	1992	X	CO_2 (6)		Acetone (7)		−40/80	[91]
Moreira-da-Silva et al. (Spain)	2019		CO_2 (6)		Acetone (7)		−40/80	[92]
Aldás (Spain)	2020		CO_2 (6)		Acetone (7)		−40/80	[93]

Table 2. *Cont.*

Organic Refrigerant								
Endo et al. (Japan)	2007		DME [8]		MeOH [9]		−30/200	[94]
Kawada et al. (Japan)	1991	X	TFE [10]		TEGDME [11]		75/200	[95]
Nogues et al. (Spain)	1997		TFE [10], MeOH [9]		TEGDME [11]		65/200	[96]
Bourouis et al. (Spain)	2000		TFE [6]/H_2O [2]		TEGDME [11]		75/200	[97]
Mestra et al. (Spain)	2003	X	TFE [10], MeOH [9],		PEGDME 500 [12]	n/s	65/200	[98]
	2005		HFIP [13]					[99]

Explanations: Exp.: Experimental work available; **GHS:** Globally Harmonized System of Classification and Labelling of Chemicals; **T_{min}/T_{max}:** Applicable temperature range; n/s: not specified; CAS: Chemical Abstracts Service; MAK: Maximum workplace concentration; [1] **Ammonia (NH_3)** | 7664-41-7—CAS Registry Number | 14 (mg/m^3)—MAK value; [2] **Water (H_2O)** | n/s—CAS Registry Number | n/s (mg/m^3)—MAK value; [3] **Lithium bromid (LiBr)** | 7550-35-8—CAS Registry Number | n/s (mg/m^3)—MAK value; [4] **Sodium thiocyanate (NaSCN)** | 540-72-7—CAS Registry Number | n/s (mg/m^3)—MAK value; [5] **Lithium nitrate ($LiNO_3$)** | 7790-69-4—CAS Registry Number | n/s (mg/m^3)—MAK value; [6] **Carbon dioxide (CO_2)** | 124-38-9—CAS Registry Number | 9100 (mg/m^3)—MAK value; [7] **Acetone** | 67-64-1—CAS Registry Number | 1200 (mg/m^3)—MAK value; [8] **Dimethyl ether (DME)** | 115-10-6—CAS Registry Number | 1900 (mg/m^3)—MAK value; [9] **Methanol (MeOH)** | 67-56-1—CAS Registry Number | 130 (mg/m^3)—MAK value; [10] **2,2,2-Trifluoroethanol (TFE)** | 75-89-8—CAS Registry Number | n/s (mg/m^3)—MAK value; [11] **Tetraethylene glycol dimethyl ether (TEGDME)** | 143-24-8—CAS Registry Number | n/s (mg/m^3)—MAK value; [12] **Polyethylene glycol dimethyl ether (PEGDME 500)** | 24991-55-7—CAS Registry Number | n/s (mg/m^3)—MAK value; [13] **Hexafluoroisopropanol (HFIP)** | 920-66-1—CAS Registry Number | n/s (mg/m^3)—MAK value.

There were 13 alternative working fluid pairs investigated in the literature, divided into inorganic and organic refrigerants with TFE and HFIP as the only non-natural refrigerants. Except for CO_2/Acetone and NH_3/NaSCN, the applicable temperature range is always 200 °C or higher. However, the minimum temperature depends strongly on the refrigerant selected and is generally lower for inorganic refrigerants. A further comparison of the cycle performance among the working fluid pairs is not appropriate due to the large differences in vapor pressure.

Åhlby and Hodgett (1990) [84] as well as Chatzidakis and Rogdakis (1992) [85], added LiBr as absorbent to the ammonia-water mixture and studied the suitability of the three-component mixture for the ACHP cycle. They stated inconsistent results regarding the improvement potential and recommended further investigations. Tarique and Siddiqui (1999) [86] and Hannl (2015) [87] investigated NH_3 paired with salts to increase the amount of refrigerant in the gas phase, eliminating the separation that may be required at increased source temperatures to reduce the water content in the vapor phase. Conducted experiments demonstrated the general functionality of this approach, although further research is required to establish prototypes and applications. The investigations on H_2O/LiBr in a temperature range between 2 °C and 35 °C, done by Ansari et al. (2018) [89], and in double-effect cycles, done by Herold et al. (1991) [88], are both far from practical application. Gudjonsdottir et al. (2017) [90] paired NH_3 with CO_2 and H_2O in a wet compression cycle. The simulations of these cycles predict advantages in efficiency by increasing the amount of CO_2. However, there are many uncertainties like the formation of solid phases, ternary property data and the compressor model used so that the authors suggest experimental validation as a necessary next step. CO_2/Acetone is an interesting working fluid pair for safety aspects, but with standard components only feasible below 80 °C. Experiments by Groll and Kruse (1992) [91] and Groll (1994) [100] revealed poor heat transfer properties with the coaxial heat exchangers used and little further experience with this working fluid pair in the literature. In recent years, the thermodynamic properties have been increasingly studied experimentally, and Moreira-da-Silva et al. (2019) [92] simulated the usability for ACHP cycles in automotive air conditioning based on the available composition data. Aldás (2020) [93] conducted thermodynamic modelling and simulation of the cycle and theoretical-experimental investigations of the desorption process in a PHE.

DME/MeOH was theoretically investigated by Endo et al. (2007) [94] in the temperature range between 7 °C and 60 °C for the single stage cycle and the DAHX cycle. The differences in efficiency between pure DME and the mixture in both cycles were small. They suggest to further proof their findings in experiments. TEGDME or PEGDME as solvent use flammable and toxic TFE or MeOH as the refrigerant. These mixtures are suitable for temperatures above 65 °C and PEGDME for cases where the compressor may be lubricated by the lean solution [98]. Kawada et al. (1991) [95] stated that TFE/TEGDME shows good thermal stability and no corrosion on copper or carbon steel up to 180 °C. Nogues et al. (1997) [96] investigated the performance for TFE/TEGDME and MeOH/TEGDME for use in the single-stage and DAHX cycles. They reported interesting features for use in high temperature applications with better results for TFE/TEGDME and suggested further investigations. Bourouis et al. (2000) [97] conducted further investigations for a three-component mixture with additional water and reported further benefits such as an improvement in performance. Mestra et al. (2003) [98] investigated the working pairs TFE/PEGDME and MeOH/PEGDME to develop a 15 kW pilot plant. Here, MeOH was selected as the refrigerant for further investigations due to the lower pressure ratio required. In addition, Mestra (2005) [99] investigated the working pair HFIP/PEGDME, which was not tested experimentally. Besides theoretical studies, so far, there is only little experimental experience with the use of alternative working fluid pairs in ACHP cycles. Therefore, further investigations are essential for a successful implementation.

4.5. Summary of Existing Solutions

Figure 6 summarizes recent developments and existing solutions for the realization of ACHP systems. The classification is based on the previously presented and discussed solutions. The fields highlighted in green indicate the currently most frequently used solutions for commercial applications of each system part. All other solutions have at least been tested on a laboratory scale and often need further investigation for commercial use.

Figure 6. Overview of recent developments and existing solutions for the realization of ACHP systems (fields highlighted in green indicate the currently most frequently used solutions for commercial applications of each system part).

Four different cycle configurations were discussed for the design of the ACHP system, whereby the ACHP with single-stage solution circuit was most frequently investigated and is used commercially today. The compressor, as a major component and constraint for achieving higher sink discharge temperatures, features a wide range of solutions. Against the background of reducing occurring compressor outlet temperatures and costs, several types with different compression stages and lubrication solutions were used and studied. For commercial applications, oil-lubricated reciprocating compressors with two-stage compression and intercooling are currently employed. For the absorber and desorber, vertically aligned PHEs are used in different operating modes with the associated mixing devices. The specific design and operation remain a subject of ongoing research to further increase the efficiency while reducing the required size and costs. In addition to the general low placement of the solution pump and the design of the pipes with as little pressure loss as possible, a high static height of the liquid level upstream the pump inlet is achieved by the strategic design of the liquid–vapor separator. There have been many primarily

theoretical studies on alternative working fluid pairs, yet experimental experience for use in ACHP systems is limited to ammonia-water. The use and combination of other presented solutions are explicitly not excluded to overcome existing challenges. Depending on the circumstances, a follow-up and combination of other solutions can be a promising approach to improve the achievable operating parameter and efficiency to increase the suitable application range and competitiveness compared to VCHPs and conventional solutions for industrial high temperature applications.

5. Future Trends

In recent years, there has been a growing demand in the utilization of ACHPs with ammonia-water as working fluid for high temperature industrial applications [18,25]. The research focuses on achieving higher sink temperatures and system efficiencies to increase the suitable application range and competitiveness compared to VCHPs and conventional solutions. Here, the aim is to describe possible future trends to overcome the identified challenges by using conducted research and recent developments and solutions as a source of ideas for potential approaches for further research. Various approaches are used for achieving this aim:

- For the general system design, the ACHP with single-stage solution circuit has been used commercially. Nevertheless, there is still potential for further improvements, such as the optimized system control in case of varying operating conditions [18].
- To increase the application range and competitiveness of the ACHP, cost-effective and simple compressor solutions will be utilized. Besides using multistage oil-lubricated reciprocating compressors, the single-stage screw compressors with liquid injection and lubrication with the solution will be implemented as an alternative. In contrast to dry compression, the advantages of wet compression with reduced superheating and low discharge temperature can be beneficial [63]. In addition, the removal of the lubricating oil can lead to a reduction in the complexity and cost of the system. However, recent studies by Ahrens et al. (2019) [75,101] and Gudjonsdottir et al. (2019) [66] have indicated that suitable compressors are not yet commercially available and require further research and development. Insights and findings can be gained from related studies dealing with oil (Wu et al. (2017) [102]) or pure refrigerants as ammonia (Tian et al. (2017) [65]) and water (Wu et al. (2020) [5]).
- For the design and operation of absorber and desorber, there is a clear trend towards vertical PHE. This is often associated with factors such as compact design and cost-effective production. However, important factors for the efficiency, such as the liquid–vapor mixing and distribution, are often difficult to determine and thus challenging to predict for varying operating parameters [73]. The application of additive manufacturing techniques to produce plates and the liquid–vapor distribution may offer interesting possibilities. Solving the distribution challenge and being able to determine and predict the required parameters more accurately for the design and controlling of ACHP cycles, especially considering the desired high temperature operation, is an important goal of further research.
- In addition to the static height, a possible sub-cooling of the lean solution upstream of the inlet can result in a sustainable operation of the solution pump.
- For the use of alternative working fluid pairs in ACHP cycles, there is so far only little experimental experience apart from theoretical studies besides ammonia-water, as presented in Section 4.4. However, the use of alternative working fluid pairs is a promising solution.

In summary, different research trends for the use of ACHP systems at high temperature operation can be identified. To address the identified challenges and increase the application range and competitiveness with respect to other systems, future research should focus on the development of (oil-free) liquid-injected compressors and the efficient design and operation of the absorber and desorber.

6. Conclusions

This work presents the current state of technology and aims to identify existing challenges and future trends for the utilization of ACHPs at high temperature operation. Different modifications of the ACHP cycle were presented and discussed in detail. Furthermore, a comprehensive overview of conducted experimental work was given concerning the described cycle modifications and existing challenges were identified. Recent developments and possible solutions were discussed based on current research activities and summarized in a detailed mind map. Finally, possible future trends for further research activities were defined. The following conclusions for the ACHP technology can be drawn:

- Interest in the ACHP system has grown in recent years and has been supported by the successful implementation of first commercial units.
- Many studies, both theoretical and experimental, focused on improving the achievable operating parameter and system efficiency to increase the competitiveness compared to VCHPs and conventional solutions for industrial high temperature applications.
- Various configurations of the ACHP system with special characteristics have been developed and studied. The ACHP with a single-stage solution circuit was most widely investigated and is the only configuration in commercial use today. With the aim of further optimization of the ACHP system, existing challenges for the main components such as compressor, absorber/desorber and solution pump were identified based on the conducted research.
- Compressors used so far have been positive displacement compressors such as reciprocating, screw and scroll. For the achievable parameters of the ACHP system, the compressor is a constraining component and associated with challenges, such as discharge temperature, lubrication, efficient and oil-free operation of the system. A variety of possible solutions to address these challenges, such as multi-stage compression with intercooling or liquid injection, were investigated.
- Different types and configurations of heat exchangers have been used. For the design and operation of absorber and desorber, a clear trend towards vertically arranged PHEs has emerged. However, there are still challenges associated with the optimal design to achieve good liquid–vapor distribution and achieving high overall heat transfer coefficients. The ability to determine and predict the parameters required for the design and control of absorber and desorber more accurately is an important goal in further disseminating ACHP technology for use in industrial applications.
- Various strategies to avoid cavitation in the solution pump have been successfully implemented and tested, thus this problem discussed in earlier literature was solved.
- In addition to ammonia-water, a variety of alternative working fluid pairs for use in ACHP systems have been investigated. Further research and development are required to evaluate the reported potential improvements in a practical application.
- Based on the conducted investigations as well as recent developments and solutions, the future trends for further research were defined for all identified challenges.
- For the increased use of ACHP systems in high temperature applications, future research should focus on the development of (oil-free) liquid-injected compressors and the efficient design and operation of the absorber and desorber.

Author Contributions: Conceptualization, M.U.A., M.L., I.T., A.H., S.K., R.W. and T.M.E.; methodology, M.U.A., M.L. and I.T.; investigation, M.U.A., M.L. and I.T.; resources, M.L., A.H., S.K., R.W. and T.M.E.; writing—original draft preparation, M.U.A.; writing—review and editing, M.U.A., M.L., I.T., A.H., S.K., R.W. and T.M.E.; visualization, M.U.A.; supervision, I.T., A.H., S.K., R.W. and T.M.E.; project administration, M.U.A.; funding acquisition, A.H., R.W. and T.M.E. All authors have read and agreed to the published version of the manuscript.

Funding: This research was funded by Research Council of Norway as part of HighEFF—Centre for an Energy Efficient and Competitive Industry for the Future, an 8-year Research Centre under the FME-scheme (Centre for Environment-friendly Energy Research, 257632).

Institutional Review Board Statement: Not applicable.

Informed Consent Statement: Not applicable.

Data Availability Statement: Data sharing not applicable.

Acknowledgments: The work is part of HighEFF—Centre for an Energy Efficient and Competitive Industry for the Future, an 8-year Research Centre under the FME-scheme (Centre for Environment-friendly Energy Research, 257632). The authors gratefully acknowledge the financial support from the Research Council of Norway and user partners of HighEFF.

Conflicts of Interest: The authors declare no conflict of interest.

Abbreviations

The following abbreviations are used in this manuscript:

ACHP	Absorption–compression heat pump
CAS	Chemical Abstracts Service
CFC	Chlorofluorocarbons
COP	Coefficient of performance
DAHX	vapor compression cycle with solution circuit and desorber/absorber heat exchange
GHG	Greenhouse gas
GHS	Globally Harmonized System of Classification and Labelling of Chemicals
GWP	Global warming potential
HTHP	High temperature heat pump
IHX	Internal heat exchanger
MAK	Maximum workplace concentration
ODP	Ozone depletion potential
PHE	Plate heat exchanger
VCHP	Vapor compression heat pump

References

1. Conti, J.; Holtberg, P.; Diefenderfer, J.; LaRose, A.; Turnure, J.T.; Westfall, L. *International Energy Outlook 2016 with Projections to 2040*; USDOE Energy Information Administration (EIA): Washington, DC, USA, 2016.
2. Oluleye, G.; Jobson, M.; Smith, R. Process integration of waste heat upgrading technologies. *Process. Saf. Environ. Prot.* **2016**, *103*, 315–333. [CrossRef]
3. Kosmadakis, G. Estimating the potential of industrial (high-temperature) heat pumps for exploiting waste heat in EU industries. *Appl. Therm. Eng.* **2019**, *156*, 287–298. [CrossRef]
4. Xu, Z.Y.; Wang, R.Z.; Yang, C. Perspectives for low-temperature waste heat recovery. *Energy* **2019**, *176*, 1037–1043. [CrossRef]
5. Wu, D.; Hu, B.; Wang, R.Z.; Fan, H.; Wang, R. The performance comparison of high temperature heat pump among R718 and other refrigerants. *Renew. Energy* **2020**, *154*, 715–722. [CrossRef]
6. Bamigbetan, O.; Eikevik, T.M.; Nekså, P.; Bantle, M. Review of vapour compression heat pumps for high temperature heating using natural working fluids. *Int. J. Refrig.* **2017**, *80*, 197–211. [CrossRef]
7. Yan, H.; Wang, R.; Du, S.; Hu, B.; Xu, Z. Analysis and Perspective on Heat Pump for Industrial Steam Generation. *Adv. Energy Sustain. Res.* **2021**, *2000108*, 2000108. [CrossRef]
8. Ommen, T.; Jensen, J.K.; Markussen, W.B.; Reinholdt, L.; Elmegaard, B. Technical and economic working domains of industrial heat pumps: Part 1—Single stage vapour compression heat pumps. *Int. J. Refrig.* **2015**, *55*, 168–182. [CrossRef]
9. Jensen, J.K.; Ommen, T.; Markussen, W.B.; Reinholdt, L.; Elmegaard, B. Technical and economic working domains of industrial heat pumps: Part 2—Ammonia-water hybrid absorption–compression heat pumps. *Int. J. Refrig.* **2015**, *55*, 183–200. [CrossRef]
10. Jensen, J.K.; Markussen, W.B.; Reinholdt, L.; Elmegaard, B. On the development of high temperature ammonia-water hybrid absorption–compression heat pumps. *Int. J. Refrig.* **2015**, *58*, 79–89. [CrossRef]
11. Farshi, L.G.; Khalili, S. Thermoeconomic analysis of a new ejector boosted hybrid heat pump (EBHP) and comparison with three conventional types of heat pumps. *Energy* **2019**, *170*, 619–635. [CrossRef]
12. Zhang, J.; Zhang, H.H.; He, Y.L.; Tao, W.Q. A comprehensive review on advances and applications of industrial heat pumps based on the practices in China. *Appl. Energy* **2016**, *178*, 800–825. [CrossRef]
13. Schlosser, F.; Jesper, M.; Vogelsang, J.; Walmsley, T.G.; Arpagaus, C.; Hesselbach, J. Large-scale heat pumps: Applications, performance, economic feasibility and industrial integration. *Renew. Sustain. Energy Rev.* **2020**, *133*. [CrossRef]
14. Arpagaus, C.; Bless, F.; Uhlmann, M.; Schiffmann, J.; Bertsch, S.S. High temperature heat pumps: Market overview, state of the art, research status, refrigerants, and application potentials. *Energy* **2018**, *152*, 985–1010. [CrossRef]

15. Wu, D.; Jiang, J.; Hu, B.; Wang, R.Z. Experimental investigation on the performance of a very high temperature heat pump with water refrigerant. *Energy* **2020**, *190*, 116427. [CrossRef]
16. Frate, G.F.; Ferrari, L.; Desideri, U. Analysis of suitability ranges of high temperature heat pump working fluids. *Appl. Therm. Eng.* **2019**, *150*, 628–640. [CrossRef]
17. Zühlsdorf, B.; Jensen, J.K.; Cignitti, S.; Madsen, C.; Elmegaard, B. Analysis of temperature glide matching of heat pumps with zeotropic working fluid mixtures for different temperature glides. *Energy* **2018**, *153*, 650–660. [CrossRef]
18. Jensen, J.K. Industrial Heat Pumps for High Temperature Process Applications. Ph.D. Thesis, Technical University of Denmark, Kongens Lyngby, Denmark, 2015.
19. Osenbrück, A. Verfahren zur Kälteerzeugung bei Absorptionsmaschinen. Deutsches Patent 84084, 1895.
20. Altenkirch, E. Kompressionskältemaschine mit Lösungskreislauf. *Kältetechnik* **1950**, *2*, 251–259, 279–284, 310–315.
21. Groll, E.A. Current status of absorption/compression cycle technology. In Proceedings of the ASHRAE Transactions: Tecnical and Symposium Papers, Philadelphia, PA, USA, 24–28 February 1997; Volume 103, pp. 361–374.
22. Baksaas, H.S.; Grandum, S. Initial tests of high temperature absorption/compression heat pump. In Proceedings of the International Sorption Heat Pump Conference, Munich, Germany, 24–26 March 1999; pp. 477–482.
23. Risberg, T.; Horntvedt, B.; Madland, D.; Nordtvedt, S.R. Process dynamics in an industrial prototype compression/absorption heat pump. In *Proceedings of the 6th IIR Gustav Lorentzen Conference*; International Institute of Refrigeration: Glasgow, Scotland, 2004.
24. Nordtvedt, S.R.; Horntvedt, B.R.; Eikefjord, J.; Johansen, J. Hybrid Heat Pump for Waste Heat Recovery in Norwegian Food Industry. In Proceedings of the 10th International Heat Pump Conference, Tokyo, Japan, 16–19 May 2011; pp. 1–5.
25. Ahrens, M.U.; Foslie, S.S.; Moen, O.M.; Bantle, M.; Eikevik, T.M. Integrated high temperature heat pumps and thermal storage tanks for combined heating and cooling in the industry. *Appl. Therm. Eng.* **2021**, *189*, 10. [CrossRef]
26. Van De Bor, D.M.; Infante Ferreira, C.A.; Kiss, A.A. Optimal performance of compression-resorption heat pump systems. *Appl. Therm. Eng.* **2014**, *65*, 219–225. [CrossRef]
27. Jensen, J.K.; Reinholdt, L.; Markussen, W.B.; Elmegaard, B. Investigation of ammonia/water hybrid absorption/compression heat pumps for heat supply temperatures above 100 °C. In *Proceedings of the International Sorption Heat Pump Conference*; Center for Environmental Energy Engineering, University of Maryland: Washington, DC, USA, 2014; pp. 1–10.
28. Gao, P.; Chang, M.M.; Zhang, C.L.; Shao, L.L. System principles and applications of hybrid sorption–compression heat pump—A review. *Int. J. Refrig.* **2019**, *108*, 14–25. [CrossRef]
29. Qing, C.; Gao, P.; Zhang, C.L. Thermodynamic analysis on feasible operating region of two-stage hybrid absorption–compression heat pump cycles. *Int. J. Refrig.* **2021**, *121*, 43–50. [CrossRef]
30. Jung, C.W.; Song, J.Y.; Kang, Y.T. Study on ammonia/water hybrid absorption/compression heat pump cycle to produce high temperature process water. *Energy* **2018**, *145*, 458–467. [CrossRef]
31. Farshi, L.G.; Khalili, S.; Mosaffa, A.H. Thermodynamic analysis of a cascaded compression—Absorption heat pump and comparison with three classes of conventional heat pumps for the waste heat recovery. *Appl. Therm. Eng.* **2018**, *128*, 282–296. [CrossRef]
32. Gao, P.; Qing, C.; Chang, M.M.; Shao, L.L.; Zhang, C.L. Hybrid absorption–compression heat pump with two-stage rectification and subcooler. *Appl. Therm. Eng.* **2020**, *181*, 116027. [CrossRef]
33. Amrane, K.; Rane, M.V.; Radermacher, R. Performance curves for single-stage vapor compression cycles with solution circuit. *J. Eng. Gas. Turbines Power* **1991**, *113*, 221–227. [CrossRef]
34. Hultén, M.; Berntsson, T. The compression/absorption heat pump cycle—Conceptual design improvements and comparisons with the compression cycle. In *Proceedings of the International Journal of Refrigeration*; Elsevier: New York, NY, USA, 2002; Volume 25, pp. 487–497.
35. Bergmann, G.; Hivessy, G. Experimental Hybrid Heat Pump of 1000kW heating capacity. In Proceedings of the 4th International Conference on Applications and Efficiency of Heat Pump Systems, Munich, Germany, 1–3 October 1990; pp. 27–40.
36. Itard, L.C.M.; Machielsen, C.H.M. Considerations when modelling compression/resorption heat pumps. *Int. J. Refrig.* **1994**, *17*, 453–460. [CrossRef]
37. Itard, L.C.M. Wet compression versus dry compression in heat pumps working with pure refrigerants or non-azeotropic mixtures. *Int. J. Refrig.* **1995**, *18*, 495–504. [CrossRef]
38. Radermacher, R. An Example of the Manipulation of Effective Vapor Pressure Curves. *J. Eng. Gas. Turbines Power* **1988**, *110*, 647–651. [CrossRef]
39. Rane, M.V.; Radermacher, R. Experimental investigation on a two stage vapor compression heat pump with solution circuits: Performance enhancement with a bleed line. In Proceedings of the Absorption Heat Pump Conference, Tokyo, Japan, 30 September–2 October 1991; pp. 96–102.
40. Rane, M.V.; Radermacher, R. Feasibility study of a two-stage vapour compression heat pump with ammonia-water solution circuits: Experimental results. *Int. J. Refrig.* **1993**, *16*, 258–264. [CrossRef]
41. Rane, M.V.; Amrane, K.; Radermacher, R. Performance enhancement of a two-stage vapour compression heat pump with solution circuits by eliminating the rectifier. *Int. J. Refrig.* **1993**, *16*, 247–257. [CrossRef]
42. Groll, E.A.; Radermacher, R. Vapor Compression heat pump with solution circuit and desorber/absorber heat exchange. In Proceedings of the International Absorption Heat Pump Conference, New Orleans, LA, USA, 19–21 January 1994; pp. 463–469.

43. Zhou, Q.; Radermacher, R. Development of a vapor compression cycle with a solution circuit and desorber/absorber heat exchange. *Int. J. Refrig.* **1997**, *20*, 85–95. [CrossRef]
44. Nordtvedt, S.R. Experimental and Theoretical Study of a Compression/Absorption Heat Pump with Ammonia/Water as Working Fluid. Ph.D. Thesis, Norweigan University of Science and Technology, Trondheim, Norway, 2005.
45. Bercescu, V. Aspects du fonctionnement d'une installation experimentale de pompe de chaleur avec compression mecanique et circulation additionelle de la solution. In Proceedings of the 16th International Congress of Refrigeration, Paris, France, 31 August–7 September 1983.
46. Pop, M.G.; Chiriac, F.; Ghitulescu, M.; Gardus, V.; Negrea, A.; Minea, V. 7.5 Gcal/h Hot Houshold Water Preparation Facility with an Absorbtion–Compression Heat Pump. In Proceedings of the Symposium on Rational Utilization of Secondary Forms of Energy in the Economy, particularly in Industry, Bucharest, Romania, 10–14 October 1983.
47. Minea, V.; Chiriac, F. Hybrid absorption heat pump with ammonia/water mixture—Some design guidelines and district heating application. *Int. J. Refrig.* **2006**, *29*, 1080–1091. [CrossRef]
48. Mučić, V.; Scheuermann, B. Zweistoff-Kompressions-Wärmepumpe mit Lösungskreislauf. *Fernwärme Int.* **1984**, *13*, 79–81.
49. Stokar, M.; Trepp, C. Compression heat pump with solution circuit Part 1: Design and experimental results. *Int. J. Refrig.* **1987**, *10*, 87–96. [CrossRef]
50. Mučić, V. Resorption Compression Heat Pump with Solution Circuit for Steam Generation Using Waste Heat of Industry as Heat Source. *Newsl. IEA Heat Pump Cent.* **1989**, *7*, 14–15.
51. Rane, M.V.; Radermacher, R.; Herold, K.E. Experimental investigation of a single stage vapor compression heat pump with solution circuit. In Proceedings of the Advances in Industrial Heat Pumps Technology, San Francisco, CA, USA, 10–15 December 1989.
52. Mongey, B.; Hewitt, N.J.; McMullan, J.T.; Henderson, P.C.; Molyneaux, G.A. Performance trends and heat transfer considerations in an ammonia-water resorption cycle. *Int. J. Energy Res.* **2001**, *25*, 41–51. [CrossRef]
53. FKW. *Entwicklung einer Absorptions-Kompressionswärmepumpe mit dem Stoffpaar Ammoniak/Wasser für die Anwendung als Hochtemperatur-Wärmepumpe*; Forschungszentrum für Kältetechnik und Wärmepumpen GmbH: Hannover, Germany, 2003.
54. Kim, J.; Park, S.R.; Baik, Y.J.; Chang, K.C.; Ra, H.S.; Kim, M.; Kim, Y. Experimental study of operating characteristics of compression/absorption high-temperature hybrid heat pump using waste heat. *Renew. Energy* **2013**, *54*, 13–19. [CrossRef]
55. Jung, C.W.; An, S.S.; Kang, Y.T. Thermal performance estimation of ammonia-water plate bubble absorbers for compression/absorption hybrid heat pump application. *Energy* **2014**, *75*, 371–378. [CrossRef]
56. Markmann, B.; Tokan, T.; Loth, M.; Stegmann, J.; Hartmann, K.H.; Kruse, H.; Kabelac, S. Experimental results of an absorption–compression heat pump using the working fluid ammonia/water for heat recovery in industrial processes. *Int. J. Refrig.* **2019**, *99*, 59–68. [CrossRef]
57. Malewski, W.F. Integrated absorption and compression heat pump cycle using mixed working fluid ammonia and water. In Proceedings of the 2nd International Workshop on Research Activities on Advanced Heat Pumps, Graz, Austria, 26–29 September 1988; pp. 35–44.
58. Torstensson, H.; Nowacki, J.-E. A sorption/compression heat pump using exhaust air as heat source. In Proceedings of the Absorption Heat Pump Conference, Tokyo, Japan, 30 September–2 October 1991; pp. 103–108.
59. Itard, L.C.M. Wet Compression-Resorption Heat Pump Cycles: Thermodynamic Analysis and Design. Ph.D. Thesis, Delft University of Technology, Delft, The Netherlands, 25 May 1998.
60. Zaytsev, D.V. Development of Wet Compressor for Application in Compression-Resorption Heat Pumps. Ph.D. Thesis, Delft University of Technology, Delft, The Netherlands, 8 April 2003.
61. Lorenz, H. Die Ermittlung der Grenzwerte der thermodynamischen Energieumwandlung. *Z. Gesammte Kälteindustrie* **1895**, *2*, 1–3, 6–12.
62. Stene, J. Design and Application of Ammonia Heat Pump Systems for Heating and Cooling of Non-Residential Buildings. In Proceedings of the 8th IIR Gustav Lorentzen Conference on Natural Working Fluids, Copenhagen, Denmark, 7–10 September 2008.
63. Zaytsev, D.; Infante Ferreira, C.A. Screw Compressor for Ammonia-Water Heat Pump Lubricated by the Process Mixture. In Proceedings of the International Compressor Engineering Conference School, West Lafayette, IN, USA, 16–19 July 2002.
64. Infante Ferreira, C.A.; Zamfirescu, C.; Zaytsev, D. Twin screw oil-free wet compressor for compression-absorption cycle. *Int. J. Refrig.* **2006**, *29*, 556–565. [CrossRef]
65. Tian, Y.; Yuan, H.; Wang, C.; Wu, H.; Xing, Z. Numerical investigation on mass and heat transfer in an ammonia oil-free twin-screw compressor with liquid injection. *Int. J. Therm. Sci.* **2017**, *120*, 175–184. [CrossRef]
66. Gudjonsdottir, V.; Infante Ferreira, C.A.; Goethals, A. Wet compression model for entropy production minimization. *Appl. Therm. Eng.* **2019**, *149*, 439–447. [CrossRef]
67. Ziegler, F. State of the art in sorption heat pumping and cooling technologies. In *Proceedings of the International Journal of Refrigeration*; Elsevier: New York, NY, USA, 2002; Volume 25, pp. 450–459.
68. Lima, A.A.S.; Leite, G.D.N.P.; Ochoa, A.A.V.; Santos, C.A.C.D.; Costa, J.A.P.D.; Michima, P.S.A.; Caldas, A.M.A. Absorption Refrigeration Systems Based on Ammonia as Refrigerant Using Different Absorbents: Review and Applications. *Energies* **2020**, *14*, 48. [CrossRef]
69. Reay, D.A. Compact heat exchangers, enhancement and heat pumps. *Int. J. Refrig.* **2002**, *25*, 460–470. [CrossRef]
70. Pratihar, A.K.; Kaushik, S.C.; Agarwal, R.S. Simulation of an ammonia—Water compression—Absorption refrigeration system for water chilling application. *Int. J. Refrig.* **2010**, *33*, 1386–1394. [CrossRef]

71. Kang, Y.T.; Akisawa, A.; Kashiwagi, T. Analytical investigation of two different absorption modes: Falling film and bubble types. *Int. J. Refrig.* **2000**, *23*, 430–443. [CrossRef]
72. Pratihar, A.K.; Kaushik, S.C.; Agarwal, R.S. Performance evaluation of a small capacity compression-absorption refrigeration system. *Appl. Therm. Eng.* **2012**, *42*, 41–48. [CrossRef]
73. Markmann, B. Wärmeübergang bei der Absorption Ammoniakreichen Dampfes Durch Wässrige Lösung im Plattenwärmeübertrager. Ph.D. Thesis, Leibniz Universität Hannover, Hannover, Germany, 2020.
74. An, S.S.; Jung, C.W.; Kim, M.; Park, S.R.; Kang, C.; Kang, Y.T. Experimental and simulation study on the plate absorber for hybrid heat pump system. *J. Mech. Sci. Technol.* **2013**, *27*, 3903–3909. [CrossRef]
75. Ahrens, M.U.; Hafner, A.; Eikevik, T.M. Development of ammonia-water hybrid absorption–compression heat pumps. In *Proceedings of the 25th IIR International Congress of Refrigeration*; IIF-IIR: Montréal, QC, Canada, 2019; pp. 4942–4949.
76. Lee, K.B.; Chun, B.H.; Lee, J.C.; Lee, C.H.; Kim, S.H. Experimental analysis of bubble mode in a plate-type absorber. *Chem. Eng. Sci.* **2002**, *57*, 1923–1929. [CrossRef]
77. Nordtvedt, S.R. Performance analysis of a plate type heat exchanger used as absorber in a combined compression/absorption heat pump. In Proceedings of the International Sorption Heat Pump Conference, Shanghai, China, 24–27 September 2002; pp. 235–239.
78. Táboas, F.; Vallès, M.; Bourouis, M.; Coronas, A. Flow boiling heat transfer of ammonia/water mixture in a plate heat exchanger. *Int. J. Refrig.* **2010**, *33*, 695–705. [CrossRef]
79. Sun, J.; Fu, L.; Zhang, S. A review of working fluids of absorption cycles. *Renew. Sustain. Energy Rev.* **2012**, *16*, 1899–1906. [CrossRef]
80. European Parliament and the Council of the European Union. Regulation (EU) No 517/2014 of the European Parliament and of the Council of 16 April 2014 on fluorinated greenhouse gases and repealing Regulation (EC) No 842/2006. *Off. J. Eur. Union* **2014**, *150*, 195–230.
81. European Parliament and the Council of the European Union. Directive 2006/40/EC of the European Parliament and of the Council of 17 May 2006. *Off. J. Eur. Union* **2006**, *161*, 1–11.
82. IFA. GESTIS-Stoffdatenbank. Available online: https://gestis.dguv.de/ (accessed on 19 March 2021).
83. DFG. MAK- und BAT-Werte-Liste 2020. *Maximale Arbeitsplatzkonzentrationen und Biologische Arbeitsstofftoleranzwerte.* Available online: http://dx.doi.org/10.34865/mbwl_2020_deu (accessed on 19 March 2021).
84. Åhlby, L.; Hodgett, D. The Compression-Absorption Cycle: A High-Temperature Application. In Proceedings of the 4th International Conference on Applications and Efficiency of Heat Pump Systems, Munich, Germany, 1–3 October 1990; pp. 59–68.
85. Chatzidakis, S.; Rogdakis, E. Das Verhalten der Zwei- und Dreistoffkompressionskältemaschine mit Lösungskreislauf. *KI Klima-Kälte-Heizung* **1992**, *7–8*, 255–258.
86. Tarique, S.M.; Siddiqui, M.A. Performance and economic study of the combined absorption/compression heat pump. *Energy Convers. Manag.* **1999**, *40*, 575–591. [CrossRef]
87. Hannl, D. Absorptions/Kompressions-Wärmepumpe für Hochtemperaturanwendung mit dem Arbeitsstoffgemisch Ammoniak/Lithiumnitrat. Ph.D. Thesis, Technische Universität Graz, Graz, Austria, 2015.
88. Herold, K.E.; Howe, L.A.; Radermacher, R. Analysis of a hybrid compression-absorption cycle using lithium bromide and water as the working fluid. *Int. J. Refrig.* **1991**, *14*, 264–272. [CrossRef]
89. Ansari, N.A.; Arora, A.; Manjunath, K. Optimum Performance Analysis of a Hybrid Cascade Refrigeration System Using Alternative Refrigerants. *Mater. Today Proc.* **2018**, *5*, 28374–28383. [CrossRef]
90. Gudjonsdottir, V.; Infante Ferreira, C.A.; Rexwinkel, G.; Kiss, A.A. Enhanced performance of wet compression-resorption heat pumps by using NH_3-CO_2-H_2O as working fluid. *Energy* **2017**, *124*, 531–542. [CrossRef]
91. Groll, E.A.; Kruse, H. Kompressionskältemaschine mit Lösungskreislauf—Einsatzmöglichkeiten für die Arbeitsstoffpaare R23/DEGDME und CO2/Aceton. *DIE KÄLTE Klimatech.* **1992**, *45*, 206–218.
92. Moreira-Da-Silva, R.J.B.; Salavera, D.; Coronas, A. Modelling of CO_2/acetone fluid mixture thermodynamic properties for compression/resorption refrigeration systems. *IOP Conf. Ser. Mater. Sci. Eng.* **2019**, *595*, 1–13. [CrossRef]
93. Aldás, P.S.D. Bomba de Calor de Compresión/Resorción con CO_2/Acetona: Modelización Termodinámica del Ciclo y Estudio Teórico-Experimental del Proceso de Desorción en un Intercambiador de Calor de Placas. Ph.D. Thesis, Universitat Rovira i Virgili, Tarragona, Spain, 2020.
94. Endo, N.; Maeda, T.; Hasegawa, Y. Performance Estimation of Absorption/Compression Cycle Using Working Pair Dimethyle Ether/Methanol. *Transactions of the JSRAE*. 2007, Volume 24, No. 3. pp. 193–204. Available online: https://ui.adsabs.harvard.edu/abs/2012TRACE..24..193E/abstract (accessed on 15 May 2021).
95. Kawada, A.; Otake, M.; Toyofuku, M. Absorption Compression Heat Pump using TFE/E181. In Proceedings of the Absorption Heat Pump Conference, Tokyo, Japan, 30 September–2 October 1991; pp. 121–126.
96. Nogués, M.; Bourouis, M.; Boer, D.; Coronas, A. Absorption/compression heat pumps using methanol—TEGDME and trifluoroethanol—TEGDME. In *Proceedings of the Heat Pump Systems, Energy Efficiency, and Global Warming*; IIF-IIR: Linz, Austria, 1997; pp. 197–204.
97. Bourouis, M.; Nogués, M.; Boer, D.; Coronas, A. Industrial heat recovery by absorption/compression heat pump using TFE-H_2O-TEGDME working mixture. *Appl. Therm. Eng.* **2000**, *20*, 355–369. [CrossRef]

98. Mestra, A.M.; Vallès, M.; Bourouis, M.; Coronas, A. Absorption/compression heat pump with organic fluid mixtures for industrial waste heat recovery. Cycle performance and first experimental results. In Proceedings of the Eurotherm Seminar 72, Valencia, Spain, 31 March–2 April 2003; pp. 397–402.
99. Mestra Rodríguez, A.M. Revalorización Energética de Residuos Térmicos Mediante Ciclos de Compresión Mecánica de Vapor con Circuito de Solución. Ph.D. Thesis, Universitat Rovira i Virgili, Tarragona, Spain, 2005.
100. Groll, E.A. Experimentelle und theoretische Untersuchungen von Kompressionskältemaschinen mit Lösungskreislauf. Ph.D. Thesis, University of Hannover, Hannover, Germany, 1994.
101. Ahrens, M.U.; Hafner, A.; Eikevik, T.M. Compressors for ammonia-water hybrid absorption–compression heat pumps. In Proceedings of the 8th Conference on Ammonia and CO2 Refrigeration Technology, Ohrid, North Macedonia, 11–13 April 2019; pp. 366–373.
102. Wu, X.; Xing, Z.; He, Z.; Wang, X.; Chen, W. Effects of lubricating oil on the performance of a semi-hermetic twin screw refrigeration compressor. *Appl. Therm. Eng.* **2017**, *112*, 340–351. [CrossRef]

Article II

M.U. Ahrens, S.S. Foslie, O.M. Moen, M. Bantle and T.M. Eikevik (2021). **Integrated high temperature heat pumps and thermal storage tanks for combined heating and cooling in the industry.** In: *Applied Thermal Engineering* 189, 2021, 116731. DOI: 10.1016/j.applthermaleng.2021.116731

Author contributions: Conceptualization: M.U. Ahrens, S.S. Foslie, O.M. Moen, M. Bantle and T.M. Eikevik; Methodology: M.U. Ahrens, S.S. Foslie and O.M. Moen; Software: M.U. Ahrens, S.S. Foslie and O.M. Moen; Investigation: M.U. Ahrens, S.S. Foslie and O.M. Moen; Resources: M. Bantle and T.M. Eikevik; Writing - Original Draft: M.U. Ahrens; Writing - Review and Editing: M.U. Ahrens, S.S. Foslie, O.M. Moen, M. Bantle and T.M. Eikevik; Visualization: M.U. Ahrens, S.S. Foslie and O.M. Moen; Supervision: M. Bantle and T.M. Eikevik; Funding Acquisition: M. Bantle and T.M. Eikevik.

Applied Thermal Engineering 189 (2021) 116731

Contents lists available at ScienceDirect

Applied Thermal Engineering

journal homepage: www.elsevier.com/locate/apthermeng

Integrated high temperature heat pumps and thermal storage tanks for combined heating and cooling in the industry

Marcel Ulrich Ahrens [a,*], Sverre Stefanussen Foslie [b], Ole Marius Moen [b], Michael Bantle [b], Trygve Magne Eikevik [a]

[a] NTNU, Department of Energy and Process Engineering, Kolbjørn Hejes vei 1B, 7491 Trondheim, Norway
[b] SINTEF Energy Research, Sem Sælands vei 11, 7034 Trondheim, Norway

ARTICLE INFO

Keywords:
Industrial application
High temperature heat pump
Thermal storage tanks
Process integration
Heat recovery
Natural refrigerants

ABSTRACT

This study investigates the integrated heat pump system of a green-field dairy located in Bergen, Norway. The purpose of the study is to determine the energy consumption and system performance. The dairy features a novel and innovative solution of a fully integrated energy system, employing high temperature heat pumps such as the hybrid absorption-compression heat pump (HACHP) with natural refrigerants to provide all temperature levels of heating and cooling demands. To evaluate the performance an energy analysis has been performed based on available process data for a comparatively energy-intensive week in February. The results have shown that the integrated system is able to meet the occurring demands. Furthermore, the specific energy consumption with 0.22 kWh l^{-1} product can outperform the annual average value of the replaced dairy even under difficult conditions. However, it is expected that the specific energy consumption will be further reduced on an annual basis. Through measures such as the extensive use of waste heat recovery accounting for 32.7% of the energy used, energy consumption was reduced by 37.9% and greenhouse gas (GHG) emissions by up to 91.7% compared to conventional dairy systems. Simultaneous, the process achieves a waste heat recovery rate of over 95%. Furthermore, demand peaks were compensated and a system coefficient of performance (COP) of 4.1 was achieved along with the identification of existing potential for further improvements.

1. Introduction

Climate change is one of the most significant topics of modern society. The energy demand and thus greenhouse gas (GHG) emissions of industrial processes are continuously increasing, with a clear trend for the coming years [1]. To achieve environmentally friendly, cheap and sustainable energy systems, it is now globally recognized that there is a necessity to increase the energy efficiency of industrial processes and reduce direct GHG emissions, e.g. from the burning of fossil fuels [2]. Simultaneously, large amounts of low-grade waste heat are available for potential waste heat utilization in various industrial processes, which are not directly usable and therefore are not exploited [3–5]. Due to this situation, it is essential to develop more efficient and environmentally friendly ways to provide thermal energy as usable heat and cold for industrial applications.

A promising approach to achieve these goals, which has been increasingly investigated in recent years, is the integrated use of high temperature heat pumps in combination with thermal storage tanks for combined heating and cooling demands in industrial applications [6–8]. Of special interest regarding environmental sustainability is the use of natural refrigerants with low global warming potential (GWP) and known effects on the atmosphere for the operation of heat pump and refrigeration systems to avoid undesirable side effects [2]. Food processing plants in particular offer great potential for initial improvement measures due to the simultaneous cooling and heating requirements in achievable temperature ranges for heat pump solutions that are currently ready for the market [9]. This observation corresponds with the results of comprehensive studies on the food industry, which state that a considerable amount of energy is required for evaporation and freezing processes [10]. Currently, most of this energy is generated using fossil fuels and the decarbonisation of these processes is key for a green transition of the industry [11].

Dairy plants were found to be very well suited for implementing high temperature heat pump systems due to the given process requirements. Processing of dairy products involves a combined application of product heating (thermal treatment) and cooling. In a conventional dairy the heating demand is traditionally covered by fossil fuel boilers, while the

* Corresponding author.
E-mail address: marcel.u.ahrens@ntnu.no (M.U. Ahrens).

https://doi.org/10.1016/j.applthermaleng.2021.116731
Received 19 November 2020; Received in revised form 20 January 2021; Accepted 10 February 2021
Available online 16 February 2021

Nomenclature

Abbreviations

CIP	Cleaning-in-place
DH	District heating
DHW	Domestic hot water
EB	Electric boiler
EU	European Union
GHG	Greenhouse gas
GWP	Global warming potential
HACHP	Hybrid absorption/compression heat pump
IHPS	Integrated heat pump system
NGB	Natrual gas boiler
NH_3 HP	Ammonia heat pump
NO	Norway
PV	Photovoltaic

Roman letters

COP	Coefficient of performance [–]
h	Specific enthalpy [kJ·kg^{-1}]
$\dot{m}$	Mass flow rate [kg·s^{-1}]
$\dot{Q}$	Thermal load [kW]
T	Temperature [°C]
$\dot{W}$	Power [kW]

Greek symbols

ρ	Density [kg·m^{-3}]

Subscripts

el	Electrical
eq	Equivalent
i	Index
in	Inlet
out	Outlet

cooling demand is covered by a separate refrigeration system. By integrating an industrial heat pump that can deliver both process cooling and heating, the need for fossil fuel is eliminated. A large share of emissions from dairy products is emitted during processing within the dairy [12], meaning there is great potential for improvements [13]. Thereby varying developments can be observed in the various countries within the European Union (EU), both concerning the treatment methods used and the primary energy sources used [14,15]. Here, the Scandinavian countries in particular achieve the lowest values in product-specific energy consumption [16].

Published work in the literature shows that several approaches can be followed to improve energy efficiency and reduce GHG emissions of industrial processes. In recent years, many studies were conducted on food processing plants and the associated processes, aiming to improve energy efficiency and reducing the energy consumption with the associated reduction of GHG emissions. On one side, there is a great effort to increase the efficiency of certain processes in terms of the technology used and the operating conditions, such as dryers [17]. On the other side, the way energy is provided [18] and controlled [19] within the plant is extensively investigated, as even a minimum of energy consumption is necessary with improved processes. With a focus on optimising individual processes as well as the overall system, several scientific and engineering methods are employed and continuously improved [20]. These include the use of energy, exergy and pinch analyses, as well as the development and implementation of advanced mathematical approaches for the optimal design and integration of industrial heat pumps for a variety of industrial processes [21,22]. For many of the investigations carried out and methods used, primarily case studies of existing plants were employed to identify the potential for optimisation in the scope of improved process control and/or waste heat recovery.

The present work aims to support the described trend in the scientific field focusing on integrating high temperature heat pumps with a high degree of waste heat recovery to minimise external energy consumption and GHG emissions of food processing plants. Unlike previous work based on simulations and theoretical case studies, this study demonstrates the performance of a fully integrated energy system of a greenfield dairy with real operational data. To authors' best knowledge, the new dairy is the first in the world to operate without fossil fuel or direct electric heating, for which it won the "Heat Pump City of the Year 2019 award" in the DecarbIndustry category [23]. The aim of this study is to demonstrate that high temperature heat pumps using natural refrigerants can provide further improvements even for comparatively good systems and thus substitute conventional fossil fuel-based solutions. Furthermore, the demonstration of possible applications and operating data of integrated high temperature heat pumps in combination with thermal storage tanks increase confidence in such systems among plant owners and key decision makers. Moreover, the present work can reduce non-technical barriers due to uncertainties based on a lack of experience among the potential users.

For this reason, this study investigates the energy consumption and system performance of the fully integrated heat pump system of a new dairy in Bergen, Norway. At first, both the system configuration and the process parameters are presented. Subsequently, the data collection and evaluation methods used are described. By using available operational data for one energy-intensive production week from the process instrumentation, an energy analysis is performed to evaluate the performance. For an environmental analysis, the conducted results are evaluated and compared with conventional reference dairy systems. Based on the process integration and system performance, further optimisation potentials are identified and discussed.

2. System description

The following case study was conducted for a green-field dairy in Bergen, Norway, which was commissioned in 2018 with an innovative integrated heat pump system to provide cooling and heating at all temperature levels required for the production process. The dairy has a size of 20,000 m^2 and a forecasted annual production of 43.4 million litres, divided into fluid milk (83.1%), cream (3.7%) and juice (13.2%), with fluid milk dominating the production. On the roof 6000 m^2 of photovoltaic (PV) solar panels are installed, generating approximately 0.5 GWh of electricity annually. The dimensioning was based on a replaced dairy in Minde, Norway, with an annual energy consumption of 10.1 GWh (6.8 GWh electricity and 3.9 GWh district heating) resulting in a specific annual energy consumption of 0.24 kWh l^{-1} product for the year 2015. The targeted specific energy consumption for the new dairy was defined at 0.15 kWh l^{-1} product on an annual average, with production taking place only on weekdays and not at weekends. This value is a realistic target based on the experience of the plant owner on branch-typical energy demands. In the following, the specific energy consumption for the investigated dairy is calculated and benchmarked against the targeted and reference values.

Production processes within the dairy can be divided into several consumers at different temperature levels. The dairy uses the excess heat from cooling processes provided by ammonia chillers and upgrades this heat to supply usable process heat for heating demands. This enables process heat at different temperature levels of 40 °C, 67 °C and 95 °C. The integrated heating and cooling system of the dairy is visualized in Fig. 1, including three different heat pump systems and six temperature

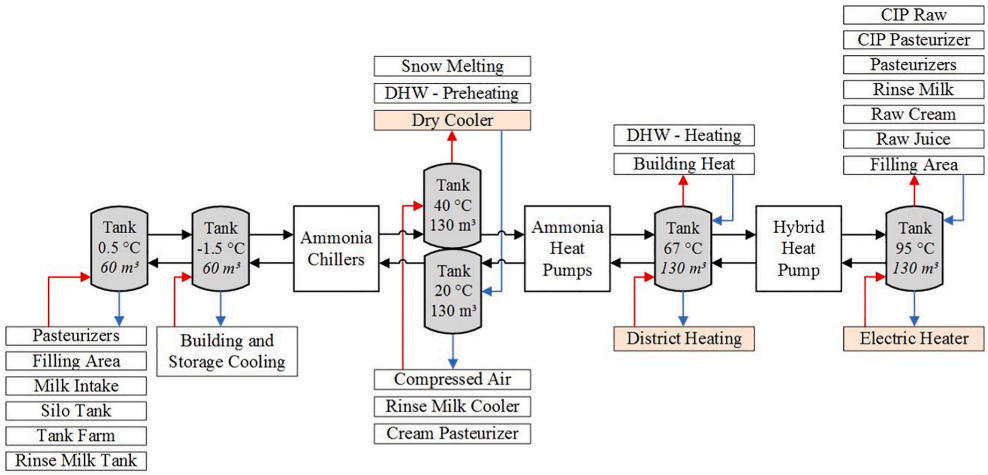

Fig. 1. Integrated energy supply system including heat pump systems and thermal storage tanks.

levels provided to the different consumers.

Ammonia chillers supply cold glycol at −1.5 °C to the building and storage cooling and via a heat exchanger to the ice water circuit at 0.5 °C, which provides cooling to different consumers, such as pasteurizers, filling area and milk intake. On the condenser side, the chillers produce hot water at 40 °C, which is accumulated in a storage tank. From the 40 °C tank, the hot water is distributed to the snow melting, the preheating of domestic hot water (DHW) and to the ammonia heat pumps (NH_3 HPs). The return water enters another storage tank at 20 °C before being heated by the condenser side of the chillers. From the 20 °C tank, cooling is provided to the compressed air system, rinse milk cooler and cream pasteurizer. If the NH_3 HPs are unable to provide sufficient cooling for the 20 °C/40 °C circuit, the dry cooler ensures the required deficit.

Using the 20 °C/40 °C circuit as heat source, the NH_3 HPs produce hot water at 67 °C, which is then accumulated in a storage tank. The 67 °C tank supplies heating for the building heat system, DHW heating and the high temperature heat pump. Eventual capacity deficits are compensated using district heating (DH). The installed hybrid absorption/compression heat pump (HACHP), operating as high temperature heat pump, produces hot water at 95 °C for a further storage tank. The tank distributes the hot water to consumers, such as the cleaning-in-place (CIP) processes, pasteurizers and filling area. In case of a heat deficit in the 95 °C circuit, an electric heater serves as reserve source.

The heat pump systems are designed to be able to provide nearly all required cooling and heating demands at the dairy, with the dry cooler, electric heater and DH as backup resources. Table 1 contains a detailed overview of the installed heat pump systems including refrigerant, number of units, heat source and sink temperatures and total capacities.

The chillers and NH_3 HPs are designed as single stage vapour compression heat pump systems with ammonia as refrigerant. Ammonia is a popular working fluid for both industrial refrigeration systems (chillers) and large NH_3 HP systems due to excellent heat transfer properties and high volumetric heat capacity [24], which reduces the required compressor swept volume. The HACHP system uses the zeotropic ammonia/water mixture as refrigerant and is based on the Osenbrück cycle [25], which extents a vapour compression cycle with an additional solution circuit [26]. This extension offers the typical features of HACHP systems, such as high achievable sink temperatures at comparably low-pressure levels in combination with non-isothermal heat transfers [27]. The volumes of the storage tanks (see Fig. 1) were selected in relation to the required and available process demands and the objective of efficient operation with continuous supply to all process consumers.

Table 1
Overview of installed heat pump systems.

System	Refrigerant	Units	Source	Sink	Total capacity
Chillers	NH_3	3	4 °C/ −1.5 °C	20 °C/ 40 °C	2400 kW (cooling)
NH_3 HPs	NH_3	2	40 °C/20 °C	60 °C/ 67 °C	1577 kW (heating)
HACHP	NH_3-H_2O	1	67 °C/60 °C	73 °C/ 95 °C	940 kW (heating)

3. Data collection and evaluation methods

The data used in this analysis were collected for one week in the period from February 10th (00:00 CET) to February 17th (00:00 CET) 2020. The period of one full week was selected to identify cross-production influences that would not be noticeable in a daily analysis. At the same time, due to the comparatively short time from commissioning and the resulting constant changes in the operation control, it was not meaningful to conduct an analysis of a longer period including different seasonal influences. This increases to a certain degree the uncertainty regarding the full-year values and reduces the possibility of a direct comparison with annual values. During the installation of the dairy, a significant number of sensors were installed, which made it possible to closely monitor the process. For all heat pump systems, thermal energy storages and consumers, the inlet and return temperatures were determined using PT100 temperature sensors (iTHERM TM411, Class A, $\pm\ 0.15 + 0.002 \cdot T$ [°C]). Volume flows measurements in each fluid line were conducted using Coriolis flow sensors (Promass F300 Hart, ± 0.1%) and electromagnetic flow sensors (Promag H300 ProfiNet, ± 0.2%). Values for total power consumption and specific power consumption for the various heat pumps and the electric heater were determined using power meters (PowerLogic PM3000, ± 0.5%). From this information, an average relative uncertainty was determined for each measurement point. These values were then used to determine the combined relative measurement uncertainty of the various system parameters including all contributing variables by applying the Root Sum of Square method [28].

For size reduction of measurement data, the value at a certain time is only logged by the measurement system if it differs from the value in the

previous time step within a defined range. Since the time steps for the different measurements consisting of temperatures, flow rates, and power consumption were not the same, this led to many empty cells when merging the logged values. Linear interpolation between two known values was used to fill all empty cells. For the further use, the recorded data was resampled, and the average values were calculated on a minute basis. The programming language Python was used for data collection, data handling and energy balance calculations. Specifically, the data analysis library Pandas was used for data processing, while the CoolProp package was used to calculate energy balances.

3.1. Energy analysis

The conducted energy analysis is based on the logging values from the heating and cooling distribution system. It does therefore not consider any inefficiencies of the processing equipment itself, but merely studies how much energy is required to operate the dairy. Due to the absence of energy meters within the system, the specific thermal loads, $\dot{Q}_i$ [kW], are determined using the specific energy balance for each consumer, i, as shown in Eq. (1).

$$\dot{Q}_i = \dot{m}_i \cdot \left(h_{out,i} - h_{in,i}\right) \pm 3.0\% \tag{1}$$

Pressures for water streams at all temperatures were assumed as 1 bara and glycol streams as 3.5 bara based on information from the dairy. Since flow measurements were volumetric, mass flow rates were calculated using the densities for constant temperatures based on the mean values of the respective temperature levels (see Table 1). The specific enthalpies at the inlet and outlet of each component or process were determined using the respective measured inlet and outlet temperatures and assumed pressures. The average value of the calculated measurement uncertainty [%] based on the measurement system used is presented in the equation [29].

3.2. Environmental analysis

To provide an environmental perspective of the benefits of the integrated energy system, energy savings and GHG emissions were investigated. Based on the energy analysis a comparison between the energy system of the investigated dairy and a reference system with separated cooling and heating systems has been made, using the same energy requirement for each process. Here, cooling is provided using the chillers and dry cooler against the ambient temperature. It can be assumed that the power demand for a refrigeration system rejecting all its heat to the ambient will be lower than for a system rejecting heat to an integrated heat pump system (IHPS) due to lower condensing temperatures [30]. The supply of the heating demand was divided into two scenarios: 1. EB + DH scenario with electric boiler (EB) for 95 °C consumers and DH for the remaining heating demands; 2. NGB scenario with natural gas boiler (NGB) for all heating demands. A thermal efficiency of 95% was assumed for the heat transfer to process heat from electricity, gas and DH. For a comprehensive consideration of the GHG emissions savings, these have been determined for Norwegian (NO) and EU emission cases. For electricity, an equivalent CO_2 emission factor of 17 g $CO_{2,eq}$ kWh^{-1} is assumed in the NO case, based on the Norwegian energy mix for electricity consumption in 2019 [31]. In the EU case, the emission factor for electricity is 295.8 g $CO_{2,eq}$ kWh^{-1}, based on the EU energy consumption in 2016 [32]. For DH, the emissions factor is 23.4 g $CO_{2,eq}$ kWh^{-1}, based on the energy mix of the local district heating provider BKK in 2019 [33]. This value does not include CO_2 emissions associated with the combustion of bio waste, which in most cases can be justified as it is part of the natural carbon cycle. The emission factor associated with natural gas consumption is 205 g $CO_{2,eq}$ kWh^{-1} [34].

3.3. Performance analysis

The performance of the individual heat pump systems is evaluated through the respective coefficient of performance (COP). It relates the total amount of heat supplied to (for heating) or extracted from (for cooling) a system to the total amount of work required to achieve that effect, hence indicating the efficiency of the heat pump or refrigeration system:

$$COP_{Heating} = \frac{\sum \left|\dot{Q}_{Heating}\right|}{\sum \dot{W}_{el}} \pm 3.6\% \tag{2}$$

$$COP_{Cooling} = \frac{\sum \left|\dot{Q}_{Cooling}\right|}{\sum \dot{W}_{el}} \pm 3.6\% \tag{3}$$

where $\dot{Q}_{Heating}$ is the useful heat supplied to the system and $\dot{Q}_{Cooling}$ is the useful heat removed from the system. For the work required, the value determined by the power meters is used, which includes losses in the inverter, motor, and compressor. Other values for auxiliary equipment such as pumps are not included. The theoretical maximum for the COP of a heat pump or refrigeration system operating between heat source and sink with constant temperatures is defined by the Carnot process, which is given by

$$COP_{Carnot\ \ Heating} = \frac{T_{sink}}{T_{sink} - T_{source}} \tag{4}$$

$$COP_{Carnot\ \ Cooling} = \frac{T_{source}}{T_{sink} - T_{source}} \tag{5}$$

where T_{sink} and T_{source} are in [K], respectively. In this case there is a small temperature difference between the input and output of the heat source and heat sink, and the temperatures are not constant, so the average output temperatures are used for the calculation. To evaluate the system performance, the Carnot efficiency, η_{Carnot}, is determined as the ratio of the COP to the theoretically achievable Carnot COP, as shown in Eq. (6) [35].

$$\eta_{Carnot} = \frac{COP}{COP_{Carnot}} \tag{6}$$

The overall system COP is defined as the ratio of the sum of the useable thermal heating and cooling loads to the total electricity consumption of the heat pump systems, using Eq. (7):

$$COP_{system} = \frac{\sum \left|\dot{Q}_{Heating}\right| + \sum \left|\dot{Q}_{Cooling}\right|}{\sum \dot{W}_{el}} \pm 8.7\% \tag{7}$$

4. Results and discussion

The results of the conducted analysis are based on the investigated production week in February. The total amount of product was 733,957 L, corresponding to a production capacity of 88%, divided into 589,399 L of fluid milk (80.2%), 26,045 L of cream (3.5%) and 119,513 L of juice (16.3%). When comparing this amount to the total energy consumption of electricity (138.6 MWh) and DH (26.6 MWh), excluding the electricity generated by PV solar panels (0.8 MWh), this results in a specific energy consumption of 0.22 kWh l^{-1} product. The period studied covers one week in winter with temperatures below zero degree and snowfall, when energy consumption is generally higher than in summer. Therefore, it is expected that specific energy consumption will be reduced on an annual basis and full production volume. And despite the difficult conditions, the investigation already indicates a reduction of about 10% compared to the specific energy consumption of the replaced dairy, which was 0.24 kWh l^{-1} product on an annual basis. As

the operational experience with this dairy is new, it is also expected that with increasing knowledge of process equipment and optimization techniques, the specific energy consumption will continue to decrease over time, thus reaching the targeted 0.15 kWh l^{-1} product on an annual basis. To identify potential improvements for the further reduction of the energy consumption, an energy and environmental analysis were performed, and the process integration and system performance investigated.

4.1. Energy analysis

Table 2 gives an overview of the energy demands with amount [MWh] and share [%] of the various process consumers. The list includes only end consumers of energy and intermediate consumers of heat and electricity, such as the heat pump systems, are not included.

The process consumer labelled "Other" has the largest single share (33.7%) and consists of a collection of consumers which includes electrical consumption from building lighting, the air compressor and fans, pumps and other auxiliary processing equipment, DH not used directly in the dairy process and waste heat, where individual values were not available. This value was obtained from subtracting the known consumers of electricity and DH from the total consumption. The second and third biggest energy consumers are the heat consumers at 95 °C (22.3%) and 67 °C (17.3%). Overall, heating processes thus account for the largest share of energy demand (41.6%).

To provide the required energy demands, electricity and DH were used as external energy sources, and waste heat recovery was utilized by the heat pump systems. Energy sources used in the dairy with their respective amounts [MWh] and shares [%] are shown in Table 3.

The total value of 245.5 MWh includes all energy consumed in the dairy, with electricity covering most of the energy demand (56.5%). Except for the electricity generated from the installed PV solar panels (0.3%), this energy is supplied together with DH (10.8%) from external sources and contribute to GHG emissions. With a share of 0.3%, PV solar panels contribute little to reducing total external energy consumption. However, as the data collection period was in February, a week with cloudy weather and regular snowfall, their contribution is expected to be significantly higher on average over a whole year. Waste heat recovery is accountable for 32.7% of the energy supplied and is provided by two main sources, the chillers (28.7%) and cooling of the compressor, the rinse milk and cream pasteurizer (4.0%). With the integration of the waste heat from the chillers into the dairy process being by far the largest contribution to waste heat recovery. For further utilization in the process, the waste heat recovered from the chillers is increased by the electricity consumption, as the electricity required for cooling is unavoidable. In contrast, cooling of the compressor, the rinse milk and cream pasteurizer can take place above the ambient temperature and therefore do not require additional energy. However, in this case the heat is used within the process via heat recovery. These results show that despite the modest reduction in specific energy consumption, without waste heat utilization, the consumption of electricity and DH would be considerably higher. The contradictory results indicate that this was a week where energy demands per litre product were higher than average.

Table 2
Energy demands of the various process consumers.

Energy consumers	Amount [MWh]	Share [%]
Heating processes at 95 °C	**72.7**	**22.3**
– Process Heat	72.7	22.3
Heating processes at 67 °C	**56.4**	**17.3**
– Building Heat	50.0	15.3
– DHW – Heating	6.4	2.0
Heating processes at 40 °C	**6.6**	**2.0**
– DHW – Preheating	5.0	1.5
– Snow Melting	1.6	0.5
Cooling processes at 20 °C	**9.9**	**3.0**
– Comp. /Rinse Milk/Cream Past.	9.9	3.0
Cooling processes at 0.5 °C	**30.9**	**9.5**
– Process Cooling	30.9	9.5
Cooling processes at −1.5 °C	**39.5**	**12.1**
– Building and Storage Cooling	39.5	12.1
Other	**109.8**	**33.7**
Total	**325.8**	**100.0**

Table 3
Energy sources with amount and share.

Energy sources	Amount [MWh]	Share [%]
Electricity	**138.6**	**56.5**
– From grid	137.8	56.2
– From PV solar panels	0.8	0.3
District heating	**26.6**	**10.8**
Waste heat recovery	**80.3**	**32.7**
– Chillers	70.4	28.7
– Comp./Rinse Milk/Cream Past.	9.9	4.0
Total	**245.5**	**100.0**

4.2. Environmental analysis

Based on the energy demands presented in Table 2, a comparison was made between the IHPS and a reference system with separated cooling and heating system, as described in Chapter 3.2. When using dry cooling in the IHPS, the return temperature after cooling was on average about 7 °C lower than the return temperature of the other cooling sources, making it clear that the cooling efficiency was to some extent sacrificed to achieve the utilization of surplus heat. The cooling system for the reference system can achieve a higher COP due to the reduced condensing temperature, resulting in lower power consumption. For the calculation of the electricity demand for the chillers in the reference scenarios, it was therefore assumed that the exclusive use of dry cooling leads to 7 °C lower condensing temperatures. This results in a Carnot COP of 9.5, which with an expected Carnot efficiency of 60% gives a COP of 5.7. Cooling requirements at 20 °C are not included as energy demand since it requires no additional energy input from either system. Data including additional power consumption from auxiliary equipment related to the heat pumps and thermal storage tanks was not available, so that this part has been neglected. Table 4 shows the comparison of the investigated energy systems based on the determined energy input values.

Based on the values in Table 2 and by excluding the 20 °C processes,

Table 4
Comparison between the IPHS and a reference energy system.

		IHPS		Reference	
Process	Required [MWh]	Source	Amount [MWh]	Source	Amount [MWh]
Heating at 95 °C	72.7	HTHP EB	11.7 3.7	EB/ NGB	76.5
Heating at 67 °C	56.4	NH3 HP DH	20.1 3.2	DH/ NGB	59.4
Heating at 40 °C	6.6	Chillers	0.0	DH/ NGB	6.9
Cooling at 0.5 °C/ −1.5 °C	70.4	Chillers	16.7	Chillers	12.3
Other	109.8	El. Grid El. Solar DH	85.6 0.8 23.4	El. Grid DH/ NGB	86.4 23.4
Total	**315.9**		**164.4**		**264.9**

the total energy demand of the dairy is 315.9 MWh. The IHPS requires an external energy input of 164.4 MWh to cover this demand, reduced by the 0.8 MWh of energy generated by the PV solar panels. For the reference system, the total energy consumption is 264.9 MWh, resulting in a total external energy saving for the IHPS of 100.5 MWh (37.9%). Compared to the EB + DH scenario (using electric boiler and DH), this corresponds to electricity savings of 37.4 MWh (21.3%) and DH savings of 63.1 MWh (70.4%). In the NGB scenario, 98.7 MWh were provided by electricity and 166.1 MWh by the NGB. For the investigation of the GHG emissions, the determined external energy consumption was projected over a period of one year and multiplied by the corresponding equivalent CO_2 emission factors. Fig. 2 shows the calculated GHG emissions in tons CO_2 equivalent projected for the period of one year [t $CO_{2,eq}$ $year^{-1}$] of the investigated scenarios for the NO and EU case, respective.

The reduction in GHG emissions for the IHPS in the NO case is 41.6% compared to the EB + DH scenario and 91.7% compared to the NGB scenario. The relatively low emission factor for electricity is responsible for the large GHG emission savings compared to the energy savings. A reduction in GHG emissions will also be achieved in the EU case, even though the savings are proportionally lower with 23.2% (EB + DH) and 34.3% (NGB) respectively. These results are consistent with the findings of [36] and [37], which stated that the use of high temperature heat pumps and EB can substitute conventional NGB and lead to large savings in primary energy consumption and GHG emissions, especially in countries with a high share of renewable energy sources in their energy mix.

4.3. Process integration

A well-integrated process is necessary to compensate for peak energy loads, time differences between available heat surplus and demand, and temperature differences. Fig. 3 presents an overview of the energy flows [MWh] in the dairy processing plant using a Sankey diagram [38]. The diagram shows the integration of energy consumers, heat pump systems and thermal storage tanks at different temperature levels. Individual energy consumers of the corresponding temperature levels were summarized. The diagram does not include an overview of the power consumption of auxiliary equipment such as lighting, air compressors, fans, and other devices, as these were not provided individually. Energy flows are directed from left to right and the line width represents the respective quantity. Therefore, it is visible for each stage which energy flows enter and exit. Discrepancies between entering and leaving energy flows for single components in the diagram are caused by differences between the calculated values on both sides. Reasons for these discrepancies may be based on several factors, such as measurement uncertainties and data processing methods. The largest differences were observed where cyclical processes with rapid changes in temperatures and volume flows occur. It is therefore assumed that these, in combination with a periodically low measurement resolution, are the main causes for discrepancies between the determined results.

The analysis of the energy flows indicates that the amounts of energy

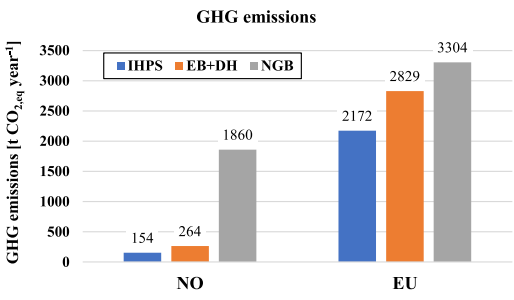

Fig. 2. GHG emissions of the investigated scenarios for the NO and EU case.

from the use of DH (3.2 MWh) and the electric heater (3.7 MWh) to cover the peak heat demand at 67 °C and 95 °C are small compared to the heat supplied by the heat pumps (105.9 MWh and 69.2 MWh). Likewise, the use of dry cooling (4.3 MWh) is limited compared to the amount of surplus heat provided by the chillers (87.2 MWh). This results in a waste heat recovery rate for the entire process of more than 95%. This indicates that the utilization of heat pump systems and thermal storage tanks are well integrated into the dairy process and sufficiently dimensioned. An investigation of hourly heat demands was made to further evaluate this integration. Fig. 4 shows the hourly thermal load profiles for the process consumers and suppliers over the period of the investigated week. The stacked chart area represents the sum of the thermal load for all consumers of heat, while the solid line represents the supply of heat from the recovered waste heat from cooling processes, including the heat generated from the electrical power to the heat pumps and the various dashed lines represent the use of the respective backup sources.

The illustration indicates a good match between heat supply and demand for most of the time. Occurring demand peaks and associated heat deficits are often managed without use of DH or electrical heater as backup sources. On the other hand, surplus heat is usually handled without the use of dry cooling. This indicates that the thermal storage tanks provide a reasonable compensation for the imbalance between the required process heat and the heat supplied by the heat pump systems.

During weekdays, the dairy processing is performed during daytime, resulting in the highest thermal peak loads. The cyclical behaviour of the load is highly affected by the load variations from the 95 °C processes. Peak loads from the 95 °C processes exceed the high-temperature heat pump capacity of 940 kW on a daily basis, proving again that the thermal storage tanks are used to overcome peak loads. The use of the electric heater is mainly limited to the start-up of the process, which is caused by the support of the high temperature heat pump start in the morning. Load variations in the 67 °C circuit are smaller than in the 95 °C circuit, as many of the consumers such as building heating and DHW require a continuous heat supply. Peak loads are usually well within the total heat pump capacity of 1577 kW. The increasing use of DH during the week therefore indicates a shortage of available waste heat from cooling processes.

During the weekend, the heat demand is reduced by more than half and remains more constant compared to weekdays. In particular, the heat demand for the 95 °C circuit is reduced and yet the electric heater is used more extensively. On the other hand, dry cooling is also being used more frequently in the same period. The backup source is thus used to cover a heat deficit with a simultaneous available heat surplus. The integration and evaluation of the data for the weekend indicates that by using the dry cooler, a total of 2.9 MWh of surplus heat was not utilized, which was almost twice as much as the amount of heat generated by the electric heater at 1.5 MWh. An explanation for this behaviour requires more insight into the process control system. In any case, these findings indicate that there is improvement potential for the energy utilization. For a more detailed analysis, the load profiles of HACHP and electric heater are plotted together with the temperatures from and to the 95 °C tank over the weekend (see Fig. 5). The solid lines represent the supplied heat load from both HACHP, and electric heater and the dotted lines represent the inlet and return temperatures before and after the systems.

With closer examination it becomes clear that the HACHP works in a cyclic manner together with the electric heater, but not at the same time. These systems are operated to maintain a certain temperature level in the thermal storage tank. If the temperature in the tank drops (indicated by the blue dotted line), the HACHP is operated until a defined set point temperature is reached and then stops operating. When the return temperature (orange dotted line) is too low or the required capacity is too small, the electric heater is used to raise the temperature. The missing ability of the HACHP to further reduce capacity could lead to this cyclical behaviour until it improves with increasing demand towards the end of the weekend. This is an indication that the system is not

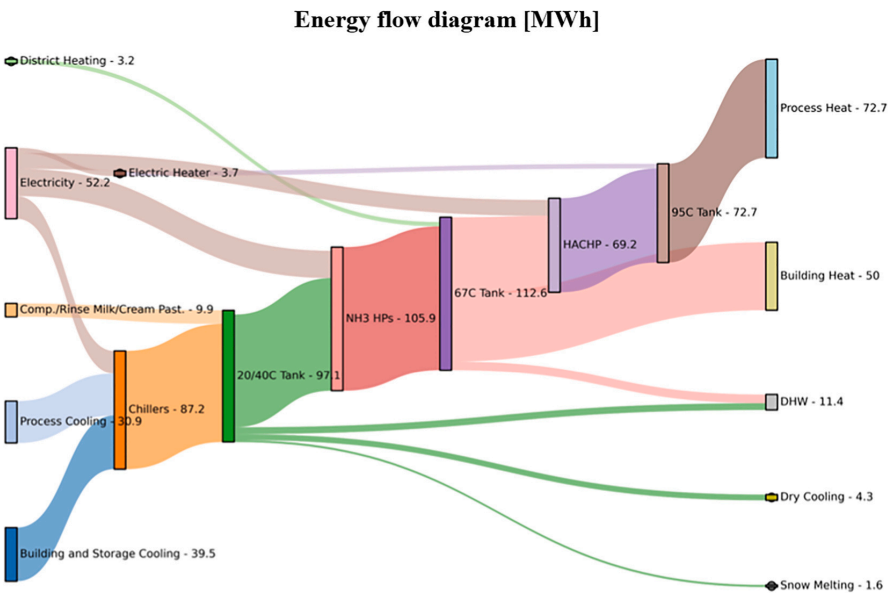

Fig. 3. Sankey diagram of energy flows in the dairy process.

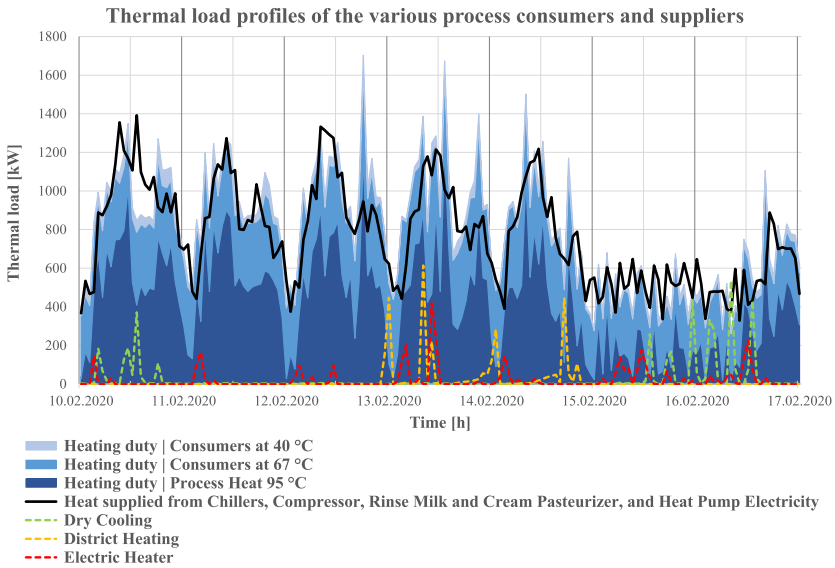

Fig. 4. Hourly thermal load profiles of the various process consumers and suppliers.

tuned for operation at half thermal load and further potential for improvement is available here. Possible approaches are the adaptation of the selected temperature set points. Thereby the temperature for the start of the electric heater could be reduced to limit the usage. In addition, if feasible, the minimum temperature level for the tank could be lowered on weekends to extend the charging times of the HACHP.

4.4. Performance analysis

In this section, the results of the performance analysis of the specific heat pump systems as well as the overall system are presented. Fig. 6 shows the thermal load profiles of the heat pump systems during the investigated week.

The thermal loads for all heat pump systems were mostly well below the installed total capacity. As previously discussed, thermal loads for both heating and cooling are mainly affected by the high temperature processes at 95 °C, causing the cyclic heat demand during weekdays at daytime. The demand for building and storage cooling ensures that the chillers are in continuous operation throughout the week. The building heat and DHW ensure a stable heat demand in the 67 °C circuit, while

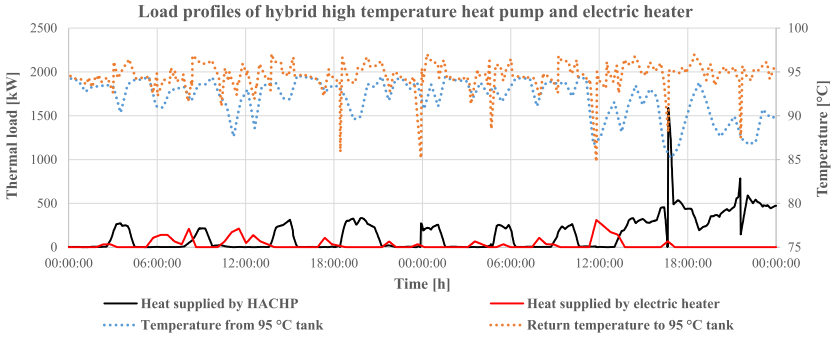

Fig. 5. Load profiles of high temperature heat pump and electric heater over the weekend.

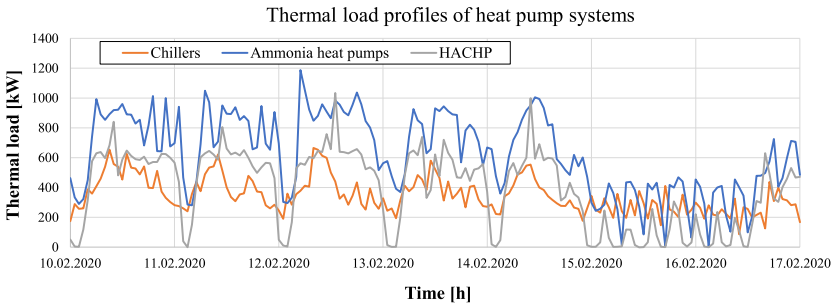

Fig. 6. Thermal load profiles of the heat pump system.

the total heat load is significantly reduced at weekends and the NH_3 HPs are operated cyclically. The HACHP system operates in the most cyclical way, as it only supplies heat to the 95 °C processes and is not in operation during the night on weekdays. This is also due to the fact of having only one unit which restricts the possible capacity control. Table 5 shows the results of the conducted performance analysis for the different heat pump systems.

During the investigated period, the average COP for the chillers was 4.2 with a Carnot efficiency of 55%. As already discussed in chapter 4.2, the use of dry cooling was minimal compared to the total amount of waste heat used for snow melting, DHW and the NH_3 HPs. However, when dry cooling was used, the return temperature after cooling was about 7 °C lower than the return temperature of the other cooling sources. This suggests that cooling efficiency has to some extent been sacrificed to achieve utilization of surplus heat. The average COP for NH_3 HP was 5.3, resulting in a Carnot efficiency of 65%, which is in the upper range for large scale industrial heat pumps [39]. The HACHP achieved an average COP of 5.9, resulting in a Carnot efficiency of 53%, which is within the expected range for state-of-the-art high temperature heat pumps on the market [9]. For the calculation of the overall system performance, all provided cooling and heating loads were summed up based on Table 2, excluding "Others", resulting in a value of 216.0 MWh.

Table 5
Performance data of the heat pump systems.

System	Heat supply [MWh]	Power consumption [MWh]	COP [–]	COP_{Carnot} [–]	η_{Carnot} [%]
Chillers	70.4	16.7	4.2	7.7	55
NH_3 HPs	105.9	20.1	5.3	8.1	65
HACHP	69.2	11.7	5.9	11.2	53

The required work was determined to be 52.2 MWh based on the electricity consumption in Fig. 3. This results in a total system COP of 4.1 for the examined week in February. The presented performance values were achieved during an energy-intensive week, so it can be stated that the IHPS can certainly compete with conventional solutions.

5. Conclusion

This study investigates the energy consumption and system performance of an integrated energy system of a green-field dairy located in Bergen, Norway. The dairy features a novel and innovative solution of a fully integrated energy system. The system features high temperature heat pumps using natural refrigerants to provide all temperature levels of heating and cooling demands, enabling significant energy savings compared to the replaced dairy and other conventional dairy systems. By using available operation data for an energy-intensive week, an energy analysis has been performed to evaluate the system performance. The results were compared against reference dairy scenarios using conventional methods for providing the heating and cooling demands.

The results obtained show a specific energy consumption of 0.22 kWh l^{-1} product for the investigated week, allowing the integrated dairy to outperform the annual average of the replaced dairy despite challenging conditions. The energy analysis indicated that 33.0% of all energy sources in the new dairy already come from either waste heat recovery or solar energy, while the process achieves a waste heat recovery rate of over 95%.

By using the determined energy demand of the dairy for the week, the external energy consumption and GHG emissions for a corresponding reference system were calculated. The integrated dairy achieved external energy savings of up to 37.9%, while GHG emission reductions of 23.2% to 91.7% are achievable, depending on the respective scenario and case. The continuing trend towards an increasing share of renewable

energy in the electricity mix has a positive effect on the competitiveness of the integrated system.

The detailed evaluation of the process integration revealed a good match between the heat supply from cooling processes and the heat demand from heating processes both in terms of overall load and the simultaneousness between supply and demand. Thermal storage tanks cover peak loads and provide useful heat storage, especially for the 95 °C circuit. A very modest use of backup resources in the process supports these findings, while further improvement potential was identified for the operation of these.

The results obtained clearly demonstrate that the integrated energy system with high temperature heat pumps and thermal storage tanks is suitable for providing all cooling and heating demands of the investigated dairy. The achieved performance values with a total system COP of 4.1 despite an energy-intensive operation period can certainly compete with conventional solutions. Thus, a further reduction of the specific energy consumption to the target value of 0.15 kWh l^{-1} product on an annual average appears feasible. To support the conclusions of this paper, further work should include an analysis over a longer period, considering various seasonal influences.

Declaration of Competing Interest

The authors declare that they have no known competing financial interests or personal relationships that could have appeared to influence the work reported in this paper.

Acknowledgements

This publication has been funded by HighEFF - Centre for an Energy Efficient and Competitive Industry for the Future, an 8-years' Research Centre under the FME-scheme (Centre for Environment-friendly Energy Research, 257632). The authors gratefully acknowledge the financial support from the Research Council of Norway and user partners of HighEFF. We would like to thank Mr. Kim Andre Lovas and Tine SA as well as Mr. Bjarne Horntvedt and Mr. Stein Rune Nordtvedt of Hybrid Energy AS for in-depth system details and access to their system data.

References

[1] J. Conti, P. Holtberg, J. Diefenderfer, A. LaRose, J.T. Turnure, L. Westfall, International Energy Outlook 2016 With Projections to 2040, 2016. https://doi.org/10.2172/1296780.
[2] O. Bamigbetan, T.M. Eikevik, P. Nekså, M. Bantle, Review of vapour compression heat pumps for high temperature heating using natural working fluids, Int. J. Refrig. 80 (2017) 197–211, https://doi.org/10.1016/j.ijrefrig.2017.04.021.
[3] C. Forman, I.K. Muritala, R. Pardemann, B. Meyer, Estimating the global waste heat potential, Renew. Sustain. Energy Rev. 57 (2016) 1568–1579, https://doi.org/10.1016/j.rser.2015.12.192.
[4] H. Jouhara, N. Khordehgah, S. Almahmoud, B. Delpech, A. Chauhan, S.A. Tassou, Waste heat recovery technologies and applications, Therm. Sci. Eng. Prog. 6 (2018) 268–289, https://doi.org/10.1016/j.tsep.2018.04.017.
[5] S. Broberg Viklund, M.T. Johansson, Technologies for utilization of industrial excess heat: potentials for energy recovery and CO2 emission reduction, Energy Convers. Manag. 77 (2014) 369–379, https://doi.org/10.1016/j.enconman.2013.09.052.
[6] J. Zhang, H.H. Zhang, Y.L. He, W.Q. Tao, A comprehensive review on advances and applications of industrial heat pumps based on the practices in China, Appl. Energy 178 (2016) 800–825, https://doi.org/10.1016/j.apenergy.2016.06.049.
[7] G. Kosmadakis, Estimating the potential of industrial (high-temperature) heat pumps for exploiting waste heat in EU industries, Appl. Therm. Eng. 156 (2019) 287–298, https://doi.org/10.1016/j.applthermaleng.2019.04.082.
[8] R. Bergamini, J.K. Jensen, B. Elmegaard, Thermodynamic competitiveness of high temperature vapor compression heat pumps for boiler substitution, Energy 182 (2019) 110–121, https://doi.org/10.1016/j.energy.2019.05.187.
[9] C. Arpagaus, F. Bless, M. Uhlmann, J. Schiffmann, S.S. Bertsch, High temperature heat pumps: market overview, state of the art, research status, refrigerants, and application potentials, Energy 152 (2018) 985–1010, https://doi.org/10.1016/j.energy.2018.03.166.
[10] A. Ladha-Sabur, S. Bakalis, P.J. Fryer, E. Lopez-Quiroga, Mapping energy consumption in food manufacturing, Trends Food Sci. Technol. 86 (2019) 270–280, https://doi.org/10.1016/j.tifs.2019.02.034.
[11] J.-M. Clairand, M. Briceño-León, G. Escrivá-Escrivá, A.M. Pantaleo, Review of energy efficiency technologies in the food industry: trends, barriers, and opportunities, IEEE Access 8 (2020) 48015–48029, https://doi.org/10.1109/ACCESS.2020.2979077.
[12] IDF Bulletin 436, Environmental/Ecological Impact of the Dairy Sector: Literature review on dairy products for an inventory of key issues; List of environmental initiatives and influences on the dairy sector, 2009. http://www.ukidf.org/documents/Bulletin436.pdf.
[13] M. Philipp, G. Schumm, P. Heck, F. Schlosser, R.H. Peesel, T.G. Walmsley, M. J. Atkins, Increasing energy efficiency of milk product batch sterilisation, Energy 164 (2018) 995–1010, https://doi.org/10.1016/j.energy.2018.09.002.
[14] C.A. Ramírez, M. Patel, K. Blok, From fluid milk to milk powder: energy use and energy efficiency in the European dairy industry, Energy 31 (2006) 1984–2004, https://doi.org/10.1016/j.energy.2005.10.014.
[15] M. Philipp, G. Schumm, R.H. Peesel, T.G. Walmsley, M.J. Atkins, F. Schlosser, J. Hesselbach, Optimal energy supply structures for industrial food processing sites in different countries considering energy transitions, Energy 146 (2018) 112–123, https://doi.org/10.1016/j.energy.2017.05.062.
[16] S.J. Rad, M.J. Lewis, Water utilisation, energy utilisation and waste water management in the dairy industry: a review, Int. J. Dairy Technol. 67 (2014) 1–20, https://doi.org/10.1111/1471-0307.12096.
[17] J.F. Wang, C. Brown, D.J. Cleland, Heat pump heat recovery options for food industry dryers, Int. J. Refrig. 86 (2018) 48–55, https://doi.org/10.1016/j.ijrefrig.2017.11.028.
[18] P.O. Kapustenko, L.M. Ulyev, S.A. Boldyryev, A.O. Garev, Integration of a heat pump into the heat supply system of a cheese production plant, Energy 33 (2008) 882–889, https://doi.org/10.1016/j.energy.2008.02.006.
[19] K. Semkov, E. Mooney, M. Connolly, C. Adley, Efficiency improvement through waste heat reduction, Appl. Therm. Eng. 70 (2014) 716–722, https://doi.org/10.1016/j.applthermaleng.2014.05.030.
[20] F. Bühler, T. Van Nguyen, J.K. Jensen, F.M. Holm, B. Elmegaard, Energy, exergy and advanced exergy analysis of a milk processing factory, Energy 162 (2018) 576–592, https://doi.org/10.1016/j.energy.2018.08.029.
[21] A.S. Wallerand, M. Kermani, I. Kantor, F. Maréchal, Optimal heat pump integration in industrial processes, Appl. Energy 219 (2018) 68–92, https://doi.org/10.1016/j.apenergy.2018.02.114.
[22] J.A. Stampfli, M.J. Atkins, D.G. Olsen, M.R.W. Walmsley, B. Wellig, Practical heat pump and storage integration into non-continuous processes: a hybrid approach utilizing insight based and nonlinear programming techniques, Energy 182 (2019) 236–253, https://doi.org/10.1016/j.energy.2019.05.218.
[23] European heat pump association, Winners of the Heat Pump City of the Year award - 2019 edition, 2019. https://www.ehpa.org/about/news/article/winners-of-the-heat-pump-city-of-the-year-award-2019-edition/ (accessed January 19, 2020).
[24] J. Stene, Design and Application of Ammonia Heat Pump Systems for Heating and Cooling of Non-Residential Buildings, in: Gustav Lorentzen Conf. Nat. Work. Fluids, Copenhagen, 2008, pp. 1–8.
[25] A. Osenbrück, Verfahren zur Kälteerzeugung bei Absorptionsmaschinen, DPR 84084, 1895.
[26] J.K. Jensen, W.B. Markussen, L. Reinholdt, B. Elmegaard, On the development of high temperature ammonia-water hybrid absorption-compression heat pumps, Int. J. Refrig. (2015), https://doi.org/10.1016/j.ijrefrig.2015.06.006.
[27] S.R. Nordtvedt, B.R. Horntvedt, J. Eikefjord, J. Johansen, Hybrid heat pump for waste heat recovery in norwegian food industry, in: 10th Int. Heat Pump Conf., 2011, pp. 1–5.
[28] R.J. Moffat, Describing the uncertainties in experimental results, Exp. Therm. Fluid Sci. 1 (1988) 3–17, https://doi.org/10.1016/0894-1777(88)90043-X.
[29] S. Smitt, I. Tolstorebrov, A. Hafner, Integrated CO2 system with HVAC and hot water for hotels: field measurements and performance evaluation, Int. J. Refrig. 116 (2020) 59–69, https://doi.org/10.1016/j.ijrefrig.2020.03.021.
[30] K.H. Kvalsvik, M. Bantle, Generating hot water for food processing plant using waste heat, high temperature heat pump and storage, in: Proc. 13th IIR-Gustav Lorentzen Conf. Nat. Refrig., International Institute of Refrigeration, 2018, pp. 92–99. https://doi.org/10.18462/iir.gl.2018.1111.
[31] NVE, Hvor kommer strømmen fra?, Nor. Water Resour. Energy Dir. - NVE. (2020). https://www.nve.no/energibruk-effektivisering-og-teknologier/energibruk/hvor-kommer-strommen-fra/?ref=mainmenu (accessed October 6, 2020).
[32] European Environment Agency, Overview of electricity production and use in Europe, 2018. https://www.eea.europa.eu/data-and-maps/indicators/overview-of-the-electricity-production-2/assessment-4 (accessed November 5, 2020).
[33] Multiconsult, Varedeklarasjon fjernvarme BKK – BREEAM-NOR 2016 for nybygg ver. 1.2, 2019.
[34] R. Scoccia, T. Toppi, M. Aprile, M. Motta, Absorption and compression heat pump systems for space heating and DHW in European buildings: energy, environmental and economic analysis, J. Build. Eng. 16 (2018) 94–105, https://doi.org/10.1016/j.jobe.2017.12.006.
[35] L. Reinholdt, J. Kristófersson, B. Zühlsdorf, B. Elmegaard, J. Jensen, T. Ommen, P. H. Jørgensen, Heat pump COP, part 1: Generalized method for screening of system integration potentials, in: Proc. 13th IIR-Gustav Lorentzen Conf. Nat. Refrig., International Institute of Refrigeration, 2018: pp. 1097–1104. https://doi.org/10.18462/iir.gl.2018.1380.
[36] M. Jarre, M. Noussan, M. Simonetti, Primary energy consumption of heat pumps in high renewable share electricity mixes, Energy Convers. Manag. 171 (2018) 1339–1351, https://doi.org/10.1016/j.enconman.2018.06.067.

[37] C. Mateu-Royo, S. Sawalha, A. Mota-Babiloni, J. Navarro-Esbrí, High temperature heat pump integration into district heating network, Energy Convers. Manag. 210 (2020), https://doi.org/10.1016/j.enconman.2020.112719.
[38] K. Soundararajan, H.K. Ho, B. Su, Sankey diagram framework for energy and exergy flows, Appl. Energy 136 (2014) 1035–1042, https://doi.org/10.1016/j.apenergy.2014.08.070.
[39] F. Schlosser, M. Jesper, J. Vogelsang, T.G. Walmsley, C. Arpagaus, J. Hesselbach, Large-scale heat pumps: applications, performance, economic feasibility and industrial integration, Renew. Sustain. Energy Rev. 133 (2020), https://doi.org/10.1016/j.rser.2020.110219.

Article III

M.U. Ahrens, I. Tolstorebrov, E.K. Tønsberg, A. Hafner, R.Z. Wang and T.M. Eikevik (2022). **Numerical investigation of an oil-free liquid-injected twin screw compressor with ammonia-water as refrigerant for high temperature heat pump applications.** In: *Applied Thermal Engineering* 219, 2023, 119425. DOI: 10.1016/j.applthermaleng.2022.119425

Author contributions: Conceptualization: M.U. Ahrens, I. Tolstorebrov, E.K. Tønsberg, A. Hafner, R. Wang and T.M. Eikevik; Methodology: M.U. Ahrens, I. Tolstorebrov and E.K. Tønsberg; Software: M. U. Ahrens and E.K. Tønsberg; Investigation: M.U. Ahrens, I. Tolstorebrov and E.K. Tønsberg; Resources: A. Hafner, R. Wang and T.M. Eikevik; Writing - Original Draft: M.U. Ahrens; Writing - Review and Editing: M.U. Ahrens, I. Tolstorebrov, E.K. Tønsberg, A. Hafner, R. Wang and T.M. Eikevik; Visualization: M.U. Ahrens; Supervision: I. Tolstorebrov, A. Hafner, R. Wang and T.M. Eikevik; Project Administration: M.U. Ahrens; Funding Acquisition: A. Hafner, R. Wang and T.M. Eikevik.

Applied Thermal Engineering 219 (2023) 119425

Contents lists available at ScienceDirect

Applied Thermal Engineering

journal homepage: www.elsevier.com/locate/apthermeng

Research Paper

Numerical investigation of an oil-free liquid-injected screw compressor with ammonia-water as refrigerant for high temperature heat pump applications

Marcel Ulrich Ahrens [a,*], Ignat Tolstorebrov [a], Even Kristian Tønsberg [a], Armin Hafner [a], R.Z. Wang [b], Trygve Magne Eikevik [a]

[a] NTNU, Department of Energy and Process Engineering, Kolbjørn Hejes vei 1B, 7491 Trondheim, Norway
[b] SJTU, Institute of Refrigeration and Cryogenics, Shanghai Jiao Tong University, 200240 Shanghai, China

ARTICLE INFO

Keywords:
Modelica modeling
Liquid injection
Oil-free screw compressor
Ammonia-water mixture
Absorption-compression heat pump
High temperature heat pump

ABSTRACT

This study investigates a numerical model of an oil-free twin screw compressor with an ammonia-water mixture as refrigerant and liquid injection. The compressor was identified as the main constraint to increase the heat sink temperature of absorption-compression heat pump systems past 120 °C. Liquid injection can reduce the superheating of the vapor during compression, while an existing liquid film can provide lubrication and sealing, enabling oil-free operation. A quasi-one-dimensional numerical model was developed using the Modelica language. It considers the effects of liquid injection flows and injection positions, leakages, heat losses, and variation in ammonia mass fractions. The results revealed a strong influence of occurring internal leakages, varying ammonia mass fractions of the injected solution and changing injection flows and positions on the evolution of temperature, pressure, and compression power. The injection with a lower ammonia mass fraction is beneficial for reducing the discharge temperature, discharge pressure and compression power. The increase in injection flow led to a further reduction in the values obtained. Continuous wet compression, required for sufficient sealing and lubrication of the compressor, was achieved with injection at 360° at the beginning of the compression phase and an injection rate of about 10% of the compressor's suction mass flow. By distributing the injection to two injection ports, wet compression can be supported and occurring under-compression and backflow can be reduced.

1. Introduction

Thermal processes in the industry are responsible for increasing energy consumption and the associated CO_2 emissions [1]. It is therefore of great interest to improve the energy efficiency of heat supply systems to reduce the consumption of energy and resources [2]. At the same time, large amounts of low-grade waste heat are available for potential waste heat recovery in various industrial processes [3]. For example, the waste heat potential in the EU is estimated at approx. 300 TWh/year, of which one third is at the temperature level below 200 °C, often referred to as low-temperature waste heat [4]. The use of high temperature heat pumps with natural working fluids, such as ammonia and water, instead of conventional boilers is an effective measure to exploit available waste heat while reducing the consumption of energy and dependency of fossil fuels, as outlined by Bergamini et al. [5] in a thermodynamic system comparison. Ahrens et al. [6] supported this statement by presenting operational performance results of an integrated energy system of an existing dairy plant, using heat pumps entirely for all cooling and heating applications. Many authors such as Arpagaus et al. [7], Kosmadakis [8], Marina et al. [9], and Jiang et al. [10] investigated and summarized the possibilities of using high temperature heat pumps and found great potential for the application in various industrial sectors for the supply of process heat with sink temperatures above 100 °C.

One of the suitable heat pump solutions for various industrial high temperature applications is the absorption-compression heat pump (ACHP) system with the zeotropic ammonia-water mixture as working fluid. The ACHP system combines the advantages of achievable sink temperatures up to 120 °C with large temperature lifts (>60 K) and non-isothermal heat transfers (>30 K) [11]. To increase the system efficiency and further extend the range of applications by achieving higher sink outlet temperatures and associated pressure levels, the compressor was

* Corresponding author.
E-mail address: marcel.u.ahrens@ntnu.no (M.U. Ahrens).

https://doi.org/10.1016/j.applthermaleng.2022.119425
Received 2 June 2022; Received in revised form 24 August 2022; Accepted 28 September 2022
Available online 3 October 2022

Nomenclature

Abbreviations

ACHP	Absorption compression heat pump
CFD	Computational fluid dynamics
CV	Control volume
IHX	Internal heat exchanger

Roman Letters

A	Flow area [m^2]
f	Operational frequency [Hz]
h	Specific enthalpy [J/kg]
$\dot{m}$	Mass flow rate [kg/s]
p	Pressure [bar]
$\dot{Q}$	Heat transfer rate [W]
T	Temperature [°C]
u	Specific internal energy [J/kg]
V	Volume [m^3]
W	Work [J]
$\dot{W}$	Power [W]
x	Ammonia mass fraction [-]

Greek symbols

α	Heat transfer coefficient [W/m^2K]
θ	Rotational angle of male rotor [rad]
ν^j	Built-in volume ratio [-]
ρ	Density [kg/m^3]
ω	Angular velocity [rad/s]

Subscripts

body	Compressor body
comp	Compression
dis	Discharge
disp	Displacement
eff	Effective flow area
in	Inlet
inj	Injection
j	Index
leak	Leakage
lean	Lean solution
max	Maximum
out	Outlet
rich	Rich solution
suc	Suction

identified as the main constraint due to limitations in the manageable compressor discharge temperature [12]. During his investigations, Zaytsev [13] identified the use of liquid-injected screw compressors (in operation as wet compression) as a potential solution to the problem of occurring superheat during the compression of ammonia vapor.

The general objectives of liquid injection during the compression process in a screw compressor include the reduction of occurring leakages along with the reduction of superheating, resulting in improved efficiency of the compressor [14]. Furthermore, this can lead to an oil-free operation of the ACHP system, promising further benefits including lower installation costs due to fewer components (oil separator and cooler) and higher efficiencies due to improved heat transfer and reduced heat losses without the use of oil. Given the elimination of oil stability issues in oil-free operation, an increased compressor discharge temperature can be accepted and exploited to potentially increase the achievable heat sink temperatures, as outlined by Infante Ferreira et al. [15]. Zaytsev et al. [16] stated that providing the compressor with sufficient liquid injection for lubrication and sealing is essential to increase the compressor's efficiencies and maintain the thermal limits of the compressor's material by providing cooling.

The process of liquid injection in twin screw compressors was investigated by several authors, both theoretical and experimental, for different refrigerants and working conditions. For the theoretical investigation, a variety of models with mostly numerical approaches were developed using different methods [17]. As reviewed by Wang et al. [18], these range from quasi-one-dimensional models to more complex computational fluid dynamics (CFD) models with varying degrees of complexity by incorporating different assumptions (homogenous or heterogenous model, losses considered, etc.) and phenomena occurring (heat and mass transfer). Stosic et al. [19] investigated the influence of oil injection and analysed widely the effects of various parameters such as oil flow rate, inlet temperature, droplet atomization, oil injection port position and compressor speed on the performance of a twin screw compressor. The authors concluded that the parameters have varying influences on the performance and an optimal oil injection quantity can be found. In another study of oil-free compressors, Stosic et al. [20] demonstrated that injecting small amounts of water to control the rotor temperature was sufficient to operate single-stage compressors at higher pressure ratios with only minor modifications required. Yang et al. [21] conducted an experimental investigation of a water-injected process-gas screw compressor and found that the liquid injection could reduce the compressor discharge temperature significantly while increasing the capacity. The authors further stated that an optimal mass flow of injected water exists to effectively lower the discharge temperature while sealing the gap between the female and male rotors. Tian et al. [22] investigated a water-injected twin-screw compressor for water vapor compression and demonstrated that the injection rate must be adjusted to the respective rotor speed and operating point. The aim is to achieve saturated discharge temperature and to avoid flooding with too much liquid water, as this results in the highest efficiencies. Furthermore, a uniform and fine atomization by using nozzles is advantageous, while the injection temperature revealed only little effect on the cooling effect. Basha et al. [23] numerically investigated the implementation of the oil injection for a twin screw compressor. They found that the distribution of the injection over multiple injection ports for the same total liquid quantity revealed a positive influence on the compression process and the parameter achieved. These findings were confirmed by Tian et al. [24] in an additional numerical investigation on mass and heat transfer in an ammonia oil-free twin-screw compressor with liquid injection. The obtained results indicated that the average droplet diameter of the injected liquid should be less than 100 μm to ensure a sufficient cooling effect and improve the performance of the compressor. Furthermore, an optimization method for the positioning of the injection nozzle and the amount of injected liquid was proposed. Based on their results, the authors recommended adding a second injection nozzle. This should be placed after the starting point of the compression process, where the temperature gradient is greatest, and should receive about 70 % of the total injected amount. Patel and Lakhera [25] conducted a comprehensive review of experimental studies related to twin screw compressors. They concluded that for oil-free operation the understanding of improved thermal management through the usage of liquid injection along with self-lubricated bearings must be further explored.

The conducted literature review revealed that many investigations were performed on liquid injection in twin screw compressors using pure refrigerants and oil injection. It was stated that liquid injection had an overall positive influence on the achievable efficiency and the reduction of superheating. Thereby, it is important to maintain a high vapor quality of the compressed fluid while avoiding the flooding of the compressor with too much liquid. This results in an optimization

problem for the liquid injection flow. For the implementation of the injection, both the positioning of the injection port in the compression cycle and the distribution over a single port or multiple port injection revealed impact on the compression process. Furthermore, improved cooling effects were obtained with smaller droplet diameters, which can be provided by using nozzles and other devices.

Recent studies on the oil-free operation of the screw compressor and the use of ammonia-water mixture are limited to the conducted studies on wet compression with liquid injection in the suction and compression phases investigated by Gudjonsdottir et al. [26] and Gudjonsdottir and Infante Ferreira [27]. However, the system setup used, as well as the operating conditions investigated, deviate from the envisaged objectives of this study. Thus, a research gap exists for the planned integration of an oil-free twin screw compressor with liquid injection into the ACHP system at high temperature operation. For this, the effects on the compression process of different injected liquid rates, injection positions and injection distributions for changing ammonia mass fractions of the ammonia-water mixture must be investigated.

To address the identified research questions, this study introduces and investigates the quasi-one-dimensional model of an oil-free liquid-injected twin screw compressor for use in the ACHP system at high temperature operation. The purpose is to improve the understanding of the thermodynamic behaviour and expected results during the compression process with varying liquid injection parameters. Furthermore, the obtained results provide information for the preferred design of the liquid injection when integrated into ACHP systems and support the planning of necessary experimental investigations.

2. Background

In this section, the theoretical background for the conducted research is presented. First, the ACHP system using ammonia-water mixture as working fluid is described, with a special focus on the compressor to be investigated and the discussion of possibilities for implementing liquid injection. The subsequent thermodynamic analysis provides the basis for the development of the simulation model and the evaluation and assessment of the achieved results.

2.1. The absorption-compression heat pump system

A schematic illustration of the ACHP system, often referred to as Osenbrück cycle in recognition of its inventor Osenbrück (1895) [28], is presented in Fig. 1. For the focus of this study, two possible options for the desired implementation of liquid injection in the screw compressor under investigation were identified: injection of lean solution (Option 1) and injection of rich solution (Option 2).

In the ACHP, the desorber and absorber transfer heat with the heat source and sink. The ammonia-rich solution enters the desorber at low pressure (10). As the temperature increases, the solubility of the ammonia in water decreases, causing ammonia vapor to expel. As a result, a two-phase mixture leaving the desorber towards the liquid–vapor separator (1). The low-pressure vapor and lean solution are separated in the liquid–vapor separator before being directed to the compressor (2) and solution pump (4). The compressor increases the pressure and temperature of the vapor (2 to 3), while the pump elevates the pressure of the lean solution correspondingly (4 to 5). To improve the cycle performance, an internal heat exchanger (IHX) is installed to interconnect the solution streams. Heat is exchanged between the lean and rich solution, resulting in a temperature increase of the lean solution (5 to 6) and a decrease of the rich solution (8 to 9). At the high-pressure side, the lean solution (6) is then mixed with the superheated NH_3 vapor from the compressor (3) at the inlet of the absorber (7). In the absorber, vapor is absorbed by the liquid and the generated heat is transferred to the heat sink fluid. During the absorption process, the NH_3 mass fraction in the solution phase gradually increases and a saturated solution emerges at the outlet of the absorber. The ammonia-rich solution then flows through the IHX before being throttled down to desorber's pressure (8 to 9 to 10) and thus completing the cycle.

2.2. Possibilities for liquid injection

For the study of compression with liquid injection, the effects with varying NH_3 mass fraction of the injected solution (x_{inj}), injected mass flow rate $\left(\dot{m}_{inj}\right)$ and position of injection (θ_{inj}) are investigated. With respect to the structure of the ACHP system (see Fig. 1), two possible options for the arrangement of the injection line are highlighted. Option

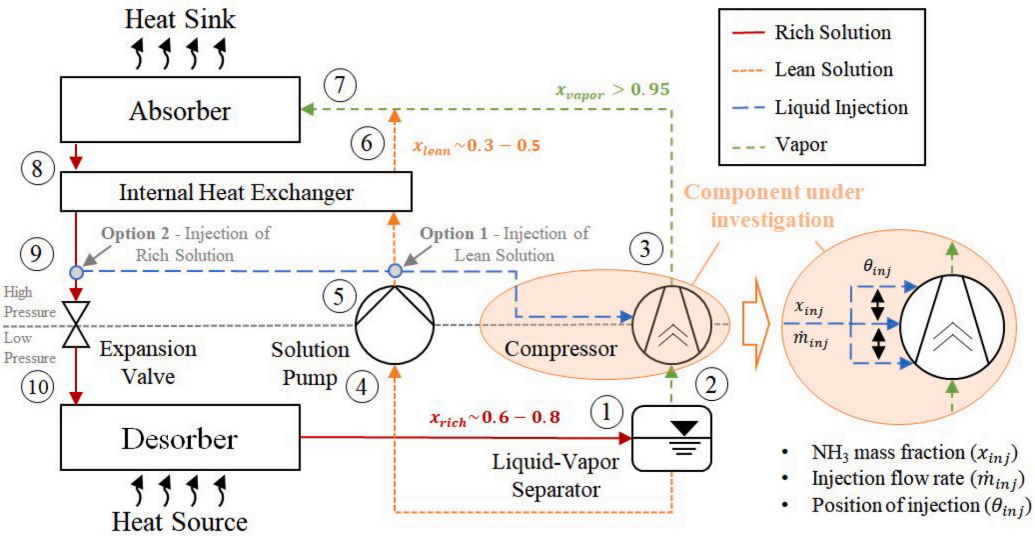

Fig. 1. Schematic illustration of ACHP system including possible liquid injection options.

1 - Injection of the lean solution: extraction of the lean solution (x_{lean} 0.3 −0.5) downstream of the solution pump, where the solution is significantly subcooled due to the previous pressure rise from the saturated state. Option 2 - Injection of the rich solution: extraction of the rich solution (x_{rich} 0.6 −0.8) downstream of the IHX and upstream of the expansion valve. In this case, the solution remains at high pressure and was subcooled by the lean solution. Thus, the solution for injection will be present in highly subcooled liquid state for both options. Depending on the position of the injection, subcooled solution will be injected into increasingly superheated vapor with the start of the compression phase. In this case, the solution is not in a state of equilibrium in terms of pressure and temperature. The equilibrium state of the solution parameters is strongly influenced by the injection flow rate and possibility of injection at multiple positions between suction, compression, and discharge phases, along with internal flows due to leakage. Furthermore, the thermodynamic properties of the solution and vapor phases change as a function of temperature, pressure, and NH_3 mass fraction. It is therefore important to further describe and analyse the expected thermodynamic behaviour of the NH_3-H_2O mixture during occurring parameter changes.

2.3. Thermodynamic analysis

The NH_3-H_2O mixture used in the ACHP system is a zeotropic mixture consisting of two solution components with different boiling points [29]. Fig. 2 shows the temperature-NH_3 mass fraction (T −x) diagram with bubble point and dew point lines at different pressure levels.

The indicated example is valid for liquid–vapor equilibrium conditions and illustrates the thermodynamic behaviour of the NH_3-H_2O mixture at a constant NH_3 mass fraction x_1 of 0.5 and pressure p_1 of 5 bar during the temperature change from subcooled solution state (0) to superheated vapor state (4). The injected solution (lean or rich) is in the subcooled state (0). The temperature of the solution is gradually increased due to the contact with the superheated vapor in compressor. At the boiling point (1′) the saturated vapor of NH_3 and H_2O is formed (1″). The further increasing of the solution's temperature (2) results in desorption of NH_3 and the NH_3 mass fraction in the liquid phase drops (1′ −3′), while vapor fraction of NH_3 is increasing (1″ −3″). In the superheated state (4) is the solution fully evaporated. Rising the pressure (p_1 to p_3) leads to increasing temperatures of the bubble point and dew point lines. Thus, the degree of subcooling of the solution at a higher pressure is increasing. It should be noted that the equilibrium state of the solution is not defined by pressure and temperature only. The significant amount of NH_3 in the superheated vapor shifts the equilibrium state of the NH_3-H_2O vapor mixture. Thus, the evaporation of saturated solution will continue to compensate for the low partial pressure of H_2O vapor in the gas mixture [24]. Due to this, in the case of low mass flow rates of the injected solution, the full evaporation will occur irrespectively on the temperature and pressure. When used in ACHP systems, however, remaining liquid and wet compression are essential for sufficient sealing and lubrication of the compressor.

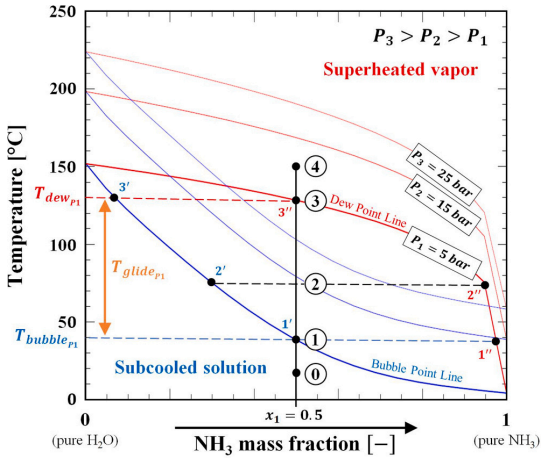

Fig. 2. Temperature-NH_3 mass fraction (*T*-x) diagram with bubble point and dew point lines for NH_3-H_2O mixture at different pressure levels.

3. MODELICA twin screw compressor model

The developed model of the oil-free liquid-injected twin screw compressor is a quasi-one-dimensional numerical model with multiple control volumes (CV), each representing the volume of one rotor cavity, and follows the concepts presented by Chamoun et al. [30] and Tian et al. [22]. The model was written in the object-oriented Modelica language [Modelica Association] and was implemented and solved in the Dymola 2020 simulation environment using the ESDIRK23A standard solver by Dassault Systèmes [31]. Two commercial Modelica libraries were used for the implementation, namely TIL-Suite 3.5 and TILMedia 3.5 provided by TLK-Thermo GmbH [32,33]. TIL-Suite is a component library for steady-state and transient simulation of thermodynamic systems, while TILMedia provides methods and data for calculating the properties of thermophysical substances. The model considers the effects of liquid injection, leakage flows, and heat losses and is designed to investigate various arrangements of liquid injection and operating conditions.

3.1. Description of the control volume

The change in the boundaries (volume) of each CV occurs with time, often expressed as rotational angle of the male rotor. Thereby, the total rotation time/angle that one cavity undergoes during a complete compression cycle depends on the length and pitch of the rotors. This is applied from the beginning of the suction phase to the end of the discharge phase. When a CV enters the suction phase its volume increases, while it decreases during the compression and discharge phases. The underlying volume alteration throughout an entire compression cycle is defined by the compressor's geometry. This is identical for all CVs but contains a time delay between individual CV. Thus, the leading cavity (e.g., CV_j) can simultaneously undergo a volume reduction, while the trailing cavity (CV_{j-1}) still undergoes a volume increase. Each CV is an open system with three inlet paths (suction, leak-in and liquid injection) and two outlet paths (discharge and leak-out). Additionally, the system receives compression power from the rotor ($\dot{W}_{comp}$) and dissipates heat to the compressor body and ambient ($\dot{Q}_{loss}$). As a result, pressure, temperature, mass, internal energy and NH_3 mass fraction differ in each CV at any point in time. Fig. 3 illustrates the simplified mass and energy balance associated with each CV.

3.2. Basic equations for the control volume

Based on a set of differential equations for the conservation of mass and energy, the model simulates the processes (heat and mass flow) of the twin screw compressor in each CV at any time. Since there are leakage flows and the cavities are periodically connected to suction, injection and discharge, the CV is treated as an open system which can be described by the first law of thermodynamics [35]. Neglecting kinetic energy and gravitational energy, and expressing the equations based on rotational angle of the male rotor (θ), the mass and energy balances can be expressed as [36,37]:

$$\frac{d(m)}{d\theta} = \sum \frac{dm_{in}}{d\theta} - \sum \frac{dm_{out}}{d\theta} \quad (1)$$

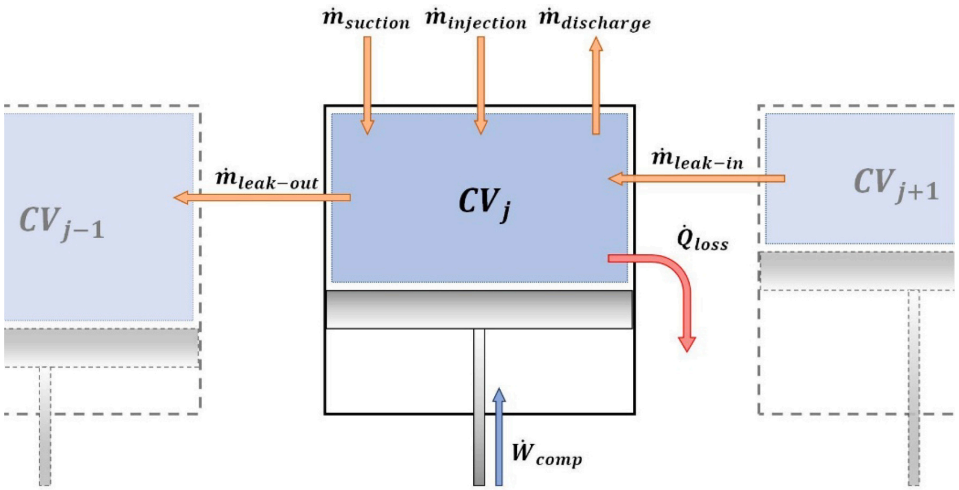

Fig. 3. Simplified mass and energy balance associated with each control volume ().
adapted from [34]

$$\frac{d(mx)}{d\theta} = \sum \frac{dm_{in}}{d\theta} x_{in} - \sum \frac{dm_{out}}{d\theta} x_{out} \tag{2}$$

$$\frac{d(mu)}{d\theta} = \sum \frac{dm_{in}}{d\theta} h_{in} - \sum \frac{dm_{out}}{d\theta} h_{out} + \frac{dW_{comp}}{d\theta} - \frac{dQ_{loss}}{d\theta} \tag{3}$$

where m is mass, x is NH_3 mass fraction, u is specific internal energy, h is specific enthalpy, W is compression work and Q is heat between the working fluid and compressor body. As the working fluid is a mixture, Eq. (2) is required in addition to Eq. (1) to determine the composition of the mixture. At an angular velocity of $\omega = d\theta/dt$, the equations can be formulated as [30]:

$$\omega \frac{d(m)}{d\theta} = \sum \dot{m}_{in} - \sum \dot{m}_{out} \tag{4}$$

$$\omega \frac{d(mx)}{d\theta} = \sum \dot{m}_{in} x_{in} - \sum \dot{m}_{out} x_{out} \tag{5}$$

$$\omega \frac{d(mu)}{d\theta} = \sum \dot{m}_{in} h_{in} - \sum \dot{m}_{out} h_{out} + \dot{W}_{comp} - \dot{Q}_{loss} \tag{6}$$

With the compression power expressed as:

$$\dot{W}_{comp} = -\omega p \frac{dV}{d\theta} = -p \frac{dV}{dt} \tag{7}$$

where p is pressure in the CV and dV/dt is the time derivative of the cavity volume. For this investigation, a mechanical efficiency of 100 % is assumed and friction losses as a function of the compression power and rotation speed are neglected. The temperature of the working fluid is substantially higher than the temperature of the ambient air surrounding the compressor. Therefore, heat losses to the compressor body and the ambient should be assessed. The heat transfer rate from the working fluid to the compressor body is determined as [38]:

$$\dot{Q}_{loss} = \alpha V^{2/3} (T - T_{body}) \tag{8}$$

Where α is the heat transfer coefficient between working fluid and compressor body, $V^{2/3}$ denotes the available heat transfer area of the cavity volume, T is the temperature of the working fluid, and T_{body} is the average surface temperature of the compressor body. Determining the temperature of the compressor body is not trivial and is generally influenced by the heat transferred by the working fluid and additional factors such as mechanical heat losses. The temperature of the working fluid and the influence of other factors vary greatly along the length of the compressor during the compression process. However, the thermal conductivity of the compressor body made of steel is relatively high, and uniform temperature distribution can be simplified assumed.

3.3. Determination of thermodynamic state properties

By solving the mass and energy equations, the pressure, specific internal energy, and NH_3 mass fraction of the NH_3-H_2O mixture are determined for each CV throughout the entire compression cycle continuously. With the assumption of liquid vapor equilibrium conditions, the thermodynamic state properties of the NH_3-H_2O mixture in each CV were determined using the calculation procedures provided by the TILMedia library [33]. Here, pressure, specific enthalpy and NH_3 mass fraction are used as input parameters. By using the specific internal energy calculated from Eq. (6), the specific enthalpy in the CV can be obtained:

$$h = u + \frac{p}{\rho} \tag{9}$$

where ρ is the density of the working fluid. The density is obtained from the TILMedia property calculation procedure [33] and with $m = \rho V$ also utilized when calculating the total mass in the CV.

3.4. Determination of flow rates

As illustrated in Fig. 3, there are different paths through which the working fluid can flow throughout an entire compression cycle. The mass flow rates for the suction, discharge and leakage paths are determined using [39]:

$$\dot{m} = A_{eff} \bullet \sqrt{2 \bullet \rho \bullet \Delta p} \tag{10}$$

where A_{eff} is the effective flow area of the flow path in m^2, ρ is the density of the working fluid upstream of the flow, and Δp is the pressure difference across the flow area. When calculating suction mass flow rates, for instance, A_{eff} represents the effective flow area of the suction port, ρ the density of the working fluid in the suction line, and Δp the pressure difference between the suction line and the connected CV. Thereby, A_{eff} varies with time as the CV goes through the suction phase, while it is set to zero during the compression and discharge phases. The same applies adjusted for the discharge path and phase. The

characteristics of the A_{eff} curves are dependent on the set built-in volume ratio (V^i) and are defined by the geometry of the respective ports and the rotor profile [40]. Contrary to the other paths, the injection mass flow rate is defined as a fixed value. The injection starts when a CV reaches the injection port location (θ_{inj}). It remains active until the trailing cavity reaches the injection port location, determined by the existing phase shift between the CVs.

Occurring leakage flows within the compressor are considered by linking adjacent CVs. The leakage path represents the gap between the rotor tips and the compressor housing, as it is one of the paths with the greatest impact on compressor performance [41]. Here, A_{eff} depends on the length of the sealing line, and it is assumed to be directly proportional to the cavity volume. Furthermore, it is assumed that the length of the sealing line between two adjacent CVs is determined by the smallest cavity volume at each point in time. Thus, the effective leakage area is calculated using the leakage area function as follows:

$$A_{eff,leak} = C_{leak} \bullet \min\left(V_{CV_{j-1}}, V_{CV_j}\right) \tag{11}$$

where C_{leak} represents the leakage flow coefficient, an estimated constant ranging from 0 to 1 [m^{-1}]. $V_{CV_{j-1}}$ and V_{CV_j} represent the adjacent trailing and leading cavity volumes behind and in front of the sealing line.

3.5. Model parameter

To perform the simulations in this investigation, the model input parameters listed in Table 1 were used to define the screw compressor model.

The compressor model is divided into eight control volumes, resulting in a phase shift of 90° between each CV. It is assumed that for each CV the total rotation angle during a compression cycle (θ_{cycle}) is 720°. Under the assumption that the male rotor spins at an operational frequency (f) of 50 Hz, it takes 40 ms to complete one entire cycle. The displacement volume (V_{disp}) is set to 335 cm^3 with a $\nu^i = (V_{disp}/V_{dis})$ of 3.65. The maximum effective flow areas are set at 50 cm^2 for the suction path (A_{suc}) and 10 cm^2 for the discharge path (A_{dis}). Fig. 4 shows the volume evolutions for two adjacent CVs with 90° phase shift and the resulting effective flow area $A_{eff,leak}$ of the leakage path through the gap between rotor tips and compressor housing using Eq. (11) with a C_{leak} value of 0.05 m^{-1}.

The evolution of the effective flow area A_{eff} depends on the smallest volume of the adjacent CVs. While one of the CVs remains in the compression phase (from V_{disp} to V_{dis}) starting from state (1) and ending at state (2), an effective flow area exists, and leakage flow occurs. If both CVs are in the suction phase (from 0 to V_{disp}) or discharge phase (from V_{dis} to 0), the respective path openings represent a much larger area, and the leakage area is set to zero. The same applies when the leading CV (CV_j) enters the suction phase, since the CVs are on opposite sides of the compressor and there is no leakage connection between them.

3.6. Simulation setup

The developed screw compressor model can be used as a stand-alone model or integrated into a larger system model. For this study, the model was used as stand-alone and connected with boundaries defining the conditions for suction, injection, and discharge ports. Each boundary is defined by three parameters: pressure, temperature and NH_3 mass fraction. Fig. 5 illustrates the simulation setup with the defined boundary conditions for the suction, injection, and discharge ports.

Table 1
Model input parameter used.

Parameter	# of CV	θ_{cycle}	f	V_{disp}	ν^i	A_{suc}	A_{dis}
Value	8	720°	50 Hz	335 cm^3	3.65	50 cm^2	10 cm^2

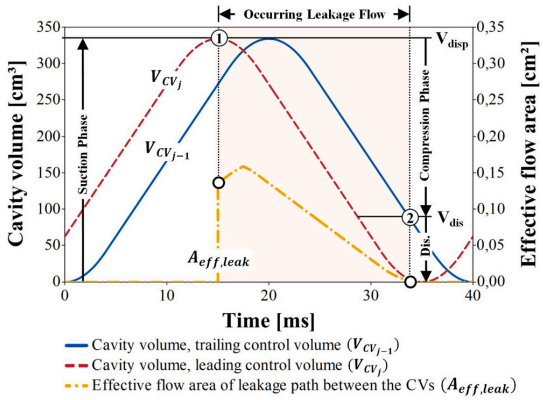

Fig. 4. Evolution of cavity volumes of two adjacent CVs and resulting effective flow area of the implemented leakage path through the gap between rotor tips and compressor housing.

The defined boundary conditions are based on the expected operating conditions for the screw compressor in the ACHP system (see Section 2). The desorber and absorber pressures are assumed to be 5 bar and 25 bar, respectively, corresponding to the suction (p_{suc}) and discharge (p_{dis}) pressure of the compressor model. The NH_3 mass fraction of the rich solution is set to 0.7 with a temperature of 55 °C in the liquid–vapor separator. In liquid–vapor equilibrium, this results in the NH_3 mass fraction of 0.985 in the vapor phase (x_{suc}). The injection boundary pressure, p_{inj}, is set to the high-pressure side of 25 bar and the injection temperature, T_{inj}, to 55 °C. During injection, an adjustment with the prevailing pressure in the CV takes place. Thus, the injection pressure at the respective injection port is adjusted depending on the positioning. The NH_3 mass fraction of the injected liquid, x_{inj}, is defined as variable (var.) since simulations with varying values are to be performed. The values for T_{dis} and x_{dis} of the discharge boundary are the result of the compression in the compressor model. In addition to the model input parameters given in Table 1, values for C_{leak}, the injection angle (θ_{inj}) and the injection mass flow rate ($\dot{m}_{inj}$) were defined and varied to perform the simulations.

3.7. Model validation

The purpose of the present study is to improve and discuss the understanding of the thermodynamic behaviour of an oil-free twin-screw compressor with NH_3-H_2O mixture as refrigerant and liquid injection during the compression process. Achievable efficiencies and other performance parameters are influenced by occurring leakages, mechanical losses, and heat losses, and other component and/or operation specific parameters. These are difficult to predict without detailed data on the geometry and operational performance and require experimental investigations. Since this study is a preliminary theoretical investigation without an existing prototype and detailed experimental data for validation, a component-based validation is performed to verify the reliability of the achievable results.

For this, the component models used in the developed model are checked and validated with respect to their physical and thermodynamic properties and reliability. The TILMedia 3.5 library [33] provides the determined thermo-physical properties of the investigated NH_3-H_2O mixture for each time point. The operating parameters are within the valid working range and can therefore be assumed to be sufficiently accurate. Further, TIL-Suite 3.5 [33] model components such as ports were utilized, which are commonly used and provide reliable results. Smitt et al. [42] used these libraries for a variety of components to study integrated energy systems and obtained less than 10 % deviation from

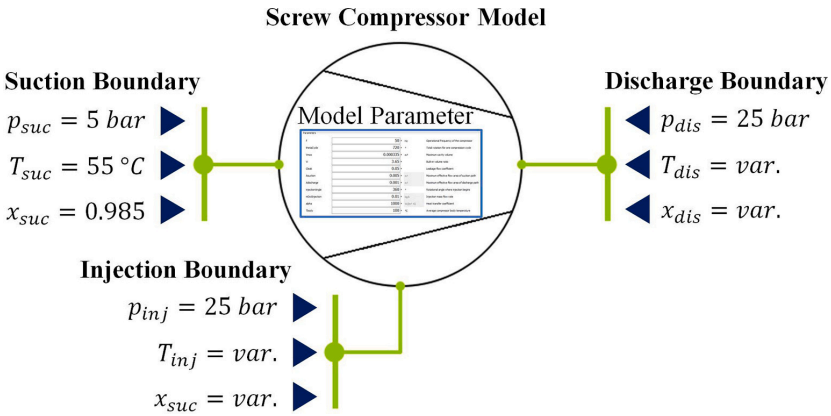

Fig. 5. Simulation setup of the screw compressor model with defined boundary conditions.

the experimentally determined readings. Chamoun et al. [30] used a Modelica-based model for the comprehensive analysis of an experimentally tested twin screw compressor. Although no explicit validation of the model results was performed, it can be assumed that the deviation of the simulation results was within an acceptable range.

Occurring flow rates are implemented using Eq. (10), which is widely used for investigations of this phenomena in screw compressors [38,39]. Required area functions for inlet and outlet ports in this study are defined following the extensive investigation by Zaytsev [13]. The same applies to the implemented leakage flows, which are calculated using Eq. (11). The curves of the cavity volume and the resulting effective flow area are shown in Fig. 4 and are comparable to the results presented by Zaytsev [13]. For the implemented control volume, homogeneous pressure and liquid–vapor distribution are assumed, and mechanical losses are neglected. With these assumptions, the compression process in the CV can be compared with isentropic compression and for a case without leakage and liquid injection compared with adiabatic compression. In this context, the obtained results are presented and discussed in the next section.

4. Results and discussion

The aim of this study was to investigate the effects of different parameters on the compressor's discharge temperature and pressure, and compression power throughout the compression process. The discharge temperature of the compressor was identified as the main constraint for the ACHP system in achieving higher heat sink temperatures and system efficiency. For this, the examined results focus on one control volume passing through an entire compression cycle.

4.1. Leakage flow coefficient

Internal leakage influences the performance of screw compressors [13,41]. It is therefore essential to apply an appropriate value for the leakage flow coefficient, C_{leak}, in the model. Simulations were performed with varying C_{leak} values ranging from 0 m^{-1} to 0.1 m^{-1} without liquid injection ($\dot{m}_{inj}$ set to 0). Fig. 6 presents the resulting pressure evolution throughout a whole compression cycle of a CV in a pressure–volume diagram.

The pressure curves indicate that increasing C_{leak} values accelerate the pressure evolution, as reflected by higher pressures at a respective volume. Moreover, it results in higher degree of over-compression at the end of the compression phase when reaching the discharge port and increases the required compression power. With further increasing of leakage ($C_{leak} > 0.1\ m^{-1}$), over-compression is decreasing and even

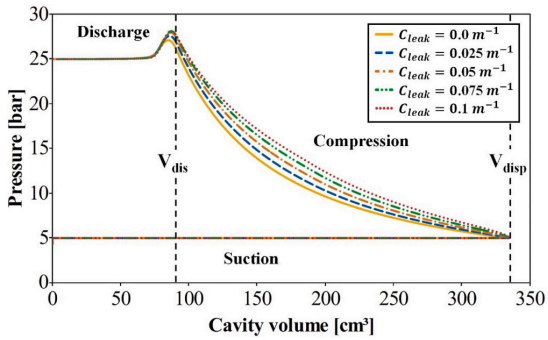

Fig. 6. Pressure-volume diagram for different C_{leak} values without liquid injection ($\dot{m}_{inj} = 0\ kg/s$).

under-compression can be observed, due to excessive backflow of working fluid at a fixed built-in volume ratio (not shown at Fig. 6). At the same time, high leakage increases the discharge temperatures, as heated vapor flows back from volume cavities at higher pressure levels towards the suction port and is partly re-compressed. The maximum temperature reached 243 °C at C_{leak} of 0.1 m^{-1}, and it was 40 K higher when compared with the ideal case without leakage. The pressure curve without leakage ($C_{leak} = 0.0\ m^{-1}$) and with no liquid injection can be used as a reference for adiabatic compression since other losses are neglected. The plotted curve patterns are qualitatively comparable with other literature results [15].

During the suction phase, leaking vapor occupies a fraction of the available suction volume, thus decreasing the volumetric efficiency occurs. With a C_{leak} value of 0.1 m^{-1}, the reduction in volumetric efficiency was calculated at 13 %. Fleming and Tang (1995) [41] stated that the implemented leakage path between the rotor tips and the compressor housing contributes to a 2 % to 3 % reduction in volumetric efficiency compared to a scenario without leakage. An equivalent result can be obtained with a value of C_{leak} between 0.025 m^{-1} and 0.035 m^{-1}. However, to compensate for the additional reductions in volumetric efficiency caused by leakage paths other than those considered in the model, a C_{leak} value of 0.05 m^{-1} was used for the further investigation of liquid injection. This leads to a reduction in volumetric efficiency of about 5 % compared to the ideal case without leakage.

4.2. Heat losses to compressor body and ambient

The temperature of the working fluid in the CV rises significantly during the compression process, similar to the increase in pressure (see Fig. 6). Thus, there is a very large temperature difference between the working fluid and the ambient at the end of the compression phase, implying that large heat losses can occur. On the other hand, the volume of the compression cavity, and thus the available transfer area, decreases continuously towards the end of compression. These opposing trends lead to uncertainties on whether the heat losses to the compressor body and ambient have a significant impact on the compression parameters. It is often argued in the literature that the heat loss to the casing and the environment can be neglected because the heat transfer coefficient between the steam and the compressor casing is small [20]. Tian et al. [22], in their investigation of water-injected screw compressors, further specified that the cooling effect of the injected liquid has greater influence and heat losses to the ambient are neglected.

To evaluate the effects of heat losses to the compressor body and ambient, an investigation was performed for a case without liquid injection ($\dot{m}_{inj}$ set to 0) and a C_{leak} value of 0.05 m^{-1}, assuming a uniform T_{body} value of 80 °C and a varying α value from 0 up to an unlikely high value of 5000 W/m^2K. The achieved results revealed that the influence of heat losses is minimal, even with an unreasonably high value for α, such as 5000 W/m^2K. The working fluid is slightly heated during the suction phase, and there is a slight cooling effect on the last section during discharge, but apart from this the temperature curves are almost identical. The same results are obtained for pressure and compression work. Change rates are below ± 1.0 % for the observed maximum values. Furthermore, as described by Stosic et al. [20], the temperature profile in an actual screw compressor is not uniform during operation and the temperature of the compressor body is higher on the discharge end compared to the suction end. Thus, it can be argued that the temperature differences between the working fluid and the compressor body will be smaller, and less heat will be transferred than in the simulation when using an average body temperature. This strongly suggests that heat losses to the compressor body can be neglected in this study. Therefore, the α value is set to zero for the following simulations and heat losses are not considered.

4.3. NH_3 mass fraction of the injection liquid

The NH_3 mass fractions of the various streams in ACHP systems change depending on the design and operating conditions. To investigate the effects on the compression process, the NH_3 mass fraction of the injection liquid was varied from pure water ($x_{inj} = 0$) to pure ammonia ($x_{inj} = 1$) at a constant injection angle of 360° (beginning at the start of the compression phase and active for a rotational angle of 90°) and injection mass flow rate of 0.01 kg/s, corresponding to about 5 % of the

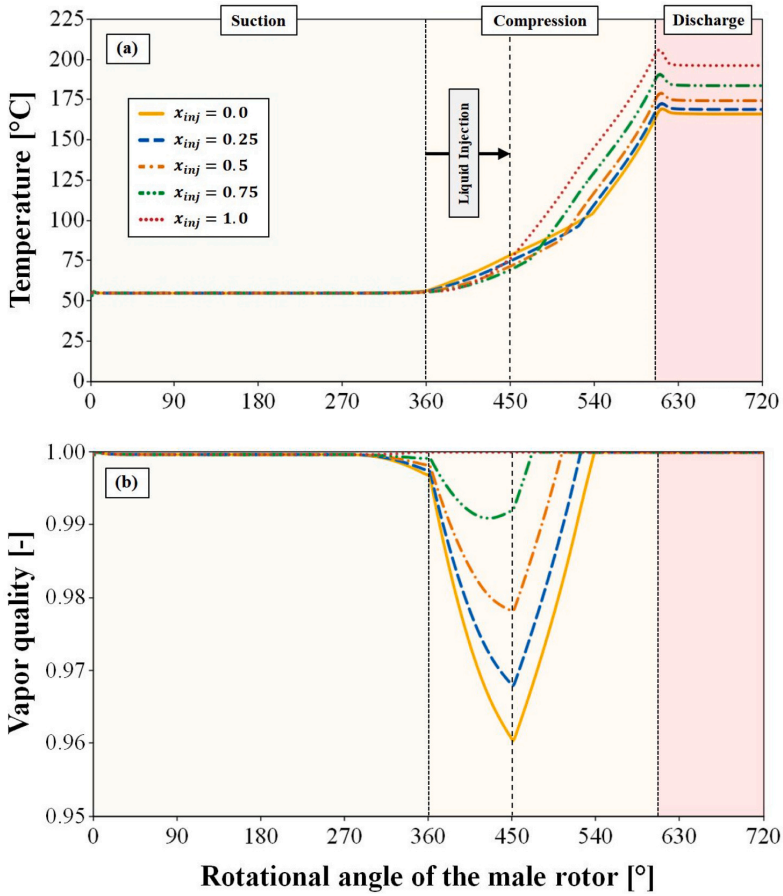

Fig. 7. (a) Temperature and (b) vapor quality evolution for different x_{inj} values at constant $C_{leak} = 0.05\ m^{-1}$, $\theta_{inj} = 360^{\circ}$ and $\dot{m}_{inj} = 0.01\ kg/s$.

compressor's suction mass flow rate. Fig. 7 illustrates the temperature and vapor quality evolution for different ammonia-water solutions.

The lowest discharge temperature was obtained when the injection liquid was pure water ($x_{inj} = 0$), while the highest discharge temperature was obtained for pure ammonia ($x_{inj} = 1$), Fig. 7a. Characteristics of the different curves were very similar, with a relatively low temperature rise during the first part of the compression phase. At a certain point, the gradient of the respective curve changes, and the temperature rises more sharply when the liquid fraction is fully evaporated. This inflection point occurred earlier for higher NH_3 mass fraction of the injection liquid, and it resulted in higher discharge temperature as well. This can be explained by increased evaporation of liquid and differences in heat capacity and saturation temperature for different NH_3 mass fractions of the ammonia-water mixture (see Fig. 2). Once the liquid injection stops and all remaining liquid is evaporated, the temperature increases sharply.

The plotted evolution of the vapor quality, Fig. 7b, helps to understand the temperature profile alteration shown on Fig. 7a. Except for pure ammonia, the vapor quality drops into the two-phase region when liquid is injected into the CV, but it immediately rises again after the injection stops and the volume is further compressed. The wet compression occurs in all such cases. The length of the wet compression strongly depends on the NH_3 mass fraction in the injected solution: the longest wet compression was observed for pure water and none for pure ammonia. The NH_3 mass fraction in the CV varies from 0.985 at suction and ranges between 0.941 and 0.987 at the discharge for pure water and ammonia, respectively. The extremums for temperature and pressure, and compression power are given in Table 2.

The highest temperature, pressure and compression power were observed when injecting pure ammonia. The high temperature is beneficial for oil-free high temperature heat pumps; however, it can be limited by the material properties of the compressor. At the same time, for the investigated case, where the pressure in absorber was set to 25 bar, the injection of pure ammonia resulted in the highest degree of over-compression, when compared with pure water. Due to this, an increased compression power was observed.

4.4. Injection mass flow rate

Previous results have indicated that remaining liquid in the CV (vapor quality less than 1) during the compression process influences the discharge temperature, degree of over-compression and compressor power. Therefore, it is expected that besides the NH_3 mass fraction, the injected mass flow rate has a significant influence on the compression process. In the further investigation, the NH_3 mass fraction of the injection fluid is set to 0.4 and 0.7, respectively, which are feasible values for the lean and rich solution in the ACHP system. The injection mass flow rate varied from 0.00 kg/s to 0.02 kg/s at a constant C_{leak} value of 0.05 m^{-1} and injection angle of 360°. This corresponded to a range between 0 % and 10 % of the compressor's suction mass flow rate. Fig. 8 shows the temperature evolution for different liquid injection mass flow rates with NH_3 mass fraction of 0.4.

The results indicate a significant influence of the injection mass flow rate on the temperature evolution and maximum discharge temperature. The discharge temperature is the highest with zero injection and decreases with higher injection mass flow rates. The inflection point of temperature evolution was observed when the liquid fraction was fully evaporated. This trend was similar with the findings from Fig. 7a. With higher injection rates, the inflection point shifts towards the end of the compression phase. At an injection mass flow rate of 0.02 kg/s, wet compression occurs during the entire compression phase. With increased NH_3 mass fraction of 0.7, complete wet compression occurs first at a value between 0.02 kg/s and 0.025 kg/s. The extremums for temperature and pressure, and compressor power for different injection mass flow rates with NH_3 mass fractions of 0.4 and 0.7 are given in Table 3.

The discharge temperature was influenced by the injected mass flow rates and solution mass fraction. The lowest discharge temperature was observed for injected mass flow rates of 0.02 kg/s and lean solution with NH_3 mass fraction of 0.4. The injection of rich solution ($x_{inj} = 0.7$) shows the same trend as lean solution, but discharge temperature, pressure and compression power were higher. The discharge NH_3 mass fractions in the CV range from 0.985 to 0.937 and to 0.962 for injection mass flow rates from 0.0 kg/s to 0.02 kg/s with NH_3 mass fractions of 0.4 and 0.7, respectively. The increasing of the injected mass flows leads to under-compression within the CV when reaching the discharge port at a rotational angle of 605°. As shown in Fig. 9, this can result in backflow from the discharge port into the CV, generating pressure and flow pulsation.

Pressure and flow pulsation result in additional mechanical stress on the compressor and noise generation. To avoid over- or under-compression, an injection mass flow rate of approx. 0.01 kg/s for an NH_3 mass fraction of 0.4 is recommended. Here, only the leakage flow into the trailing CV was compensated, but no excessive backflow into the CV was generated. With an NH_3 mass fraction of 0.7, the recommended rate is between 0.01 kg/s and 0.015 kg/s. For application in the ACHP system, an optimization problem arises that must be solved depending on the specific operating conditions, considering all system parameters.

4.5. Positioning of injection ports

The influence of the position of the injection port was investigated. The injection angle (θ_{inj}) was set up at 360°, 405°, 450°, 495° and 540°. The injection mass flow rate was set to 0.01 kg/s with NH_3 mass fractions of 0.4 and 0.7. Fig. 10 shows the example of temperature evolution in relation to the injection angle.

The increasing of the injection angle resulted in the increasing of the discharge temperature, discharge pressure and required compression power. That was true for both lean and rich solutions. The injection is characterised by the change of slope of the temperature increasing. The model indicated that wet compression occurs when the solution is injected at 360° and 405°. For the injection at 360°, this is clearly indicated by the temperature line inflection shown in Fig. 10. Further increase of the injection angle did not show the presence of the liquid fraction (vapor quality = 1) except at the injection point. This happens due to the high degree of superheat at an injection angle over 405°. At the time, the cooling of the superheated gas before reaching the injection point was observed for all investigated cases. This was explained by the leakage of cooled gas towards the suction port. The injection mass flow rate of 0.01 kg/s at 360° and 405° did not provide wet compression for the whole length of the compressor, which means it is insufficient for good lubrication. The mass flow analysis revealed that the injection of 0.01 kg/s does not generate backflow from the discharge port into the compression chamber, and under-compression was not observed for both the lean and rich solutions, irrespectively on the injection angle.

Three different injection mass flow rates (0.01 kg/s, 0.015 kg/s and 0.02 kg/s) were investigated with respect to the set injection angles. Increasing the injection mass flow rate lowers the discharge temperature, pressure, and compression power, as observed in Section 4.4. At the same time, the increase of the injection angle results in the decrease of the under-compression and backflow. For injection of lean solution, it was found that under-compression and backflow occurred with an injected mass flow rate of 0.015 kg/s for injection angles up to 450° and with 0.02 kg/s for injection angles up to 495°. At an injection angle of

Table 2
Results for different x_{inj} values at constant $C_{leak} = 0.05\ m^{-1}$, $\theta_{inj} = 360^{\circ}$ and $\dot{m}_{inj} = 0.01\ kg/s$.

x_{inj} [-]	0.0	0.25	0.5	0.75	1.0
T_{max} [°C]	169.2	172.6	179.2	191.2	207.3
p_{max} [bar]	25.82	25.96	26.24	26.85	27.65
$\dot{W}_{comp}$ [kW]	54.07	54.35	54.94	56.21	57.89

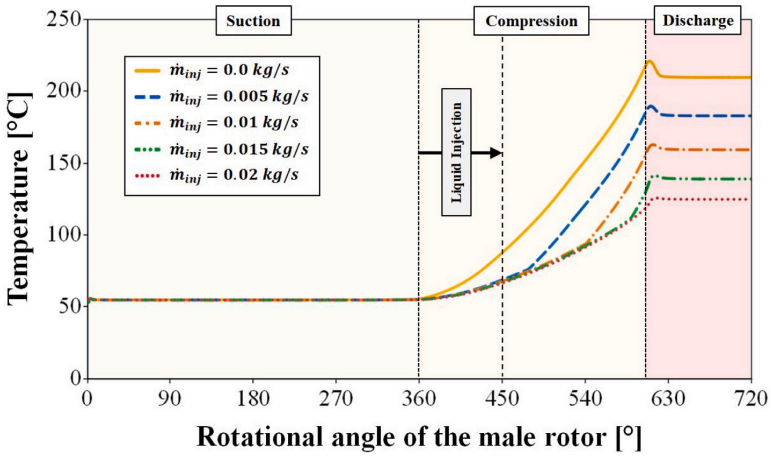

Fig. 8. Temperature evolution for different $\dot{m}_{inj}$ values with $x_{inj} = 0.4$ at constant $C_{leak} = 0.05$ m^{-1} and $\theta_{inj} = 360^{\circ}$.

Table 3
Results for different $\dot{m}_{inj}$ values with $x_{inj} = 0.4$ and 0.7 at constant $C_{leak} = 0.05$ m^{-1} and $\theta_{inj} = 360^{\circ}$.

$\dot{m}_{inj}$ [kg/s]	0.0	0.005	0.01	0.015	0.02
		x_{inj} = 0.4			
T_{max} [°C]	221.4	189.9	163.0	141.7	126.0
p_{max} [bar]	27.99	26.76	25.95	25.71	25.55
$\dot{W}_{comp}$ [kW]	58.61	56.04	54.33	53.84	53.49
		x_{inj} = 0.7			
T_{max} [°C]	221.4	196.2	173.3	153.3	136.7
p_{max} [bar]	27.99	27.15	26.45	25.95	25.78
$\dot{W}_{comp}$ [kW]	58.61	56.85	55.38	54.33	53.97

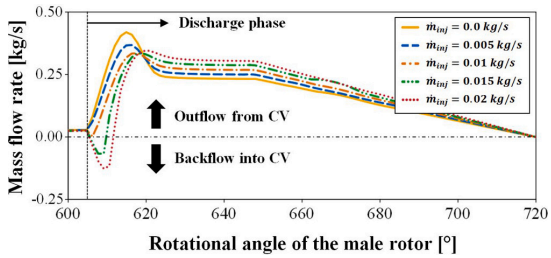

Fig. 9. Mass flow rate evolution for a CV during transition from compression to discharge phase for different $\dot{m}_{inj}$ values with $x_{inj} = 0.4$ at constant $C_{leak} = 0.05$ m^{-1} and $\theta_{inj} = 360^{\circ}$.

540°, no under-compression and backflow were observed. For injection of rich solution, the under-compression and backflow with an injected mass flow rate of 0.015 kg/s occurred only for an injection angle of 360° and with 0.02 kg/s for injection angles up to 450°. More detailed information is presented in Table 4.

The analysis on the provision of wet compression revealed that higher mass flow rates are required for later injection positions. Wet compression was not observed for injection at 540°, while in all other cases sufficient wet compression occurred at injection rates of 0.02 kg/s at the latest. As indicated in Fig. 10 and Table 4, injection at the beginning of the compression phase (360°) shows the best effect on the resulting parameters. However, to ensure continuous wet compression throughout the entire compression phase, larger mass flow rates (min. 0.02 kg/s corresponding to approx. 10 % of the compressor's suction mass flow rate) must be injected. To limit a further increase in the required injection flow rate with the resulting effects such as increased under-compression and backflow, the distribution of the injection over multiple injection ports can be considered, as the single port solution becomes insufficient. Here, a portion of the solution is injected at the beginning of the compression phase at 360°, with the remaining portion injected at a later stage to ensure continuous wet compression for sufficient lubrication and sealing effects.

An investigation with different injection positions (360°, 450° and 495°) and mass flow rates was conducted to evaluate the distribution through two injection ports. The first injection was placed at 360°, the only position capable of ensuring wet compression from the beginning of the compression phase. The second injection port was located either at 450° or 495° to support continuous wet compression towards the end of the compression phase, see Fig. 10. Total injection rates of 0.01 kg/s, 0.015 kg/s and 0.02 kg/s were distributed to both ports with varying injection flow ratios for each port in steps of 0.005 kg/s. The analysis for the case with injection ports located at 360° and 450° revealed that with increasing total injection rate, the discharge temperature, discharge pressure and compressor power decrease, as shown in Table 4. At the same time, the length of the occurring wet compression increases. Increasing the injected flow over the port at 450° (while keeping the total injection flow constant) resulted in slightly increased values for discharge temperature, discharge pressure, and compressor power compared to single port injection (see Table 4). Furthermore, a flattening of the vapor quality curves was accompanied by a lower degree of under-compression and backflow when compared with single port injection and increased injection flow at 360° (two port injection). The analysis for the case with injection ports located at 360° and 495° indicated a similar behaviour with slightly increased values for discharge temperature, discharge pressure and compression power. Unlike the previous case with the second injection at 450°, it is important to note that with a low injection rate of 0.005 kg/s at 360°, no continuous wet compression was achieved with total injection rates of 0.01 kg/s and 0.015 kg/s. Once wet compression stops, it is difficult to regain it at a later stage due to the increased temperature. Therefore, an attempt should be made to ensure continuous wet compression. Based on these results, it is suggested to split the injection over two ports located at 360° and 450°, with the larger proportion of 0.015 kg/s (75 %) injected through the port at 450°. In this case, an injection flow of approx. 0.02 kg/s is still required for complete wet compression. However, the resulting pressure is around 0.01 bar higher, and less under-

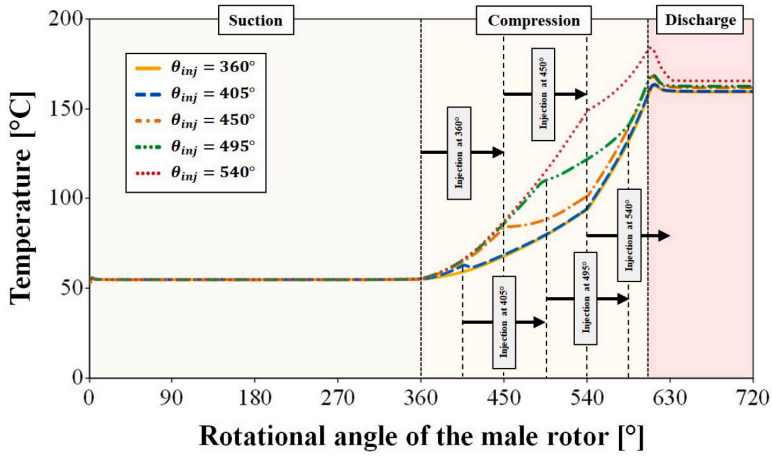

Fig. 10. Example of temperature evolution for different θ_{inj} values with $x_{inj} = 0.4$ at constant $C_{leak} = 0.05\ m^{-1}$ and $\dot{m}_{inj} = 0.01\ kg/s$.

Table 4
Results for different θ_{inj} and $\dot{m}_{inj}$ values with $x_{inj} = 0.4$ and 0.7 at constant $C_{leak} = 0.05\ m^{-1}$.

	$x_{inj} = 0.4$					$x_{inj} = 0.7$				
θ_{inj} [°]	360	405	450	495	540	360	405	450	495	540
					$\dot{m}_{inj} = 0.01$kg/s					
T_{max} [°C]	163.0	163.6	168.2	172.1	184.4	173.3	172.6	177.1	178.1	190.2
p_{max} [bar]	25.95	26.02	26.70	26.78	27.09	26.45	26.49	26.90	26.92	27.22
$\dot{W}_{comp}$ [kW]	54.33	54.49	55.89	56.07	56.71	55.38	55.46	56.31	56.37	57.00
					$\dot{m}_{inj} = 0.015$kg/s					
T_{max} [°C]	141.7	141.5	143.7	147.9	167.1	153.3	154.3	156.6	160.2	175.5
p_{max} [bar]	25.71	25.71	25.83	26.24	26.65	25.95	25.99	26.36	26.49	26.87
$\dot{W}_{comp}$ [kW]	53.84	53.82	54.08	54.94	55.79	54.33	54.42	55.18	55.46	56.25
					$\dot{m}_{inj} = 0.02$kg/s					
T_{max} [°C]	126.0	126.0	126.2	129.3	150.6	136.7	135.8	138.1	142.7	161.2
p_{max} [bar]	25.55	25.56	25.62	25.80	26.23	25.78	25.76	25.84	26.11	26.46
$\dot{W}_{comp}$ [kW]	53.49	53.51	53.63	54.01	54.91	53.97	53.94	54.09	54.67	55.41

compression and backflow will occur.

4.6. Variation of compressor speed

In the intended operation of a compressor in the ACHP system, the compressor speed will vary depending on the required operating condition. As outlined in a review by Wang et al. [18], investigations in the literature show that changes in speed affect the different performance parameters of the compressor. To gain a better understanding of the achievable performance parameters at varying operating points of the compressor, the influence of the operational frequency was investigated. The operational frequency was set to 62.5 Hz (125 %), 50 Hz (100 %), 37.5 Hz (75 %) and 25 Hz (50 %) with a constant C_{leak} value of 0.05 m^{-1} and single-port injection at an injection angle of 360°. The liquid injection rate with respect to the specific compressor suction mass flow rate was varied from 0 %, 5 %, and 10 %, with NH_3 mass fractions of 0.4 and 0.7.

The suction mass flow rate of the compressor for the ideal case without leakage ($C_{leak} = 0.0\ m^{-1}$) and no liquid injection ($\dot{m}_{inj}$ set to 0) increases linearly with increasing operational frequency. Under consideration of internal leakage ($C_{leak} = 0.05\ m^{-1}$), the results revealed that a decrease in the operational frequency causes an increase in the occurring leakage flow. Due to reduced rotor speed, the residence time of the working fluid in the cavity volume during the compression process is extended, and leakages increase. Fig. 11 presents the achieved volumetric efficiencies compared to the reference case without leakage for the investigated operational frequencies and liquid injection flow rates corresponding to 0 %, 5 % and 10 % of the respective suction mass flow rates.

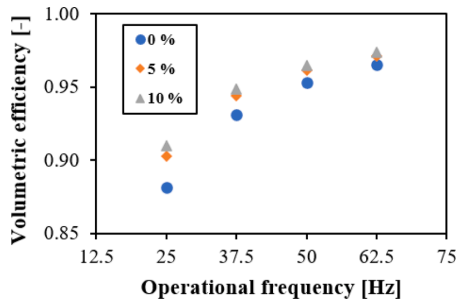

Fig. 11. Volumetric efficiency for varying f and liquid injection flow rates from 0 %, 5 % and 10 % with $x_{inj} = 0.4$ at constant $C_{leak} = 0.05\ m^{-1}$ and $\theta_{inj} = 360°$.

The results demonstrate that the volumetric efficiency increases for higher operational frequencies. Moreover, the increase in the injection rate provides an improvement in the volumetric efficiency at constant frequencies. Here, the difference from 0 % to 5 % is larger than from 5 % to 10 %, indicating that the liquid has a positive effect on the occurring leakages, although there is a maximum possible value that can be

achieved.

The same trends are observed for the other investigated parameters. The maximum temperature reached decreases for increasing operational frequencies from 238.9 °C at 25 Hz to 218.3 °C at 62.5 Hz with no injection. When the injection rates are increased to 5 %, both the respective temperatures and the total variation decrease (174.1 °C at 25 Hz and 161.6 °C at 62.5 Hz). At an injection rate of 10 %, full wet compression is achieved for all cases studied, and the temperatures are greatly reduced to 130.5 °C at 25 Hz and 125.8 °C at 62.5 Hz. Therefore, to obtain the same temperature as in cases with higher operational frequency, a higher injection ratio is required. The same beneficial impact of the injection is observed for the changes in the maximum pressure (from 28.08 bar to 26.14 bar to 25.71 bar at 62.5 Hz and from 27.53 bar to 25.61 bar to 25.24 bar at 25 Hz), and the maximum required compression power (from 73.79 kW to 68.42 kW to 67.28 kW bar at 62.5 Hz and from 28.82 kW to 26.81 kW to 26.42 kW at 25 Hz), with the lowest values are obtained with 10 % injection rate.

The determination of isentropic and adiabatic efficiency for the comparison and evaluation of the achieved efficiency is complicated in the present study. Due to the liquid injection, a continuous heat transfer takes place, which is often solved by splitting the compression process, as described by Tian et al. [22] and Di et al. [43]. However, the NH_3 mass fraction also changes continuously, complicating the calculation and making comparison difficult. For this reason, the specific power is calculated as the ratio of the maximum total compression power to the suction mass flow rate. Fig. 12 shows the determined specific power for the investigated operational frequencies and liquid injection flow rates corresponding to 0 %, 5 % and 10 % of the respective suction mass flow rates.

The results indicate that the specific power required for compression decreases as the operational frequency increases. In addition, a higher injection rate ensures a further reduction in specific power. Here, the characteristics are similar to the previously described trends. It can be concluded that the injection rate and ratio must be adapted and controlled according to the compressor speed. These observations are consistent with the results presented in the literature by various authors such as Tian et al. [22], Wang [39] and Li et al. [44].

4.7. Discussion of results and model limitations

The results and model limitations are discussed with respect to the conducted investigation of the liquid injection for an oil-free twin screw compressor within the ACHP system. The objective of the developed MODELICA screw compressor model was to improve the understanding of thermodynamic behaviour during the compression process using NH_3-H_2O mixture as refrigerant and liquid injection with varying NH_3 mass fractions. The preliminary analysis indicated that both desorption of ammonia from the liquid phase and full evaporation are achievable,

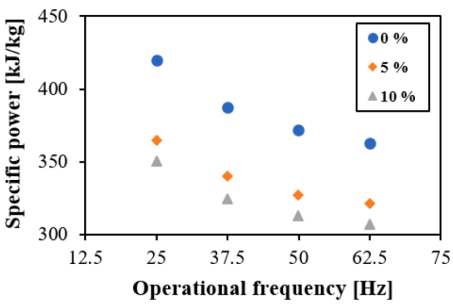

Fig. 12. Specific power (compression power to compressed working fluid flow) for varying f and liquid injection flow rates from 0 %, 5 % and 10 % with $x_{inj} = 0.4$ at constant $C_{leak} = 0.05\ m^{-1}$ and $\theta_{inj} = 360^{\circ}$.

irrespective of the subcooled state of the injected lean or rich solution.

The developed model consists of moving control volumes containing the working fluid in liquid vapor equilibrium and performing the compression process without mechanical losses. To consider occurring leakages across the rotor tips and housing, a function was implemented, and a leakage coefficient (C_{leak}) was defined. The analysis with different values indicated the influence on the pressure evolution and resulting over- or under-compression. A suitable value of 0.05 m^{-1} was selected for the further investigation to also consider additional losses of other leakage paths. Heat losses to the compressor body and ambient were not considered for further investigations after assessing their influence.

The study of the NH_3 mass fraction revealed that a reduction in the ammonia content resulted in decreasing values for discharge temperature, discharge pressure and compression power at a constant injection mass flow rate. It was demonstrated that the presence and duration of wet compression (for lubrication and sealing of the compressor) are a function of the NH_3 mass fraction of the injected solution. The best results were obtained with pure water, and it is therefore preferable to inject a solution with low NH_3 mass fraction, such as the lean solution in the ACHP system.

The investigation of the injection mass flow rates demonstrated that wet compression throughout the whole compression phase is possible with an increase in the injection quantity. However, if the injection flow becomes too large, negative effects such as under-compression and backflow from the discharge port will occur. At constant injection flow rates, these effects are less significant with an increased NH_3 mass fraction. An optimum of 0.01 kg/s for the lean solution and between 0.01 kg/s and 0.015 kg/s for the rich solution was determined.

The positioning of injection ports revealed a strong influence on the results obtained. Wet compression was observed with an injection flow of 0.01 kg/s for injection at 360° and 405°. However, this did not occur for the entire compression phase. For this injection rate, no under-compression or backflow was observed for both lean and rich solution. To achieve complete wet compression, larger injection flows up to 0.02 kg/s are required, corresponding to approx. 10 % of the compressor's suction mass flow. At the same time, the provision of complete wet compression through the injection at 360° with 0.02 kg/s led to the highest under-compression and backflow from the discharge port. The split of two injection ports was investigated to evaluate further options to ensure continuous wet compression. It was found that injection at 360° and 450° with a higher injection rate of 0.015 kg/s (75 % of total injection) at 450° leads to higher pressures of 0.01 bar with a reduction in occurring under-compression and backflows. The analysis of varying compressor speed revealed that leakage flows increase at reduced operational frequency. This results in an increased temperature and higher required liquid quantities. It can be concluded that the injection rate must be adapted to the respective operating conditions.

For the comprehensive evaluation of the obtained results, the given model limitations are addressed and discussed. Occurring leakages, mechanical and heat losses, and other component and/or operation specific parameters are difficult to predict without detailed geometry and data and often require experimental investigations. The implemented model of leakage allows to understand and adjust different leakage paths and their geometries. At the same time, the absence of a specific liquid film due to the homogeneous vapor–liquid equilibrium approach of each CV hampers the accurate determination of occurring leakage flows and achievable efficiencies. Since the compressor efficiencies were not a primary concern in this study, the assumption of 100 % mechanical efficiency is reasonable. However, this assumption neglects the fact that mechanical losses under real conditions can influence the temperature evolution of the working fluid by generating heat and thus effect all other operational parameters. This may be compensated for to some extent, as additionally counteracting heat losses to the compressor body were not considered.

The solution is injected in a highly supercooled state and the time to achieve eventual liquid–vapor equilibrium becomes extremely limited

due to the high rotational speeds and relatively short residence time. Furthermore, the liquid–vapor surface area is further reduced due to imperfect dispersion without the use of atomizing nozzles or similar devices. Forces resulting from the rotational motion of the rotors cause the liquid droplets to move toward the rotor tips and/or the compressor housing, which impedes uniform dispersion. All these factors can hamper substantial heat and mass transfer under real operating conditions, resulting in the presence of simultaneously remaining liquid in the CV despite superheated vapor being present. Compared to this, the assumption of liquid–vapor equilibrium with homogeneous distribution in the CV can lead to an overestimation of the pressure and an underestimation of the temperature evolution. Due to these known limitations and further unknown uncertainties, the results are considered as a kind of best-case analysis.

5. Conclusion

The objective of this study was to develop an oil-free twin screw compressor model with NH_3-H_2O mixture as refrigerant and liquid injection to improve the understanding of thermodynamic behaviour during the compression process and to discuss the integration into the ACHP system. The preliminary thermodynamic analysis indicated that both desorption of ammonia from the liquid phase and full evaporation are achievable during the compression process with liquid injection, irrespective of the subcooled state of the injected lean or rich solution. For a comprehensive investigation, a quasi-one-dimensional numerical model was developed using the Modelica language that considers the effects of liquid injection, leakage flows, and heat losses. The model was designed to investigate various arrangements of liquid injection and operating conditions and consists of eight control volumes moving in a continuous compression cycle, containing the working fluid in liquid vapor equilibrium. It is suitable for both transient and steady-state analysis and was used to study the effects of varying NH_3 mass fractions, injection amounts and injection positions during the compression process.

The analysis of the obtained results revealed a strong influence of the investigated parameters on the compression process and the evolution of temperature, pressure, and compression power.

- For the application in the ACHP system, it was concluded that the injection of solution with a low NH_3 mass fraction (see Fig. 1 - Option 1: Injection of lean solution) should be preferred. It was observed that a lower NH_3 mass fraction resulted in decreased discharge temperature, discharge pressure, and compression power. The lowest values were obtained for the injection of pure water. High temperature is generally beneficial for oil-free high temperature heat pumps; however, it can be limited by the material properties of the compressor.
- With the injection of 0.01 kg/s (about 5 % of the compressor's suction mass flow rate) of lean solution, the temperature was sufficiently reduced, and the pressure evolution was adapted to the externally applied pressure ratio. Thereby, under-compression and backflow from the discharge were minimized, which is important for the efficient and sustainable operation of the compressor.
- Wet compression was observed during the injection at the beginning of compression but was not continuous throughout the entire compression phase. To ensure a continuous liquid film that provides sufficient lubrication and sealing throughout the compression process, the injection rate must be increased to about 10 % of the compressor's suction mass flow rate (0.02 kg/s).
- When injecting through a single port, full wet compression was observed only when injected at 360° (at the beginning of the compression phase), regardless of the injection rate. Thus, the placement of one port at 360° is important for ensuring a continuous liquid film.
- To further optimize the achievable results, injection through an additional port in the mid-compression phase (450° or 495°) was investigated. Compared to the single-port injection, the distribution over two injection ports, with the smaller portion (approx. 25 %) injected at 360° at the beginning of the compression process and the greater portion (approx. 75 %) injected at 450°, can support the provision of wet compression and reduce occurring under-compression.
- An investigation with varying compressor speed revealed the influence on the investigated compressor parameters. It was concluded that the injection rate and ratio must be adjusted and controlled to achieve identical temperatures depending on the operating point.

The limitations of the existing model due to the assumptions for the working fluid in each control volume with homogeneous behaviour and liquid vapor equilibrium, as well as the simplified representation of leakage paths and other losses were discussed. Due to these known limitations and further unknown uncertainties, the results are considered as a kind of best-case analysis. However, the conducted investigation fulfils the purpose to provide information about the expected behaviour and the preferred integration into ACHP systems. Furthermore, it provides results for the lowest required injection mass flow and the distribution of injection positions to improve the planning of necessary experimental investigations. The adaptability of the model also provides a comparatively simple increase in the degree of detail for further investigations.

Further research will focus on the experimental investigation and realization of oil-free operation by lubricating and cooling the bearings with the injected solution. This can be supported by a comprehensive life cycle assessment to investigate how the use of more specialized materials like oil-free bearings and more advanced sealings compares to a potential complete elimination of lubrication oil and oil separation equipment. Furthermore, an exergy analysis can be conducted to investigate the influence on the overall ACHP system performance.

Declaration of Competing Interest

The authors declare that they have no known competing financial interests or personal relationships that could have appeared to influence the work reported in this paper.

Data availability

Data will be made available on request.

Acknowledgements

This publication has been funded by HighEFF - Centre for an Energy Efficient and Competitive Industry for the Future, an 8-years' Research Centre under the FME-scheme (Centre for Environment-friendly Energy Research, 257632). The authors gratefully acknowledge the financial support from the Research Council of Norway and user partners of HighEFF.

References

[1] International Energy Agency, Energy Efficiency 2018: Analysis and outlooks to 2040, 2018. Available from: <https://www.iea.org/reports/energy-efficiency-2018>.
[2] International Energy Agency, Net Zero by 2050 - A Roadmap for the Global Energy Sector, 2021. Available from: <https://www.iea.org/reports/net-zero-by-2050>.
[3] E. Woolley, Y. Luo, A. Simeone, Industrial waste heat recovery: a systematic approach, Sustain. Energy Technol. Assessments 29 (2018) 50–59, https://doi.org/10.1016/j.seta.2018.07.001.
[4] M. Papapetrou, G. Kosmadakis, A. Cipollina, U. La Commare, G. Micale, Industrial waste heat: estimation of the technically available resource in the EU per industrial sector, temperature level and country, Appl. Therm. Eng. 138 (2018) 207–216, https://doi.org/10.1016/j.applthermaleng.2018.04.043.

[5] R. Bergamini, J.K. Jensen, B. Elmegaard, Thermodynamic competitiveness of high temperature vapor compression heat pumps for boiler substitution, Energy 182 (2019) 110–121, https://doi.org/10.1016/j.energy.2019.05.187.

[6] M.U. Ahrens, S.S. Foslie, O.M. Moen, M. Bantle, T.M. Eikevik, Integrated high temperature heat pumps and thermal storage tanks for combined heating and cooling in the industry, Appl. Therm. Eng. 189 (2021) 10, https://doi.org/10.1016/j.applthermaleng.2021.116731.

[7] C. Arpagaus, F. Bless, M. Uhlmann, J. Schiffmann, S.S. Bertsch, High temperature heat pumps: market overview, state of the art, research status, refrigerants, and application potentials, Energy 152 (2018) 985–1010, https://doi.org/10.1016/j.energy.2018.03.166.

[8] G. Kosmadakis, Estimating the potential of industrial (high-temperature) heat pumps for exploiting waste heat in EU industries, Appl. Therm. Eng. 156 (2019) 287–298, https://doi.org/10.1016/j.applthermaleng.2019.04.082.

[9] A. Marina, S. Spoelstra, H.A. Zondag, A.K. Wemmers, An estimation of the European industrial heat pump market potential, Renew. Sustain. Energy Rev. 139 (2021), 110545, https://doi.org/10.1016/j.rser.2020.110545.

[10] J. Jiang, B. Hu, R.Z. Wang, N. Deng, F. Cao, C.-C. Wang, A review and perspective on industry high-temperature heat pumps, Renew. Sustain. Energy Rev. 161 (2022), 112106, https://doi.org/10.1016/J.RSER.2022.112106.

[11] J.K. Jensen, W.B. Markussen, L. Reinholdt, B. Elmegaard, On the development of high temperature ammonia-water hybrid absorption-compression heat pumps, Int. J. Refrig. 58 (2015) 79–89, https://doi.org/10.1016/j.ijrefrig.2015.06.006.

[12] M.U. Ahrens, M. Loth, I. Tolstorebrov, A. Hafner, S. Kabelac, R. Wang, T. M. Eikevik, Identification of existing challenges and future trends for the utilization of ammonia-water absorption-compression heat pumps at high temperature operation, Appl. Sci. 11 (2021) 4635, https://doi.org/10.3390/app11104635.

[13] D. Zaytsev, Development of wet compressor for application in compression-resorption heat pumps, Technische Universiteit Delft, 2003. Available from: <http://repository.tudelft.nl/view/ir/uuid%3Aca640a9d-6fe1-4a59-b42c-594213703f07/>.

[14] J. Shen, Z. Xing, K. Zhang, Z. He, X. Wang, Development of a water-injected twin-screw compressor for mechanical vapor compression desalination systems, Appl. Therm. Eng. 95 (2016) 125–135, https://doi.org/10.1016/j.applthermaleng.2015.11.057.

[15] C.A. Infante Ferreira, C. Zamfirescu, D. Zaytsev, Twin screw oil-free wet compressor for compression-absorption cycle, Int. J. Refrig. (2006), https://doi.org/10.1016/j.ijrefrig.2005.10.006.

[16] D. Zaytsev, C.A. Infante Ferreira, Screw compressor for ammonia-water heat pump lubricated by the process mixture, in: Int. Compress. Eng. Conf. Sch., 2002.

[17] M.A. Heiyanthuduwage, S. Mounoury, A. Kovacevic, Performance prediction methods for screw compressors, in: 7th Int. Conf. Compressors Their Syst. 2011, Woodhead Publishing Limited, London, 2011, pp. 411–420, doi: 10.1533/9780857095350.8.411.

[18] C. Wang, B. Wang, M. Liu, Z. Xing, A review of recent research and application progress in screw machines, 10 (2022) 62, doi: 10.3390/MACHINES10010062.

[19] N. Stošic, L. Milutinović, K. Hanjalić, A. Kovačević, Investigation of the influence of oil injection upon the screw compressor working process, Int. J. Refrig. 15 (1992) 206–220, https://doi.org/10.1016/0140-7007(92)90051-U.

[20] N. Stosic, I.K. Smith, A. Kovacevic, Estimation and control of heat transfer in screw compressor rotors, in: Proc. IMECE04, 2004 ASME Int. Mech. Eng. Congr. Expo., Anaheim, 2004, pp. 441–446, doi: 10.1115/IMECE2004-60516.

[21] Q. Yang, C. Liu, Q. Zhang, G. Liu, Y. Zhao, L. Li, Experimental investigation of the water-injected process-gas screw compressor, J. Process Mech. Eng. 232 (2018) 3–11, https://doi.org/10.1177/0954408916666573.

[22] Y. Tian, J. Shen, C. Wang, Z. Xing, X. Wang, Modeling and performance study of a water-injected twin-screw water vapor compressor, Int. J. Refrig. 83 (2017) 75–87, https://doi.org/10.1016/j.ijrefrig.2017.04.008.

[23] N. Basha, A. Kovacevic, S. Rane, Numerical investigation of oil injection in screw compressors, Appl. Therm. Eng. 193 (2021), 116959, https://doi.org/10.1016/J.APPLTHERMALENG.2021.116959.

[24] Y. Tian, H. Yuan, C. Wang, H. Wu, Z. Xing, Numerical investigation on mass and heat transfer in an ammonia oil-free twin-screw compressor with liquid injection, Int. J. Therm. Sci. (2017), https://doi.org/10.1016/j.ijthermalsci.2017.06.007.

[25] H.H. Patel, V.J. Lakhera, A critical review of the experimental studies related to twin screw compressors, J. Process Mech. Eng. 234 (2020) 157–170, https://doi.org/10.1177/0954408919869534.

[26] V. Gudjonsdottir, C.A. Infante Ferreira, A. Goethals, Wet compression model for entropy production minimization, Appl. Therm. Eng. 149 (2019) 439–447, https://doi.org/10.1016/j.applthermaleng.2018.12.065.

[27] V. Gudjonsdottir, C.A. Infante Ferreira, Technical and economic analysis of wet compression–resorption heat pumps, Int. J. Refrig. 117 (2020) 140–149, https://doi.org/10.1016/j.ijrefrig.2020.05.010.

[28] A. Osenbrück, Verfahren zur Kälteerzeugung bei Absorptionsmaschinen, DPR 84084, 1895.

[29] N.S. Ganesh, T. Srinivas, Evaluation of thermodynamic properties of ammonia-water mixture up to 100 bar for power application systems, J. Mech. Eng. Res. 3 (2011) 25–39.

[30] M. Chamoun, R. Rulliere, P. Haberschill, J.L. Peureux, Modelica-based modeling and simulation of a twin screw compressor for heat pump applications, Appl. Therm. Eng. (2013), https://doi.org/10.1016/j.applthermaleng.2013.04.020.

[31] Dassault Systems, DYMOLA Systems Engineering: Multi-Engineering Modeling and Simulation based on Modelica and FMI, 2022. Available from: <https://www.3ds.com/products-services/catia/products/dymola/>.

[32] TLK-Thermo GmbH, TIL Suite – Simulates thermal systems, 2022. Available from: <https://www.tlk-thermo.com/index.php/en/software/til-suite>.

[33] TLK-Thermo GmbH, TILMedia Suite – Software package for calculating the properties of thermophysical substances, 2022. Available from: <https://www.tlk-thermo.com/index.php/en/software/tilmedia-suite>.

[34] M.U. Ahrens, E.K. Tønsberg, I. Tolstorebrov, A. Hafner, T.M. Eikevik, Modelling approach for a liquid-injected ammonia-water screw compressor, in: 10th IIR Conf. Compressors Refrig., Bratislava, 2021, pp. 13–15, doi: 10.18462/iir.compr.2021.0385.

[35] A. Bejan, Advanced Engineering Thermodynamics, 4th ed., John Wiley & Sons, Inc., 2016, doi: 10.1002/9781119245964.

[36] N. Stosic, I.K. Smith, A. Kovacevic, Optimisation of screw compressors, Appl. Therm. Eng. 23 (2003) 1177–1195, https://doi.org/10.1016/S1359-4311(03)00059-0.

[37] J. Li, H. Wu, B. Wang, Z. Xing, P. Shu, Research on the performance of water-injection twin screw compressor, Appl. Therm. Eng. 29 (2009) 3401–3408, https://doi.org/10.1016/J.APPLTHERMALENG.2009.05.018.

[38] W. Huagen, X. Ziwen, S. Pengcheng, Theoretical and experimental study on indicator diagram of twin screw refrigeration compressor, Int. J. Refrig. 27 (2004) 331–338, https://doi.org/10.1016/J.IJREFRIG.2004.01.004.

[39] C. Wang, Z. Xing, W. Chen, S. Sun, Z. He, Analysis of the leakage in a water-lubricated twin-screw air compressor, Appl. Therm. Eng. 155 (2019) 217–225, https://doi.org/10.1016/j.applthermaleng.2019.04.001.

[40] M.G. Read, I.K. Smith, N. Stosic, Influence of rotor geometry on tip leakage and port flow areas in gerotor-type twin screw compressors, Proc. Inst. Mech. Eng. Part E J. Process Mech. Eng. 236 (1) (2022) 94–102.

[41] J.S. Fleming, Y. Tang, The analysis of leakage in a twin screw compressor and its application to performance improvement, Proc. Inst. Mech. Eng. Part E J. Process Mech. Eng. 209 (2) (1995) 125–136.

[42] S. Smitt, I. Tolstorebrov, A. Hafner, Performance improvement of integrated CO2 systems with HVAC and hot water for hotels, Therm. Sci. Eng. Prog. 23 (2021), https://doi.org/10.1016/J.TSEP.2021.100869.

[43] D. Wu, J. Jiang, B. Hu, R.Z. Wang, Experimental investigation on the performance of a very high temperature heat pump with water refrigerant, Energy 190 (2020), 116427, https://doi.org/10.1016/j.energy.2019.116427.

[44] Y. Li, J. Wang, Y. Wu, B. Lei, R. Zhi, L. Shen, Influence of water injection parameters on the performance of a water-lubricated single-screw air compressor, J. Mech. Sci. Technol. 36 (2022) 445–456, doi: 10.1007/S12206-021-1242-4.

Paper I

M.U. Ahrens, A. Hafner and T.M. Eikevik (2019). **Compressors for ammonia-water hybrid absorption-compression heat pumps.** In: *Proceedings of the 8th IIR International Conference on Ammonia and CO2 Refrigeration Technologies*, Ohrid, Republic of North Macedonia, 11-13 April.

Author contributions: Conceptualization: M.U. Ahrens, A. Hafner and T.M. Eikevik; Methodology: M.U. Ahrens; Investigation: M.U. Ahrens; Resources: A. Hafner and T.M. Eikevik; Writing - Original Draft Preparation: M.U. Ahrens; Writing - Review and Editing: M.U. Ahrens, A. Hafner and T.M.E., Visualization: M.U. Ahrens, Supervision: A. Hafner and T.M. Eikevik; Funding Acquisition: T.M. Eikevik.

Paper II

M.U. Ahrens, A. Hafner and T.M. Eikevik (2019). **Development of Ammonia-Water Hybrid Absorption-Compression Heat Pumps.** In: *Proceedings of the 25th IIR International Congress of Refrigeration*, Montreal, Canada, 24-30 August.

Author contributions: Conceptualization: M.U. Ahrens, A. Hafner and T.M. Eikevik; Methodology: M.U. Ahrens; Investigation: M.U. Ahrens; Resources: A. Hafner and T.M. Eikevik; Writing - Original Draft Preparation: M.U. Ahrens; Writing - Review and Editing: M.U. Ahrens, A. Hafner and T.M.E., Visualization: M.U. Ahrens, Supervision: A. Hafner and T.M. Eikevik; Funding Acquisition: T.M. Eikevik.

Paper III

M.U. Ahrens, I.S. Ertesvåg and T.M. Eikevik (2020). **Exergy analysis of a combined absorption-compression heat pump with ammonia-water mixture as working fluid.** In: *Proceedings of the 14th IIR Gustav Lorentzen Conference on Natural Refrigerants*, Kyoto (Online), Japan, 6-9 December.

Author contributions: Conceptualization: M.U. Ahrens, I.S. Ertesvåg and T.M. Eikevik; Methodology: M.U. Ahrens and I.S. Ertesvåg; Investigation: M.U. Ahrens; Resources: I.S. Ertesvåg; Writing - Original Draft Preparation: M.U. Ahrens; Writing - Review and Editing: M.U. Ahrens, I.S. Ertesvåg and T.M. Eikevik; Visualization: M.U. Ahrens; Supervision: I.S. Ertesvåg and T.M. Eikevik; Funding Acquisition: T.M. Eikevik.

Paper IV

M.U. Ahrens, E.K. Tønsberg, I. Tolstorebrov, A. Hafner and T.M. Eikevik (2021). **Modelling approach for a liquid-injected ammonia-water screw compressor.** In: *Proceedings of the 10th International Conference on Compressors and Coolants,* Bratislava (Online), Slovakia, 13-15 January.

Author contributions: Conceptualization: M.U. Ahrens, E.K. Tønsberg, I. Tolstorebrov, A. Hafner and T.M. Eikevik; Methodology: M.U. Ahrens, E.K. Tønsberg and I. Tolstorebrov; Investigation: M.U. Ahrens, E.K. Tønsberg and I. Tolstorebrov; Resources: A. Hafner and T.M. Eikevik; Writing - Original Draft: M.U. Ahrens and E.K. Tønsberg; Writing - Review and Editing: M.U. Ahrens, E.K. Tønsberg, I. Tolstorebrov, A. Hafner and T.M. Eikevik; Visualization: M.U. Ahrens and E.K. Tønsberg; Supervision: I. Tolstorebrov, A. Hafner and T.M. Eikevik; Funding Acquisition: T.M. Eikevik.

Paper V

M.U. Ahrens, H. Selvnes, L. Henke, M. Bantle and A. Hafner (2021). **Investigation on heat recovery strategies from low temperature food processing plants: Energy analysis and system comparison.** In: *Proceedings of the 9th IIR International Conference on Ammonia and CO2 Refrigeration Technologies*, Ohrid (Online), Republic of North Macedonia, 16-18 September.

Author contributions: Conceptualization: M.U. Ahrens, H. Selvnes, L. Henke, M. Bantle and A. Hafner; Methodology: M.U. Ahrens and H. Selvnes; Investigation: M.U. Ahrens, H. Selvnes and L. Henke; Resources: M. Bantle and A. Hafner; Writing - Original Draft: M.U. Ahrens and H. Selvnes; Writing - Review and Editing: M.U. Ahrens, H. Selvnes, L. Henke, M. Bantle and A. Hafner; Visualization: M.U. Ahrens and H. Selvnes; Supervision: M. Bantle and A. Hafner; Funding Acquisition: M. Bantle and A. Hafner.

Paper VI

M.U. Ahrens, E.K. Tønsberg, I. Tolstorebrov, A. Hafner and T.M. Eikevik (2022). **Modeling and simulation of oil-free liquid-injected screw compressors using ammonia-water mixture as working fluid.** In: *Proceedings of the 15th IIR Gustav Lorentzen Conference on Natural Refrigerants*, Trondheim, Norway, 13-15 June.

Author contributions: Conceptualization: M.U. Ahrens, E.K. Tønsberg, I. Tolstorebrov, A. Hafner and T.M. Eikevik; Methodology: M.U. Ahrens and E.K. Tønsberg; Investigation: M.U. Ahrens, E.K. Tønsberg and I. Tolstorebrov; Resources: A. Hafner and T.M. Eikevik; Writing - Original Draft: M.U. Ahrens; Writing - Review and Editing: M.U. Ahrens, E.K. Tønsberg, I. Tolstorebrov, A. Hafner and T.M. Eikevik; Visualization: M.U. Ahrens and E.K. Tønsberg; Supervision: I. Tolstorebrov, A. Hafner and T.M. Eikevik; Funding Acquisition: T.M. Eikevik.

Paper VII

M.U. Ahrens, A. Brækken, S.S. Foslie, O.M. Moen, K.A. Lovas, M. Bantle, A. Hafner and T.M. Eikevik (2022). **Performance analysis of high temperature heat pumps and thermal energy storages for a dairy.** In: *Proceedings of the 15th IIR Gustav Lorentzen Conference on Natural Refrigerants*, Trondheim, Norway, 13-15 June.

Author contributions: Conceptualization: M.U. Ahrens, A. Brækken, S.S. Foslie, O.M. Moen, K.A. Lovas, M. Bantle and T.M. Eikevik; Methodology: M.U. Ahrens, S.S. Foslie and O.M. Moen; Software: M.U. Ahrens, S.S. Foslie and O.M. Moen; Investigation: M.U. Ahrens and A. Brækken; Resources: K.A. Lovas, M. Bantle and T.M. Eikevik; Writing - Original Draft: M.U. Ahrens and A. Brækken; Writing - Review and Editing: M.U. Ahrens, A. Brækken, S.S. Foslie, O.M. Moen, K.A. Lovas, M. Bantle and T.M. Eikevik; Visualization: M.U. Ahrens and A. Brækken; Supervision: T.M. Eikevik; Funding Acquisition: M. Bantle and T.M. Eikevik.